HYDROLOGIC OPTICS

Volume I. Introduction

R.W. PREISENDORFER

U.S. DEPARTMENT OF COMMERCE
NATIONAL OCEANIC & ATMOSPHERIC ADMINISTRATION
ENVIRONMENTAL RESEARCH LABORATORIES

HONOLULU, HAWAII
1976

HYDROLOGIC OPTICS

Volume I. Introduction

R.W Preisendorfer

Joint Tsunami Research Effort
Honolulu, Hawaii

1976

U.S. DEPARTMENT OF COMMERCE
National Oceanic and Atmospheric Administration
Environmental Research Laboratories
Pacific Marine Environmental Laboratory

Nothing that is seen is seen at once
in its entirety

EUCLID
(First theorem, The Optics of Euclid [36])

CONTENTS

Volume I

PART I BASIC PRINCIPLES

Chapter 1

Introduction to Hydrologic Optics

1.0 Hydrologic Optics: Definition, Domain and Desiderata 1

The Problems of Hydrologic Optics 2
The Aims and Desired Goals of This Work 3
The Plan and Scope of This Work 4

1.1 A Primer of Geometrical Radiometry and Photometry 6

The Nature of Radiant Flux 6
The Unpolarized-Flux Convention 7
Geometrical Channeling of Radiant Flux 9
Operational Definitions of the Densities 10
Field and Surface Interpretations of Radiant Flux and its Densities 12
Operational Definitions of Field and Surface Quantities 12
Summary of Concepts and Some Principal Formulas of Geometrical Radiometry 14
n^2-Law for Radiance 18
The Bridge to Geometrical Photometry 18

1.2 A Survey of Natural Light Fields 22

The Solar Constant 22
General Irradiance Levels at Earth's Surface 24
General Illuminance Levels at Earth's Surface 25
Gross Features of Atmospheric Radiative Transfer 27
Radiative Transfer Across the Air-Water Surface 28
Glitter Patterns on the Air-Water Surface 32
Subsurface Refractive Phenomena 33
The Decay of the General Light Field with Depth 37
Behavior of Radiance Distributions with Depth 39
The Asymptotic Radiance Hypothesis 41
Underwater Irradiance Distributions 42
Subsurface Contrast Reduction by Scattering and Absorbing Effects 44
Subsurface Contrast Reduction by Refractive Effects 48
The Polarization of Underwater Light Fields 50
Biological Sources of Submarine Light Fields 53

1.3 Three Simple Models for Light Fields 55

The Two-Flow Model 55
The Radiance Model 58
The Diffusion Model 61

1.4 Some Deductions from the Light Field Models 66

The Decay of the General Light Field with Depth 66
Reflectance and Transmittance of Finitely Deep Hydrosols 68
Invariant Imbedding Relations for Irradiance 71
A Theoretical Basis for the Law:

$$N_* (z,\theta) = N_* (0,\theta)\, e^{-kz}$$ 81

Computing Radiances from the Simple Model 84
Derivation of the Contrast Transmittance Law and the Radiance Difference Law 89
Contrast Transmittances for General Backgrounds 92
The Multiplicative Property of Contrast Transmittance 93
Theory of the Secchi and Duntley Disks 96
Theory of Absorption Measurements in Natural Hydrosols 103

1.5 Some Properties of Artificial Light Fields in Natural Waters 109

The Pure Absorption Case 109
Derivation of the Semi-empirical Diffusion Model for Point Sources 110
Two Examples of the Empirical Diffusion Model 112
Radiance Distribution Produced by a Submerged Uniform Point Source 113
An Empirical Study of Light Fields Produced by Collimated Sources 114

1.6 Inherent and Apparent Optical Properties of Hydrosols 118

Operational Definitions of the Inherent Optical Properties 119
The Volume Attenuation Function 119
The Volume Scattering Function 122
Volume Total Scattering Function and Volume Absorption Function 123
Selected Physical Measurements of the Inherent Optical Properties 125
Operational Definitions of the Apparent Optical Properties 135
Preliminary Observations on the Classification of Natural Hydrosols 138

1.7 Some General Modes of Classification of Natural Optical Media 139

Modes of Classification 139

1.8 Colorimetric Radiative Transfer 142

The Quantitative Description of Color 143
An Example of Experimentally Determined Chromaticity Coordinates 149
On the Use of Simple Models for Theoretical Predictions of Chromaticity Coordinates 151

1.9 Applications of Hydrologic Optics to Underwater Visibility Problems 154

Introduction to the Nomographs 154

A. Selection of the Proper Chart 156
A.1 Introduction 156
A.2 Natural Illumination 156
A.3 Effect of Depth and Water Clarity 157
Stratified Water 157
Effect of Sea-State 157
Examples 160
A.4 Adaptation Level 160
Inclination Factor 160
Bottom Influence 162
A.5 Calculation of Adaptation Luminance 162
A.6 Chart Selection 163

B. Using the Nomographs 163
B.1 Introduction 163
Objects on the Bottom 163
Object Size and Shape 163
Vertical Path of Sight 163
Inclined Paths of Sight 165
B.3 The Secchi Disk 169
B.4 Target Markings 170
B.5 The Measurements of Target Reflectance 170
B.6 Horizontal Paths of Sight 170
B.7 The R_∞ *Correction* 172
B.8 Correction of the Sighting Range 172

C. Interpretation of Sighting Range 193
C.1 Introduction 193
C.2 Effect of Lack of Warning 193
C.3 Effect of Observer Training 193
C.4 Effect of Observer Visual Capability 194

D. Visualization of Water Clarity 194
D.1 Introduction 194
D.2 Estimation of Sighting Range 194
D.3 Estimation of Adaptation Luminance 195
D.4 Estimation of α *and* K 195
D.5 Characterization of Natural Waters 195

1.10 Applications of Hydrologic Optics to the Food-Chain Problem in the Sea 196

The General Exponential Law of Change 197
The Volterra Prey-Predator Equations 198
The General Food-Chain Equations 199
An Illustration of the Food-Chain Theory with a Radiant Energy Term 201

1.10 Applications of Hydrologic Optics to the Food-Chain Problem in the Sea (Continued)

The General Three-Term Equations 202
The Quasi-Steady State Equations 202
The Equilibrium Solutions 203
Some General Properties of Equilibrium Solutions 204

1.11 Future Problems of Hydrologic Optics 205

Problem One: To Establish Theoretically the Physical Basis of the Inherent Optical Properties of Natural Hydrosols 206
Problem Two: To Establish Complete Empirical Classifications of Natural Hydrosols 207
Problem Three: To Establish a Unified Automatic Computation Program for Prediction Computations and Data Reduction Computations in Geophysical Optics (the GEOVAC) 208

1.12 Bibliographic Notes for Chapter 1 208

Volume II

Chapter 2

Radiometric and Photometric Concepts

2.0 Introduction

2.1 Radiant Flux

Basic Photoelectric Effects
Operational Definition of Radiant Flux

2.2 The Meaning of 'Radiant Flux'

2.3 Fundamental Geometric Properties of Radiant Flux

2.4 Irradiance and Radiant Emittance

Definition of Irradiance
The Meaning of 'Irradiance'
Terrestrial Coordinate Systems
Representation of Irradiance in Terrestrial Frames
The Cosine Law for Irradiance
Radiant Emittance

2.5 Radiance

Radiance Distributions
Irradiance from Radiance
Radiance from Irradiance

2.5 Radiance (Continued)
Field Radiance vs Surface Radiance

2.6 An Invariance Property of Radiance
The Radiance-Invariance Law
The Operational Meaning of Surface Radiance
The n^2-Law for Radiance

2.7 Scalar Irradiance, Radiant Energy, and Related Concepts
Radiant Density
Scalar Irradiance
Spherical Irradiance
Hemispherical Irradiance
Radiant Energy over Space
Radiant Energy over Time
Scalar Radiant Emittance

2.8 Vector Irradiance
A Mechanical Analogy
General Definition of Vector Irradiance
The General Cosine Law for Irradiance

2.9 Radiant Intensity
Operational Definition of Empirical Radiant Intensity
Field Intensity vs Surface Intensity
Theoretical Radiant Intensity
Radiant Intensity and Point Sources
Cosine Law for Radiant Intensity
Generalized Cosine Law for Radiant Intensity

2.10 Polarized Radiance
Operational Definition of Polarized Radiance
The Standard Stokes and Standard Observable Vectors
Analytic Link Between **S** and **N**
Standard and Local Reference Frames
Radiant Flux Content of Polarized Radiance

2.11 Examples Illustrating the Radiometric Concepts
1. Radiance of the Sun and Moon
2. Radiant Intensity of the Sun and Moon
3. Radiant Flux Incident on Portions of the Earth
4. Irradiance Distance-Law for Spheres
5. Irradiance Distance-Law for Circular Disks; Criterion for a Point Source
6. Irradiance Distance-Law for General Surfaces
7. Irradiance via Line Integrals
8. Solid Angle Subtense of Surfaces

2.11 Examples Illustrating the Radiometric Concepts (Continued)

9. Irradiance via Surface Integrals
10. Radiant Flux Calculations
11. Intensity Area-Law for General Surfaces
12. On the Possibility of Inverse nth Power Irradiance Laws
13. Irradiance from Elliptical Radiance Distributions
14. Irradiance from Polynomial Radiance Distributions
15. On the Formal Equivalence of Radiance and Irradiance Distributions

2.12 Transition from Radiometry to Photometry

The Individual Luminosity Functions
The Standard Luminosity Functions
Photometric Bedrock: the Lumen
Luminance Distributions
Transition to Geometrical Photometry
General Properties of the Radiometric-Photometric Transition Operator
The Mathematical Basis for Geometrical Photometry
Summary and Examples (Tables of Radiometric and Photometric Concepts)

2.13 Generalized Photometries

Linear Photometries
Nonlinear Photometries

2.14 Bibliographic Notes for Chapter 2

Chapter 3

The Interaction Principle

3.0 Introduction

The Physical Basis of the Linearity of the Interaction Principle
Plan of the Chapter

3.1 A Preliminary Example

Empirical Reflectances and Transmittances for Surfaces
The Problem
The Present Instance of the Interaction Principle
Solution of the Problem

3.1 A Preliminary Example (Continued)

Discussion of Solution
Related Problems and Their Solutions
An Alternate Form of the Principle
The Natural Mode of Solution

3.2 The Interaction Principle

Discussion of the Interaction Principle
The Place of the Interaction Principle in Radiative Transfer Theory
The Levels of Interpretation of the Interaction Principle

3.3 Reflectance and Transmittance Operators for Surfaces

Geometrical Conventions
The Empirical Reflectances and Transmittances
The Theoretical Reflectances and Transmittances
Variations of the Basic Theme

3.4 Applications to Plane Surfaces

Example 1: Irradiances on Two Infinite Parallel Planes
Example 2: Irradiances on Two Infinite Parallel Planes, Reexamined. A First Synthesis of the Interaction Method
Example 3: Irradiances on Finitely Many Infinite Parallel Planes
Example 4: Irradiances on Infinitely Many Infinite Parallel Planes
Example 5: The Algebra of Reflectance and Transmittance Operators for Planes. Radiometric Norm. Iterated Operators. Operator Algebras and Radiative Transfer.
Example 6: Radiances of Infinite Parallel Planes
Example 7: Terminable and Non Terminable Interreflection Calculations. A Terminable Calculation. Truncation Error Estimates. Quantum-terminable Calculations.
Example 8: Two Interacting Finite Plane Surfaces

3.5 Applications to Curved Surfaces

Example 1: Open Concave Surfaces
Example 2: Closed Concave Surfaces; the Integrating Sphere
Example 3: Open and Closed Convex Surfaces
Example 4: General Two-Sided Surfaces
Example 5: General One-Sided Surfaces

3.6 Reflectance and Transmittance Operators for Plane-Parallel Media

Geometrical Conventions
The Empirical Reflectances and Transmittances

3.6 Reflectance and Transmittance Operators for Plane-Parallel Media (Continued)

The Theoretical Reflectances and Transmittances
Variations of the Basic Theme

3.7 Applications to Plane-Parallel Media

Example 1: Irradiances on Plane-Parallel Media
Example 2: Radiances in Plane-Parallel Media
Example 3: The Classical Principles of Invariance
Example 4: The Invariant Imbedding Relation
Example 5: Semigroup Properties of Transmitted and Reflected Radiant Flux
Example 6: The Generalized Invariant Imbedding Relation
Example 7: Group-Theoretic Structure of Natural Light Fields. Group Theory, Radiative Transfer and Quantum Theory.

3.8 Interaction Operators for General Spaces

Geometrical Conventions
The Empirical Scattering Functions
The Theoretical Scattering Functions
Variations of the Basic Theme

3.9 Applications to General Spaces

Example 1: Principles of Invariance for Spherical, Cylindrical, Toroidal Media
Example 2: Invariant Imbedding Relation for One-Parameter Media
Example 3: One-Parameter Media with Internal Sources
Example 4: Principles of Invariance for General Media
Example 5: Invariant Imbedding Relation in General Media
Example 6: Reflecting Boundaries and Interfaces
Example 7: The Unified Atmosphere-Hydrosphere Problem
Example 8: Several Interacting Separate Media

3.10 Derivation of the Beam Transmittance Function

3.11 Derivation of the Volume Attenuation Function

3.12 Derivation of Path Radiance and Path Function

The Path Radiance
The Path Function
The Connection Between Path Function and Path Radiance

3.13 Derivation of Apparent-Radiance Equation

3.14 Derivation of the Volume Scattering Function

Regularity Properties of σ
The Integral Representation of the Path Function

3.15 The Equation of Transfer for Radiance

Steady State Equation of Transfer
Time Dependent and Polarized Equations of Transfer

3.16 On The Integral Structure of the Interaction Operators

The Mathematical Prerequisites
Interaction Operators for Surfaces
Interaction Operators for General Media
Interaction Measures and Kernels

3.17 Further Examples of the Interaction Method

Example 1: The Path Function Operator
Example 2: The Path Radiance Operator
Example 3: The Volume Transpectral Scattering Operator
Miscellaneous Examples

3.18 Summary of the Interaction Method

Summary of the Interaction Method
Remarks on the Stages of the Interaction Method
The Interaction Method and Quantum Theory
The Interaction Principle as a Means and as an End
Conclusion

3.19 Bibliographic Notes for Chapter 3

Volume III

PART II THEORY OF LIGHT FIELDS

Chapter 4

Canonical Forms of the Equation of Transfer

4.0 Introduction

4.1 Radiance in Transparent Media

4.2 Radiance in Absorbing Media

4.3 Koschmieder's Equation for Radiance

4.4 The Classical Canonical Equation

4.5 The General Canonical Equation for Radiance
Canonical Representation of Apparent Radiance
The Canonical Form for Stratified Media

4.6 Canonical Representation of Polarized Radiance
A Simple Model for Polarized Light Fields
Experimental Questions

4.7 Abstract Versions of Canonical Equations

4.8 Bibliographic Notes for Chapter 4

Chapter 5

Natural Solutions of the Equation of Transfer

5.0 Introduction

5.1 The n-ary Radiometric Concepts
n-ary Radiance
n-ary Scalar Irradiance
n-ary Radiant Energy
General n-ary Radiometric Functions

5.2 Equation of Transfer for n-ary Radiance, Diffuse Radiance, and Path Function

5.3 Canonical Equations for n-ary Radiance
Concluding Observations

5.4 The Natural Solution for Radiance

5.5 Truncated Natural Solutions for Radiance

5.6 Optical Ringing Problem. One Dimensional Case.
Geometry of the Time-Dependent Light Field
The Equation of Transfer
Operator Form of the Equation of Transfer
The Natural Solution
An Example
Concluding Observations

5.7 Optical Ringing Problem. Three Dimensional Case.

The Characteristic Ellipsoid
Time Dependent **R** and **T** Operators and the Natural Solution
Truncated Natural Solution

5.8 Transport Equation for Residual, Directly Observable, and n-ary Radiant Energy

Residual Radiant Energy
Transport Equation for Residual Radiant Energy
The Attenuation Time Constant
General Representation of Residual Radiant Energy
Transport Equation for n-ary Radiant Energy
Transport Equation for Directly Observable Radiant Energy
The Natural Solution for Directly Observable Radiant Energy

5.9 Solutions of the n-ary Radiant Energy Equations

Natural Integral Representations of n-ary Radiant Energy
Natural Closed Form Representations of n-ary Radiant Energy
General Integral Representations of n-ary Radiant Energy
Standard Growth and Decay Formulas for n-ary Radiant Energy

5.10 Properties of Time Dependent n-ary Radiant Energy Fields and Related Fields

Some Fine-Structure Properties of n-ary Radiant Energy
Scattered, Absorbed, and Attenuated Radiant Energies
Representations of $U(t;\alpha)$, $U(t;s)$, and $U(t;a)$

5.11 Dimensionless Forms of n-ary Radiant Energy Fields and Related Fields

Conversion Rules for Dimensionless Quantities
Dimensionless Forms for $U^{o}(t)$
Dimensionless Forms for $U^{n}(t)$
Dimensionless Forms for $U^{*}(t)$
Dimensionless Forms for $U(t)$
Dimensionless Forms for $U(t;\alpha)$, $U(t;a)$
Some Graphical Representations of Solutions in Dimensionless Form
A Discussion of Time Constants

5.12 Global Approximations of General Radiance Fields

Global Approximations of Higher Order

5.13 Light Storage Phenomena in Natural Optical Media

Everyday Examples of Light Storage
Storage Capacity
Methods of Determining Storage Capacity
Example

5.14 Operator-Theoretic Basis for the Natural Solution Procedure

5.15 Bibliographic Notes for Chapter 5

Chapter 6

Classical Solutions of the Equations of Transfer

6.0 Introduction

6.1 The Bases of the Spherical Harmonic Method

Physical Motivations
An Algebraic Setting for Radiance Distributions

6.2 Abstract Spherical Harmonic Method

Finite Forms of the Abstract Harmonic Equations

6.3 Classical Spherical Harmonic Method; General Media

The Orthonormal Family
Properties of the Orthonormal Family
General Equations for Spherical Harmonic Method

6.4 Classical Spherical Harmonic Method: Plane-Parallel Media

A Formal Solution Procedure
A Truncated Solution Procedure
Vector Form of the Truncated Solution
Summary

6.5 Three Approaches to Diffusion Theory

The Approach via Fick's Law
The Approach via Spherical Harmonics
Radiance Distributions in Diffusion Theory

6.5 Three Approaches to Diffusion Theory (Continued)

Approaches via Higher Order Approximations
The Approach via Isotropic Scattering

6.6 Solutions of the Classical Diffusion Equations

Plane-Parallel Case
Point Source Case
Discrete Source Case
Continuous Source Case
Primary Scattered Flux as Source Flux
Higher Order Scattered Flux as Source Flux
Time Dependent Diffusion Problems

6.7 Solutions of the Exact Diffusion Equations

Infinite Medium with Point Source
Infinite Medium with Arbitrary Sources
Semi-infinite Medium with Boundary Point Source
Semi-infinite Medium with Internal Point Source
Observations on the Functional Relations for f_c and f_o

6.8 Bibliographic Notes for Chapter 6

Volume IV

Chapter 7

Invariant Imbedding Techniques for Light Fields

7.0 Introduction

7.1 Differential Equations Governing the Steady State R and T Operators

Local Forms of the Principles of Invariance
The Differential Equations for R and T
Discussion of the Differential Equations
Functional Relations for Decomposed Light Fields

7.2 Differential Equations Governing the Time Dependent R and T Operators

Time Dependent Local Forms of the Principles of Invariance
Time Dependent Invariant Imbedding Relation
Integral Representation of Time Dependent $\mathcal{R}$ and $\mathcal{T}$ Operators
Time Dependent Principles of Invariance
Differential Equations for the Time Dependent R and T Operators

7.2 Differential Equations Governing the Time Dependent R and T Operators (Continued)

Discussion of the Differential Equations

7.3 Algebraic and Analytic Properties of the R and T Operators

Partition Relations for R and T Operators
Alternate Derivations of the Differential Equations for R and T Operators
Asymptotic Properties of R and T Operators

7.4 Algebraic Properties of the Invariant Imbedding Operators

The Operator M(x,z)
The Connections Between M(x,z), $\mathcal{M}(x,z)$, and $\mathcal{M}(z,x)$
Invertibility of Operators
Representations for the Components of $\mathcal{M}(x,z)$, $\mathcal{M}(z,x)$
The Isomorphism ϕ Between $\Gamma_2(a,b)$ and $G_2(a,b)$
The Physical Interpretation of the Star Product
The Link Between $\mathcal{M}(a,x,b)$ and $\mathcal{M}(a,y,b)$
Representation of $\mathcal{M}(x,y,z)$ by Elements of $\Gamma_2(a,b)$
A Constructive Extension of the Domain of $\mathcal{M}(x,y,z)$
Representation of $\mathcal{M}(v,z;u,y)$ by Elements of $\Gamma_2(a,b)$ and $\Gamma_3(a,b)$
The Connection Between $\Psi(x,y)$ and $\mathcal{M}(s,y)$
A Star Product for the Operators $\mathcal{M}(x,y,z)$
Possibilities Beyond $\mathcal{M}(v,x;u,w)$
Possibilities Beyond $\Gamma_2(a,b)$

7.5 Analytic Properties of the Invariant Imbedding Operators

Differential Equations for $\mathcal{M}(x,y)$
Differential Equations for $\mathcal{M}(x,y,z)$
Differential Equations for $\mathcal{M}(v,x;u,w)$
Differential Equations for M(x,y) and $\Psi(s,y)$
Analysis of the Differential Equation for R(y,b)

7.6 Special Solution Procedures for R(a,b) and T(a,b) in Plane-Parallel Media

The General Equation for $R(a,b;\xi',\xi)$
The Isotropic Scattering Case for R
A Sample Numerical Solution for $r(x;\mu',\nu)$
The General Equation for $T^*(a,b;\xi';\xi)$
The Isotropic Scattering Case for T^*

7.7 General Solution Procedures for R(a,b) and T(a,b) in Plane-Parallel Media

7.8 The Method of Modules for Deep Homogeneous Media

The Invariant Imbedding Relation for Deep Hydrosols
The Module Equation
Empirical Bases for the Use of the Module Equations

7.9 The Method of Semigroups for Deep Homogeneous Media

The Semigroup Equations for $\mathcal{T}(z)$
The Infinitesimal Generator A

7.10 The Method of Groups for Deep Homogeneous Media

The Return of the Group $\Gamma_2(0,\infty)$
The Infinitesimal Generator of $\Gamma_2(0,\infty)$
The Exponential Representation of $\mathcal{M}(y)$ and N(y)
The Exponential Representation of $\mathcal{A}(y)$
Numerical Procedures of N(y): The Exponential Technique
The Characteristic Representation of N(y)
Asymptotic Property of N(y)
Asymptotic Properties of Polarized Radiance Fields

7.11 Method of Groups for General Optical Media

Analysis of the Group Method: Initial Data
Analysis of the Group Method: Limitations of the Equation of Transfer
Analysis of the Group Method: Summarized
The General Method of Groups
Observations on the Method of Groups
The Method of Groups and the Inner Structure of Natural Light Fields

7.12 Homogeneity, Isotropy and Related Properties of Optical Media

Local Concepts
Global Concepts
Summary
Conclusion

7.13 Functional Relations for Media with Internal Sources

Preliminary Relations
Integral Representations of the Local Ψ-Operators
Integral Representations of the Global Ψ-Operators
Incipient Patterns and Nascent Methods

7.13 Functional Relations for Media with Internal Sources (Continued)

Dual Integral Representations of the Global Ψ-Operators
Logical Descendants of Ψ(s,y;a,b)
Differential Equations for the Dual Operators
A Colligation of the Component Ψ-Operator Equations
Asymmetries of the Ψ-Operator
A Royal Road to the Internal-Source Functional Equations
Summary and Prospectus
Final Observations on the Relations Between the Operators $\mathcal{M}(v,x;u,w)$ and Ψ(s,y;a,b)

7.14 Invariant Imbedding and Integral Transform Techniques

An Integral-Transform Primer
Time-Dependent Radiative Transfer
Heterochromatic Radiative Transfer
Multidimensional Radiative Transfer
Conclusion

7.15 Bibliographic Notes for Chapter 7

Volume V

Chapter 8

Models for Irradiance Fields

8.0 Introduction

8.1 Invariant Imbedding Relation for Irradiance Fields

8.2 General Irradiance Equations

8.3 Two-Flow Equations: Undecomposed Form

Equilibrium Form of the Two-Flow Equations
Ontogeny of the Two-Flow Equations

8.4 Two-Flow Equations: Decomposed Form

Principles of Invariance for Diffuse Irradiance
Classical Models for Irradiance Fields
Collimated-Diffuse Light Field Models
Isotropic Scattering Models
Connections with Diffusion Theory

8.5 Two-D Models for Irradiance Fields

On the Depth Dependence of the Attenuating Functions
Two-D Model for Undecomposed Irradiance Fields
Two-D Models for Internal Sources
Two-D Model for Decomposed Irradiance Fields
Inclusion of Boundary Effects

8.6 One-D and Many-D Models

One-D Models for Undecomposed Irradiance Fields
One-D Model for Internal Sources
One-D Model for Decomposed Irradiances
Many-D Models

8.7 Invariant Imbedding Concepts for Irradiance Fields

Example 1: $\mathscr{R}$ and $\mathscr{T}$ Factors in Two-D Models
Example 2: $\mathscr{R}$ and $\mathscr{T}$ Factors in One-D Models
Example 3: Differential Equations for R and T Factors
Example 4: Third Order Semigroup Properties of $\mathscr{R}$ and $\mathscr{T}$ Factors
Example 5: Systematic Analyses of Boundary Effects
Example 6: Invariant Imbedding Operator for Interacting Media
Example 7: Differential Equations Governing $\mathscr{R}$ and $\mathscr{T}$ Factors
Example 8: Method of Modules for Irradiance Fields
Example 9: Method of Semigroups for Irradiance Fields
Example 10: Irradiance Fields Generated by Internal Sources

8.8 A Model for Vector Irradiance Fields

The Quasi-Irrotational Light Field in Natural Waters
Interpretations of the Integrating Factor
The Curl and Divergence of the Submarine Light Field
General Representation of the Submarine Light Field
Example 1: The Case of Isotropic Scattering
Example 2: Asymptotic Form of the Light Field
Global Properties of the Irradiance Field

8.9 Canonical Representation of Irradiance Fields

8.10 Bibliographic Notes for Chapter 8

PART III THEORY OF OPTICAL PROPERTIES

Chapter 9

General Theory of Optical Properties

9.0 Introduction

9.1 Basic Definitions for Optical Properties

9.2 Directly Observable Quantities for Light Fields in Natural Hydrosols

Introduction
Classical Two-Flow Theory: The Theoretical K-Functions
Diffuse Absorption Coefficient k
The R-Infinity Formulas
The Inequalities
Observations on Inadequacies of Classical Theory
Exact Two-Flow Theory: Experimental K-Functions and R-Functions
The Basic Reflectance Relation
The Exact Inequalities
The Significance of the Condition $0 \leq K(z,+)$
Relative Magnitudes of H and K-Functions
Characteristic Equation for $K(z,\pm)$
The Depth Rate of Change of $R(z,-)$
Connections Among the K-Functions
K-Function for Radiance
General K-Functions
Integral Representations of the K-Functions
Integral Representations of the Irradiance and Radiance Fields

9.3 The Covariation of the K-Functions for Irradiance and Distribution Functions

Some Elementary Physical and Geometrical Features of $K(z,-)$ and $D(z,-)$
The General Law Governing $K(x,-)$ and $D(z,-)$
The Absorption-Like Character of $K(z,-)$
Forward Scattering Media
The Covariation Rule for $K(z,-)$ and $D(z,-)$
Illustrations of the Rule
The Contravariation of $K(z,+)$ and $D(z,+)$
A Covariation Rule of Thumb

9.4 General Analytical Representations of the Observable Reflectance Function

The Differential Equation for $R(\cdot,-)$: Unfactored Form

9.4 General Analytical Representations of the Observable Reflectance Function (Continued)

The Differential Equation for R(•,-): Factored Form
Second-Order Form of Differential Equation for R(•,-)
The Equilibrium-Seeking Theorem for R(•,-): Preliminary Observations
The Equilibrium-Seeking Theorem for R(•,-)
Observation 1
Observation 2
The Integral Representations of R(z,-)
Applications
Special Closed Form Solution
Differential Analyzer or Digital Solutions
Series Solutions
Equivalence Theorem for R(•,-)
Connections with the Two-Flow Theory
Summary

9.5 The Contrast Transmittance Function

The Concept of Contrast
Regular Neighborhoods of Paths
Contrast Transmittance and Its Properties
Alternate Representations of Contrast Transmittance
Contrast Transmittance as an Apparent Optical Property
On the Multiplicity of Apparent Radiance Representations

9.6 Classification of Optical Properties

9.7 Bibliographic Notes for Chapter 9

Chapter 10

Optical Properties at Extreme Depths

10.0 Introduction

10.1 On the Structure of the Light Field at Shallow-Depths: Introductory Discussion

10.2 Experimental Basis for the Shallow-Depth Theory

Summary of the Experimental Evidence

10.3 Formulation of the Shallow-Depth Model for K- and R-Functions

Formulas for H(z,±)

10.3 Formulation of the Shallow-Depth Model for K- and R-Functions (Continued)

Formulas for $K(z,\pm)$
Formula for $R(z,-)$
Comparisons of Experimental Data with Calculations Based on the Model
Hypotheses on the Fine Structure of Light Fields in Natural Hydrosols

10.4 Catalog of K-Configuration for Shallow Depths

Some Special Fine Structure Relations
Conclusion

10.5 A General Proof of the Asymptotic Radiance Hypothesis

Introduction
Preliminary Definitions
Formulation of the Problem
The Functions P,Q,R
The Limit of $K_q(\cdot,\mu,\phi)$
The Limit of $K(\cdot,\mu,\phi)$
Notes and Observations

10.6 On the Existence of Characteristic Diffuse Light: A Special Proof of the Asymptotic Radiance Hypotheses

Introduction
Physical Background of the Method of Proof
The Proof
The Equation for the Characteristic Diffuse Light

10.7 Some Practical Consequences of the Asymptotic Radiance Hypothesis

Basic Formulas: The Irradiance Quartet
The D- and R-Functions
The K-Functions
The K-Characterization of the Hypothesis
The Basic Transfer Equations
Consequences for Directly Observable Quantities: The Equation for the Asymptotic Radiance Distribution
The Limits of the K-Functions
The Limits of the D- and R-Functions
Consequences for Some Simple Theoretical Models: The Two-D Model for Irradiance Fields
Critique of Whitney's "General Law"
The Simple Model for Radiance Distributions
Further Consequences of Asymptoticity
The Standard Ellipsoid
Expressions for $D(\pm)$ and R
The Determination of ε
An Heuristic Proof of the Hypothesis
A Criterion for Asymptoticity

10.8 Simple Formulas for the Volume Absorption Coefficient in Asymptotic Light Fields

Introduction
Short Derivation of I
Derivation of II
Applied Numerology: A Rule of Thumb

10.9 Bibliographic Notes for Chapter 10

Chapter 11

The Universal Radiative Transport Equation

11.0 Introduction

11.1 Transport Equations for Radiometric Concepts

Equation of Transfer for Radiance
Transport Equations for $H(z,\pm)$
Transport Equations for $h(z,\pm)$
Transport Equation for Scalar Irradiance
Preliminary Unification and Preliminary Statement of the Equilibrium Principle

11.2 Transport Equations for Apparent Optical Properties

Canonical Forms of Transport Equations for K-Functions
Dimensionless Transport Equation for $K(\mathcal{P})$
Transport Equation for $K(z,\theta,\phi)$
Transport Equations for $K(z,\pm)$
Transport Equations for $k(z,\pm)$ and $k(z)$
Transport Equation for $R(z,-)$

11.3 Universal Radiative Transport Equation and the Equilibrium Principle

11.4 Some Additional Transport Equations Subsumed by the Universal Transport Equation

Summary and Conclusion

11.5 Bibliographic Notes for Chapter 11

Volume VI

Chapter 12

Optical Properties of the Air-Water Surface

12.0 Introduction

12.1 Reflectance and Transmittance Properties of the Static Surface

The Geometric Law of Reflection
The Geometric Law of Refraction
The Fresnel Laws for Reflectance
The Fresnel Laws for Transmittance
Example 1: Reflectance Under Uniform Radiance Distributions
Example 2: Reflectance Under Cardioidal Radiance Distributions
Example 3: Reflectance Under Zonal Radiance Distributions

12.2 Radiative Transfer and the Static Surface

Irradiance Interaction Between the Surface and the Hydrosol
The Three-fold Irradiance Interaction: Aerosol, Air-Water Surface, and Hydrosol
The Three-fold Radiance Interaction: for the Static Surface
Contrast Transmittance Formulas for the Static Surface
Contrast Transmittance Formulas for Extended Paths Across the Static Air-Water Surface

12.3 Elementary Hydrodynamics of the Air-Water Surface

The Fluid Transfer Process
Physics of the Fluid Transfer Process
General Equations of Motion of a Fluid
Special Equations of Motion for the Air and Water Masses
Surface Kinematic Condition
Surface Pressure Condition
Sinusoidal Wave Forms
Linearized Equations of Motion
Classical Wave Model
Kelvin-Helmholtz Model
Kelvin-Helmholtz Instability
Capillary and Gravity Waves
Energy of Waves
Superposition of Waves
Spectrum of the Air-Water Surface

12.4 Harmonic Analyses of the Dynamic Air-Water Surface

The Roots of Harmonic Analysis
Harmonic Synthesis vs. Harmonic Analysis
Integrals vs. Series in Harmonic Analysis
Fourier Series Representations of the Air-Water Surface
Hydrodynamic Basis for Harmonic Analysis of Air-Water Surfaces
The Periodogram Basis of the Energy Spectrum
Fourier Integral Representations of the Air-Water Surface. Case 1: The Surface is Aperiodic
Fourier Integral Representations of the Air-Water Surface. Case 2: The Surface is Periodic or Random
A Working Representation of the Dynamic Air-Water Surface and its Directional Energy Spectrum
Geometrical Applications of the Directional Energy Spectrum

12.5 Wave Slope Data

The Logarithmic Wind Profile Model
Visual Observations on Wave Slopes
Hulburt's Observations of Wave Slopes
Duntley's Immersed-Wire Measurements of Wave Slopes
Intuitive Picture of the Gaussian Slope Distribution
The Wave-Slope Wind-Speed Law (Duntley)
Cox and Munk's Photographic Analysis of the Glitter Pattern
The Wave-Slope Wind-Speed Law (Cox and Munk)
Schooley's Flash Photography Measurements of Wave Slopes

12.6 Wave Generation and Decay Data

Generation of Waves: Shallow Depths, Small Fetches
Generation of Waves: Deep Depths, Large Fetches
Decay of Waves

12.7 Wave Spectrum Data

Wave Spectra by Aerial Stereo Photography
Wave Spectra by Floating-Buoy Motion
Wave Spectra from Submarine Echo Recordings

12.8 Empirical Wave Spectra Models

The Neumann Spectrum
Derivation of the Neumann Spectrum
Three Laws Derived from the Neumann Spectrum
Alternate Forms of the One-Dimensional Spectrum

12.8 Empirical Wave Spectra Models (Continued)

General Properties of Gamma Type Spectra
Wind Speed, Wave Length, and Wave Energy

12.9 Theoretical Wave Spectra Models

The Wave Elevation Distribution
The Wave Slope Distribution
The Wavelength Distribution
The Bretschneider Spectrum
The Wave Height Distribution
Models of Wind-Generated Spectra
Spectral Transport Theory

12.10 Instantaneous Radiance Field Over A Dynamic Air-Water Surface

The Geometrical Setting
The Integral Equation for the Instantaneous Surface Radiance $N^{\ddagger}(S)$

12.11 Time Averaged Radiance Field Over A Dynamic Air-Water Surface

Direct and Indirect Radiance Averages
The Stationarity Condition
The Independence Condition
The Weighting Functions
The Time Averaged Integral Equation for $N^{\ddagger}(S)$
Structure of the Weighting Functions
The Instantaneous and Time Averaged Equations for $N^{\pm}(S)$

12.12 Instantaneous and Time-Averaged Radiance Fields Within A Natural Hydrosol

Two Types of Time-Averaged Radiance Fields
Equations of Transfer for Time-Averaged Radiance Fields
Connection Between Fixed Depth and Cosurface Time-Averaged Radiances

12.13 Synthesis of Time-Averaged Radiance Fields

Comparison with the Static Case

12.14 Observations on the Theory of Time-Averaged Radiance Fields for Dynamic Air-Water Surfaces

A Hierarchy of Approximate Theories
Illustrations of Some Classical Partial Theories
Concluding Observations

12.15 Simulation of the Reflectance of the Air-Water Surface by Mechanical Devices

The Central Idea of the Sea State Simulator
Ergodic Hypothesis
The Discrete Case
The Continuous Case
Some General Observations on the Ergodic Cup Device
Sea Simulator Devices Beyond the Ergodic Cup

12.16 Bibliographic Notes for Chapter 12

Chapter 13

Operational Formulations of Concepts for Experimental Procedures

13.0 Introduction

13.1 Operational Definitions of the Principal Radiometric Concepts

13.2 Operational Definition of Beam Transmittance

General Two-Path Method
General One-Path Method

13.3 Operational Definitions of Path Radiances and Path Functions

Operational Formulation of Path Radiance
Operational Formulation of Path Function

13.4 Operational Definition of Volume Attenuation Function

13.5 A General Theory of Perturbed Light Fields, with Applications to Forward Scattering Effects in Beam Transmittance Measurements

Introduction
General Representation of a Perturbed Light Field
Linearized Representation of Slightly Perturbed Light Fields
Application to Bright-target Technique
Application to Dark-target Technique
An Outline of Possible Experimental Procedures of α in Perturbed Light Fields
Order of Magnitude Estimates
Summary and Conclusions

13.6 Operational Definition of Volume Scattering Function

σ-Recovery Procedures
Determining the Volume Scattering Matrix in the Polarized Case

13.7 Direct Measurement of the Volume Total Scattering Function

The General Method
Observations
Two Special Methods
Cylindrical Medium
Spherical Medium

13.8 Operational Definition of Volume Absorption Function

Procedures for Stratified Light Fields
Procedures for Deep Media
General Global Method
Further Procedures for General Media

13.9 Operational Procedures for Apparent Optical Properties

The Fundamental Irradiance Quartet
Discussion of the Distribution Functions
Discussion of the K-Functions

13.10 Theory of Measurement of Local and Global R and T Properties

Example 1: R and T Factors in Homogeneous Polarity-Free Settings
Example 2: Homogeneous Media with Polarity
Example 3: Forward and Backward Scattering Functions
Example 4: R and T Operators for Radiance
General Observations on Inverse Problems in Hydrologic Optics

13.11 On the Consistency of the Operational Formulations

On the Relative Consistency of the Unpolarized and Polarized Theories of Radiative Transfer

13.12 Bibliographic Notes for Chapter 13

PREFACE

In this work I conclude my studies of radiative transfer theory begun in the monograph, "Radiative Transfer on Discrete Spaces." In that monograph the main goal was the founding of the interaction principle underlying the phenomenological theory of light in scattering-absorbing media. In this treatise, I systematically construct from the interaction principle those basic laws and formulas of the discipline of radiative transfer that pertain to hydrologic optics. Thus while the first work was concerned with the gathering together of many single threads of theory converging on the notion of the principle of interaction, the present study starts with the principle as a base, deduces the superstructure of general radiative transfer theory, and applies it to the special case of light in the sea. This task is essentially carried out in Chapter 3 and culminates in the classical principles of invariance and in the equation of transfer for radiance. Concurrent with this is the deduction of the existence of the fundamental optical properties used in the equation of transfer, namely the volume attenuation and volume scattering functions. Some of the remaining chapters of the book (Chapters 4, 5, 6, 7, 8, 11) are devoted to deductions from the principles of invariance and the equation of transfer of those laws of radiative transfer and those properties of natural optical media which are particularly suited to the study of radiant energy transfer in the sea and other natural bodies of water. Actually, many hydrologic optics principles discussed in this work can also describe radiative transfer phenomena in general optical media, such as those encountered in both the astrophysical and geophysical (including industrial) settings. However these principles have often been deliberately phrased for use within the context of hydrologic optics in order to retain the concreteness and practical utility of the theory. The quest for generality was fulfilled in the discrete-space monograph.

In completing the preceding task, I brought to a close a long and almost circular conceptual odyssey which began for me during a summer eighteen years ago (1950) when I was a student at the Massachusetts Institute of Technology. I was given the problem of determining the reduction of visibility of submerged objects as seen along inclined paths of sight through the wind-crinkled, air-water surface. The odyssey was 'circular' in the sense that my preoccupations in this field began and ended essentially with the problem of radiative transfer through the wind-blown air-water surfaces of natural hydrosols (Chapter 12). Between these end points concerned with the initial and final studies of this problem, I travelled a conceptual journey which for long periods was

occupied with the search for the most basic principles and concepts underlying the solution of this and related problems of light in the sea. As explained in the preface of the first work, that search was guided by a personal interest in carrying the theory of hydrologic optics to its highest level of geometric and algebraic perfection.

During the past eighteen years the theory was most intensively pursued within the period of seven years from 1953 to 1960 and during a brief period around 1964-1965. The remaining periods of time were occupied at first with student studies and later with writing, teaching, travels, and applied and pure mathematical studies in other fields. In particular, the manuscript for the present work was first drafted in rough outline in the spring of 1958. Successive drafts were enriched as additional theory was created. The motivations of these additions were through the experimental findings of my colleagues and my own imperfect applications of the rough theory. The roots of the present work extend back to a series of lectures I gave on hydrologic and atmospheric optics in the fall of 1953 and the spring of 1954, and earlier still to the joint work in 1950-1952 with Duntley summarized in the first four chapters of "The Visibility of Submerged Objects." The final and main manuscript of the present work was essentially completed in the summer of 1965, after approximately 20 months of writing which was begun hard on the heels of finishing my monograph. During this period large parts of Chapters 2, 3, 6, 7, and 12 were originated as the writing proceeded. In general, every chapter had new material of some kind added at this time. The present work then lay dormant for nearly three years, awaiting final proofreading, while I was occupied with new teaching and research responsibilities. On recently re-reading the manuscript and teaching from parts of it, I find that the fundamental theory has mellowed well; it has reached a stage of internal completeness which will be adequate to the needs of all advanced experimental and theoretical work in the forseeable future.

Those points in the present study where contact is made with physical reality, in the form of useful illustrative experimental data on the radiance of submerged light fields and in instructive listings of optical properties of various seas and lakes, are due principally to the labors of my colleagues Dr. S.Q. Duntley and Mr. J.E. Tyler. Their key measurements of the basic radiometric quantities and optical properties of these media provided some of the original impetus toward my construction of the theory of hydrologic optics. The construction was undertaken as an attempt to conceptually sort and order the many empirical laws of light in the sea which their probings uncovered. My indebtedness to these men actually is deeper than this, and I would like to record here the following observations in this regard.

To Dr. Duntley I owe much of the support of my work during all the past years through his various contracts with the Bureau of Ships and the Office of Naval Research of the United States Navy. The early years were interspersed with conversations and working sessions in which I received from him some of my first glimpses of a possible theory of

hydrologic optics. In the summer of 1950 at the Diamond Island Experimental Station in Lake Winnipesaukee, New Hampshire he described his important empirical discovery of the elliptical hydrologic range law made during some underwater experiments. The hint of theoretical order in that experimental polar plot of hydrologic range versus downward angle of sight inspired me subsequently to fathom first the physical and then the mathematical laws underlying that phenomenon. The ensuing summer was spent happily in my sun-baked cabin on that tiny island as I tackled my first independent scientific studies. These resulted in the deduction of the elliptical hydrologic range law and also the simplest radiance-propagation laws for lines of sight through air-ruffled water surfaces and along inclined paths of sight through deep regions of seas and lakes. Duntley's influence on my studies occurred not only in the experimental quarter, but also on first reading his distinguished contributions to the Schuster two-flow theory: I recall the train ride through New Hampshire countryside from Boston which began that summer of 1950 and which is forever linked with the conceptual revelations experienced as I read his two papers on "Optical Properties of Diffusing Materials" and "The Mathematics of Turbid Media." The first paper pointed the way toward the improvement of the Schuster two-flow theory. The latter paper was eventually to provide an instance of the interaction principle in the form of Schuster's "principle of self-illumination." A dozen years were to pass and a score or more of distinct manifestations of the principle of interaction were to be discovered before its universality was to become manifest in my mind. It was also Duntley's exposition of L.V. King's integral equation method and especially the closing remarks in the latter paper that eventually encouraged me to create the discrete space theory of radiative transfer. This theory on the one hand retains the generality of the integral equation approach and on the other leads without modification to numerical determinations of light fields in general optical media. The requisite procedure is given by the Categorical Analysis Method in my monograph.

I wish also to note in some detail the profound influence of the work of Tyler on my constructions of hydrologic optics theory. Unquestionably his experimental measurements on the "Radiance distribution as a function of depth in an underwater environment", was for me a watershed of at least a dozen incipient theoretical laws of hydrologic optics. It provided, for example, the definitive experimental data needed to verify L.V. Whitney's conjecture on the existence of "characteristic diffuse light" deep below the surface of every natural optical medium and which belongs exclusively to that medium regardless of the lighting conditions above its surface. These findings encouraged my search for theoretical expressions of the fundamental properties of real light fields far from the boundaries of deep optical media. It was also Tyler's accumulation of data by means of ever more precise radiometric measurements in oceans and lakes that led us both to realize the inherent limitations of the classical Schuster two-flow (one-D) model of the light field in handling such data: his measurements of upward and downward irradiance flows, for example, were uncovering new kinds of

depth behavior of the diffuse attenuation and reflectance functions of such subtle and delicate forms that they lay far beyond the descriptive powers of the classical theory. This state of affairs eventually led me to formulate the theory of directly observable optical properties of light fields in real stratified media. These formulas for directly observable properties were subsequently applied by Tyler and his colleagues in various papers, and particularly in the "Method for obtaining the optical properties of large bodies of water." The present account must also take cognizance of many conversations with Tyler on the puzzles of practical radiometry in the sea. These discussions gave me insight into the needs of the experimenter in hydrologic optics and for whom in turn Chapters 9, 10, and 13 are specifically written. In the course of the years the contents of these chapters arose in various attempts to cast into a mathematically self-consistent array of operationally meaningful forms all the fundamental concepts of radiative transfer in the sea, such as the volume attenuation, scattering, absorption, and the diffuse attenuation functions for all radiometric concepts. These concepts in other branches of radiative transfer, notably astrophysical optics, were either nonexistent or in the form of unrealizable mathematical abstractions of no use to one with direct instrumental access to the interior of the optical medium of interest; in our case, the sea. Finally, I gratefully acknowledge that a large part of the writing of this work was generously supported by portions of Tyler's National Science Foundation Grants (G 11668 and G 289).

The preceding description of the background of the present work has implicitly referred to the contents of all the chapters except the first two. The first chapter may serve as a self-contained 'short-course' on hydrologic optics. Indeed it has been used as a base for the first course on 'Radiative Transfer in the Sea' given at Scripps Institution of Oceanography in the fall of 1967. Particular attention is directed toward the three simple models for light fields in natural waters given in Chapter 1. These models constitute the minimal theoretical tools for anyone who enters the field of hydrologic optics and wishes to do productive work therein. In particular for one who plans to do experimental studies, some guidelines are necessary to first of all measure the quantities of hydrologic optics in a consistent manner and secondly, to measure something that will be useful to others in the same field. These models and the constructs from which they are fashioned supply the requisite guidelines. As one's needs for precision and comprehensiveness of concepts evolve, then the theoretical developments comprising the remaining chapters of the work will be of help in filling these needs. Attention is also directed to the section of the first chapter dealing with practical nomographs for predicting the range of visibility available to underwater swimmers in various natural hydrosols such as harbors, lakes and seas. These nomographs are based on the work of Duntley, which combines the properties of the human eye with one of the three models of the light field referred to above. Also of general interest are the many samples of magnitudes of light fields and optical constants found in natural waters. These

samples are based mainly on the field work of Tyler, Duntley, and Jerlov and serve to fix one's intuition for the sizes of the optical constants found in nature. This in turn allows intelligent derivations of new approximate formulas based on the light field models alluded to above. Finally, the presence of Chapter 2 is almost self-explanatory, being concerned with the scientific language of radiative transfer: geometrical radiometry. Students of geometrical radiometry may find the various novel formulas and laws developed throughout the chapter of independent interest. However, the chapter finds its place in this work by providing the radiometric concepts and formulations needed in the applications of the interaction principle to hydrologic optics.

The main drafts were expertly typed by Mrs. Lynn White and by Mrs. Judith Marshall. Mrs. Marshall also assisted in the preparation of various tables and graphs, and the typing of the final draft for photocopy.

R.W.P.

San Diego
December 1968

The final draft was completed while undertaking new researches in hydrodynamics with the Tsunami Research Effort (J.T.R.E.), which is part of the Environmental Research Laboratories of the National Oceanic and Atmospheric Administration. I am grateful to the Director of J.T.R.E., Dr. Gaylord Miller, for making available the Graphic Arts facilities at the Institute of Geophysics of the University of Hawaii, and particularly to Mr. Brad Evans for his art work on the figures.

R.W.P.

Honolulu
January 1972

CHAPTER 1

INTRODUCTION TO HYDROLOGIC OPTICS

1.0 Hydrologic Optics: Definition, Domain, and Desiderata

As the earth swings round the sun, it continuously turns its atmosphere, its lands and its seas to face into the steady torrent of energy streaming from that radiant star. Of the nearly 65,000,000 watts of radiant power of all wavelengths emitted from each square meter of the sun's surface, about 1,400 watts are incident on each square meter of the upper levels of the earth's atmosphere directly facing the sun, there to initiate and sustain the complex chains of meteorologic and hydrologic events among which are the important biologic links evolving in the atmosphere and the seas. In the meteorologic domain, the radiant flux from the sun is partly absorbed to warm the earth's gaseous mantle so as to generate winds and habitable climes; and partly scattered so as to help grow plants and light the ways of the creatures of the air and earth below. In the hydrologic domain the radiant flux, when in sufficient abundance, is partly absorbed to help keep the seas and lakes and other natural hydrosols in their fluid state, and is partly scattered about in their upper levels so as to light the ways and help provide sustenance for the creatures of these watery domains.

Hydrologic optics is the quantitative study of the interaction of radiant energy with hydrosols, especially the natural hydrosols of the earth such as its seas, lakes, ponds, rivers, and bays. Hydrologic optics is part of a broader discipline known as *geophysical optics* which studies the common physical and geometrical principles governing radiant energy fields in both the meteorologic and hydrologic domains. Geophysical optics together with *astrophysical optics*--in which the emission, absorption and scattering of radiant energy within general planetary and stellar atmospheres is of primary concern--fall under the aegis of *radiative transfer theory*, which is defined as the quantitative study, on a phenomenological level, of the transfer of radiant energy through media that absorb, scatter, or emit radiant energy. Radiative transfer theory, in turn, is viewable as a logical descendent of electromagnetic theory, and in this way hydrologic optics, and more generally radiative transfer theory, may take its place among the theories of modern physics. These interrelations are summarized in Fig. 1.1.

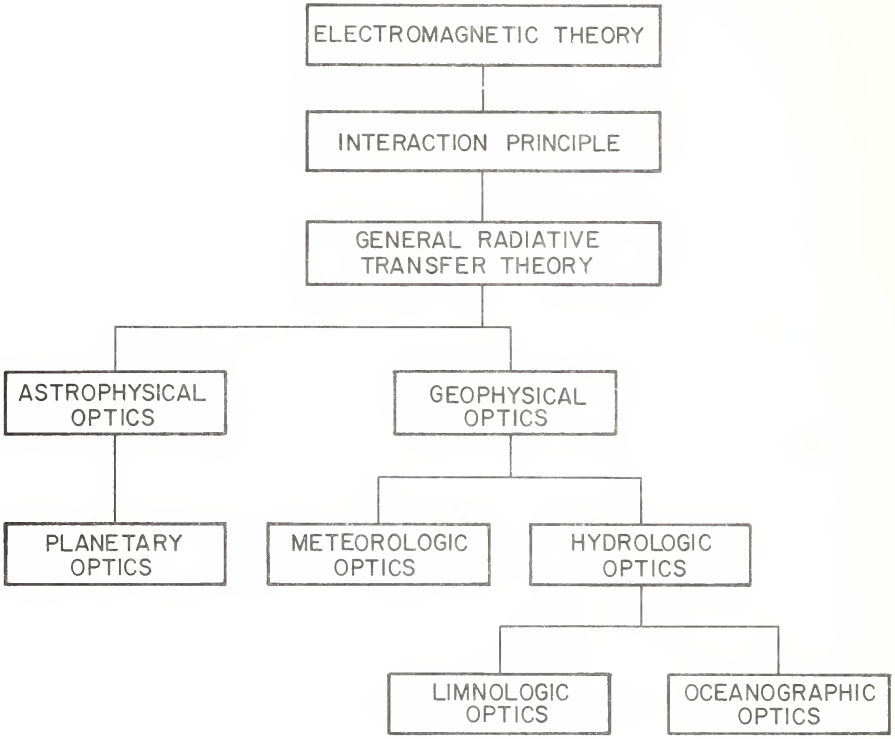

FIG. 1.1 Hydrologic optics as a logical descendant of radiative transfer theory and electromagnetic theory.

The Problems of Hydrologic Optics

The theoretical and empirical studies comprising hydrologic optics arise in the attempts to answer several diverse types of questions such as the following. How much radiant energy of a given wavelength is reflected from a sea or lake surface, and how much penetrates this surface and reaches each depth of the sea or lake? How does the amount transmitted depend on the surface winds and other factors affecting the physical, geometric, and dynamic state of the moving surface? Does the light penetrate the body of the ocean or lake in some general and predictable manner as regards depth dependence and directional dependence of the light distribution? If so, what are the pertinent physical measurements that must be made to facilitate such predictions? What effects on the light field are engendered by the proximity of the shores, bottoms and other boundaries of the hydrosols? What are the pertinent optical properties of natural hydrosols by which oceanographers and limnologists can characterize these waters? How may these scientists usefully employ these concepts in the pursuit of their special interests such as marine biology, geology, and hydrodynamics? How far can a

diver or submariner expect to see a given submerged object as he maneuvers in the submarine world of blue-green lights and shadows? How far can one expect to communicate underwater by means of given types of light sources such as lasers, point sources, etc.? Of what significance is the polarized light field to the denizens of the deep and to enterprising humans interested in navigating through the submarine world by unconventional means? These summarize some of the basic types of questions with which hydrologic optics is concerned. The questions have many variations and their resolutions are often of great difficulty,so that the theory of radiative transfer which underlies hydrologic optics is often taxed to its limits in the attempts to provide quantitative or even qualitative answers. As the discussion proceeds, we shall make clear the present status of the solutions to the general problems listed above.

The Aims and Desired Goals of This Work

In this work we shall be concerned with the systematic development of the basic physical principles and mathematical procedures of radiative transfer theory which have been found effective in solving the general types of problems cited above. The reason for selecting the domain of hydrologic optics for specific study rather than meteorologic optics or any other branch of general radiative transfer rests simply in the fact that it is in this domain that most of the practical experience of the author lies.

It should be emphasized at the outset that our primary concern is with the *principles* of hydrologic optics rather than the detailed numerical and experimental aspects of the state of the art of the discipline. These latter procedures, as important as they are in the various stages of securing our knowledge, both theoretical and empirical, are in the last analysis meaningful and efficacious only if they are based on sound physical principles and mathematical techniques. Repeated direct experiences of the author in pursuing complete or partial solutions of problems of the types listed above, have demonstrated the importance of having a well-grounded knowledge of the principles of radiometry and radiative transfer theory during the search for the solutions. It would seem to follow that anyone faced with similar problems and armed with a comparable battery of principles and laws of the subject will also eventually find his way to his own desired experimental or theoretical goals. This, then, leads to the primary aim of the present work: *to give a systematic development of the fundamental principles and procedures of radiative transfer theory which may be employed by students of the subject in the pursuit of solutions of their particular theoretical and experimental problems of geophysical optics, and especially hydrologic optics.* It has also been the experience of the author that both the theoretical and experimental practitioners of the arts of radiometry and radiative transfer are singularly independent individuals, each in his own way, and in view of this it would be somewhat futile to preoccupy the potential student and researcher with

anything but the most pertinent and general principles and procedures. This observation is cited to reinforce our aim enunciated above.

The Plan and Scope of This Work

It is in the nature of the theory of hydrologic optics that the full founding and delineation of its basic principles is tantamount to a full founding and delineation of the basic principles of radiative transfer theory itself. This fact rests on the observation that the physical-geometric problem of completely describing the structure of the scattered light field in a sea or lake is just as complex a task as that of describing the light field in the atmosphere, or for that matter in any real medium that emits or scatters light. This realization dawned very early in the author's studies of oceanographic and limnologic optics and in his theoretical excursions into the problems of meteorologic optics. It was eventually realized that the appropriate direction of study was not a problem-by-problem horizontal advance through the everyday jungle of examples, cases, and counterexamples, but rather the direction required a sharp vertical tack, straight up into the heights of abstraction, from whence one could most economically view the radiometric scenes spread out below from horizon to horizon. This attempt to escape into the thin air of general constructs and guiding principles was made as often as the exigencies of daily problems and consultations would allow, and eventually as reports and papers accumulated, there emerged a pattern of principles and procedures which could be seen to apply to all the special principles and special procedures accumulated to that time. Interestingly, it was found that the abstract principles could be phrased and assembled using very meager amounts of advanced mathematical machinery. This, coupled with the author's classroom experience that the basic constructs of radiative transfer, namely *radiant flux, scattering, absorption, volume, area,* and *length* are all readily visualizable, resulted in a theoretical framework which was readily understood and applied once a small number of academic prerequisites had been dispatched, namely the equivalent of a one year course in advanced calculus, which includes vector analysis, and first and second order ordinary differential equations.

For all these reasons it was decided in the planning stages of this work that its scope be widened to embrace, whenever possible, the completely general principles of radiative transfer theory, and to attempt a systematic development of the subject by starting from a single fundamental principle, namely that which eventually came to be called the *interaction principle* (Sec. 3.2). For, it would be inefficient and unesthetic to base a science on many seemingly unrelated principles when it is possible to employ merely one. Accordingly, in Chapter 3, after a thorough grounding in geometrical radiometry, the reader is lead through a methodical construction program of general radiative transfer theory. The elaboration of the details of this task will occupy most

of the remainder of the work, with several important chapters, included as integral parts of the main discussion, which are devoted to the richer theoretical details made possible by adopting the plane-parallel settings indigenous to hydrologic optics.

It was found possible to adopt the preceding form of development of radiative transfer theory provided some care was taken at the outset to equalize the backgrounds and intuitions of potential students of the subject. It is to such students and to the general reader that we devote this chapter. In the following sections we shall acquaint these readers with the general outlines of hydrologic optics by supplying representative radiometric examples of natural light fields and typical magnitudes of optical properties encountered in natural hydrosols. We shall also present three of the simplest models of light fields which are capable of describing a very wide number of situations encountered in practical hydrologic optics. We shall in addition illustrate the use of these models by means of explicit deductions and calculations. We shall also present graphs and tables based on these models which have been found useful in practice. Then with these introductory developments completed, we shall feel free to start from scratch in Chapter 2 and proceed rigorously with the systematic construction of the modern theory of

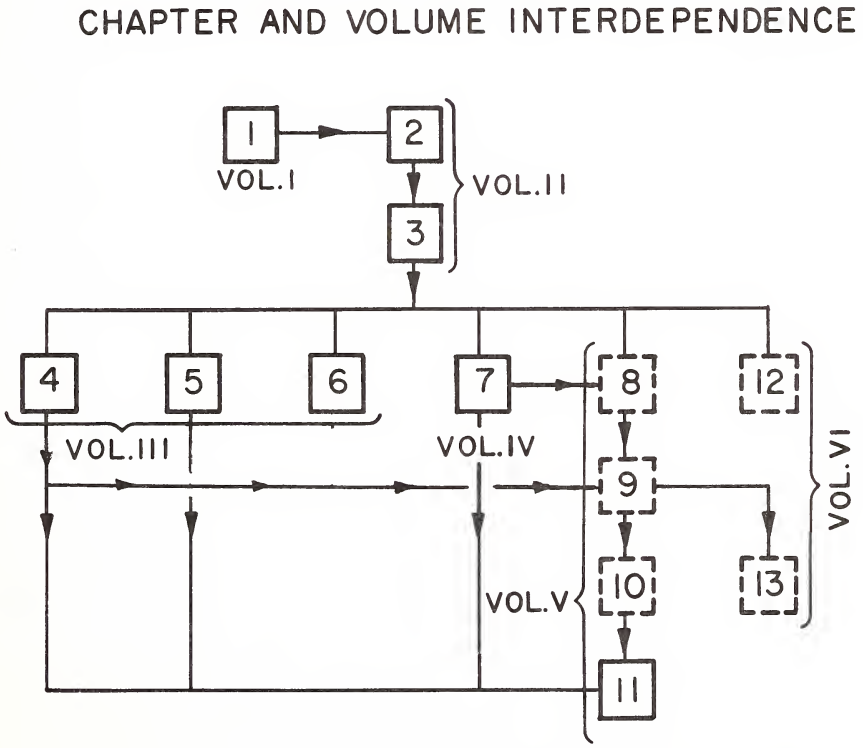

FIG. 1.2 Interdependence of the chapters of this work.

radiative transfer. The results will embody powerful extensions which appear to be capable of solving--in principle and in practice--every known current problem of applied radiative transfer theory in the domains of the air and the sea.

As an aid in studying the present work Fig. 1.2 indicates the *logical interdependence* of the various volumes and chapters. Actually every chapter is connected in some way with every other; however, some connections are stronger than others, and these are shown in the diagram. Thus the prerequisite most essential to understanding a given chapter is the chapter (or chapters) which stand immediately above it via the horizontal and vertical lines in the diagram. For example Chapter 11 depends directly on 4,5, 7 and 10, while 6 depends directly only on 3. Furthermore, the chapters whose contexts are developed on the level of general radiative transfer theory (Fig. 1.1) are outlined in heavy boxes; those that are more directly concerned specifically with hydrologic optics (or the theory of stratified plane parallel media) are outlined in the dashed boxes.

1.1 A Primer of Geometrical Radiometry and Photometry

After the solar radiant energy incident on the upper levels of the atmosphere has rapidly percolated down through the atmosphere and redistributed itself via scattering processes throughout the lower reaches and in the upper layers of the seas and lakes, its flow within these media assumes an intricate, and relatively steady geometric pattern. A particularly useful mode of representation of this flow of scattered radiant energy is possible by means of the concepts of geometrical radiometry, whose definitions and interrelations we shall now briefly study. A relatively complete and detailed study of geometrical radiometry and photometric concepts is reserved for Chapter 2.

The Nature of Radiant Flux

The radiant energy streaming in from the sun is understood to be electromagnetic energy. The atomic radiative processes of the sun generate a wide range of frequencies (or wavelengths) of electromagnetic energy, only a small part of which is visible to the human eye, or detectable by human skin, or usable by the plants and animals of the earth. The part of the electromagnetic spectrum visible to normal human eyes lies essentially in the range from 400 to 700 millimicrons wavelength, the 400 mμ light being deep blue-violet, the 700 mμ light being deep red, with all the colors of the rainbow ranging continuously between these extremes. The wavelength of electromagnetic energy evoking the greatest sensation of brightness is the yellow-green at 555 mμ under normal daylight conditions. If radiant energy of wavelengths much less than 400 or much greater than 700 mμ fall on normal retinas, there is relatively no conscious awareness of such an event by the associated brain, though--in some extraordinary cases, some ultra violet (380 mμ) and some infra red (780 mμ)

phenomena are still within the range of detectability by the human visual organs. By and large, however, the human visual sensor system effectively samples and reacts to only the minute portion of the whole outpouring of radiant energy by the sun between 400 and 700 mμ--much in the way that a taut wire of given length and diameter resonates most sharply to a single acoustic frequency and less sharply to the frequencies in a small interval surrounding the central frequency, outside of which the wire is essentially insensitive to the vibrations. Figure 1.3 depicts the place of the visible portion of the spectrum within the electromagnetic spectrum, along with schematic diagrams of those portions of which we are aware by means of various devices used to detect and measure radiant energy. (Current manufacturer's catalogs should be consulted for precise details of individual devices.) Any observable part of the electromagnetic spectrum, observable not only as visible light but also by suitable technical means, falls under the aegis of geometrical radiometry.

The central construct of geometrical radiometry is *radiant flux* which we define generally as the time rate of flow of radiant energy of given wavelength (or frequency) across a given surface. (It has dimensions of (radiant) energy per unit time per unit frequency.) Thus radiant flux is a time density* of radiant energy. For our present purposes and in the exposition of radiative transfer theory, we may imagine the flow of radiant energy to be in the form of mutually non-interfering swarms of tiny colored particles--which we call *photons*. While this may not correspond in all aspects to physical reality, it nevertheless is a helpful construct in practical work. Each photon contains a well defined amount $h\nu$--a *quantum*--of radiant energy associated with its color, or frequency ν. This means of picturing radiant energy *for the purposes of geometrical radiometry* is quite useful and correct within the modern framework of physics. It will make the exposition of the notions of geometrical radiometry a relatively simple task, and the visualizations of the various concepts an almost trivial matter. In the terminology of electromagnetic theory, we shall work with electromagnetic fields produced by mutually incoherent sources and which are studied on a macroscopic level, i.e., where the dimensions of the detectors are very large compared to the observed wavelengths.

The Unpolarized-Flux Convention

The radiant flux always will be assumed unpolarized, unless specifically noted otherwise. This will result in simplified working formulas of relatively great practical value and of adequate accuracy in the pursuit of most applications of hydrologic optics. Whenever it is necessary to indicate how the theory may be elevated to the polarized level,

---

* Because most of our discussions center on an arbitrary frequency (or wavelength) of radiant flux, the reference to the "per unit frequency" part of the dimension of radiant flux will be omitted, unless specifically noted otherwise.

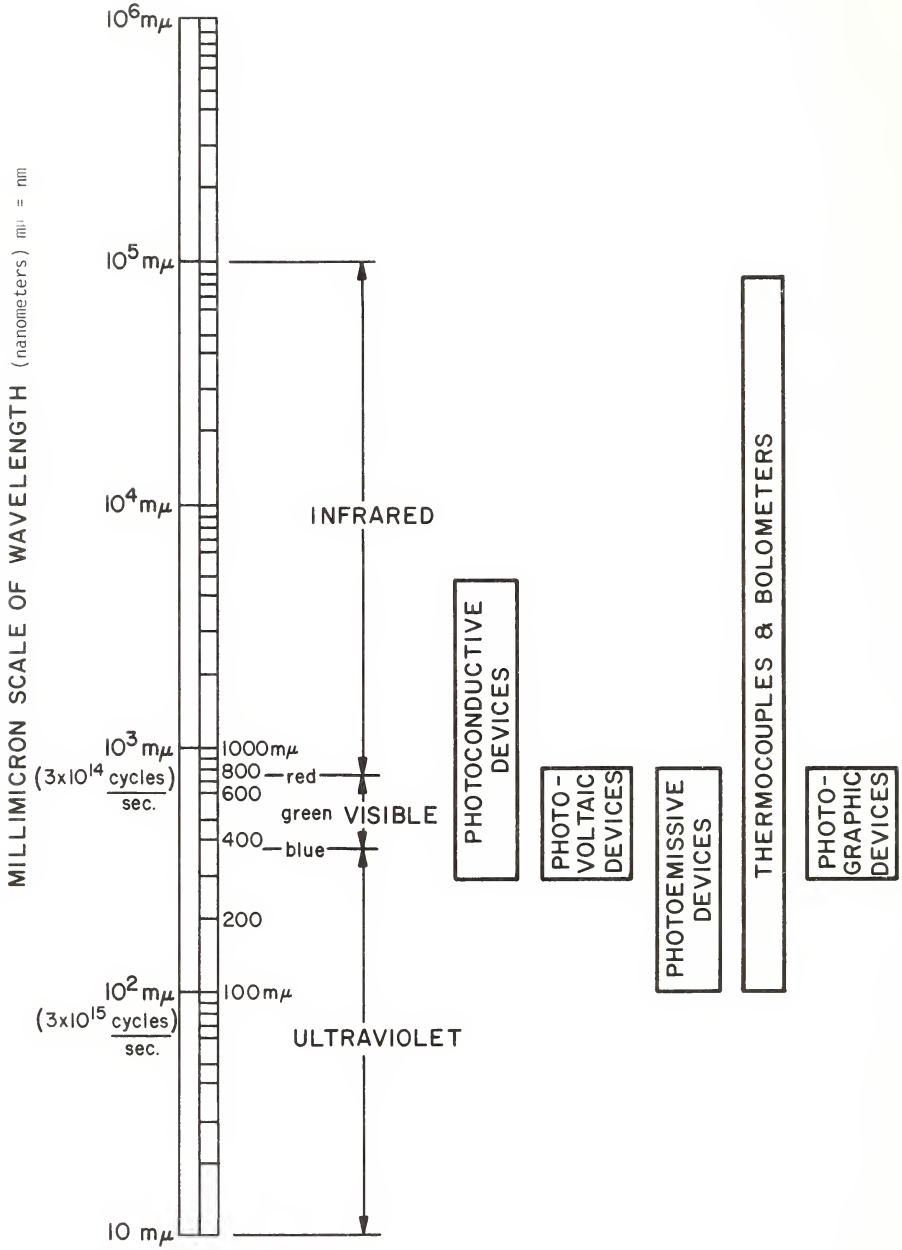

FIG. 1.3 The electromagnetic spectrum and the ranges of some typical radiant energy detector domains.

notes will be made to that effect. The general theory of polarized radiative transfer is outlined in Sec. 114 of Ref. [251], and the problem of the relative consistency of the polarized and unpolarized theories is examined in Sec. 13.11, below.

Geometrical Channeling of Radiant Flux

Once the nature of radiant flux is clarified, as above, the descriptions of the remaining concepts, theorems and procedures of geometrical radiometry are essentially geometric in nature. There are only two distinct, ideal modes of describing a flow of particles past a point in three dimensional space, and these are shown in Fig. 1.4. In part (a) of the figure a parallel flow of photons is described in terms of the passage of particles through a small region S on a plane normal to the flow around a point p on the plane. A complementary mode of the flow is in terms of the passage of particles through a small set D of directions around a given direction ξ and through the point p. Considering these two modes in a given flow of photons, let P(S) and P(Ω) be the radiant fluxes in each of these cases, with A(S) the area of S and Ω(D) the solid angle content of the bundle D of directions. Further, let the central direction ξ of the bundle D be normal to S at p. Then we write:

"P(S)/A(S)" for the area density of radiant flux

"P(D)/Ω(D)" for the solid angle density of radiant flux

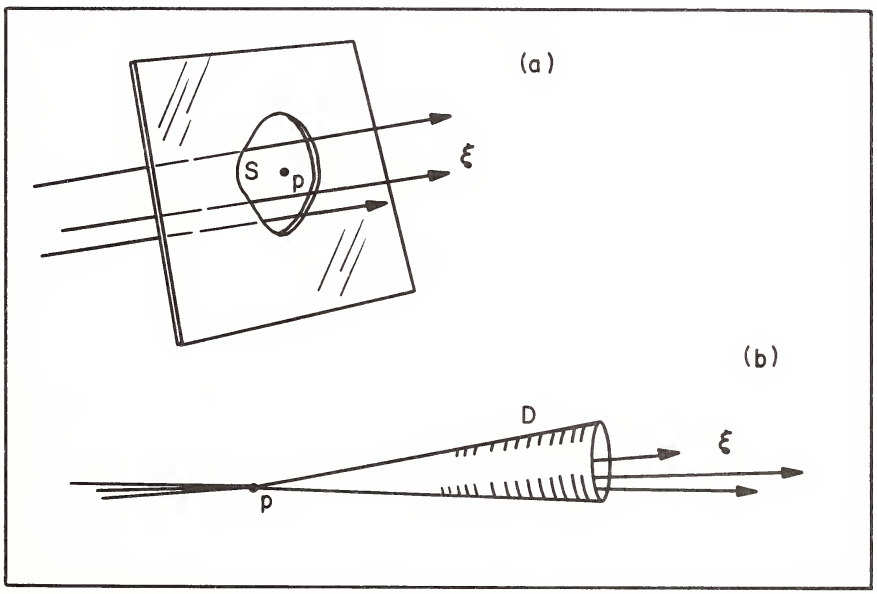

FIG. 1.4 Two geometric modes of describing radiant flux.

It is convenient in geometrical radiometry to call P(S)/A(S) simply a (radiant) *flux density* and P(D)/Ω(D) a (radiant) *intensity*.

These are the two basic modes of conceptually channeling the flow of photons in space or matter. There is an important third mode which is the result of the direct union of these two modes. If we reconsider the setting of Fig. 1.4 and imagine a narrow bundle of directions D around a central direction ξ normal to S *at each point* p of S, then there would be an associated flow P(S,D) of radiant energy across the combined set S x D of the surface set S and the direction set D. We write:

"P(S,D)/A(S)Ω(D)" for the *phase density* of radiant flux

The term "phase density" is simply a convenient descriptive term for the combined areal and directional densities, and it can be related to the phase space concept of classical statistical mechanics, though there is no need to do so here. The conventional term for phase density of radiant flux, the one we adopt for use in this work is *radiance*; it is radiance which is used to describe the monochromatic brightness of radiant flux.

Operational Definitions of the Densities

An operational definition of radiance and its companion densities is effected by means of a radiant flux meter, depicted schematically in (a) of Fig. 1.5. A radiant flux meter forms the heart of the radiance meter, as shown in (b) of Fig. 1.5, and may embody any one of several means of measurement of radiant flux, such as photoconductive, photoemissive, or photovoltaic devices (see Sec. 2.1). Before the radiant flux reaches the collecting surface S of the radiance meter, it is filtered to the desired wavelength and is also confined to flow onto S about point x through a narrow circular conical bundle D of directions whose central direction ξ is normal to S. A good radiance meter will have D so that Ω(D) is as small as practicable. A magnitude of $\Omega(D) \leq 1/30$ steradians serves well for most geophysical optics tasks. If the reading of the radiant flux meter is P(S,D) when it is located at x and oriented by ξ (see Fig. 1.5), then the associated radiance is P(S,D)/A(S)Ω(D), which we can denote by "N(x,ξ)". Here "x" denotes where the flow is, and "ξ" denotes its direction. The associated radiant intensity is P(S,D)/Ω(D) and the radiant flux density is P(S,D)/A(S). These operational definitions reduce to a practical level the ideal situations pictured in Fig. 1.4. They are ideal because in (a) of Fig. 1.4 the flow was assumed to be along a single direction and in (b) the flow was assumed to be through a single point. The operational definitions give workable approximations to these ideals and form the basis for a rigorous transition to the ideal limit, which will be made in Chapter 2.

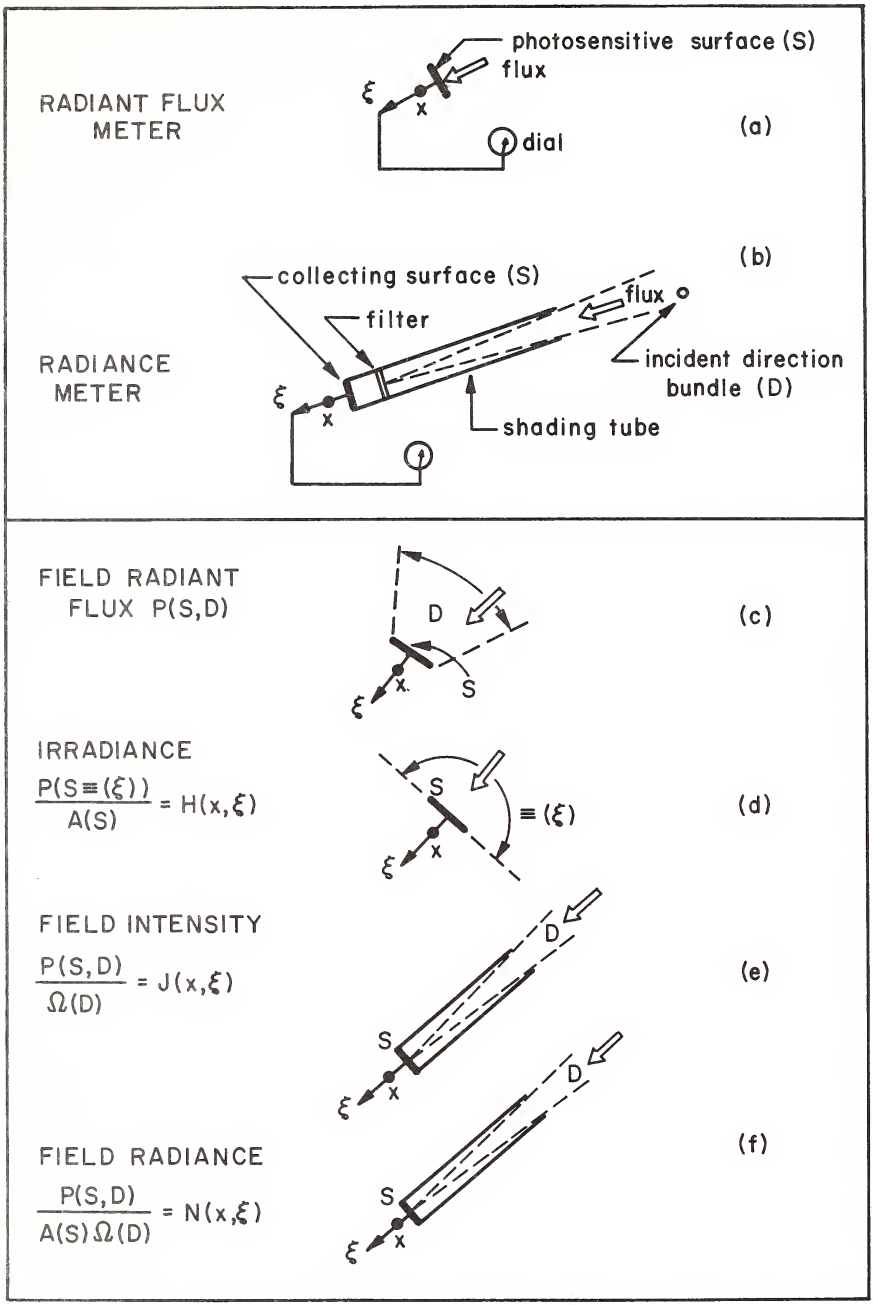

FIG. 1.5 Operational definitions of the radiometric concepts.

Field and Surface Interpretations of Radiant Flux and its Densities

In Fig. 1.4 one important fact about the radiant flux was omitted, namely its *sense* of flow. In practice we often find it useful to distinguish between the flow of radiant energy *onto* a surface S and *from* the surface S. When we do so, the three central densities introduced above each have either one of the two possible interpretations, according as the radiant flux comprising the density is viewed as flowing onto or from a surface. When radiant flux comes from the radiometric field and falls onto the collecting surface S of the radiance meter we call the associated radiance the *field radiance*. When the radiant flux is seen to leave a surface (either real or imaginary) for the surrounding radiometric field we use the term *surface radiance*. Similarly for radiant flux density: when radiant flux falls onto a surface we speak of the radiant flux density as the *irradiance* of the flux at a point, and when the radiant flux density leaves S, we speak of the *radiant emittance* of the radiant flux at a point. Similarly also for (radiant) intensity: we have *surface* (radiant) *intensity* and *field* (radiant) *intensity*. The parenthesized "radiant" indicates that this adjective can be omitted when *radiant* flux is understood to be the flux of interest.

Operational Definitions of Field and Surface Quantities

We may summarize the preceding definitions in parts (c)-(f) of Fig. 1.5. These diagrams emphasize the operational procedures used to measure the various quantities in actual radiometric environments.

Thus field radiant flux can be defined over the surface S of the radiant flux meter for an incoming bundle D of directions. The heavy arrows give the general sense of the flow. When the meter is oriented so that at point x the inward unit normal to its collecting surface is ξ, and D is opened up to be the hemisphere $\Xi(\xi)$ of all directions ξ' such that $\xi\cdot\xi' = \cos\theta \geq 0$ then by definition we measure the irradiance at x for the orientation ξ of the collector. The field (radiant) intensity $J(x,\xi)$ and the field radiance $N(x,\xi)$ are defined analogously. It is important to emphasize that the $\Omega(D)$ in the latter two cases should be on the order of 1/30 of a steradian or smaller for best results. The 'surface' counterparts to the preceding 'field' quantities may be pictured by reversing the flux arrows in parts (c) to (f) of Fig. 1.5.

Figure 1.6 shows the details of how a surface radiance may generally be assigned to a real or imaginary surface. We use the radiance invariance law (Sec. 2.6) to assign to the direction ξ at point p on S the radiance $N(x,\xi)$ when p is viewed by a radiance meter oriented as shown. This is a consistent assignation since the radiance-invariance law states that for a fixed ξ, $N(x,\xi)$ is independent of y along a

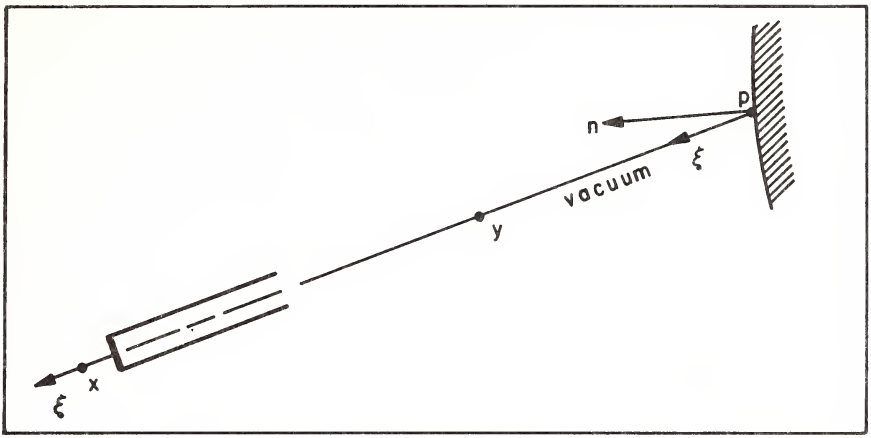

FIG. 1.6 The method of assigning radiances to real or imaginary surfaces.

vacuous path between x and p. In this way each ξ at p in the outward hemisphere $\Xi(\mathbf{n})$ of directions at p can be assigned a radiance.

A useful property of irradiance is the *cosine law*, which follows directly from the present operational considerations. Fig. 1.7 shows a thin collimated steady stream of photons incident normally on a small hypothetical plane surface S. If P(S,D) is the radiant flux produced on S by this stream, then this same flow P(S',D) exists across the surface S' whose unit normal is tilted θ' from the direction of the stream. The connection between the two irradiated areas is:

$$A(S') \cos \theta' = A(S)$$

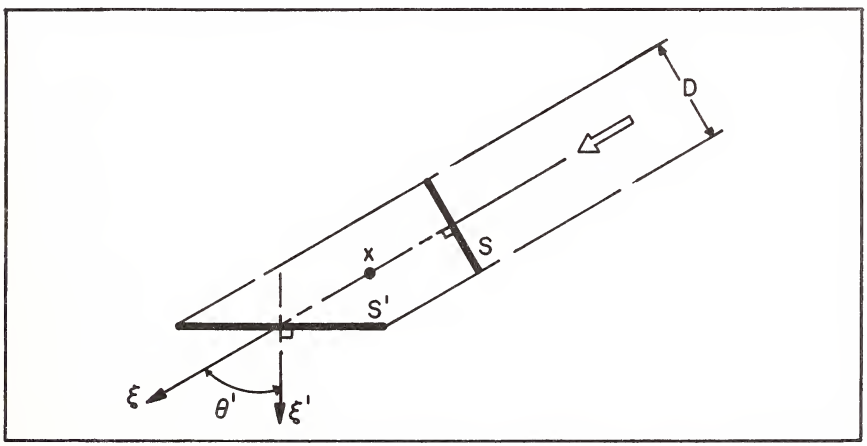

FIG. 1.7 Deriving the cosine law for irradiance.

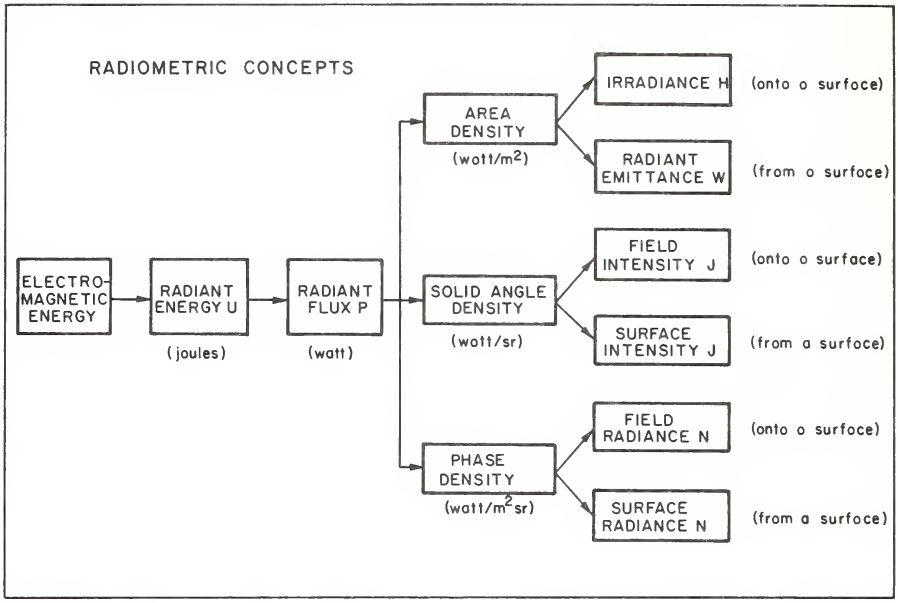

FIG. 1.8 Logical lineage of the radiometric concepts.

Hence the connection between the *irradiances* on S' and S produced by the stream is:

$$H(x,\xi') = \frac{P(S',D)}{A(S')} = \frac{P(S,D)}{A(S)} \cos\theta' = H(x,\xi)\cos\theta'$$

That is,

$$H(x,\xi') = H(x,\xi)\cos\theta'$$

which is a form of the cosine law for irradiance (the general law is given in Sec. 2.8). The companion law to this for the radiant emittance of S' is:

$$W(x,\xi') = W(x,\xi)\cos\theta'$$

Summary of Concepts and Some Principal Formulas of Geometrical Radiometry

A schematic diagram of radiometric concepts, developed in the manner described above, which summarizes the geometric derivatives of radiant energy, along with their mks units, and current standard symbols, is given in Fig. 1.8. The names of the six concepts above, and their designating symbols may come and go with the years, but the logical lineage

of the concepts depicted above, with their tap root in the concept of radiant energy and indicated branching structures, will withstand the rigors of time. For while the names in the boxes are transient conventions, the arrangement of the boxes, and the underlying concepts for which the boxes stand are simply manifestations of the way we naturally view radiant energy and the flow of radiant energy in space and time. In this sense the indicated conceptual scheme in Fig. 1.8 is immutable. The full developments of the analytical connections among the radiometric concepts are not needed in this introductory chapter, and are reserved for Chapter 2. However, a brief survey of some of the main formulas of geometrical radiometry is given here for convenient reference during the remainder of this chapter's discussions.

The primary concept of geometrical radiometry in practice is the phase density concept, namely radiance. We find it possible to describe all other concepts in terms of this density. Thus for example in the case of the flux density concept:

$$H(x,\xi) = \int_{\Xi(\xi)} N(x,\xi')\xi'\cdot\xi \, d\Omega(\xi') \quad \text{(with field radiance)} \tag{1}$$

$$W(x,\xi) = \int_{\Xi(-\xi)} N(x,\xi')\xi'\cdot\xi \, d\Omega(\xi') \quad \text{(with surface radiance)} \tag{2}$$

$H(x,\xi)$ is the irradiance at x on a surface whose inward normal is the direction ξ. The basis for (1), (2) rests in the cosine law for irradiance and the possibility of the linear superposition of radiant fluxes. The symbol "$\Xi(\xi)$" stands for the hemisphere of all directions ξ' such that $\xi'\cdot\xi > 0$, (hence $\Xi(-\xi)$ is the hemisphere of all directions ξ' such that $\xi'\cdot(-\xi) > 0$, i.e., $\xi'\cdot\xi < 0$). Here "$d\Omega(\xi')$" is short for "$\sin\theta' \, d\theta' \, d\phi'$", where (θ',ϕ') define ξ' in some reference frame. Of course $\xi'\cdot\xi$ is the scalar or dot product of the directions ξ' and ξ. The representations of the solid angle density in terms of radiance are not needed at present and may be found, along with many related concepts, in Sec. 2.9. We shall also find it convenient to introduce at this time two cousins of the flux density concept, namely *scalar* and *vector* irradiance, defined, respectively, by writing:

$$\text{"h(x)"} \quad \text{for} \quad \int_{\Xi} N(x,\xi') \, d\Omega(\xi') \quad (\text{watt/m}^2) \tag{3}$$

and:

$$\text{"H(x)"} \quad \text{for} \quad \int_{\Xi} N(x,\xi')\xi' \, d\Omega(\xi') \quad (\text{watt/m}^2) \tag{4}$$

Here Ξ is the set of all unit vectors (directions) in euclidean three space. The scalar irradiance h(x) is the total radiant flux per square meter coursing through point x in all directions. It is related to radiant energy per cubic meter

$u(x)$ (the *radiant density*: Joules/m^3) by means of the formula:

$$v(x)\ u(x) = h(x) \tag{5}$$

where $v(x)$ is the speed of light at x (in m/sec). The quantity $\mathbf{H}(x)$ is a vector; the indicated equation is really three equations: one for each of the x, y, z components of $\mathbf{H}(x)$, as given by the corresponding components of $\boldsymbol{\xi}'$. The vector $\mathbf{H}(x)$ also has units of watts per square meter: its magnitude is the maximum net irradiance attainable as one samples all possible directions ξ of flow about x. The direction of $\mathbf{H}(x)$ defines this direction of maximum net irradiance. The *net irradiance* $\bar{H}(x,\xi)$ at x in the direction ξ is defined as $H(x,\xi)-H(x,-\xi)$; see Sec. 2.8 for complete details.

It will be necessary in this introductory chapter to also consider *hemispherical scalar irradiance*, defined by writing:

$$\text{"}h(x,\xi)\text{"} \quad \text{for} \quad \int_{\Xi(\xi)} N(x,\xi')\, d\Omega(\xi') \quad (\text{watt/m}^2) \tag{6}$$

$$\text{"}h(x,-\xi)\text{"} \quad \text{for} \quad \int_{\Xi(-\xi)} N(x,\xi')\, d\Omega(\xi') \quad (\text{watt/m}^2) \tag{7}$$

where, by (3),

$$h(x) = h(x,\xi) + h(x,-\xi) \tag{8}$$

for every ξ in Ξ. A convenient terrestrial reference frame in hydrologic optics is that depicted in Fig. 1.9. We will often use the special case of (6), (7) where $\xi = \mathbf{k}$, and we shall write

$$\text{"}h(z,\pm)\text{"} \quad \text{for} \quad h(p,\pm\mathbf{k}) \tag{9}$$

where we retain only the depth variable z of the usual (x,y,z)-coordinates of the point p. Corresponding to $h(z,\pm)$ we have the companions from (1) in which $\xi = \pm\mathbf{k}$; we write

$$\text{"}H(z,\pm)\text{"} \quad \text{for} \quad H(p,\pm\mathbf{k}) \tag{10}$$

Irradiances associated with plus signs are *upwelling* (or upward) irradiances; those with minus signs are *downwelling* (or downward) irradiances. All these irradiances have units of watt/m^2. In natural hydrosols $H(z,\pm)$ can be measured by horizontal flat plate collectors, while $h(z,\pm)$ can be measured by spherical collectors, suitably shielded (see Sec. 2.7). Some useful special cases of the preceding formulas are the following.

Let $N(x,\xi)$ be uniform, i.e., independent of ξ at some x and of magnitude N; then by (1)

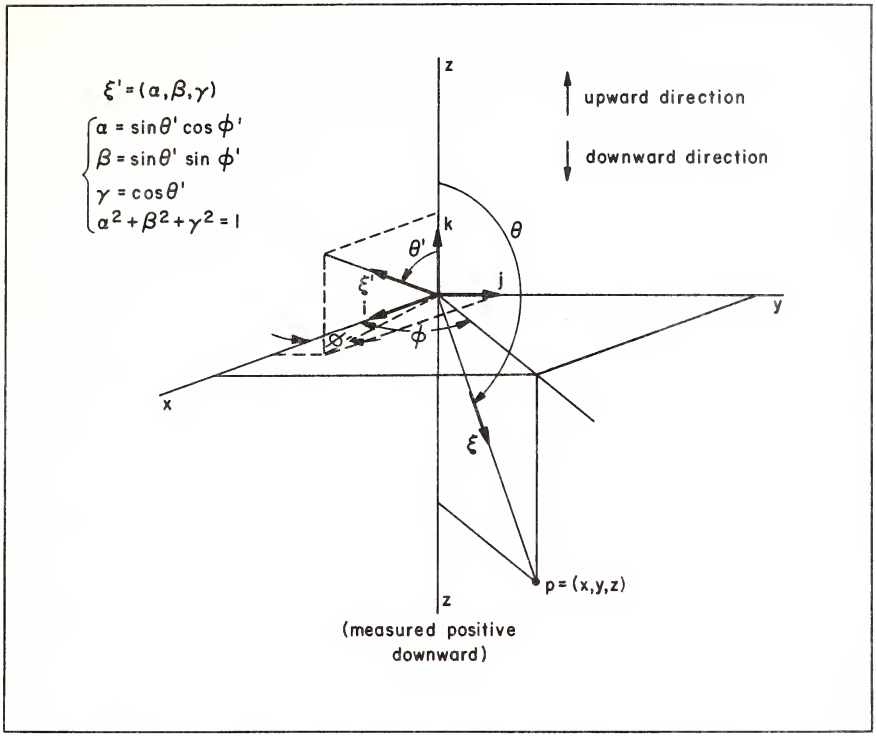

FIG. 1.9 The standard terrestrially-based coordinate system in hydrologic optics.

$$H(x,\xi) = N\int_{\Xi(\xi)} \xi'\cdot\xi \, d\Omega(\xi') = N\int_{\phi'=0}^{2\pi}\int_{\theta'=0}^{\pi/2} \cos\theta' \sin\theta' \, d\theta' d\phi'$$

$$= \pi N \tag{11}$$

which holds for all ξ at x. The computation was made with the **k** axis momentarily shifted parallel to ξ. Further, from (2), in the same way:

$$W(x,\xi) = \pi N \tag{12}$$

for all ξ at x. Next, by (3):

$$h(x) = N\int_{\Xi} d\Omega(\xi') = N\int_{\phi'=0}^{2\pi}\int_{\theta'=0}^{\pi} \sin\theta' \, d\theta' d\phi' = 4\pi N \tag{13}$$

By (4)

$$\mathbf{H}(x) = N\int_{\Xi} \xi' \, d\Omega(\xi') = 0 \tag{14}$$

By (6)

$$h(x,\xi) = 2\pi N \tag{15}$$

Observe the effect of the cosine in the integrand: for a uniform radiance distribution at x, $h(x,\xi)=2H(x,\xi)$, for every ξ. Further examples are given in Sec. 2.11.

n^2-Law for Radiance

We mention in passing an important law of geometrical radiometry concerning radiance: *If $\mathcal{P}$ is an arbitrary photon path through a transparent optical medium within which the index of refraction* n *varies continuously with location, then photon flux along the path $\mathcal{P}$ having radiance* N *moves such that* N/n^2 *is invariant along the path* (cf. Sec. 2.6). This is the n^2-law for radiance.

The Bridge to Geometrical Photometry

The conceptual bridge from geometrical radiometry to geometrical photometry is built on the empirical fact that not all wavelengths of radiant flux invoke the same sensation of brightness in the human eye. The green-yellow wavelength 555 mμ is the brightest. In fact one would require, e.g., about 2 watts of blue-green light of 510 mμ or 2 watts of orange light of 610 mμ to produce the same sensation of brightness as one watt of green-yellow light of 555 mμ. The *photopic luminosity* curve depicted in Fig. 1.10 summarizes a quantitative measure $\bar{y}(\lambda)$ of the brightness-sensation producing capabilities of a wavelength λ in the electromagnetic spectrum. Observe that for wavelengths λ below 400 mμ and above 700 mμ, electromagnetic radiation no longer is seen by normal human eyes. A fuller discussion of this curve is given in Sec. 2.12. See also Sec. 1.8.

The conversion rule from a radiometric concept to its photometric counterpart is based on the photopic luminosity curve and is given as follows:

Let $\mathcal{Q}$ be any radiometric concept (e.g., U, P, H, W, J, *or* N*) which is defined over the electromagnetic spectrum. Then the photometric concept $\mathcal{L}$ (namely* Q, F, E, L, I, *or* B, *respectively) associated with $\mathcal{Q}$ is given by*

$$\mathcal{L} = 680\int_0^{\infty} \mathcal{Q}(\lambda)\ \bar{y}(\lambda)\ d\lambda$$

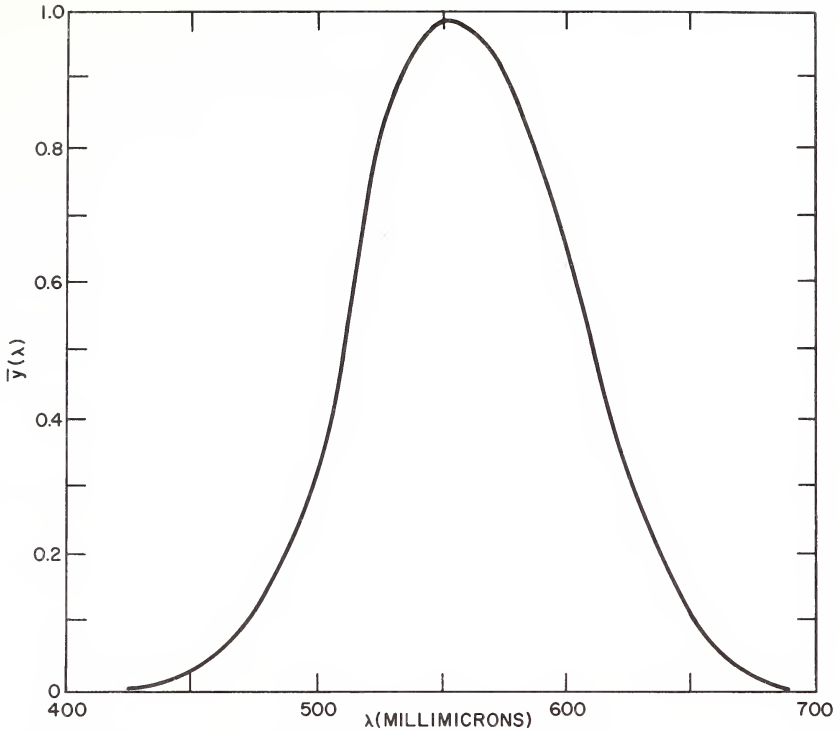

FIG. 1.10 The photopic luminosity function.

If $\mathscr{R}$ has units *watt*/(*), then $\mathscr{L}$ has units *lumen*/(*), where "(*)" stands for (meter) or (steradian) or various permissible combinations of these geometrical units. For example,

$$B(x,\xi) = 680\int_0^\infty N(x,\xi,\lambda)\ \bar{y}(\lambda)\ d\lambda \quad , \text{ lumens/m}^2\ \text{sr}$$

This gives the *luminance* (loosely, the "brightness") produced by a given sample of radiance. This is what, in essence, we can see as a result of the radiant flux of photons at x in the direction ξ. Again, for example, *illuminance* is:

$$E(x,\xi) = 680\int_0^\infty H(x,\xi,\lambda)\ \bar{y}(\lambda)\ d\lambda \quad , \text{ lumens/m}^2$$

The logical interrelations among the photometric concepts precisely parallel those of radiometry. Thus, starting with *luminous energy* Q, which, according to the rule above, we define as:

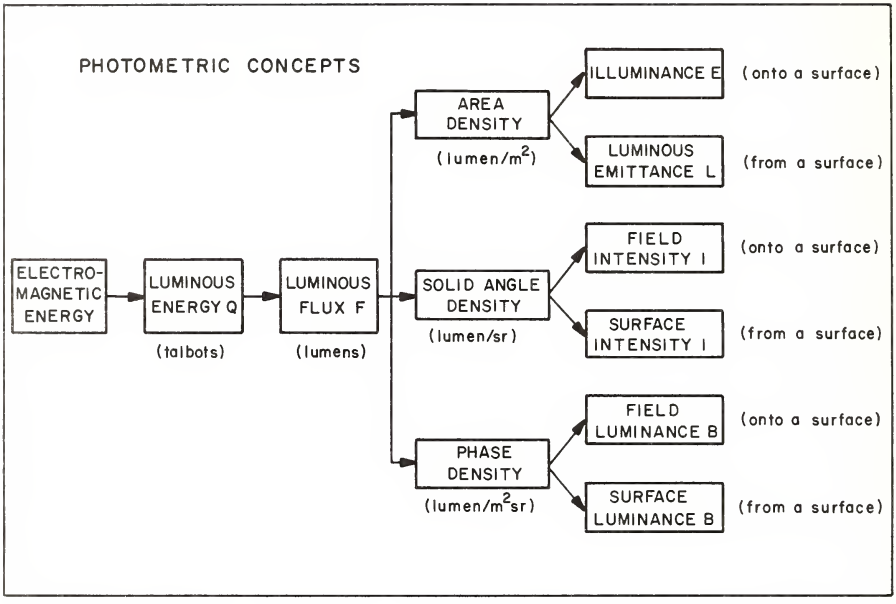

FIG. 1.11 Logical lineage of the photometric concepts.

$$Q = 680\int_0^\infty U(\lambda)\ \bar{y}(\lambda)\ d\lambda \quad ,$$

we then can construct a diagram similar to that in Fig. 1.8. This is shown in Fig. 1.11. Consequently, everything we can say about the *geometrical* properties of the radiometric concepts, we can also say about the corresponding properties of photometric concepts.

We mention in passing some classical alternate sets of photometric units:

$$1 \text{ foot candle} = 1 \text{ lumen/ft}^2 \quad \text{(area density of flux)} \tag{16}$$

$$1 \text{ candela} = 1 \text{ lumen/sr} \quad \text{(solid angle density of flux)} \tag{17}$$

$$\left.\begin{aligned} &1 \text{ (centimeter) lambert} = \tfrac{1}{\pi} \text{ lumen/cm}^2 \text{ sr} \\ &1 \text{ (meter) lambert} = \tfrac{1}{\pi} \text{ lumen/m}^2 \text{ sr} \\ &1 \text{ (foot) lambert} = \tfrac{1}{\pi} \text{ lumen/ft}^2 \text{ sr} \end{aligned}\right\} \text{(phase density of flux)} \tag{18}$$

From (17) we can compactly express luminance generally in terms of candelas/m^2 when using the mks system (the preferred system). The lambert unit arises as follows: let a surface, which has both unit reflectance with respect to irradiance for each wavelength and also a directionally uniform reflected radiance for each wavelength, be called *a perfectly diffusing* surface, for short. *By definition,* a perfectly diffusing surface irradiated by one lumen has a luminance of *one lambert.* (Use Eq. (12).) However, the conversion rules above in (18) are by convention now used under arbitrary directional and reflectance conditions.

Thus we have the general rule: *To convert* $B(x,\xi)$ *lumens/m^2sr to meter lamberts, multiply* $B(x,\xi)$ *by* π. (This follows from the fact that as defined above the meter lambert is about 1/3 of a lumen/m^2sr; so it takes about 3 meter lamberts to every lumen/m^2sr to describe the same scene.)

With due respect to the historical origins of the preceding terms, it is felt that the continued employment of "foot candle" and "lamberts" will serve no logical purpose. Their mention here simply serves to keep open the passageway to the classical literature of photometry and radiative transfer theory to which we must refer now and then during this work. New students are advised to use the lumen, meter, steradian system of units in photometry, along with the watt, meter, steradian system in radiometry in their future studies. A convenient abbreviated mks unit of radiance is the (unrationalized)* herschel:

$$1 \text{ herschel} = 1 \text{ watt/m}^2\text{sr} \tag{19}$$

and an mks unit of luminance is the (unrationalized) blondel:

$$1 \text{ blondel} = 1 \text{ lumen/m}^2\text{sr} \tag{20}$$

These abbreviations should be used only when the sheer frequency of mention of "watt/m^2sr" or "lumen/m^2sr" becomes so great in a given discussion that facile communication is impaired; otherwise they simply should be spelled out in full using watts, meters and steradians. Further discussion of the foundations of photometry is given in Sec. 2.12.

---

*An unrationalized radiance (or luminance) unit is one for which a uniform radiance distribution of magnitude N produces an irradiance of πN. A rationalized unit would associate to a uniform N the irradiance N. An unrationalized radiance unit is thus logically simpler than a rationalized unit. The term "rationalized" here means "removed π-factor". It is irrational to rationalize radiance units just because it is too tiresome to carry around a π-factor which arises in calculations with radiance distributions which in fact *do not occur in practice in real environments* in the first place! (namely directionally uniform distributions).

1.2 A Survey of Natural Light Fields

The intricate chain of radiative transfer processes within the air and seas of the earth begins with the influx of solar radiant energy at the upper levels of the atmosphere and partially ends in the depths of the seas and lakes. We shall now briefly survey the main features of the light field in the meteorologic and hydrologic domains. We conduct the survey with the purpose of establishing the general orders of magnitudes of the set of radiometric phenomena in natural optical media which the theory of radiative transfer has been evolved to describe and predict.

The Solar Constant

The *solar (irradiance) constant* is the total irradiance produced by solar radiant energy of all wavelengths at a point located outside the earth's atmosphere at the mean distance of the earth from the sun and on a plane normal to the direction of the sun's center:

$$\text{solar (irradiance) constant} = 1396 \text{ watt/m}^2 = 2.002 \text{ gm cal/cm}^2\text{min} \tag{1}$$

where

$$1 \text{ joule} = 0.2389 \text{ gm cal}$$

The quantity (1) is based on the results summarized by Johnson [128], and actually pertains to wavelengths in the range 220 to 7000 mμ. For a survey of solar constant measurements and some theoretical bases for them, see [296]. Table 1 gives a wavelength by wavelength analysis of the solar (irradiance) constant in watts/m^2×millimicron. In the table, $p(\lambda)$ is the percentage of the total solar constant included in the wavelength range from 0 to λ. It is interesting to note that this distribution of $H(\lambda)$ with λ is very close to the radiant emittance curve of a 6000°K complete radiator. The solar (illuminance) constant, i.e., the photometric counterpart to the solar (irradiance) constant is obtained by computing

$$E = 680 \int_0^\infty H(\lambda)\, \bar{y}(\lambda)\, d\lambda \tag{2}$$

in accordance with the general rules of photometry laid down in Sec. 1.1. We find:

$$\text{solar (illuminance) constant} = 136{,}700 \text{ lumens/m}^2 = 12{,}700 \text{ footcandles} \tag{3}$$

TABLE 1

Solar Spectral Irradiance Data

Wavelength in millimicrons. $H(\lambda)$ in watts/$m^2 m\mu$.

λ	$H(\lambda)$	$p(\lambda)$	λ	$H(\lambda)$	$p(\lambda)$	λ	$H(\lambda)$	$p(\lambda)$
220	0.030	0.02	420	1.92	11.7	640	1.66	42.1
225	0.042	0.03	425	1.89	12.4	650	1.62	43.3
230	0.052	0.05	430	1.78	13.0	660	1.59	44.5
235	0.054	0.07	435	1.82	13.7	670	1.55	45.6
240	0.058	0.09	440	2.03	14.4	680	1.51	46.7
245	0.064	0.11	445	2.15	15.1	690	1.48	47.8
250	0.064	0.13	450	2.20	15.9	700	1.44	48.8
255	0.10	0.16	455	2.19	16.7	710	1.41	49.8
260	0.13	0.20	460	2.16	17.5	720	1.37	50.8
265	0.20	0.27	465	2.15	18.2	730	1.34	51.8
270	0.25	0.34	470	2.17	19.0	740	1.30	52.7
275	0.22	0.43	475	2.20	19.8	750	1.27	53.7
280	0.24	0.51	480	2.16	20.6	800	1.127	57.9
285	0.34	0.62	485	2.03	21.3	850	1.003	61.7
290	0.52	0.77	490	1.99	22.0	900	8.95	65.1
295	0.63	0.98	495	2.04	22.8	950	0.803	68.1
300	0.61	1.23	500	1.98	23.5	1000	0.725	70.9
305	0.67	1.43	505	1.97	24.2	1100	0.606	75.7
310	0.76	1.69	510	1.96	24.9	1200	0.501	79.6
315	0.82	1.97	515	1.89	25.6	1300	0.406	82.9
320	0.85	2.26	520	1.87	26.3	1400	0.328	85.5
325	1.02	2.60	525	1.92	26.9	1500	0.267	87.6
330	1.15	3.02	530	1.95	27.6	1600	0.220	89.4
335	1.11	3.40	535	1.97	28.3	1700	0.182	90.83
340	1.11	3.80	540	1.98	29.0	1800	0.152	92.03
345	1.17	4.21	545	1.98	29.8	1900	0.1274	93.02
350	1.18	4.63	550	1.95	30.5	2000	0.1079	93.87
355	1.16	5.04	555	1.92	31.2	2100	0.0917	94.58
360	1.16	5.47	560	1.90	31.8	2200	0.0785	95.20
365	1.29	5.89	565	1.89	32.5	2300	0.0676	95.71
370	1.33	6.36	570	1.87	33.2	2400	0.0585	96.18
375	1.32	6.84	575	1.87	33.9	2500	0.0509	96.57
380	1.23	7.29	580	1.87	34.5	2600	0.0445	96.90
385	1.15	7.72	585	1.85	35.2	2700	0.0390	97.21
390	1.12	8.13	590	1.84	35.9	2800	0.0343	97.47
395	1.20	8.54	595	1.83	36.5	2900	0.0303	97.72
400	1.54	9.03	600	1.81	37.2	3000	0.0268	97.90
405	1.88	9.65	610	1.77	38.4	3100	0.0230	98.08
410	1.94	10.3	620	1.74	39.7	3200	0.0214	98.24
415	1.92	11.0	630	1.70	40.9	3300	0.0191	98.39

TABLE 1 (Continued)

λ	H(λ)	p(λ)	λ	H(λ)	p(λ)	λ	H(λ)	p(λ)
3400	0.0171	98.52	4400	0.0067	99.29	4900	0.0044	99.48
3500	0.0153	98.63	4500	0.0061	99.33	5000	0.0042	99.51
3600	0.0139	98.74	4600	0.0056	99.38	6000	0.0021	99.74
3700	0.0125	98.83	4700	0.0051	99.41	7000	0.0012	99.86
3800	0.0114	98.91	4800	0.0048	99.45			
3900	0.0103	98.99						
4000	0.0095	99.05						
4100	0.0087	99.13						
4200	0.0080	99.18						
4300	0.0073	99.23						

(From [128], by permission)

By dividing the solar constant by the approximate solid angle subtense of the sun at the mean distance of earth from sun, $\Omega = 6.8 \times 10^{-5}$ steradians, we obtain the approximate solar radiance and luminance constants:

$$N = 2 \times 10^{7} \text{ watts/m}^2\text{sr}$$
$$B = 2 \times 10^{9} \text{ lumens/m}^2\text{sr} \qquad (3a)$$

General Irradiance Levels at Earth's Surface

The irradiance levels at the earth's surface can vary relatively widely because of correspondingly wide variations of atmospheric clarity and elevation differences of locales above mean sea level. Hence the magnitudes to be offered here are not as unique or invariable as the solar constant given above, and must be understood as general indicators of typical irradiance levels at the earth's surface. Table 2 is adapted from one given by Moon [185]. The solar constant values in the indicated ranges have been computed from Table 1 above and included for comparison. The column marked "405 to 704 mμ" is of especial interest since it gives the irradiances in the visible portion of the spectrum. By an odd numerical fluke, the solar irradiance constant 555 watts/m^2 over the visible spectrum numerically equals the wavelength (in mμ) at which the photopic luminosity curve has its maximum. It is instructive to study the tabulated effects of moisture content of the air and altitude on the irradiance as given in Table 2. (The totals have been rounded out so as not to appear misleadingly accurate.) Quite a battery of empirical models have been evolved to predict the effects of moisture, dust, elevation of sun and of observer on the measured irradiances on the earth's surface. An excellent summary of these models may be found in [96]. Another reference, of interest to oceanographers, would be [173]. For a recent survey of solar irradiation measurements, see [296].

TABLE 2

Irradiance Data at Earth's Surface

(in watts/m^2 on a plane normal to sun's rays, within indicated portions of the electromagnetic spectrum)

Conditions	Wavelength Range				
	Below 346 mμ	346 to 405 mμ	405 to 704 mμ	Above 704 mμ	Total
Mountain tops, sun at zenith, dry clean air.	23	47	484	668	1220
Mountain tops, sun at zenith, moist dusty air.	16	43	466	534	1060
At sea level, sun at zenith, dry clean air.	16	42	472	665	1200
At sea level, sun at zenith, moist dusty air.	4	30	375	425	834
Solar (irradidiance) Constant (for comparison)	58	76	555	707	1396

(From [185], by permission)

General Illuminance Levels at Earth's Surface

An extensive photometric survey of illuminance at sea level on a horizontal plane under various sky conditions was made by Brown [35], part of which is summarized in Fig. 1.12. The graphs in Fig. 1.12 give a detailed photometric portrait of the extremes of variation and the modes of variation of natural illumination generated by the light from the sun and the moon. We have seen in (3) that the solar (illuminance) constant is 12,700 footcandles, which corresponds to a solar disk luminance of 2×10^9 blondels. This level of illumination is approached by the "unobscured sun" curve in Fig. 1.12 for zenith sun. Notice how little the average overcast conditions affect the general order of magnitude of the sea level illuminance. Inexperienced bathers who think they will be safe from sunburn under overcast skies will do well to take note of this fact which follows from Fig. 1.12: one can get baked just as severely under overcast skies as in bright direct sunlight. Moonlight bathing is harmless--photometrically speaking--for, the average level of full moonlight illuminance

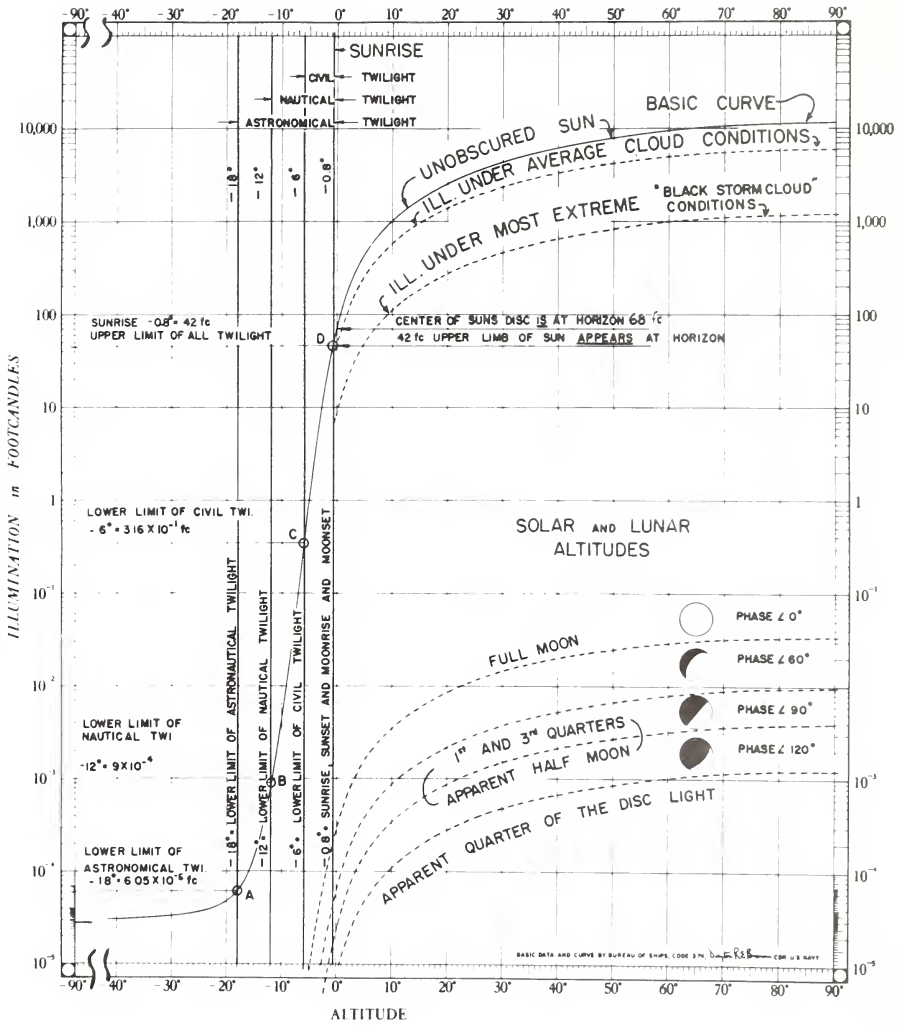

FIG. 1.12 Illuminances on a horizontal surface at sea level under indicated conditions. (From [35], by permission)

is about five orders of magnitude less than corresponding sunlight conditions. Typical clear sky luminances away from the sun are on the order of 3000 blondels, with very heavily overcast skies on the order of 300 to 1000 blondels at the zenith. For further details on the use of the graph in Fig. 1.12, one should consult the discussion given in [35].

Gross Features of Atmospheric Radiative Transfer

The tables and graphs of the irradiance and illuminance surveyed above show the great temporal and spatial variations possible in the magnitudes of these quantities. Therefore to try to assign specific numbers to the reflectance and transmittance of the atmosphere at any given time is seldom an instructive activity. However, discernable patterns and stable percentages emerge when the daily variations of the reflectances and transmittances are averaged over long times and over great areas. Such averages begin to show the general features of the radiative transfer processes extant in the atmosphere, and help us form an initial picture of the radiant energy budget of the atmosphere-surface system. Consider, for example, the average yearly irradiance (of all wavelengths) on an average horizontal surface just outside the atmosphere over the entire northern hemisphere. On purely geometrical grounds, this amounts to about one quarter of the solar constant or 340 watts/m^2 (about 0.485 gm cal/cm^2 min) over one year.

The annual radiant energy budget may be analyzed as follows: for easy visualization, we normalize the 340 watts/m^2 and start with 100 watts/m^2. Thus, if 100 units of irradiance on the average are incident on the upper atmosphere, then the general radiative transfer activities in the atmosphere at steady state are reflection, absorption, and transmission, which take up, respectively, 34, 19, and 47 of these 100 incoming units as shown in (a) of Fig. 1.13. Part (b) of Fig. 1.13 breaks the reflected and transmitted fluxes down even further. Thus, of the 34 units reflected, 25 of these are by the clouds, and 9 by the clear atmosphere. Of the 47 units transmitted, 24 of these are directly transmitted (without scattering), and 23 are transmitted via scattering. Of these 23 transmitted units 17 are transmitted by the clouds, and 6 by the clear atmosphere.

Now the 47 transmitted units are received in turn by the earth (terra firma + terra infirma), are chewed up and are eventually given back via heat radiation (14 units), or latent heat of evaporation in cloud formation (23 units) or via convection-conduction activity between the atmosphere and the earth's surface (10 units). This is shown in (c) of Fig. 1.13.

An exact mathematical formulation of these interactions can be written down using the principles of invariance for irradiance, as described generally in Sec. 8.7, assuming, e.g., a three-layer system (atmosphere + clouds + earth's surface); see in particular Examples 5 and 6 of Sec. 8.7. The numbers cited above, however, are not theoretical, but rather based on actual observations and are patterned after the

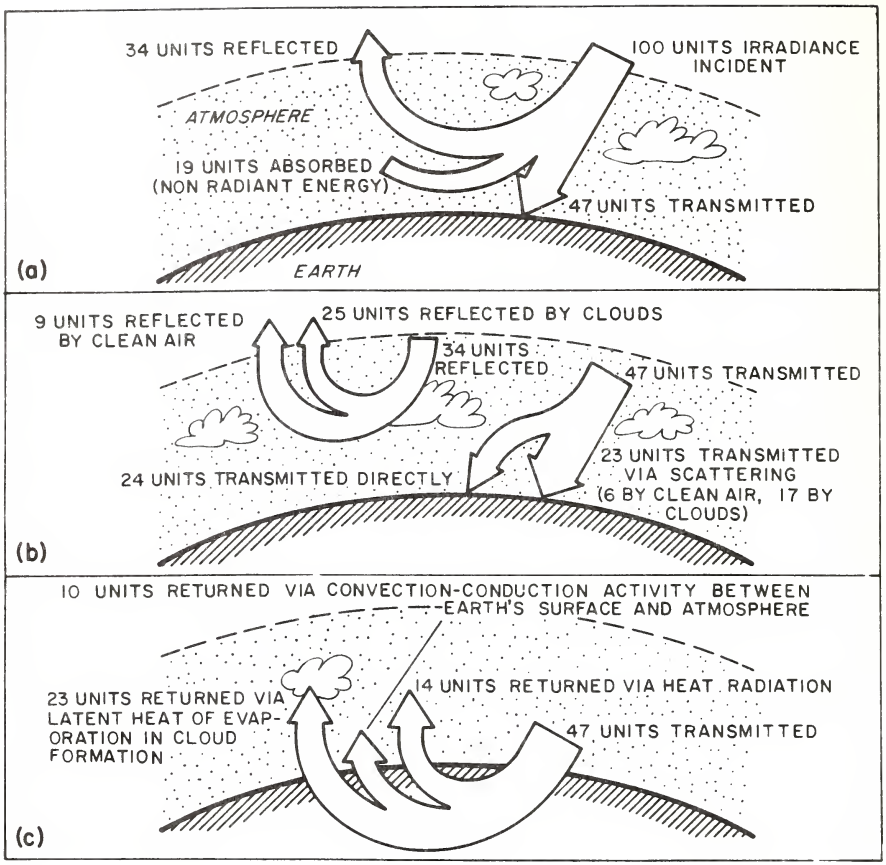

FIG. 1.13 The average yearly radiant flux budget over the sunlit hemisphere of earth. (From [96], by permission)

magnitudes summarized in [96].

Radiative Transfer Across the Air-Water Surface

The still air-water surface acts like an imperfect mirror which reflects only about 2% of an unpolarized light beam normally incident on it from the air side, and transmits about 98% of the incident flux of the beam into the water below. As the beam is tipped and all other factors the same, this reflectance stays fairly constant until, at about 45° from the vertical, the reflectance curve begins to soar to a complete reflectance of unity at grazing incidence to the air-water surface. The functional dependence of this reflectance is quite well known and is governed by Fresnel's formulas, to be studied in Sec. 12.1.

When the air-water surface is ruffled by capillary waves induced by the wind, or when the surface is heaving with gravity waves, the average amount of flux reflected from a vertical light beam incident on the moving surface over a given time can be computed, once again by means of the Fresnel reflectance function, but now with that function's values weighted by numbers between 0 and 1 which are the fraction of the given time interval the surface is tipped away from the horizontal by a given angle between 0 and 90°. The determination of these weighting factors required in such a computation is at present principally an empirical matter, and one of the first such determinations made in hydrologic optics is depicted in Fig. 1.14. This curve, based on the experimental researches by Duntley in [82], gives the number of times the water surface normal at a fixed point was observed to tip over by an amount ϕ, $0° \leq \phi \leq 90°$, during a given time period. The solid curve is for the case where the normal was observed within the up-down wind plane; the dashed curve is for the cross-wind plane case. There is very little difference between the two cases. A steady wind of 18 knots (about 9 m/sec) was blowing and maintaining a steady capillary wave and small gravity wave complex. It was found that the number n_ϕ of times the wave surface normal was tipped $\phi°$ from the vertical, during the experiment was very nearly expressible as:

$$n_\phi = n_o \, e^{-\frac{\tan^2 \phi}{2\sigma^2}} \tag{4}$$

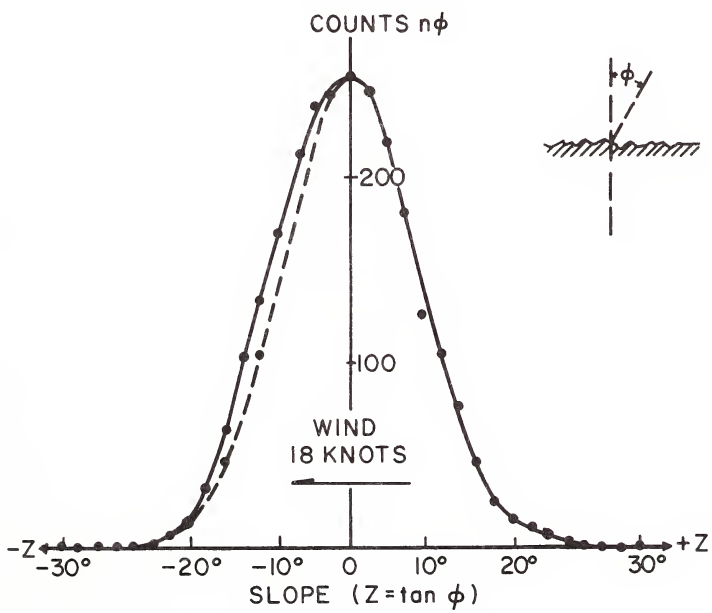

FIG. 1.14 Relative frequency of occurrence of a given tilt of a water wave facet.

In other words, n_ϕ was found to vary in a gaussian manner when tan ϕ (rather than ϕ) was used as an independent variable. The quantity σ is the usual standard deviation of the observed slopes (the mean slope tan ϕ was zero). It is clear then, that the relative number of times the wave *slopes* were tipped at tan ϕ, is given by n_ϕ/n_o. For the 18 knot wind, it turned out that σ was 0.162, which may be pictured as the tangent of a standard deviation angle of inclination of the surface normal of about 9.2 degrees from the vertical. It was also found that the square of σ, i.e., σ^2, varied nearly linearly with the surface wind speed generating and sustaining the steady wave complex. A flat calm surface clearly has a σ of 0. The preceding gaussian distribution was also found by Cox and Munk [56] in their study of the glitter patterns on the sea surface.

The preceding statistical type of description of the dynamic air-water surface can be used, under suitable conditions, to estimate the time averaged reflectance and transmittance of the air-water surface over a given time interval at a certain point; or dually, to estimate the space averaged reflectance and transmittance of the surface over a given region at a certain time instant. Table 3 displays three reflectances computed under the indicated conditions.

TABLE 3

Irradiance Reflectance H(0,+)/H(0,-) of the Air-Water Surface for Sky Light

Sky	Air-Water Surface	
	Smooth (σ=0)	Rough (σ=0.2)
Clear, sun at 60° from zenith	(no wind) .100	(13-18 knot wind) .071-.088
Uniform	.066	.050-.055
Overcast	.052	.043-.044

(From [58], by permission)

Thus under a clear sky with the sun at 60° from the zenith, a smooth sea surface will reflect about 10% of its total irradiance (H(0,-)) back into the sky, whereas, under the same sky condition, a sea driven by a steady 13-18 knot wind would reflect a slightly less amount of about 7 to 9% of the total irradiance (over the whole spectrum). This is in reasonable accordance with an intuitive estimate based on the Fresnel reflectance function for the air-water surface. In all displayed cases in Table 3, the irradiance reflectance decreases when the wind starts to blow over the surface and hence roughens the surface. As Cox and Munk observe, this fact has an important oceanographic significance, namely that in summer the open stretches of the Arctic Ocean surface (or any

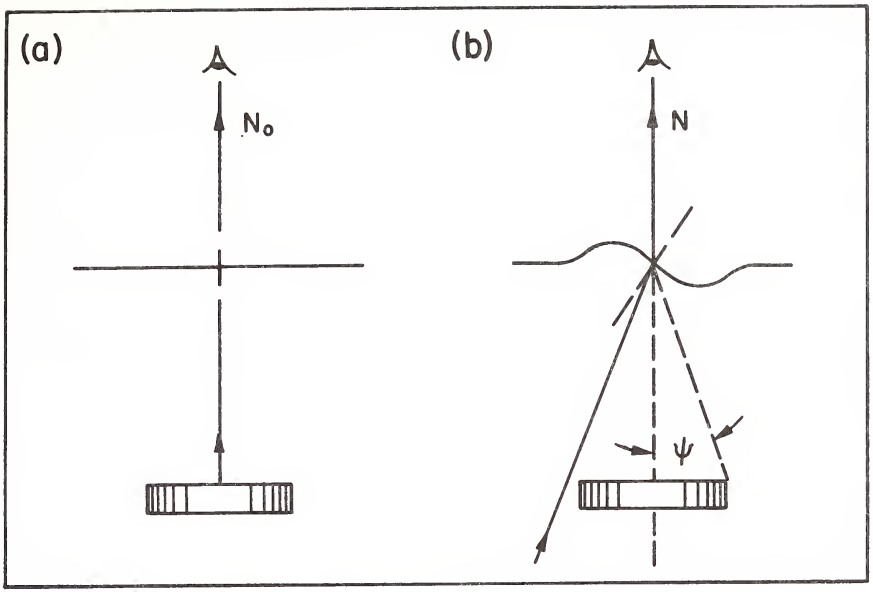

FIG. 1.15 Contrast reduction by time-averaged refraction at the air-water surface.

roughened surface for that matter) will reflect less and transmit more radiant flux than has been previously estimated using simple unweighted Fresnel reflectances (cf. [58]). More exact values of the reflectance for $\sigma = 0$ are given in Table 4 of Sec. 12.1.

A complete theory of the reflectance and transmittance of both the static and dynamic air-water surface is developed in Chapter 12 below.

Besides oceanographic applications there are also visibility applications of the observed gaussian structure of the ruffled air-water surface slopes. Thus while it is commonplace that the visibility of a submerged object below a wind blown surface as seen through the surface is less than when the surface is calm, due to the blurring action of the refracting processes at the surface, it is possible actually to make quantitative predictions of the time-averaged apparent contrast of a given submerged object against its background as a function of the size of the object and the standard deviation σ of the wave slopes through which the line of sight is directed. Part (a) of Fig. 1.15 depicts the basis of such predictions when the surface is flat and horizontal at the point of intersection with the line of sight, and when the center of the submerged object (here a circular disk) is observed to have an apparent radiance N_o. When the surface is tipped, as in (b) of the figure, the refracted line of sight picks up the apparent radiance N of the background of the object. The still water apparent contrast C of the center of

the object with respect to its water background is by definition $(N_o-N)/N$. If the time-averaged apparent contrast of the object against its background is $\overline{C}$ when the surface slopes have a standard deviation of σ, then it can be shown that:

$$\overline{C} = C\left(1-e^{-\frac{\tan^2\psi}{2\sigma^2}}\right), \qquad (5)$$

where the object has an angular radius of ψ. Observe that for $C > 0$, if σ increases, then $\overline{C}$ decreases for a given ψ, as would be expected. Further, for given σ, the time-averaged contrast $\overline{C}$ increases as ψ increases; again as would be expected, but now in a definite quantitative way. For small objects or rough seas (or both) the preceding formula yields the rule of thumb:

$$\overline{C} = C\left(\frac{\tan^2\psi}{2\sigma^2}\right) . \qquad (6)$$

These formulas, which describe the contrast reduction by time-varying refraction effects, will be developed in detail in Sec. 12.14.

Glitter Patterns on the Air-Water Surface

Sunlight reflected from a still air-water surface can be seen, by each observer, as a circular image lying angularly just as far below the observer's horizon as the sun lies above that horizon. A slight breeze disturbs the water and the single image splits into two or more irregularly shaped randomly moving images of the sun. The breeze continues and the few images ignite into a dazzling glitter pattern. To a poetically inclined observer, the glitter pattern invokes very ungeometrical and unhydrodynamical thoughts. In Russian, for example, the glitter pattern is sometimes referred to as the "road to happiness". However, to analytically inclined observers, the glitter pattern contains a wealth of information about the geometrical structure of the surface, the statistical distribution of wave slopes and, as we have seen above, important consequences for the radiative transfer processes across the air-water surface.

As an illustration of these more technical ideas consider the problem of finding the greatest occurring slopes on a rough sea surface at a given time. It is seemingly impossible to do this visually or even with photographs or other optical means until certain geometrical features of the sun's glitter pattern come under scrutiny. Then it becomes clear that in order for an observer to see the instantaneous reflected image of the sun in a wave facet, the three participants in this phenomenon, namely the sun, the facet, and the observer, must subtend very precise geometrical relations. These relations are readily calculated using a bit of analytic geometry. Figure 1.16 (adapted from Minnaert [182], in turn

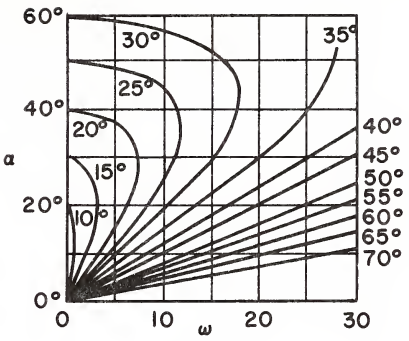

FIG. 1.16 How to find the tilt of a sun-reflecting water facet's normal knowing the sun altitude α and the horizontal angle ω of the facet from the vertical plane containing the sun. (Based on Hulburt's calculation) (From [113], by permission)

derived from [113]) summarizes one such calculation, and may be used as follows to estimate the required maximum tilt of wave facet-normals on an air-water surface which has a glitter pattern. First estimate the angular half-width ω of the pattern, and estimate the altitude α of the sun above the horizon. Suppose, e.g., $\omega = 15°$ and $\alpha = 30°$. Then the curve going through the grid point (15°, 30°) is labeled "30°" and this is the requisite maximum tilt of the normals to the glittering facets. When a grid point (such as (20°, 40°)) falls between two curves, one must visually interpolate to find the requisite maximum tilt (about 32° in this case). These and related calculations are studied further in Sec. 12.5.

It is of interest to observe that the graphs in Figure 1.16 may be used to estimate the amount of tilt of *any* observed reflecting air-water facet; furthermore the object reflected in the facet need not be the sun--any point source whose distance from the facet is several times greater than the observer-facet distance may replace the sun.

Subsurface Refractive Phenomena

Once one descends below the air-water surface a new realm of relatively strange radiative transfer phenomena is encountered. At the very instant light passes that incredibly thin air-water film the radiance function receives a jolt in the form of an abrupt increase in radiance of the sky in each observable direction. The increase is by a factor of $(4/3)^2$ or 16/9. This is a purely geometric effect due to the

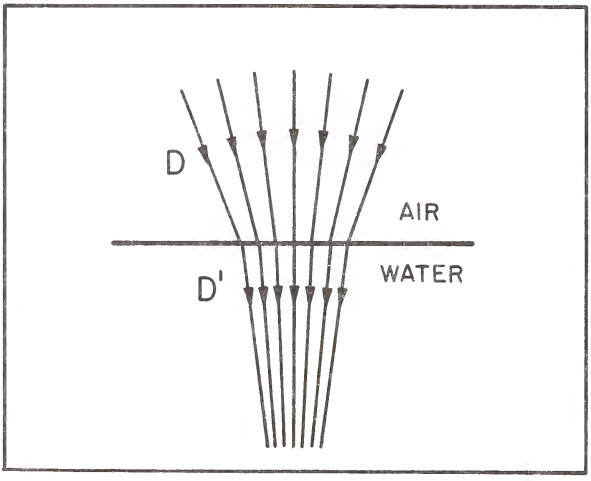

FIG. 1.17 The effect which gives rise to the n^2-law for radiance.

general narrowing of a bundle of refracted light rays as they enter the more dense water from the air (see Fig. 1.17). It is interesting to note that this phenomenon, as such, is not detectable by the unaided eye since the apparent radiance associated with a bundle of light rays depends (scattering effects aside) only on the indices of refraction at the beginning and end of the light bundle's path. Since the bundle begins in air and ends on the retina *inside* the eye, the intermediate water domain has no effect in this special geometrical sense. The full effect, however, can be measured by simple radiance meters, if they are suitably built.

The optical distortions attendant upon the refraction of the light rays at the surface are quite marked. For example as one slowly descends into a body of water with a relatively calm surface and continues to look upward, one is struck with the impression that he has just descended downward into a room with a circular hole--a "manhole"--in its ceiling. Through this manhole one sees the objects above the surface become visually compressed the closer their images lie to the rim of the hole (Fig. 1.18). Just to one side of the hole the underside of the air-water surface appears as a slightly undulating perfect mirror, in which nearby fish or other objects may be imaged--upside down. Also, if the bottom is just below the observer, he can see it mirrored on the surface above him around the rim of the manhole. As one descends further the manhole's outline is slightly dimmed by the scattering and absorbing effects of the water, but it continues to subtend the same angular radius--about 48°, the angle beyond which, according to Snell's law of refraction, total internal reflection takes place.

If the air-water surface is not calm, but ruffled with wavelets, then the ideal geometric reflection pattern is replaced by something relatively complex. Beebe [12] gives the

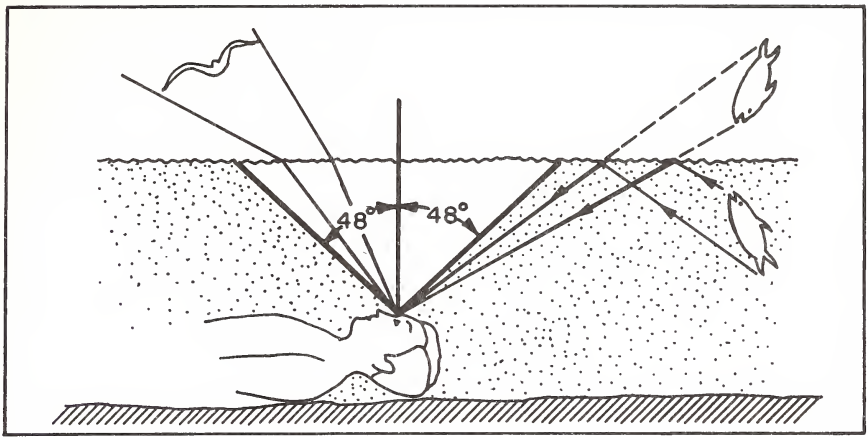

FIG. 1.18 The swimmer's optical manhole to the outside world.

following interesting account:

"As to the opacity of the ceiling, I thought it absolute until I threw my head back as far as I dared, [he was in an old fashioned iron helmet rig exploring Haiti Bay, in 1927] and saw, almost directly overhead, facets of clarity, appearing and vanishing, showing me an instant's patch of sky, a momentary glimpse of friend or boat--of that world to which it seemed at this moment inconceivable that I belonged. But anywhere except straight above me, the ceiling of the bay was watered gauze."

If the underwater observer now directs his attention downward, he may see in relatively shallow water a moving mosaic of bright and dark areas on the bottom, produced by the refracted sun's rays converging and diverging at various points on the bottom. When two bundles of rays are refracted so as to momentarily converge at a point A on the bottom (Fig. 1.19) the irradiance at A abruptly increases and is seen by the swimmer as a bright spot. On the other hand, rays could be diverted away from a point such as at B in Fig. 1.19, whereat it will be momentarily relatively dark. By knowing the statistics of the air-water surface slopes (as discussed above) it is possible to determine the statistics of the irradiance pattern on the bottom. The problem has recently been studied, e.g., by Redmond [260], and Schenck [272].

As one descends still farther, and if the water has a modicum of suspended and dissolved material which scatters light, the refracted rays of sunlight are then seen to form a pattern of moving beams and weaving, lighted, curtain surfaces very much like a watery aurora borealis or like the shafts of sunlight one sees directed earthward from rifts between clouds. These beams die away relatively quickly with depth in natural waters, at least as compared to the decay of the general diffuse light originating from the sky and clouds.

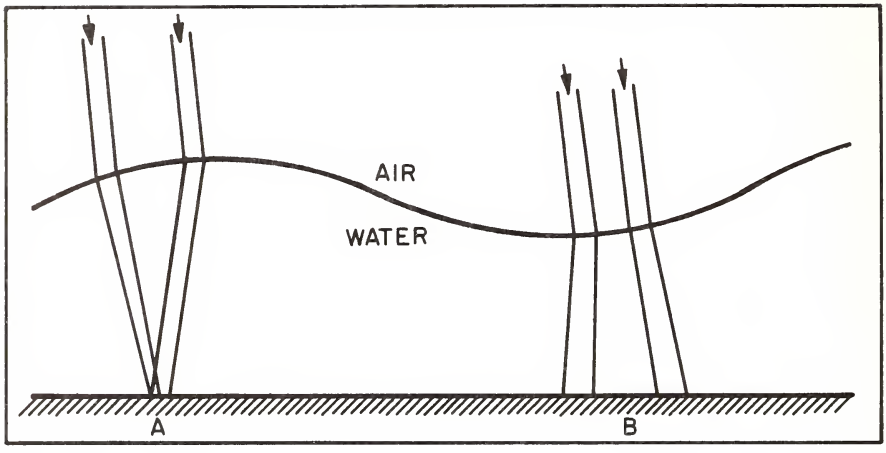

FIG. 1.19 Generating light patterns on shallow bottoms.

We shall look into this phenomenon in some detail later in this section.

One final subsurface refractive phenomenon we shall note here is that associated with the thermocline in natural hydrosols. The thermocline is the region of abrupt temperature change, (usually taking place in an extensive thin horizontal layer) found in most all natural waters, which separates a warmer layer from a cooler layer of water below it. It is detectable by means of a submersible thermometer known as a *bathythermograph*. Accompanying this temperature change is a corresponding density change of the water, and with this occurs a change in the refractive index of the water. Therefore we would expect some interesting refractive optical phenomena at the thermocline. Some observations of optical thermocline phenomena were made by Limbaugh and Rechnitzer [160] and are schematically summarized in Fig. 1.20, which is adapted from their paper. When the thermocline occurs in its more frequent guise, as a thin, horizontal, nearly motionless layer below the surface (as in the upper third of Fig. 1.20) one can actually see the thermocline from below as a smooth, nearly flat mirror-like plane boundary between the two water layers of differing temperature--and it generally manifests itself very much in the way the air-water surface does, even to the extent of having its own manhole into the warmer layer of water above. (Would one expect this manhole to subtend the same angular radius as the surface manhole?) Occasionally some rather unusual refractive phenomena may be observed when a moving tongue of cold water snakes its way through a warmer region on the bottom, (as in the lower left third of Fig. 1.20). The convex boundary of the tongue is visible all along its extent at grazing incidence, and its general appearance is reminiscent of the intertwining portions of two miscible liquids, such as clear alcohol and clear water. Finally, Limbaugh and Rechnitzer observed the optical thermocline effect in small isolated pools of relatively cold water resting

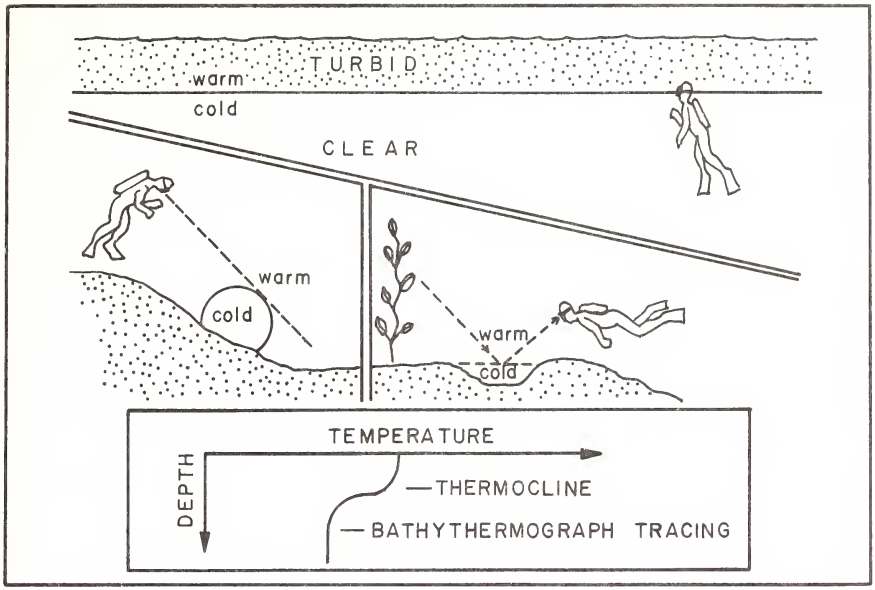

FIG. 1.20 Three interesting subsurface refractive phenomena. (From [160], by permission)

on the bottom in the midst of warmer water. These cool pools reflected light at their surfaces much in the way the still air-water surface reflects light for an observer above it.

The Decay of the General Light Field with Depth

Perhaps one of the most striking and outstanding features of the light field in deep natural waters is that it gets dark *fast* with increasing depth. For example infrared radiation (which comprises about half the irradiance at sea level on sunny noon days) is essentially absorbed in the first meter or so of most natural waters. There is a reasonably precise and simple law of darkening of the light field in this regard: the light field of any wavelength generally falls off or decays exponentially with depth. That is, if $h(z)$ is the scalar irradiance at depth z in a homogeneous, deep lake or portion of the sea, then:

$$h(z) = h(0)\, e^{-Kz} \tag{7}$$

This type of law, namely the *exponential* type, is unquestionably the most ubiquitous of all types of natural laws in geophysics: it describes thermal and radioactive decay in solids and liquids, evaporation rates of falling rain droplets, growth rates of plant and animal species, fall off of atmospheric density with altitude, only to mention a few. In our

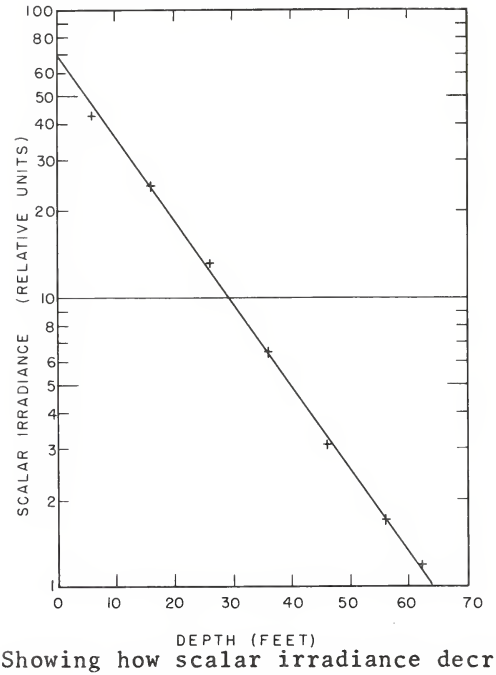

FIG. 1.21 Showing how scalar irradiance decreases exponentially with depth. Experiment by Duntley, Lake Winnipesaukee, N.H., September 1948. (Fig. 30, left diagram, from [78] by permission.)

present studies, it describes not only the decay of the natural light field with depth, but generally the decay of a beam of light with distance along its path. In the present case, the decay rate K depends on the wavelength λ of light considered (h(z) depends on λ; however for brevity, as usual we omit "λ") and of course the clarity of the water considered. Indeed, as we shall see later, in Sec. 1.7, we may use the wavelength dependence of K to help classify the optical properties of natural hydrosols.

Figure 1.21 illustrates a sample experimental determination (taken from [78]) of the depth dependence of scalar irradiance in a deep clear lake (Lake Winnipesaukee, N.H.) over a depth range of 60 feet or 18.3 m. The crosses indicate the experimental points. The straight line is the best straight line for the data, and is plotted on semilog paper. The magnitude of the constant K is: K = .066/ft. = .216/m, for green light.

In view of the preceding observations there is no need at present of giving further graphs of h(z) vs depth z in deep homogeneous media; for as the saying goes, 'if you have seen one, you have seen them all', the prototype being that displayed in Fig. 1.21. What is more worthwhile at present, is to raise such questions as: how is the exponential decay law affected if the medium is not deep, or if the bottom is clearly visible? What effects do inhomogeneities of the medium have on the exponential law? Does h(z) decay at the

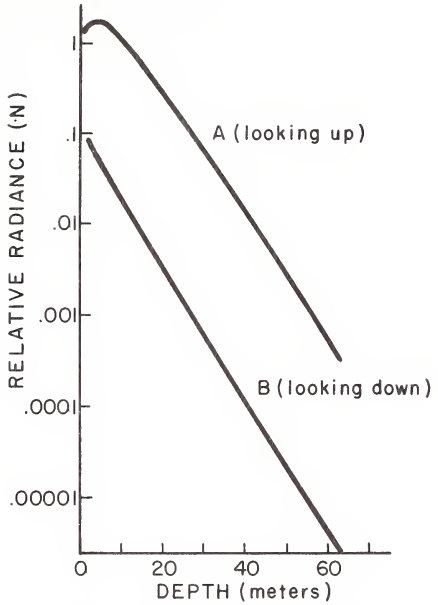

FIG. 1.22 Two experimental determinations of radiance by Tyler, Pend Oreille Lake, Idaho, April 1957. Note the general exponential decrease. Note, also, the slight buildup of radiance for the upward looking path near the surface. (From [298], by permission)

same rate at $H(z,\pm)$? (cf. (9) and (10) of 1.1). Does the exponential law hold right up to the surface, or is there a boundary effect? These and other questions are readily answered in detail by the theories developed in Chapter 8. Some simple answers are given in Sec. 1.4.

Behavior of Radiance Distributions with Depth

If we fix attention on the zenith radiance as we descend into the sea, then, aside from the effect on the radiance induced by a change of index of refraction (discussed above), there is observable a general build-up of radiance in the first meter or so below the surface. This build-up of light is depicted by Curve A of Fig. 1.22 (adapted from [298]) and is quite analogous to the increase in the light field one experiences as an airline passenger during the initial stages of the airliner's descent into a thick cloud layer lighted from above by the sun. We are observing in either case the storage of scattered radiant energy within the medium. In the case of the sea this increase in radiance is observable not only at the zenith, but in all upward looking directions, but is occasionally obscured by the refracted sunlight beams and other surface phenomena. The depth at which the maximum radiance occurs is predictable in theory and varies with the

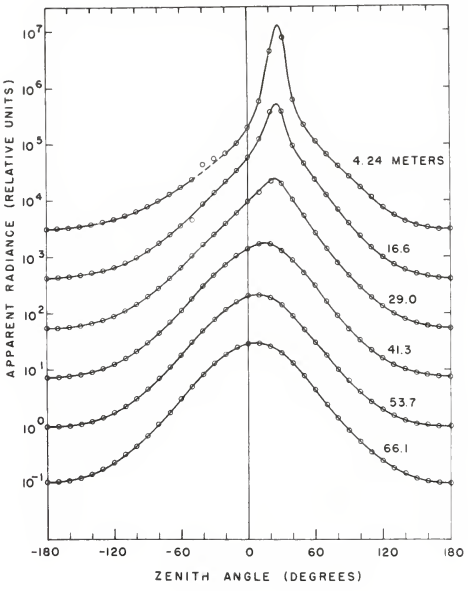

FIG. 1.23 Radiance distributions, in the vertical plane containing the sun, on a clear sunny day, at the indicated depth, in Lake Pend Oreille, Idaho, as measured by Tyler, April 1957. Observe how the shapes of the curves become similar as depth increases. (Fig. 26, from [78], by permission)

direction of sight and the clarity of the medium (cf. (12) of Sec. 4.4).

After the maximum radiance occurs in a given direction, the radiance in that direction begins to fall off rapidly with depth and soon assumes the exponential behavior that h(z) universally exhibits. This trend to exponentiality is seen quite clearly in the nadir curve B of Fig. 1.22, or more generally in Fig. 1.23, which is adapted from [78]. Fig. 1.23 is designed to show how the *shapes* of the radiance distributions vary with depth in the hydrosol. The particular graphs in Fig. 1.23 are adapted from [78] and represent the light field measured in Lake Pend Oreille, Idaho by Tyler [298]. The radiance is associated with a wavelength of 480 ± 64 mμ, in water with a K of about .170/m and (for future reference) an α of .370/m. Two important and universal properties of underwater radiance distributions are discernable in this set of curves: (i) the decrease in peakedness of the curves with depth, accompanied by a trend toward a limiting shape as depth increases, and (ii) the shift of the radiance maxima toward the zenith with increasing depth. Near the surface the peaks are pointed toward the refracted image of the sun; but this orientation is lost as depth increases. This trend toward a stable vertically-oriented smooth distribution is shown in more detail in Fig. 1.24, wherein the zenith angles of the maxima in Fig. 1.23 are plotted as a

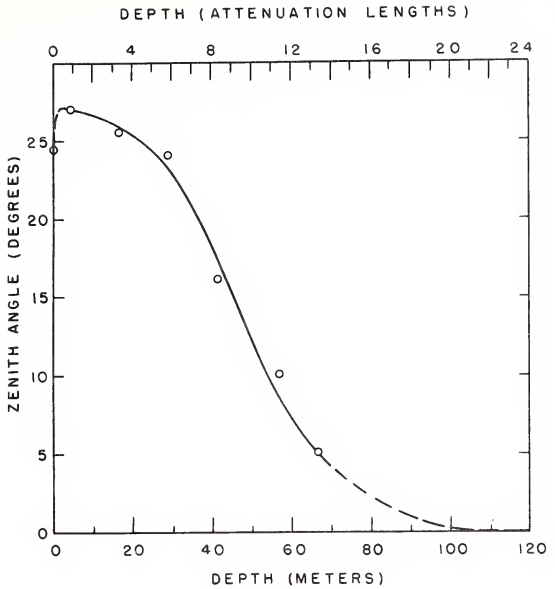

FIG. 1.24 Plot of zenith angle of the maxima of the curves of Fig. 1.23. The maxima shift toward the zenith with increasing depth. This figure and Fig. 1.23 present graphic evidence of the validity of the asymptotic radiance hypothesis. (Fig. 28 from [78], by permission)

function of depth. The problem of the description of the depth dependence of the radiance distribution in natural hydrosols is one of the principal tasks of hydrologic optics and to which much of this work is devoted.

The Asymptotic Radiance Hypothesis

The fact that the shapes of the radiance distributions in deep hydrosols approach limiting forms with increasing depth is observable in Both Figs. 1.23 and 1.24. In the former figure all the radiance curves eventually steady in shape with increasing depth. This means that eventually all radiances are decreasing at the same exponential rate with depth. Hence the evidence points to the fact that radiance distributions eventually assume certain stable shapes and these distributions subsequently shrink down exponentially in size with increasing depth, all the while preserving those shapes. The general statement of the existence of such limiting shapes in all homogeneous natural hydrosols is the *asymptotic radiance hypothesis* which was first clearly enunciated by Whitney [315] on the basis of experimental findings, and subsequently proved mathematically in [225]. The validity of the asymptotic radiance hypothesis has important consequences for the development of simple theoretical models of the light field

in the sea and in deep lakes, rivers and harbors. For example the scattering and absorption functions in the general theory depend in part on the shape of the radiance distributions. If these distributions do not vary too much with depth, vast simplifications of the general theory are possible. These matters will be pursued at some length in Chapters 6, 8 and 10.

Underwater Irradiance Distributions

The studies of visibility and biological problems--as far as they are concerned with the radiometric environment--are facilitated by knowledge of the irradiance distributions $H(z,-)$ at each depth z in the medium of interest. Figure 1.25, plotted from the tables in [304], illustrates such a distribution as a function of orientation of the collecting surface's outward normal direction (θ,ϕ) and also of depth, for a sun zenith angle of 33.4°. This graph keys in with that of Fig. 1.23, being the irradiance distribution computed from the radiance distributions in Fig. 1.23, using (1) of 1.1. The role of (θ,ϕ) is depicted in Fig. 1.26.

It is of both practical and theoretical interest to know that an irradiance distribution $H(z,\cdot)$ at a depth z contains just as much information as the radiance distribution $N(z,\cdot)$ at that depth. This will be shown in Ex. 15 of Sec. 2.11, wherein knowledge of N will be used to deduce knowledge of H, and conversely. The bridge between $N(z,\cdot)$ and $H(z,\cdot)$ is easily traversed in the direction $N\to H$ but is somewhat more difficult to traverse numerically in the direction $H\to N$, and until an efficacious numerical scheme to bridge the latter gap is devised, the radiance distribution will continue to be measured and be the favored means of cataloging natural light fields.

Some practical features of irradiance distributions are as follows. Every irradiance distribution satisfies the exact cosine law:

$$\overline{H}(z,\xi) = \overline{H}(z,\mathbf{m}) \cos\theta$$

where $\overline{H}(z,\xi)$ is the net irradiance in the direction ξ, $\mathbf{m}$ is the direction of greatest net irradiance (cf. (14) of Sec. 2.8), and θ is the angle between ξ and $\mathbf{m}$. This law shows that we need only plot or tabulate irradiance distributions $H(z,\cdot)$ for directions ξ not greater than 90° away from some arbitrary fiducial direction, say the vertical direction $\mathbf{k}$. To see this, suppose that we have $H(z,\mathbf{k})$ and $H(z,-\mathbf{k})$ and that we know $\mathbf{m}$. Then by the exact cosine law:

$$\overline{H}(z,\mathbf{k}) = H(z,\mathbf{k}) - H(z,-\mathbf{k}) = \overline{H}(z,\mathbf{m}) \cos\theta_{\mathbf{m}} \qquad (8)$$

where $\theta_{\mathbf{m}}$ is the angle between $\mathbf{k}$ and $\mathbf{m}$. From this we can compute $\overline{H}(z,\mathbf{m})$. Now suppose we know $H(z,-\xi)$ and that we want to know $H(z,\xi)$, where ξ is less than 90° from $\mathbf{k}$. Then the

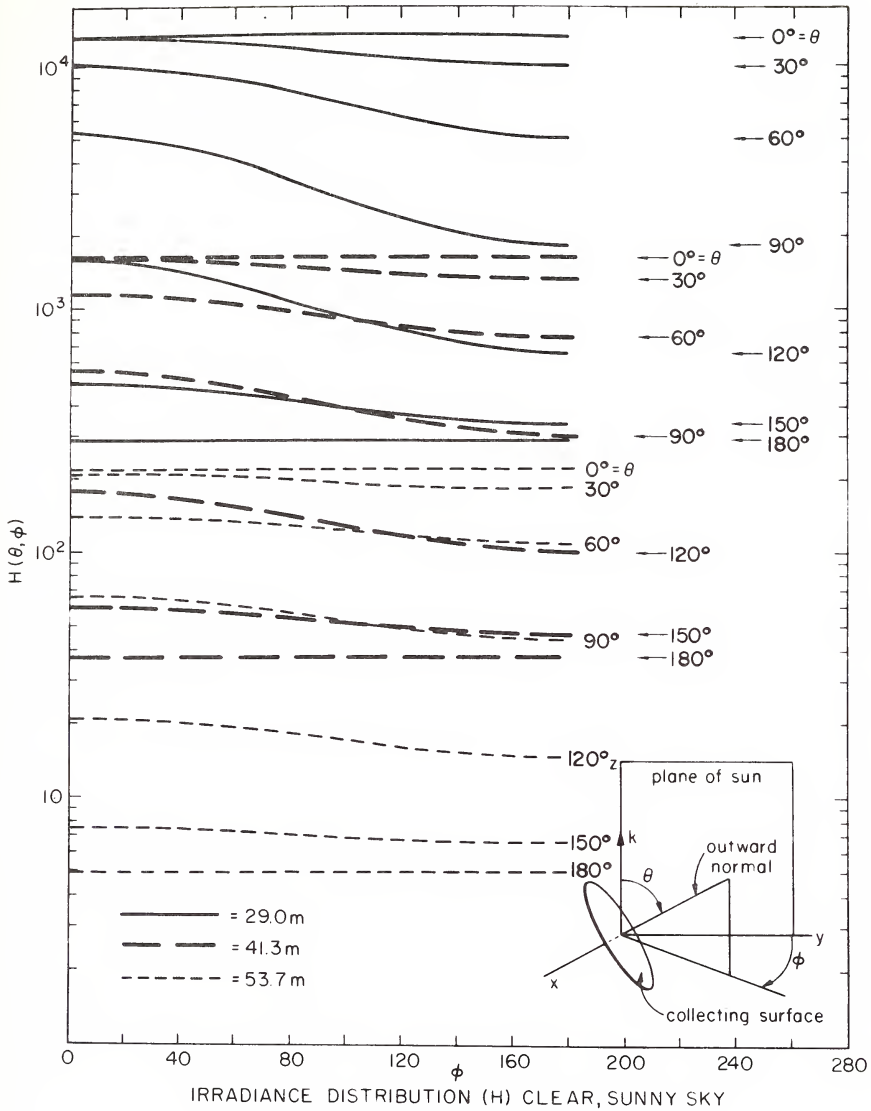

FIG. 1.25 Irradiance distribution on a clear sunny day at the indicated depths, in Lake Pend Oreille, Idaho, 28 April 1957, as computed by Schaules and Tyler from Tyler's data.

FIG. 1.26 The collecting surface receiving the irradiance recorded in Fig. 1.25.

cosine law yields:

$$H(z,\xi) = H(z,-\xi) + \bar{H}(z,\mathbf{m}) \cos\theta \qquad (9)$$

Therefore knowledge of $\mathbf{m}$ and $\bar{H}(z,\mathbf{m})$ together with $H(z,\cdot)$ over one hemisphere of directions, will yield $H(z,\cdot)$ over the remaining hemisphere.

Another practical aspect of the irradiance distribution is that is can be used to compute one of the basic optical properties--namely the volume absorption function, a --of natural optical media, by using the *divergence law*:

$$\frac{d\bar{H}(z,\mathbf{k})}{dz} = a(z)\, h(z) \qquad (10)$$

for the vector irradiance (cf. (1) of 13.8, and Sec. 1.4 below). Thus knowledge of $H(z,\cdot)$ leads to $\bar{H}(z,\mathbf{k})$ and to the latter's derivative by straightforward computations. This, together with auxiliary determinations of h, yields estimates of a.

Subsurface Contrast Reduction by Scattering and Absorbing Effects

Underwater scenes in seas, lakes and harbors are characteristically dim and blurry. The sharp outlines and stark contrasts above the surface are relatively absent from underwater scenes. Even in the clearest swimming pools, distant objects no longer have sharp edges, and contrasts are slightly but yet noticeably decreased. If one looks a bit closer at these contrast-reduction phenomena, one outstanding and fundamental fact soon becomes manifest: on the one hand, as the observer recedes from a relatively bright object, its luminance rapidly falls off and soon melts into the background luminance; on the other hand, if the object is relatively dark, its luminance rapidly increases with viewing distance and eventually also melts into the background luminance. Is there some order and regularity in these changes of apparent contrast with viewing distance? In other words is there some general law followed by these changes in apparent contrast of distantly viewed objects in underwater scenes? The answer is 'yes', provided a judicious scientific choice is made in the selection of the notion of *contrast*.

If ${}_tN_r$ is the apparent (surface) radiance of an object (the *target*) viewed at a distance r underwater, and ${}_bN_r$ is the apparent (surface) radiance of its background, then we write

$$\text{"}C_r\text{"} \quad \text{for} \quad ({}_tN_r - {}_bN_r)/{}_bN_r \qquad (11)$$

and call C_r the *apparent contrast* of the target with respect to its background. The geometry of this situation is pictured in Fig. 1.27. If r=0, we call C_0 the *inherent contrast* of the

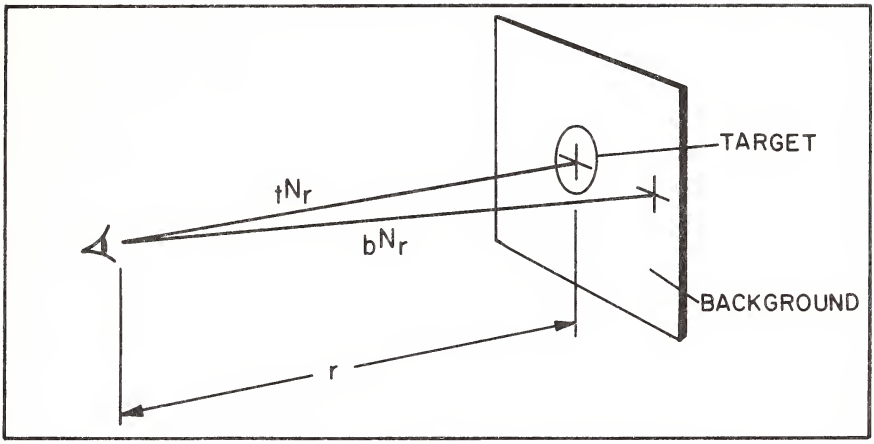

FIG. 1.27 The apparent contrast of a target against its background.

target with respect to its background.

Figure 1.28 shows an experimental arrangement, devised by Duntley [78], to study contrast reduction phenomena in Lake Winnipesaukee, N.H.. A telephotometer (i.e., a radiant flux meter attached to a telescope) was mounted on a small, hooded glass-bottomed boat which looked at a flat white target at depth r. At the time of the experiment (sometime in September 1948) the water was calm, the sky was clear, with a low sun. For later reference we will note that the lake at that time had a K of 0.216/m and an α of 0.594/m, for green light. The observation of interest at the moment is recorded in Fig. 1.29, in its original form, which shows the sought-for law governing C_r vs distance r in feet. This clearly shows an exponential decrease of C_r with r, in this case depth r below the bottom of the boat. In fact it was found, on converting to meter lengths, that:

$$C_r = C_o\, e^{-.810\ r} \quad .$$

This finding of the exponential law is in itself a remarkable one; however, the really exciting fact lay in the nature of the number .810/m(=.247/ft), the exponential decay rate of the apparent contrast. It was found that:

$$.810 = .594 + .216 = \alpha + K \quad \text{(per meter)}$$

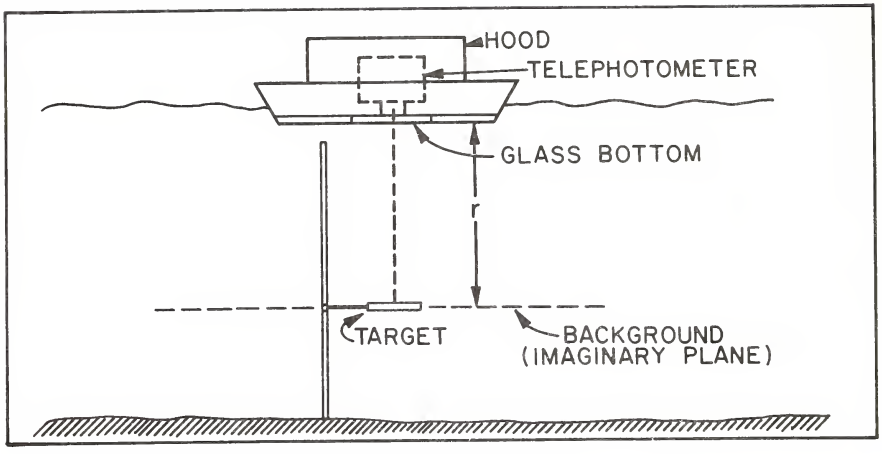

FIG. 1.28 Physical set-up for Figs. 1.29, 1.30.

To see the significance of this, recall our earlier observations on the general mode of decay of the natural light field in the water. The depth rate of decay is given by K. The α on the other hand, gives the depth rate of decay of a beam of light in the water. Therefore there are two mechanisms involved here in giving rise to contrast reduction. These are summarized by K and α, and are generally distinct. These will share our attention later. But for the moment we quietly revel in the presence of discerned order in at least one feature of the underwater radiometric environment. It was perhaps this experimental finding and the ones immediately following it, shown in Fig. 1.30, that contributed more than any others, to inspire Duntley and one of his students (the present author) to turn to the problem of explaining these interesting (and then, mysterious) manifestations of order in the submarine light field, and relating them to the general radiative transfer phenomena in scattering-absorbing media.

What is shown in Fig. 1.30 (which holds for the same setting as above) is an extension of the findings in Fig. 1.29, and once again in the original form given by Duntley. The new figure shows several things. First, it shows that the apparent contrast of an object is exponentially attenuated with target distance at the same space rate for both light and dark targets. Second, this space rate is independent of azimuth of the line of sight (here, the direction of motion of the photons) which in this experiment was inclined at an angle θ of 30° away from vertically upward, or an amount θ= 150° from vertically downward. (See Fig. 1.31) In particular the azimuths, measured from the vertical plane of the sun, are

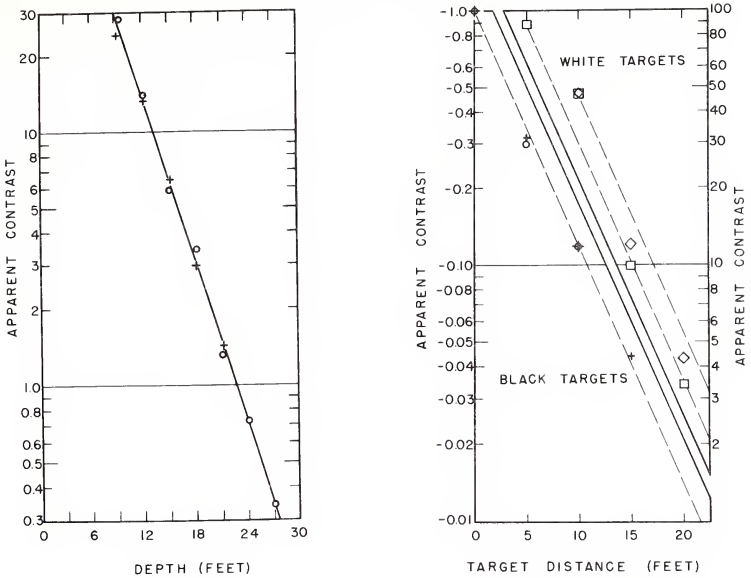

FIG. 1.29 Duntley's classic experiment showing the exponential law of decrease of apparent contrast along a vertical path in a natural hydrosol (Lake Winnipesaukee, N.H., Autumn, 1948. See also Figs. 1.28, 1.30)(Fig. 30, middle diagram, from [78], by permission)

FIG. 1.30 Further experimental evidence for the exponential apparent contrast law. (See Figs. 1.29, 1.31)(Fig. 30, right diagram, from [78], by permission)

$\phi = 0°$ (circled points), $\phi = 45°$ (crosses), $\phi = 95°$ (diamonds) and $\phi = 135°$ (squares). The dashed straight lines are drawn parallel to help judge the slope and linearity of the data and have a natural logarithmic slope of about .781/m. Once again this exponential decay rate is a source of surprise when it is observed that

$$.781 = .594 + .216 \cos 30° \quad \text{(per meter)}$$

This would lead one to conjecture that paths of sight inclined generally at θ from the vertical in homogeneous stratified media, as shown in Fig. 1.31, would have an apparent contrast C_r associated with them of the general form

$$C_r = C_o \, e^{-(\alpha + K \cos \theta) r} \qquad (12)$$

The conjecture was confirmed and a simple theoretical model underlying this contrast reduction law was soon evolved. The model will be discussed further in Sec. 1.4, in Chapter 4, and Chapter 9.

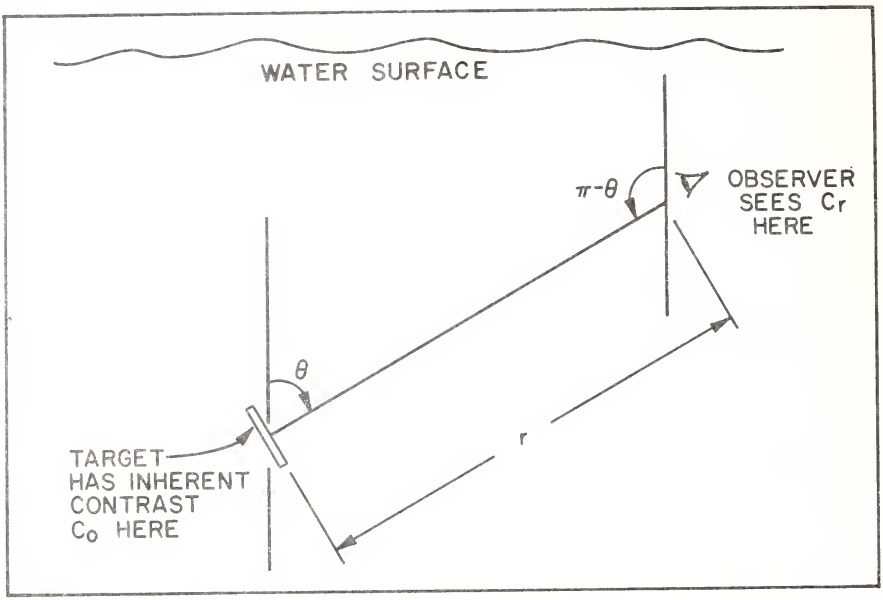

FIG. 1.31 The geometrical details for Fig. 1.30, in which $\theta = 30°$.

Subsurface Contrast Reduction by Refractive Effects

When one looks across an extensive flat stretch of the earth's surface such as a meadow or stretch of ocean on a sunny or very windy day, distant objects seem to be blurred not only by the usual atmospheric haze, but also by a rapidly varying shimmering or "heat wave" effect. This phenomenon is produced by inhomogeneities of the refractive index of the air along the line of sight and is associated with cells of air of different density. These in turn are related to uneven temperature distributions in the air mass or simply to the local mechanical compression of the air in gusts of wind on windy days. The same mechanism makes the stars twinkle at night.

It may come as a mild shock to some observers to occasionally see this same twinkling, heat-wave like effect in the otherwise cool depths of an incompressible fluid like a sea or a lake. Nevertheless, the effect exists, and on closer examination, sanity prevails: the underlying mechanism is seen to be refractive, but produced by myriads of tiny transparent plankton, whose indices of refraction differ very slightly from that of water. In some south sea waters, it is said that the concentration of such plankton is so great, the spacing between a swimmer's toes cannot be distinguished by him, though the foot is visible with high contrast against its background. A somewhat less dramatic but similar phenomenon was observed and recorded by Duntley at the Diamond Island Field Station in Lake Winnipesaukee, N.H.. Figure 1.32, from [78], shows a photograph of the light distribution on a camera

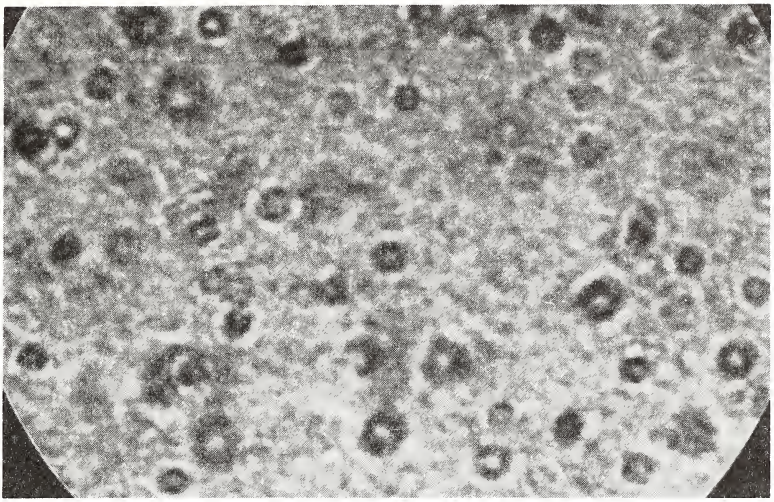

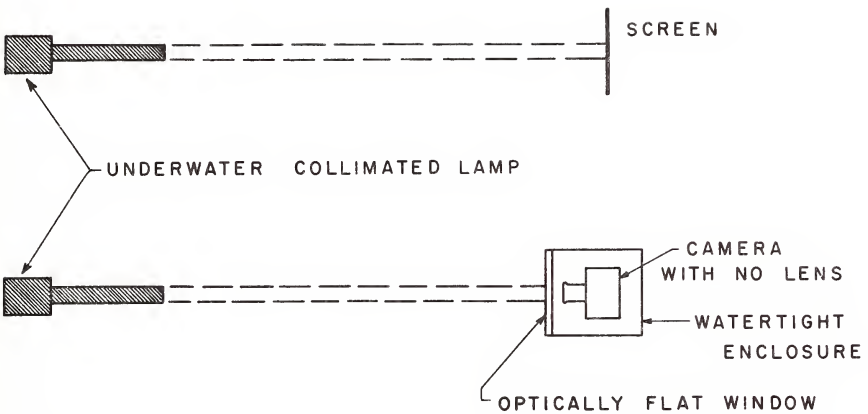

FIG. 1.32 Swarming plankton photographed in the light of a strong collimated beam, as observed by Duntley in Lake Winnipesaukee, N.H., 22 August 1961. Plankton swarms such as these may contribute to contrast reduction along underwater paths of sight. (Fig. 22 from [78], by permission)

FIG. 1.33 Arrangement for plankton photograph, Fig. 1.32. (Fig. 21 from [78], by permission)

film produced by a collimated light beam after having travelled through a horizontal 3 m water path shown in Fig. 1.33. The time of year was late August (1961) and the exposure time was 1/50 sec. on an Eastman Plus-X film with a normal D-76 development. The beam had a diameter of about 5 cm and a

spread of about 0.01°. The α of the water was .585/m, in green light. The water path between the lamp and camera was swarming with plankton, and the bright collimated beam has limned some of these on the photographic film. To judge the size of these tiny organic refractive cells, the diameter of the black circular border (caused by the camera opening) was measured to be 3.3 cm on the negative.

A theory for the loss of contrast of objects seen through atmospheric boil was evolved some time ago by the author and some of his colleagues [81]. This theory appears to be applicable also to the contrast reduction phenomenon described above. The effect, however, is generally mild when it does occur, and may for virtually all practical purposes be ignored in the problem of predicting underwater visibility. However, in passing we may note that in a natural hydrosol which has such transparent plankton distributed uniformly and densely along a path of sight of length r the theory predicts that the magnitude of the blur (the standard deviation of the angular displacement of a typically straggling light ray from observer to object plane) increases like $r^{1/2}$ and the apparent contrast of fine details in an object against the general background decreases like $1/r^3$. Thus the contrast reduction law produced by refractive inhomogeneities in a medium is, on the one hand, quite different from that produced by scattering-absorbing mechanisms in that medium, and summarized in (12). On the other hand, as a perusal of [81] would show, the theory of the present effect is quite close to that used to derive (5).

The Polarization of Underwater Light Fields

Up to now we have been describing those optical effects in natural hydrosols that have very little directly to do with the fact that photons, in their pristine state, are viewable as particles with observable spins--i.e., with an observable property we usually call *polarization*. If we now invoke the quantum theoretical wand of complementarity and imagine the photon to be not a small, hard, colored ball but, rather a relatively compact packet of electromagnetic waves whose **E** and **H** vectors vibrate in fixed mutually orthogonal planes as the packet moves along (see Fig. 1.34), then we add a new dimension to the description of radiometric phenomena. No longer is it sufficient to merely describe the unpolarized radiance of the light field, but rather we must go on to describe radiance carried by those photons at x in the direction ξ whose **E** vector is oriented by the general angle ψ with respect to some reference frame.

Suppose we place a polarizer into the radiance tube, as shown in Fig. 1.35. (Compare with (b) of Fig. 1.5.) This may be made from some commercially available polaroid material. Then if we fix x and ξ as usual, and rotate the polarizing element, we can detect the presence of polarized radiance by the varying output of the radiant flux meter's dial. Suppose we turn the polarizer one full turn. Let $N_{max}(x,\xi)$ and $N_{min}(x,\xi)$ be the maximum and minimum radiances so obtained.

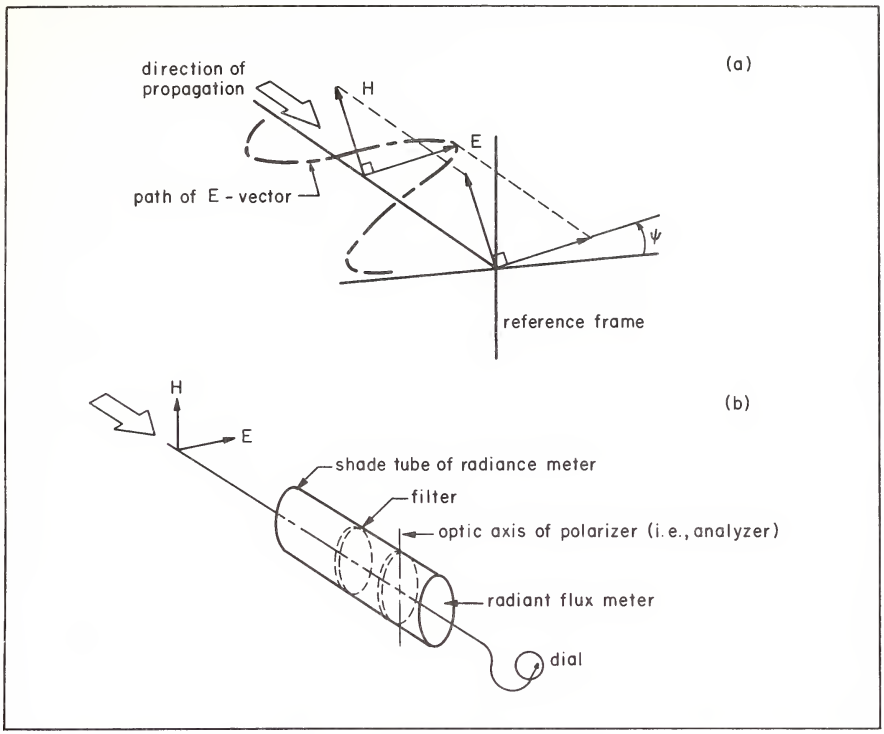

FIG. 1.34 A linearly polarized E-vector.
FIG. 1.35 The placement of a polarizer in a radiance tube preparatory to measuring the polarization of a light field.

Then we write

$$\text{"p}(x,\xi)\text{"} \quad \text{or "p"} \quad \text{for} \quad \frac{N_{max}(x,\xi) - N_{min}(x,\xi)}{N_{max}(x,\xi) + N_{min}(x,\xi)}$$

$p(x,\xi)$ is called the *polarization* of the light field at x in the direction ξ, and is a useful measure of how much polarization is present in the light field at x.

Now if we train such a polarized radiance meter at a clear sky, we find that the sky radiance is most noticeably polarized in all directions which lie in a plane normal to the direction of the sun's rays. If we go below the air-water surface we find that the light field is still polarized but to a lesser extent. The shafts of sun and skylight beaming down into and around the manhole (described above) are *scattered* into the line of sight by the water in a manner completely analogous to the sunlight streaming into and scattering within the upper atmosphere. Furthermore, the underwater light field may also be reflected into the line of sight by the underpart

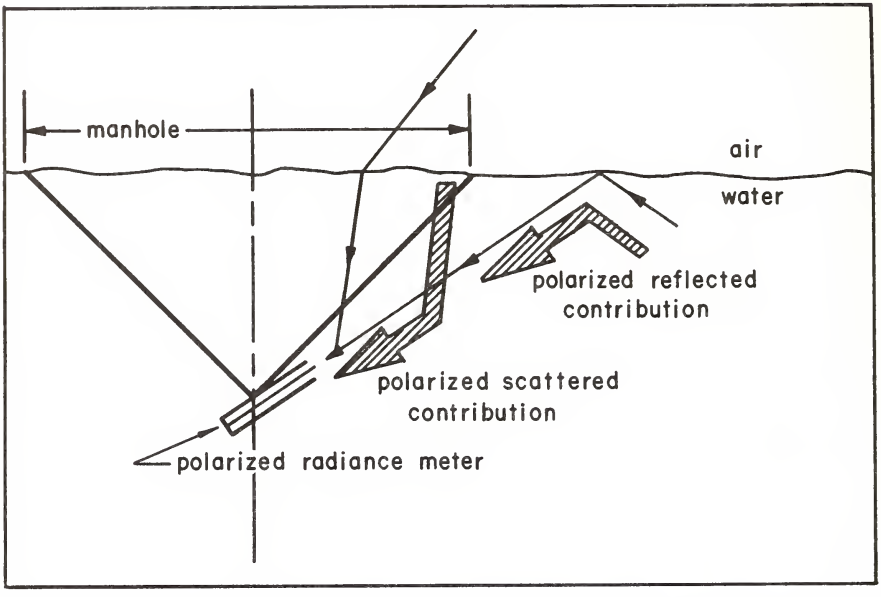

FIG. 1.36 The observed underwater polarized radiance can come from the sky via refraction through the manhole, or from the underwater domain via air-water surface reflection outside the manhole.

of the air-water surface outside the manhole (see Fig. 1.36). These two mechanisms, the scattering and reflection of underwater light, contribute the principal polarized parts to the underwater light field. On purely theoretical grounds (which need not concern us here) one would expect the scattered light to be predominantly linear, and the reflected light to be elliptical, and hence the general underwater light field to be a mixed linear-elliptical polarized field (see Sec. 2.10 and the Stokes Polarization Composition theorem).

The general features of polarized submarine light fields may be summarized, according to Ivanoff and Waterman [117], [118], as follows. In general for a fixed direction ξ the polarization $p(x,\xi)$ is greatest near the air-water surface, and diminishes rapidly with depth down to about 10-20 attenuation lengths and then settles down to an asymptotic value, which does not change with further increase of depth (this is reminiscent of the asymptotic radiance theorem described earlier; and in Sec. 4.6 the potential connections between these two ideas will be outlined). Furthermore, the limiting p value depends on the water clarity, and we would expect on theoretical grounds that it eventually be independent of surface and bottom effects provided the medium is deep enough. It is noted that, all other factors remaining fixed, polarization increases rapidly with transparency from turbid to moderately clear waters, but the increase slows down as waters become more and more transparent. In oceanic hydrosols p may vary,

e.g., from .60 at the surface to .30 as an asymptotic value. In a horizontal sweep, with low sun, the azimuth dependence of p is generally such that in directions normal to the vertical plane of the sun p is greatest, less for directly away from the sun and least of all looking toward the sun. For higher suns or for more turbid waters a horizontal sweep of the radiance tube may find little variation in p. The wavelength dependence of p is such that, with all other factors remaining fixed, p attains a minimum at the blue-green wavelengths (450 mμ)--i.e., just about where in the spectrum natural waters transmit best. This ties in with the observations cited just above about turbidity dependence of p. (Remember the proviso, "all other factors remaining fixed".) Thus both ends of the spectrum should yield higher p values, and hence more pronounced polarized fields in reddish and bluish light --of what there is to measure. The polarization of underwater light fields decreases when diffuseness of the field increases. For example, when depths are shallow, overhead cloudiness will tend to increase the diffuseness and hence decrease the polarization. Under best conditions, the elliptical component of the underwater radiance field reaches about 10% of the total radiance, and about 50% of the linear component. At very great depths the light is predominantly horizontally linearized (because the predominant flow is downward; and recall the analogy with scattered skylight).

Further details will be found in [117], [118], and also in Tyler's article [301]. A simple model for polarized light fields in the sea is developed, along with the general theory, in Sec. 4.6. Sec. 2.10 develops the essentials of the radiometry of polarized light.

Biological Sources of Submarine Light Fields

How many have ever seen the unforgettable sight of luminous bow waves of a ship plowing through nighttime tropical and semitropical waters? Many types of marine animals large and small are known to emit radiant energy when disturbed--a sort of pale cold light, obviously of chemical (quantum) rather than thermal origin. Other organisms seem to flash on and off under their own volition, deep in the sea or in nighttime waters nearer the surface.

An important study of such self-regulative radiometric-biologic phenomena was made by Kampa and Boden [133] in which detailed and careful measurements of the radiant flux output of a certain type of luminescent creatures (*Euphasia pacifica*) were made both *in situ* in the San Diego Trough, and in the laboratory. The presence of these creatures is generally noted by sonar operators because the creatures form a sonic-scattering layer in the water. By lowering a bathyphotometer (a radiant flux meter tightly encased for deep water work) down into the layer, day and night recordings of the output of the *Euphasia* were made.

It was observed that the creatures emitted flashes having a *mean* irradiance of about 1.1×10^{-4} microwatts/cm^2 throughout the day. The output was in the form of flashes

which varied in frequency as a function of time of day--greatest (42/min) during twilight when the *Euphasia* migrated upward, least (10-24/min) during midday when they were at rest in the depths, and intermediate (32/min) during the night. The color of the luminescence was blue-green, with maximum output near 478 mμ, and a secondary maximum near 520 mμ. Kampa and Boden postulate that the time dependence of the depth of the *Euphasia* scattering layer is photoregulated; that is, the creatures constantly monitor the environmental level of irradiance and according raise or lower themselves to a depth at which the total irradiance ($H(z,+) + H(z,-)$) is on the order of 10^{-4} microwatts/cm^2. All this activity transpires along with the flashing at the above-mentioned mean irradiance and frequencies. The type of flashes are temporally highly peaked and these peaks were observed to be one to two orders of magnitude greater than the total environmental irradiance (see Fig. 1.37). It appears that this is an optical means of assuring togetherness during the vertical migrations, for the eye pigment of the *Euphasia* has a greatest photosensitivity to the predominant color of its flashes.

Using the irradiance models developed in Chapter 8, it is a relatively straightforward task to describe and predict the light field generated in the sea by extensive layers of the *Euphasia* or other stratified biological sources of radiant flux. The photoregulative activities of these creatures coupled with the general food chain activities in the seas

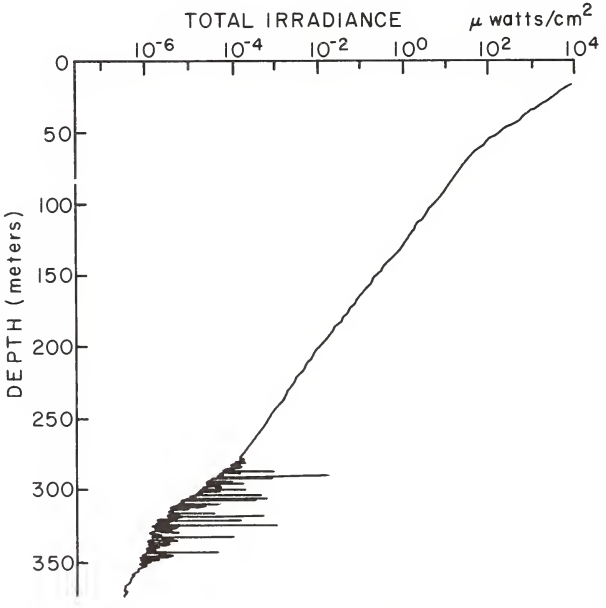

FIG. 1.37 Depth dependence of downward irradiance in which discrete flashes of light generated by *Euphasia pacifica* are evident at the depths around 300-350 meters, as observed by Kampa and Boden in the San Diego Trough, 20 February 1956. (From [133], by permission)

presents a challenging problem to hydrologic optics in the description of the dynamical interactions of plants, animals and photons in seas and lakes. We shall briefly reconsider this problem in Sec. 1.10.

1.3 Three Simple Models for Light Fields

How do we seek order in all that we have encountered above? How do we incorporate those few evidences of order, already glimpsed, into some greater scheme, satisfying for its accuracy, comprehensiveness, and relevance to the main stream of modern physical theory? The number of effects to be described is great, and their intricacy has a tendency to initially intimidate those who attempt a precise description: nature's ways are orderly but infinitely complex, the theorists are few and finite; therefore, each stage of theoretical knowledge inevitably rests on chosen compromises. Three such theoretical compromises are selected for study here; each is designed to describe one facet of the radiometric complex encountered in the seas and lakes of the earth: the first two describe the light fields generated by sunlight and skylight and give simple models for the radiance distributions and two-flow irradiance fields; the third describes artificial light fields set off in the water by man-made point sources and extended artificial sources of radiant flux.

The Two-Flow Model

The two-flow model of the light field pictures the radiant flux in a natural hydrosol X, free of internal sources, as divided into two streams at each depth z below the boundary: a downward stream of radiance H_- and an upward stream of irradiance H_+ (see Fig. 1.38). The primary purpose of the model is to predict H_+ and H_- at each depth z, given H_+ and H_- at the upper boundary, or more generally, given H_+ at some depth and H_- at another (possibly the same) depth. The hydrosol, therefore, is viewed by this model as a *plane-parallel medium*, i.e., an infinite region of space caught between two horizontal parallel planes, which are the *boundaries* of the medium. The physical properties of the hydrosol are described in the present model by means of two optical properties a, b; and the geometrical flow of the radiant energy is described by means of a *distribution factor* D. These three concepts are defined in detail as follows. We write:

"a" for the amount of irradiance *absorbed* from a narrow vertical beam of radiant flux of unit irradiance as it crosses a horizontal layer of unit thickness in X.

"b" for the amount of irradiance *back scattered* without change in wavelength from a given arbitrary stream of radiant flux of unit irradiance as it crosses a horizontal layer of unit thickness in X.

Finally, if h_+, h_- are the scalar irradiances associated with

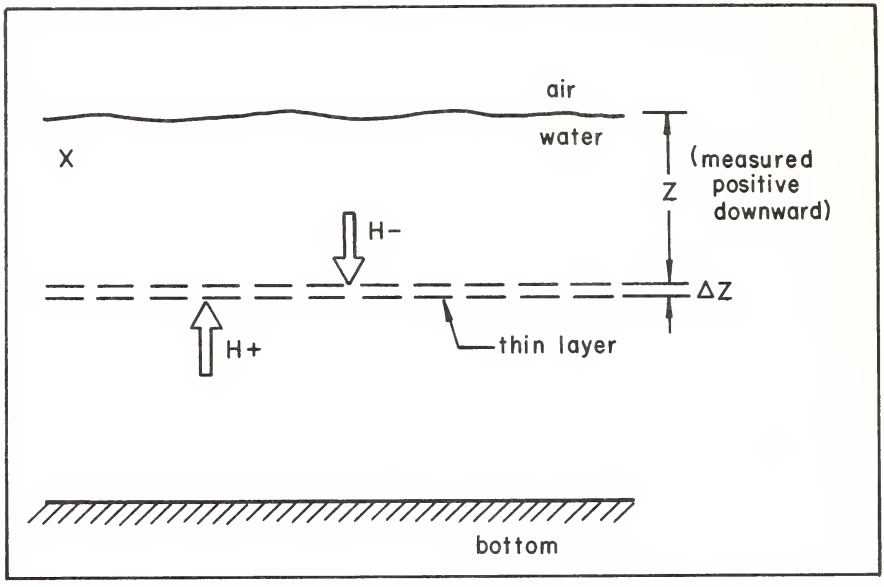

FIG. 1.38 Setting for the two-flow model for irradiance.

the two given streams of radiant flux in X, we write:

$$\text{"}D_{\pm}\text{"} \quad \text{for} \quad h_{\pm}/H_{\pm}$$

$D_{\pm}$ give the mean distances traversed by each stream through a horizontal layer of unit thickness. They are also convenient measures of the diffuseness or collimatedness of the flows. This latter interpretation can be made plausible by a few examples. If the downward stream, say, is collimated, i.e., in the form of a narrow beam which makes an angle θ with the vertical, then from (9), (10) of 1.1 it is easy to see that $D_- = \sec\theta$. Further, if the downward radiance distribution is uniform, then by (11), (15) of Sec. 1.1, we have $D_- = 2$. In the model currently under study, it is assumed that:

$$D_+ = D_- \tag{1}$$

and we shall write "D" for this common value. (On the basis of this assumption, we occasionally call the resultant two-flow model the *one*-D (*two-flow irradiance*) model.) It is easy to see that the amount of irradiance lost by absorption from a flow of unit irradiance and of distribution factor D, as it traverses a unit thickness layer in X, is aD. On the other hand the amount of loss by backscattering is simply b, with the quantity D not appearing explicitly. The reason why absorption is treated differently than scattering in the above sense, rests in the fact that these processes manifest themselves differently geometrically: when flux is absorbed it disappears from the scene; when it is scattered, it must

still be contended with in the radiometric scene. This is discussed further throughout Chapter 8, along with precise definitions of D and b.

We are now ready to derive the basic differential equations of the two-flow model.

Consider the downward stream of radiant flux as it passes through a horizontal layer of thickness Δz, where z is measured positive in the downward direction. (Fig. 1.38) As the stream progresses through the layer, it is partially absorbed and partially scattered backwards to join the upward stream of flux. The total amount of irradiance lost from H_- by these two processes is, according to the definitions of a and b:

$$aDH_-\Delta z + bH_-\Delta z$$

On the other hand, H_- will be increased by that amount of flux, namely $bH_+\Delta z$, scattered backwards from the upward stream. The net change ΔH_- of the downward irradiance, after traversing the layer of thickness Δz, is therefore:

$$\Delta H_- = -(aD + b)H_-\Delta z + bH_+\Delta z \quad . \tag{2}$$

In the same way we find that for the upward stream of radiant flux, which moves through the same layer (so that its associated Δz is negative) the net change ΔH_+ of H_+ is:

$$\Delta H_+ = -(aD + b)H_+(-\Delta z) + bH_-(-\Delta z) \quad . \tag{3}$$

Dividing each side of (2) by Δz, and each side of (3) by $-\Delta z$, and letting $\Delta z \to 0$, we have:

$$\frac{dH_-}{dz} = -(aD + b)H_- + bH_+ \quad , \tag{4}$$

$$-\frac{dH_+}{dz} = -(aD + b)H_+ + bH_- \quad . \tag{5}$$

These equations constitute the two-flow model for light fields in homogeneous stratified natural hydrosols. This model (*the one-D model*), in undecomposed form, in essence goes back to Schuster in 1905 who first formulated similar equations in the astrophysical context. In Chapter 8 we review the high points of the model's history and place it on a sound physical and mathematical basis. For the present, however, we indulge in a relatively uncluttered derivation and solution of the model, in order to point up its central ideas and its simple beauty.

The solution of the system (4), (5) is*

$$H(z,-) = m_+ g_- e^{kz} + m_- g_+ e^{-kz} \tag{6}$$

$$H(z,+) = m_+ g_+ e^{kz} + m_- g_- e^{-kz} \tag{7}$$

where m_+, m_- are arbitrary constants to be fixed by specifying either one of H_+ and H_- at each of two chosen depths (distinct or not), and where we have written:

$$\text{"}g_{\pm}\text{"} \quad \text{for} \quad 1 \pm \frac{aD}{k} \quad , \tag{8}$$

and:

$$\text{"k"} \quad \text{for} \quad [aD(aD + 2b)]^{1/2} \quad . \tag{9}$$

This completes the construction of the two-flow model. We shall put it to work in Sec. 1.4.

The Radiance Model

The radiance model connects the radiances at the beginning and end of an arbitrary path, such as AB, in a natural hydrosol X (Fig. 1.39). Thus, given the radiance at A in the direction ξ, the model yields the radiance at B in the same direction ξ. This model is quite general, for we can choose point A to be on the upper or lower boundary of X and so the radiance at the end B will give the apparent radiance of the boundary; and this is just the radiance one sees or measures at B with a radiance meter.

In order to construct such a model we need to know what happens to the radiance as it travels along a straight path in the water. If we imagine the radiance to be generated by a swarm of photons travelling along the path, then on the one hand we would expect this swarm to lose some members via scattering and absorption at each point along the path. Accordingly, let us write:

"a" for the amount of radiance *absorbed* from a narrow beam of radiant flux of unit radiance travelling a unit distance along a path.

and

"s" for the amount of radiance *scattered* without change in wavelength from a narrow beam of radiant flux of unit radiance travelling a unit distance along a path.

---

*$H(z,+)$ is the value of the function H_+ at depth z. Similarly, $H(z,-)$ is the value of H_- at z. The functional notations "$H_{\pm}$" and "$H(\cdot,\pm)$" are to be considered synonymous and may be used interchangeably.

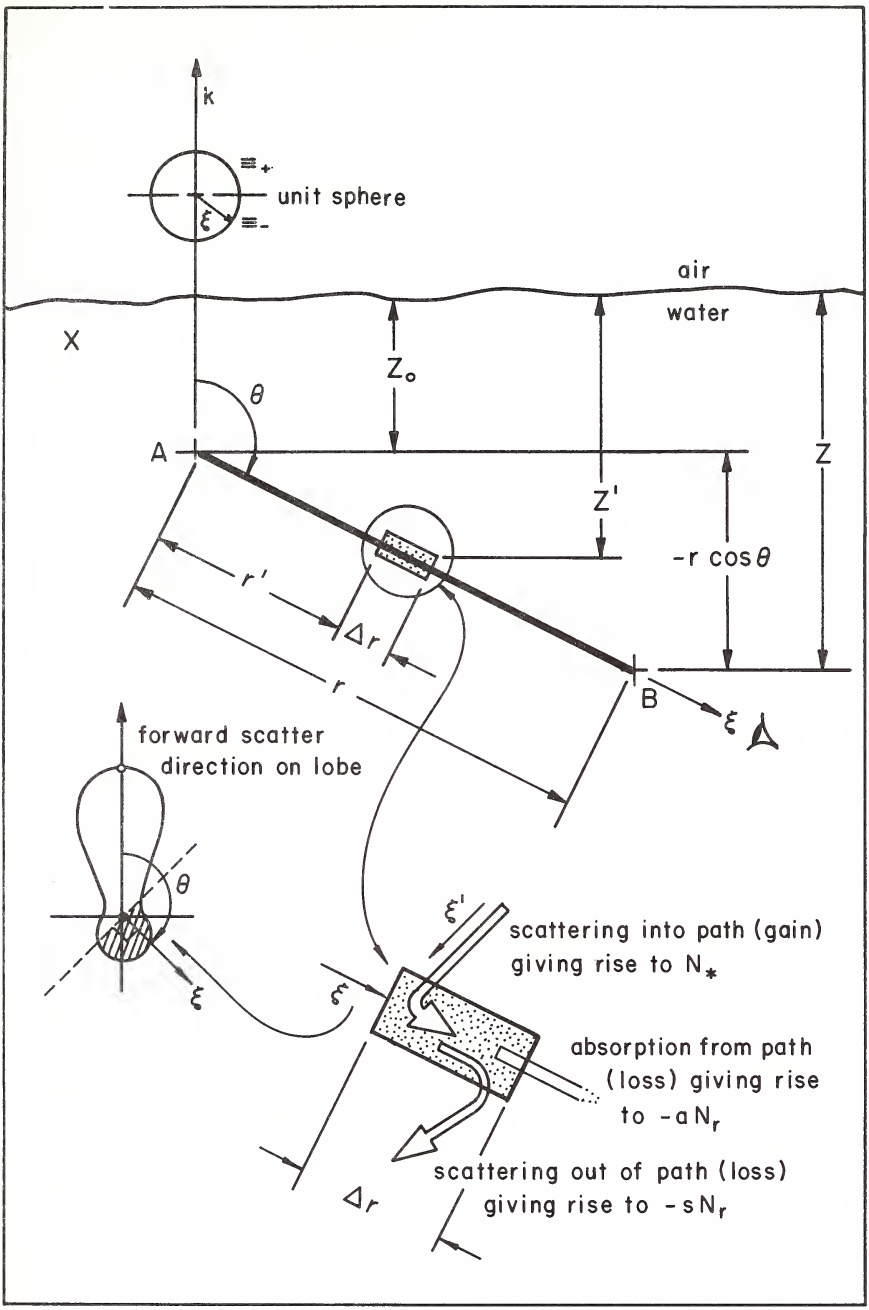

FIG. 1.39 Setting for the radiance model.

We note in passing that the *volume absorption function* a for X just defined is identical with that defined for the two-flow model. The function s is the *volume total scattering function* for X.

Now, on the other hand, we would expect the swarm of photons to gain new members from the surrounding environment simply as a result of some of the nearby photons being scattered into the swarm as it passes along a small segment of its path. Thus, let us write:

"N_*" for the amount of radiance scattered without change in wavelength into a narrow beam of radiant flux travelling a unit distance along a given path past a given point.

If N_0 is the *inherent radiance*, of the path, i.e., the beginning radiance at point A in Fig. 1.39, and N_r is the *apparent radiance* of point A as seen at point B a distance r along the path, then according to the above remarks the change ΔN_r of N_r in the next increment of distance Δr along the path is expected to be:

$$\Delta N_r = -(a + s)N_r\Delta r + N_*\Delta r$$

Dividing by Δr and letting $\Delta r \to 0$, we arrive at

$$\boxed{\frac{dN_r}{dr} = -\alpha N_r + N_*} \qquad (10)$$

where we have written

$$\text{"}\alpha\text{"} \quad \text{for} \quad a + s \quad . \qquad (11)$$

Equation (10) is the *equation of transfer* for radiance. It is the central equation of radiative transfer theory. We call α the *volume attenuation function* and N_* the *path function*. The equation is used to connect the value $N_r(z,\theta)$ of N_r at depth z, in the direction θ with the value $N_0(z_0,\theta)$ of N_0 at depth z_0 in the direction θ. (See Fig. 1.39.)

As it stands, (10) looks like a simple differential equation, and, indeed, it is readily integrated if we know α and N_* along the path. We shall assume α to be constant along the path, and N_* to be given along the path, and that N_* varies only with depth. Then it is easily verified that the general solution of (10) is (see, e.g., (1)-(3) of Sec. 3.15):

$$\boxed{N_r(z,\theta) = N_0(z_0,\theta)e^{-\alpha r} + \int_0^r N_*(z',\theta)e^{-\alpha(r-r')}dr' \qquad (12)$$

$$z' = z_0 - r'\cos\theta}$$

The simple model we are interested in at present rests on the assumption that $N_*(z,\theta)$ in optically very deep media depends only on depth z in X, in the manner:

$$N_*(z,\theta) = N_*(0,\theta)e^{-Kz} \tag{13}$$

where K is the empirical depth rate of decay of the general light field in X. For example it may be taken as the empirical K in (7) of 1.2, or the theoretical k in (9) above encountered in the two-flow model (cf. (61) of Sec. 1.4). At any rate, using (13) in (12), performing the integration and simplifying, we have:

$$N_r(z,\theta) = N_o(z_o,\theta)e^{-\alpha r} + \frac{N_*(z,\theta)}{\alpha+K\cos\theta}\left[1-e^{-(\alpha+K\cos\theta)r}\right] \tag{14}$$

This is the requisite simple model for radiance. We shall study it later to see if it helps us understand some of the observed properties of the underwater light field surveyed in Sec. 1.2. It is a simple matter to generalize (14) to the case where $N_*(z,\theta)$ depends also on the azimuth angle ϕ. (See Chapter 4.) For the present we can think of (14) holding in an arbitrary given azimuth plane.

The Diffusion Model

The diffusion model is designed to describe the spatial variation of scalar irradiance in a natural hydrosol. This model together with the two-flow model for irradiance, and the model for radiance, forms a reasonably exhaustive battery of elementary descriptions of most of the natural and artificial light fields encountered in everyday practice.

A simple and instructive route to the diffusion model can be made via the two-flow model (4), (5), as follows. Let us add together, term by corresponding term, the two equations (4), (5). We find:

$$\frac{d(H_- - H_+)}{dz} = -aD(H_+ + H_-) \tag{15}$$

Now, according to (8) of Sec. 1.1 and the definition of *net irradiance* $\overline{H}(z,+)$, which is defined by writing:

$$\text{"}\overline{H}(z,+)\text{"} \quad \text{for} \quad H(z,+) - H(z,-) \quad ,$$

or more briefly:

$$\text{"}\overline{H}_+\text{"} \quad \text{for} \quad H_+ - H_-$$

$$\text{"}\overline{H}_-\text{"} \quad \text{for} \quad H_- - H_+ \quad ,$$

we can cast (15) into the form

$$-\frac{d\bar{H}_-}{dz} = \frac{d\bar{H}_+}{dz} = ah \quad , \tag{16}$$

using the definition of the distribution factor D, and (1). This states that the depth rate of change of the net upward irradiance at a point is jointly proportional to the volume absorption coefficient and the scalar irradiance at that point.

Readers familiar with the rudiments of vector analysis will see that either derivative term on the left side of (16) is simply the negative of the divergence of the vector irradiance **H** (cf. (4) of Sec. 1.1). The other two (the x,y) derivatives of the components of H are missing from (16) because the two-flow model applies to *stratified* media, i.e., media whose properties are constant over horizontal planes in the hydrosol. However, this recognition of the nature of the left side of (16) permits us to write:

$$\nabla \cdot \mathbf{H} = -ah \tag{17}$$

in place of (16).

Equation (17), despite the route we have just taken, is a quite general law which holds in source-free media of arbitrary shape and inhomogeneities and whose light fields are of arbitrary spatial and directional structure. We have in this way made a leap from the special to the general by making a simple observation on the mathematical form of the divergence of a vector field. (For further details, see (5) of Sec. 2.8 and (15) of Sec. 8.8.) An even more general form can be obtained if we allow the presence of sources in the medium:

$$\nabla \cdot \mathbf{H} = -ah + h_\eta \tag{18}$$

where h_η is the radiant flux generated per unit volume by internal sources.

Now, the diffusion model we are interested in springs from (18) once we have made a special assumption about the behavior of the light field and the nature of the term h_η. The requisite assumption is concerned with the *scattered* light field in the medium of interest, so that we shall look only at the components of **H** and h which consist of radiant flux having been scattered at least once. In order to point this up in the notation, it can be shown that we may write (17) in a form quite analogous to (18):

$$\nabla \cdot \mathbf{H}^* = -ah^* + h_*^1 \tag{19}$$

This star notation is standard notation for scattered radiant flux. To indicate how we may arrive at (19), we first observe that the full vector and scalar irradiance fields are represented as:

$$\mathbf{H} = \mathbf{H}^{o} + \mathbf{H}^{*} \tag{20}$$

$$h = h^{o} + h^{*} \tag{21}$$

where $\mathbf{H}^{o}$, h^{o} consist of residual radiant flux directly transmitted from the sources and boundaries. When written in this form, we say that the light field $\mathbf{H}$ has been *decomposed* into its residual and scattered parts. This mode of decomposition is not new to our discussions in this chapter. For we have in effect represented the apparent radiance N_r in (12) in precisely this way. Indeed, if in the context of (12) we write

$$\text{"}N_r^{o}\text{"} \quad \text{for} \quad N_o e^{-\alpha r} \tag{22}$$

and

$$\text{"}N_r^{*}\text{"} \quad \text{for} \quad \int_0^r N_* e^{-\alpha(r-r')} dr' \quad , \tag{23}$$

then the equation (12) for apparent radiance N_r becomes (in functional form):

$$N_r = N_r^{o} + N_r^{*} \tag{24}$$

where N_r^{o} is the *residual radiance* and N_r^{*} the *path radiance*. This form is completely analogous to (20), (21). In fact, all we have to do to get (20), (21) is integrate (24) over all directions and apply (3), (4) of Sec. 1.1 (cf. Secs. 6.5 and 6.6). Hence if we integrate each side of (10) over all directions in this manner, we can obtain (19) quite rigorously. The complete details of this derivation may be found in the derivation of (63) of Sec. 6.6.

We return to (19), and make the assumption about $\mathbf{H}^{*}$ which invokes the desired diffusion model. The assumption is simply this:

$$\mathbf{H}^{*} \text{ shall be proportional to } -\nabla h^{*} \tag{25}$$

Here ∇h^{*} is the gradient of h^{*}. For example, in a stratified plane-parallel medium, this amounts to saying that:

$$\mathbf{H}^{*} = (H_-^{*} - H_+^{*})(-\mathbf{k}) = -\frac{dh^{*}}{dz}(-\mathbf{k}) \times (\text{constant})$$

i.e., that the scattered irradiance vector--which in the sea clearly points downward in the direction of greatest net irradiance--is simply the derivative of the scattered scalar irradiance times the unit downward vector $(-\mathbf{k})$, i.e., the vector pointing along the direction of increasing z. It is interesting to note that this is a sort of backwards version of

(16), obtained from the latter essentially by moving the derivative operation from its left to its right side. Notice that $\mathbf{H}^*$ is required by (25) to point in the direction of decrease of h. In natural waters dh/dz is negative (with increasing z measured downward as usual). We shall use the conventional symbol "D" for the diffusion constant of proportionality. Notice that its dimension is that of a length. (We use the letter "D" here without fear of confusion with our distribution coefficients.) Hence assumption (25) can be written as an equality:

$$\mathbf{H}^* = -D\nabla h^* \tag{26}$$

and when this assumption is used in (19) we have:

$$\nabla\cdot(-D\nabla h^*) = -ah^* + h_*^1$$

or, since D is a constant we have, finally:

$$\boxed{-D\nabla^2 h^* + ah^* = h_*^1} \quad \begin{array}{l}\text{(diffusion}\\ \text{equation for}\\ \text{decomposed}\\ \text{light field)}\end{array} \tag{27}$$

which is the present desired form of the diffusion model. The symbol "∇^2" is the laplacian operator used in vector analysis. In this model we assume that the source term h_*^1 describes the origin of the scattered scalar irradiance h^* and thereby is of the form:

$$h_*^1 = h^o s \tag{28}$$

where s is the volume total scattering coefficient defined in the preceding radiance model discussion and h^o is the scalar irradiance associated with the residual flux from the source and boundaries. The diffusion model takes its name from the assumption (26), which is *Fick's law of diffusion*, now applied to the diffusion of photons.

Equation (27) as it stands constitutes a reasonably good model of the scattered (or diffuse) scalar irradiance in both natural and artificial light fields. By way of contrast, we observe that it is more accurate than the diffusion model that comes from applying (26) (without the stars) to (18), instead of (26) to (19). For in the former case, i.e., when applying (26) (without the stars) to (18) we find

$$\boxed{-D\nabla^2 h + ah = h_\eta} \quad \begin{array}{l}\text{(diffusion}\\ \text{equation for}\\ \text{undecomposed}\\ \text{light field)}\end{array} \tag{29}$$

and even though the mathematical forms of (27) and (29) are the same, an essential difference between them arises by virtue of the nature of the source term h_η. In the case of (29), h_η for artificial point sources is a Dirac delta function, whereas in (27), as we see by (28), h_*^1 is a relatively

smoothly varying function throughout the medium. Since diffusion models become more accurate the smoother the spatial variation of the source terms, the superiority of (27) over (29) is quite clear.

However, it takes correspondingly more effort to solve (27) than it does (29). The formal solution of (29) for a point source is straightforward, and takes the form:

$$\boxed{h(r) = \frac{J_o e^{-\kappa r}}{Dr}} \quad \text{(undecomposed } h\text{, and point source)} \tag{30}$$

where we have written

$$\text{"}J_o\text{"} \quad \text{for} \quad \frac{P_o}{4\pi} \ , \tag{31}$$

and P_o is the radiant flux output of the point source, assumed to be uniform in all directions. Furthermore r is distance from the observation point to the point source, and we have written:

$$\text{"}\kappa\text{"} \quad \text{for} \quad \sqrt{\frac{a}{D}} \ , \tag{32}$$

where a is the volume absorption coefficient for the medium, and D is the diffusion constant (cf. (27) of Sec. 6.5).

The general solution of (27) is now forthcoming by means of (30) and a straightforward integration. To see this, we imagine that at each point $\mathbf{x}'$ of the Medium X (which is an extensive region without perturbing boundaries) the residual scalar irradiance $h^o(\mathbf{x}')$ is scattered, there to give rise to an entirely new point source problem whose solution at an observation point $\mathbf{x}$ is described by (30), now written in the form:

$$h_s(r) = \frac{J_o(\mathbf{x}')e^{-\kappa r}}{Dr} \tag{33}$$

where

$$r = |\mathbf{x}-\mathbf{x}'| \tag{34}$$

and

$$J_o(\mathbf{x}') = \frac{h^o(\mathbf{x}')s}{4\pi} = \frac{1}{4\pi} h^1_* \tag{35}$$

Hence if the original point source is at the origin (i.e., at $\mathbf{x}=0$), and of a relatively mild directional output, then the scalar irradiance field $h(\mathbf{x})$ at $\mathbf{x}$ is given very nearly by:

$$h(\mathbf{x}) = h^o(\mathbf{x}) + h^*(\mathbf{x}) \tag{36}$$

where

$$h^*(\mathbf{x}) = \int_X h_s(\mathbf{x}')\, dV(\mathbf{x}') \tag{37}$$

and

$$h^o(\mathbf{x}') = N^o \Omega(\mathbf{x}') e^{-\alpha r'} s \tag{38}$$

and where

$$r' = |\mathbf{x}'| \quad , \tag{39}$$

and $\Omega(\mathbf{x}')$ is the solid angular subtense of the point source as measured at $\mathbf{x}'$. The source is actually a small finite sphere of surface radiance N^o in the direction $\xi' = \mathbf{x}/|\mathbf{x}'|$. V is the volume measure in X. We shall not go into further details here. See (66) of Sec. 6.6 in particular, and Sec. 6.6 in general for complete details.

1.4 Some Deductions from the Light Field Models

The three models for natural and artificial light fields derived above allow us to explain and interrelate many of the observed features of light fields in natural hydrosols. We shall consider here and in subsequent sections a small representative sample of such activity, based on simple deductions from the three models.

The Decay of the General Light Field with Depth

We shall now show how (7) of Sec. 1.2 follows from the two-flow model for light fields. Toward this end, we let the scattering medium X be infinitely deep and be absorbing, i.e., a>0. Then we compute the net downward irradiance at a general depth, using (6), (7) of Sec. 1.3.

$$\begin{aligned} \bar{H}(z,-) &= H(z,-) - H(z,+) \\ &= (g_- - g_+)\left[m_+ e^{kz} - m_- e^{-kz} \right] \end{aligned} \tag{1}$$

Now from (16) of Sec. 1.3 we find, by integrating between depths 0 and z, and noting that h(z) is a non negative quantity for all z:

$$\bar{H}(z,-) - \bar{H}(0,-) = \int_0^z \frac{d\bar{H}(z',-)}{dz'} = -a\int_0^z h(z')\, dz' \leq 0$$

Hence for all z:

$$\bar{H}(z,-) \leq \bar{H}(0,-) \tag{2}$$

This shows that the net downward irradiance is bounded. Indeed, from Tables 2, 3 of Sec. 1.2 we can estimate an upper bound of $\bar{H}(z,-)$ as 1396 watts/m^2, and infer that $\bar{H}(z,-) \geq 0$ in real optical media. It follows that (2) and (1), along with $a > 0$, force m_+ to be zero; otherwise we could find a depth z at which (2) would be violated. Some further general inequalities related to (2) are given in Sec. 9.2.

Having established that $m_+=0$ in infinitely deep absorbing media, (6), (7), of Sec. 1.3 yield the requisite forms of $H(z,\pm)$ for every z:

$$H(z,-) = m_- g_+ e^{-kz} \tag{3}$$

$$H(z,+) = m_- g_- e^{-kz} \quad . \tag{4}$$

From (3), (4) we have, on setting z=0:

$$H(0,-) = m_- g_+$$

$$H(0,+) = m_- g_-$$

Let us write

$$\text{"}R_\infty\text{"} \quad \text{for} \quad H(0,+)/H(0,-)$$

Clearly, we then have from (3), (4):

$$R_\infty = \frac{H(0,+)}{H(0,-)} = \frac{H(z,+)}{H(z,-)} = \frac{g_-}{g_+} = \frac{1-\frac{aD}{k}}{1+\frac{aD}{k}} = \frac{k-aD}{k+aD} \tag{5}$$

This shows that the reflectance R_∞ of the medium is independent of depth and determinable once a, k, and D are known. Hence for every z,

$$H(z,+) = H(z,-)R_\infty$$

where

$$m_- = \frac{H(0,+)}{g_+ R_\infty} = \frac{H(0,+)}{g_-} = \frac{H(0,-)}{g_+}$$

Thus we have shown, among other things that:

$$H(z,\pm) = H(0,\pm)e^{-kz} \tag{6}$$

for all z.

Furthermore, by definition of the distribution factor D (cf. (1) of Sec. 1.3) we have, with the help of (8) of Sec. 1.1:

$$\begin{aligned} h(z) &= h(z,+) + h(z,-) \\ &= D(H(z,+) + H(z,-)) \\ &= D(H(0,+) + H(0,-)) \, e^{-kz} \\ &= h(0) \, e^{-kz} \end{aligned} \tag{7}$$

which is the theoretical basis for (7) of Sec. 1.2.

Observe how the assumption that a>0, is needed in various parts of the arguments above. This assumption is quite reasonable in terrestrial settings; indeed, in such settings the condition a=0 for every wavelength is never observed. What would the light field look like in an infinitely deep medium in which a=0? Equation (1) shows us that if a=0 for all wavelengths, then: since $g_- = g_+ = 1$,

$$\bar{H}(z,-) = 0$$

so that

$$H(z,-) = H(z,+)$$

at all depths z and for all wavelengths. The sea would be of the same general brightness and color of the sky in this case --at every depth!

Reflectance and Transmittance of Finitely Deep Hydrosols

The simple two-flow model allows us to estimate the reflectances and transmittances of finitely deep layers of water. We return to (6), (7) of Sec. 1.3 and consider a finitely deep homogeneous layer whose upper surface is at 0 and whose lower surface is at z. The upper surface is irradiated with a given irradiance H(0,-) and we set H(z,+)=0, which simulates zero irradiation at the lower boundary (Fig. 1.40 (a)). We then find the m_+, m_- corresponding to these two given irradiances, and solve for H(0,+). Thus, if under these conditions we write

$$\text{"}R_\gamma(\tau)\text{"} \quad \text{for} \quad H(0,+)/H(0,-)$$

then $R_\gamma(\tau)$ is the *reflectance* of the slab of (diffuse) optical depth* $\tau = kz$, and $R_\gamma(\tau)$ is found to be of the form:

$$\boxed{R_\gamma(\tau) = (1-\gamma^2) \, \frac{e^{\tau} - e^{-\tau}}{(1+\gamma)^2 e^{\tau} - (1-\gamma)^2 e^{-\tau}}} \tag{8}$$

*There are many 'optical depths' possible in radiative transfer theory; one for each scattering or absorbing concept. In the present case we use k as a base for optical depth.

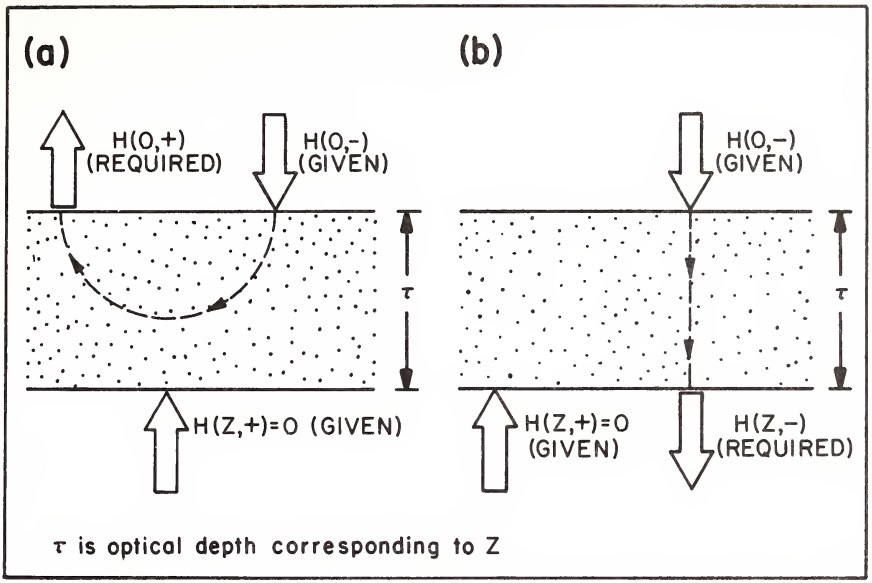

FIG. 1.40 Boundary conditions for the reflectance and transmittance of finitely deep layers in a hydrosol.

where we have written:

$$\text{"}\gamma\text{"} \quad \text{for} \quad \frac{aD}{k} \quad . \tag{9}$$

The transmittance $T_\gamma(\tau)$ of the slab of optical depth τ can be found in an analogous manner (Fig. 1.40 (b)) by now seeking $H(z,-)$ under the same conditions. Thus if we write:

$$\text{"}T_\gamma(\tau)\text{"} \quad \text{for} \quad H(z,-)/H(0,-) \quad ,$$

then it follows that:

$$T_\gamma(\tau) = \frac{4\gamma}{(1+\gamma)^2 e^{\tau} - (1-\gamma)^2 e^{-\tau}} \tag{10}$$

One should see that, because the medium is homogeneous, $R_\gamma(\tau)$ and $T_\gamma(\tau)$ depend spatially only on the optical depth τ, so that (8) and (10) pertain to any slab of thickness τ in the medium regardless of its vertical location within the medium.

It will also be interesting to look at some of the limiting values of $R_\gamma(\tau)$ and $T_\gamma(\tau)$ for various extreme values of τ and γ. For example, one may verify that:

$$\lim_{\tau \to 0} R_\gamma(\tau) = 0 \tag{11}$$

$$\lim_{\tau \to \infty} R_\gamma(\tau) = \frac{1-\gamma}{1+\gamma} = R_\infty \tag{12}$$

$$\lim_{\tau \to 0} T_\gamma(\tau) = 1 \tag{13}$$

$$\lim_{\tau \to \infty} T_\gamma(\tau) = 0 \tag{14}$$

$$\lim_{\tau \to 0} \frac{R_\gamma(\tau)}{\tau} = \frac{1-\gamma^2}{2\gamma} = \frac{b}{k} \tag{15}$$

$$\lim_{\tau \to 0} \frac{1-T_\gamma(\tau)}{\tau} = \frac{1+\gamma^2}{2\gamma} = \frac{aD+b}{k} \tag{16}$$

From (15) we see that the reflectance of very thin slabs is proportional to the backscattering coefficient b. Indeed,

$$\lim_{z \to 0} \frac{R_\gamma(\tau)}{z} = b$$

so that:

$$R_\gamma(\tau) \cong bz \tag{17}$$

for small τ. From (16) we see that the transmittance of very thin slabs is:

$$T_\gamma(\tau) = 1 - (aD+b)z \quad . \tag{18}$$

From (17), (18) we conclude that for thin slabs:

$$R_\gamma(\tau) + T_\gamma(\tau) = 1 - (aD)z$$

and if in general we write:

$$\text{"}A_\gamma(\tau)\text{"} \quad \text{for} \quad 1 - \left[R_\gamma(\tau) + T_\gamma(\tau)\right] \tag{19}$$

we see that in particular for thin slabs:

$$A_\gamma(\tau) \cong (aD)z \quad . \tag{20}$$

Clearly $A_\gamma(\tau)$ for general τ is the amount of irradiance absorbed by a slab of optical thickness τ and with optical properties a, b, and D. From (19) we have the general conservation law:

$$A_\gamma(\tau) + R_\gamma(\tau) + T_\gamma(\tau) = 1 \tag{21}$$

Figs. 1.41, 1.42 represent $R_\gamma(\tau)$ and Fig. 1.43 represents $T_\gamma(\tau)$ for a selected set of γ and τ values. Values of k and γ can be obtained by direct computation from the definitions of k and γ, or by their graphs in Figs. 1.44, 1.45. The computations were done by Mrs. Judith Marshall.

Invariant Imbedding Relations for Irradiance

We now wish to investigate a particularly interesting property of the reflectance and transmittance functions $R_\gamma(\tau)$ and $T_\gamma(\tau)$ defined above. This property will allow us to write down Eqs. (6),(7) of Sec. 1.3 by sight for homogeneous media with transparent boundaries. We shall fix attention on an arbitrary medium X whose upper boundary is at optical depth 0 and whose lower boundary is at optical depth c (= zk), where z is the geometric depth of the medium. Since X is fixed throughout the present paragraph, we can drop the "γ" from the R and T notation. Furthermore, to emphasize the geometric limits of X we shall denote it by "X(0,c)".

Now suppose X(0,c) is irradiated at the upper boundary only. Then by definition of R(c) and T(c) we have:

$$H(0,+) = H(0,-)\ R(c) \tag{22}$$

$$H(c,-) = H(0,-)\ T(c) \tag{23}$$

This is a simple application of (8) and (10) and the basic meanings of R(c) and T(c). Next, assume that X(0,c) is irradiated only on its lower boundary. Then, by the same token:

$$H(0,+) = H(c,+)\ T(c) \tag{24}$$

$$H(c,-) = H(c,+)\ R(c) \tag{25}$$

These formulas follow rigorously using the pattern of derivation leading to (8) and (10). However, they should be intuitively clear simply on the basis that T(c) and R(c) are transmittances and reflectances of homogeneous slabs of scattering absorbing material of optical thickness c in which complete symmetry of the light field has been assumed (in the form of (1) of Sec. 1.3).

Furthermore, and this is a crucial step, because the basic differential equations of the two-flow model are linear, we have at our beck and call the mathematical principle of linear superposition of solutions of these equations. Thus, if X(0,c) is irradiated simultaneously at levels 0 and c,

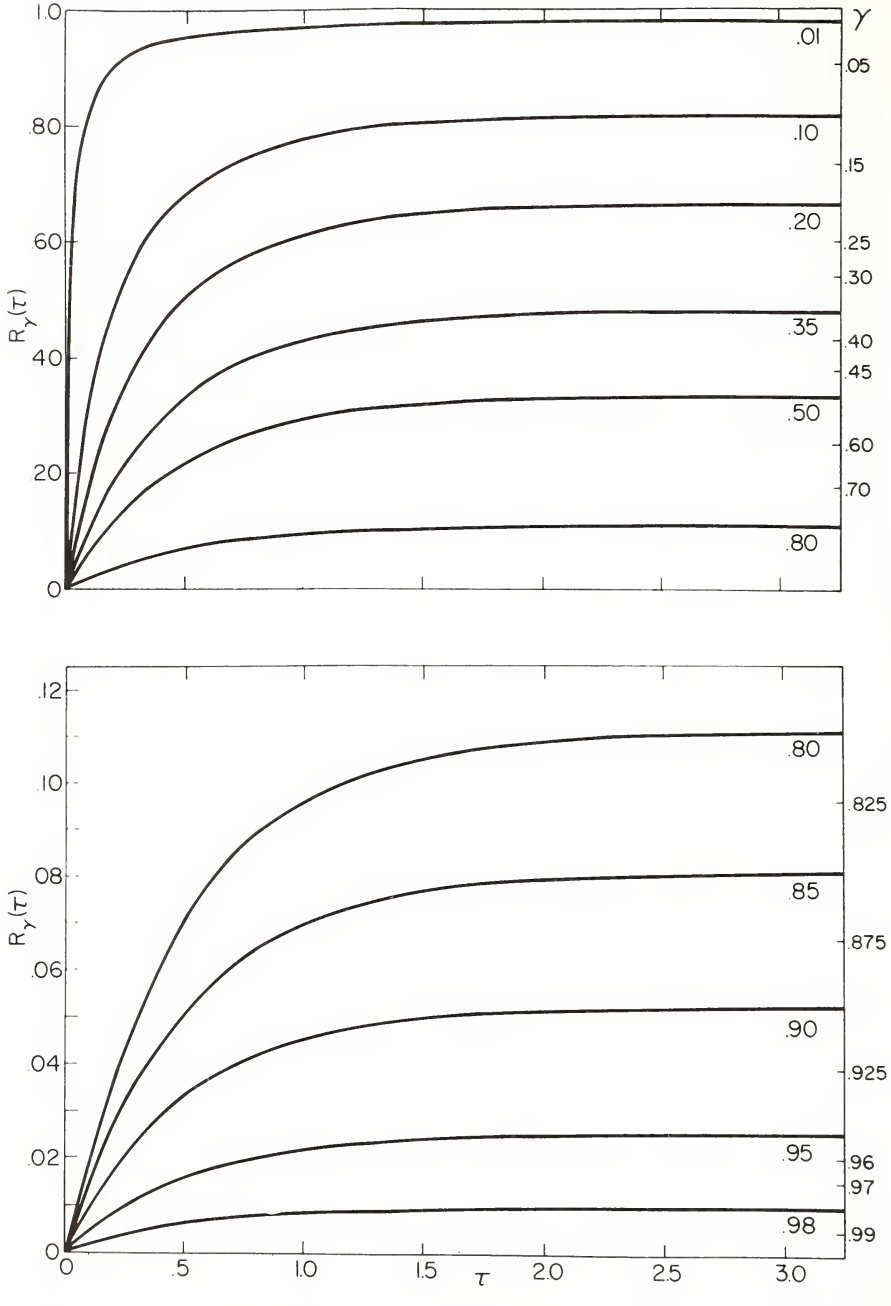

FIG. 1.41 Calculated reflectance $R_\gamma(\tau)$ versus τ, for $.01 \leq \gamma \leq .80$.

FIG. 1.42 Calculated reflectance $R_\gamma(\tau)$ versus τ, for $.80 \leq \gamma \leq .98$.

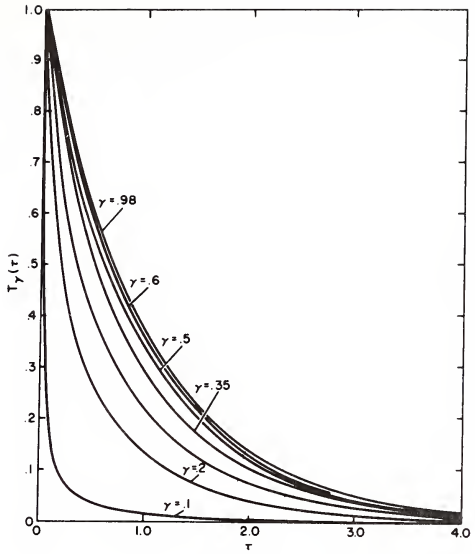

FIG. 1.43 Calculated transmittance $T_\gamma(\tau)$ versus τ, for $.01 \leq \gamma \leq .98$.

then we would be correct in writing the observed emergent irradiances at levels 0 and c as:

$$H(0,+) = H(0,-)R(c) + H(c,+)T(c) \tag{26}$$

$$H(c,-) = H(0,-)T(c) + H(c,+)R(c) \ . \tag{27}$$

These equations are readily forthcoming from (6), (7) of Sec. 1.3; however, we shall imagine for the moment that they form a relatively new basis for approaching radiative transfer problems, and that they are just as basic (as indeed they are) as the two-flow equations (4), (5) of Sec. 1.3 in setting up the foundations of the two-flow model. We shall spend much time on this point of view and its generalizations in Chapters 3, 7, and 8. For the moment we adopt it in the form of (26) and (27) and apply it in a simple and direct manner so as to explain the essential ideas behind it.

In order to illustrate in a relatively concrete manner the properties of (26) and (27), we shall consider an actual natural hydrosol in the framework of the one-D model. Thus let us suppose that

$D = 2$ (diffuse light distribution factor)

$a = .117/m$ (volume absorption coefficient)

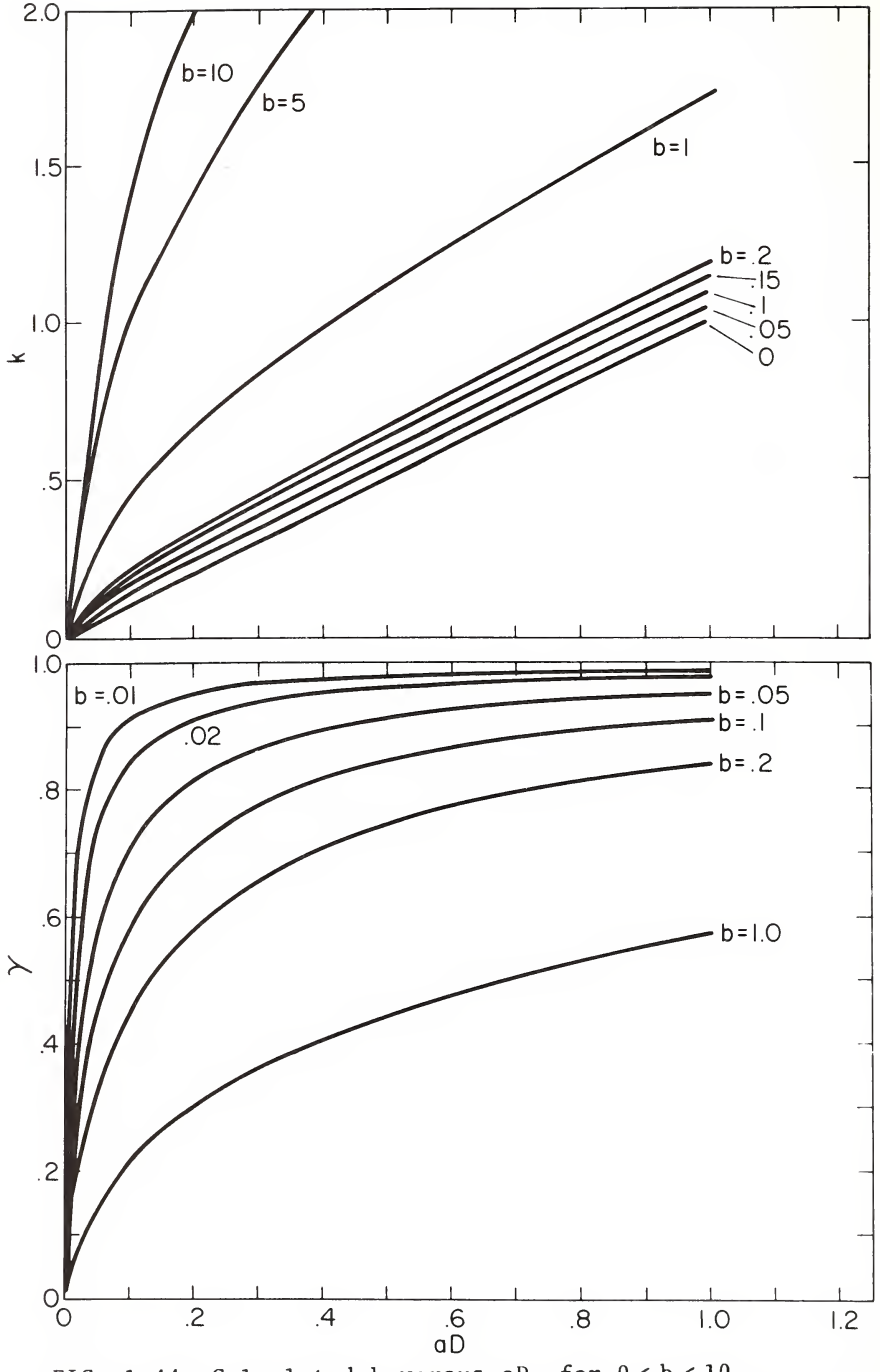

FIG. 1.44 Calculated k versus aD, for $0 \leq b \leq 10$.
FIG. 1.45 Calculated γ versus aD, for $.01 \leq b \leq 1.0$

Hence:

$aD = .234/m$ (volume absorption coefficient for diffuse light)

Further we suppose:

$s = .325/m$ (volume total scattering coefficient)

and

$b = .010/m$ (volume backward scattering coefficient for diffuse light)

From the graphs for γ, and k, we find that for this medium

$$\gamma = .96$$

$k = .250/m.$ (diffuse attenuation coefficient)

For later reference we note that:

$\alpha = a+s = .442/m$ (volume attenuation coefficient)

For a medium of depth:

$$z = 4 \text{ meters},$$

we have an optical depth of:

$$c = zk = 1.$$

According to the graphs for R and T, for such a medium:

$$R(1) = .018$$

$$T(1) = .360$$

and so:

$$A(1) = .622.$$

All these optical properties are to be considered for illustrative purposes only. In the present example, they pertain not to a single wavelength but to average values over the visible spectrum. Suppose that the medium X(0,1) has transparent upper and lower boundaries and that it is irradiated such that:

$$H(0,-) = 500 \text{ watt/m}^2$$

$$H(1,+) = 100 \text{ watt/m}^2 \ .$$

The H(0,-) chosen here simulates a typical visible spectrum irradiance produced by a noonday sun at sea level on a horizontal plane, under a sky with clear dry air (cf. Table 2 of Sec. 1.2). Then the upward irradiance at the upper boundary is, according to (26):

$$H(0,+) = 500 \times .018 + 100 \times .360$$

$$= 45 \text{ watts/m}^2 \ .$$

The downward irradiance at the lower boundary is:

$$H(1,-) = 500 \times .360 + 100 \times .018$$

$$= 182 \text{ watts/m}^2 \quad .$$

Finally, the number of incident watts absorbed per square meter of boundary within X(0,1) are:

$$(H(0,-) + H(1,+)) \times .622 = 373 \text{ watts/m}^2$$

Suppose now that X(0,1) has a reflecting lower boundary. We wish to show next that the upward irradiance H(1,+) just above the lower boundary of X(0,1) can be computed directly, if the reflectance r of the lower boundary is known. Suppose that

$$r = .050$$

and suppose that only H(0,-) is given. Let the associated light field be set up in X(0,1). Then if we know the irradiance H(1,-) on the lower boundary, we have:

$$H(1,+) = H(1,-)r \tag{28}$$

H(1,+) is the incident irradiance on the body of X(0,1) just within its lower boundary. Then, by (27),

$$H(1,-) = H(0,-)T(1) + H(1,+)R(1) \tag{29}$$

Combining (28), (29) we have, on solving for H(1,-):

$$H(1,-) = \frac{H(0,-)T(1)}{1-rR(1)} \tag{30}$$

Suppose that H(0,-) = 500 watts/m^2, then (30) yields:

$$H(1,-) = \frac{500 \times .360}{1-.05 \times .02}$$

$$= 180 \text{ watts/m}^2 \quad .$$

In other words, on comparing this H(1,-) with that worked out above, a bottom boundary reflecting by an amount r = .050 will contribute essentially nothing measurable to H(1,-). By (28) we have

$$H(1,+) = 180 \times .050 = 9 \text{ watts/m}^2$$

What should the reflectance r of the lower boundary be in order to yield the H(1,+) = 100 watts/m^2 we used in the first illustration above? Multiplying each side of (30) by r, and using (28) we have

$$H(1,+) = \frac{H(0,-)rT(1)}{1-rR(1)}$$

Solving for r:

$$r = \frac{H(1,+)}{H(1,+)R(1) + H(0,-)T(1)}$$

$$= \frac{100}{100 \times .018 + 500 \times .360}$$

$$= \frac{100}{182} = .550$$

which could for example simulate a light sandy bottom. Observe that the denominator in the preceding expression for r is simply H(1,-), under the present boundary conditions.

These examples begin to show the use of the one-D model in making elementary calculations concerning everyday matters in the study of hydrologic optics, including the effects of nontransparent boundaries.

We continue with another illustration which shows how to find the internal irradiances in X(0,1) knowing the incident irradiances on its transparent upper and lower boundaries. Suppose we have the incident irradiances:

$$H(0,-) = 500 \text{ watts/m}^2$$

$$H(1,+) = 100 \text{ watts/m}^2$$

We want to find H(1/2,±), i.e., the irradiances at the mid-level of the present medium. Now since (26), (27) hold for arbitrary media of optical depths c, let us apply them to the two subslabs X(0,1/2), and X(1/2,1) which comprise the upper and lower halves of X(0,1), respectively (see Fig. 1.46).

Applying (26), (27) to X(0,1/2):

$$H(0,+) = H(0,-)R(1/2) + H(1/2,+)T(1/2) \qquad (31)$$

$$H(1/2,-) = H(0,-)T(1/2) + H(1/2,+)R(1/2) \qquad (32)$$

Of the irradiances we know only H(0,-), and we want to find H(1/2,±). We also do not know H(0,+). We therefore need more relations. Returning to (26), (27), and applying them to X(1/2,1), we have:

$$H(1/2,+) = H(1/2,-)R(1/2) + H(1,+)T(1/2) \qquad (33)$$

$$H(1,-) = H(1/2,-)T(1/2) + H(1,+)R(1/2) \qquad (34)$$

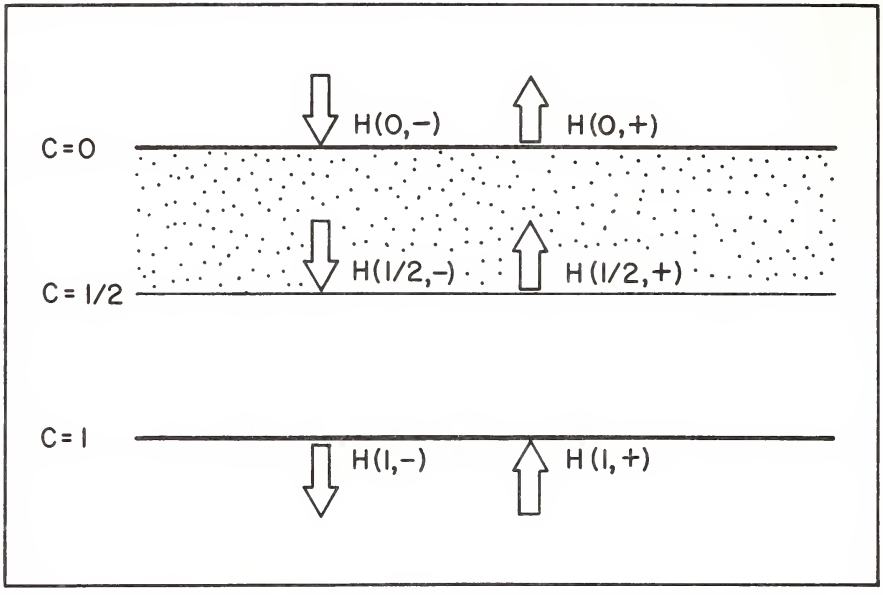

FIG. 1.46 Using invariant imbedding ideas to calculate internal irradiances from boundary irradiances.

Here we know H(1,+), and we have more relations for H(1/2,±) with another unknown H(1,-). But now we have four equations in four unknowns which we can solve for H(1/2,±), and rearrange as follows.

$$H(1/2,-) = H(0,-)\mathcal{T}(0,1/2,1) + H(1,+)\mathcal{R}(1,1/2,0) \quad (35)$$

$$H(1/2,+) = H(0,-)\mathcal{R}(0,1/2,1) + H(1,+)\mathcal{T}(1,1/2,0) \quad (36)$$

where for the present example:

$$\mathcal{R}(0,1/2,1) = \mathcal{R}(1,1/2,0) = \frac{R(1/2)T(1/2)}{1-R^2(1/2)} = .006 \quad (37)$$

$$\mathcal{T}(0,1/2,1) = \mathcal{T}(1,1/2,0) = \frac{T(1/2)}{1-R^2(1/2)} = .600 \quad (38)$$

Hence:

$$H(1/2,-) = 500 \times .600 + 100 \times .006$$

$$= 301 \text{ watts/m}^2$$

$$H(1/2,+) = 500 \times .006 + 100 \times .600$$

$$= 63 \text{ watts/m}^2$$

Equations (35)-(38) are special cases of the important invariant imbedding relations we shall study in many contexts later. If the reader has understood the deductions in this example, he will have no difficulty with the deductions in the remainder of this work concerning invariant imbedding concepts, for they are merely elaborations of the present simple example to general geometries and radiometric quantities. It suffices to observe here that the $\mathcal{R}$ and $\mathcal{T}$ factors are the *complete reflectances* and *complete transmittances* for the medium X(0,1) partitioned at level 1/2. More general partitions generally yield four such numbers.

With the preceding numerical examples in mind, we may now apply (26), (27) to the following situation which generlizes the setting of Fig. 1.46. Thus, being guided by Fig. 1.47 in which all depths are optical depths we have, for the medium X(a,b):

$$H(a,+) = H(a,-)R(b-a) + H(b,+)T(b-a) \tag{39}$$

$$H(b,-) = H(a,-)T(b-a) + H(b,+)R(b-a) \tag{40}$$

Applying (26), (27) again, now to X(b,c):

$$H(b,+) = H(b,-)R(c-b) + H(c,+)T(c-b) \tag{41}$$

$$H(c,-) = H(b,-)T(c-b) + H(c,+)R(c-b) \tag{42}$$

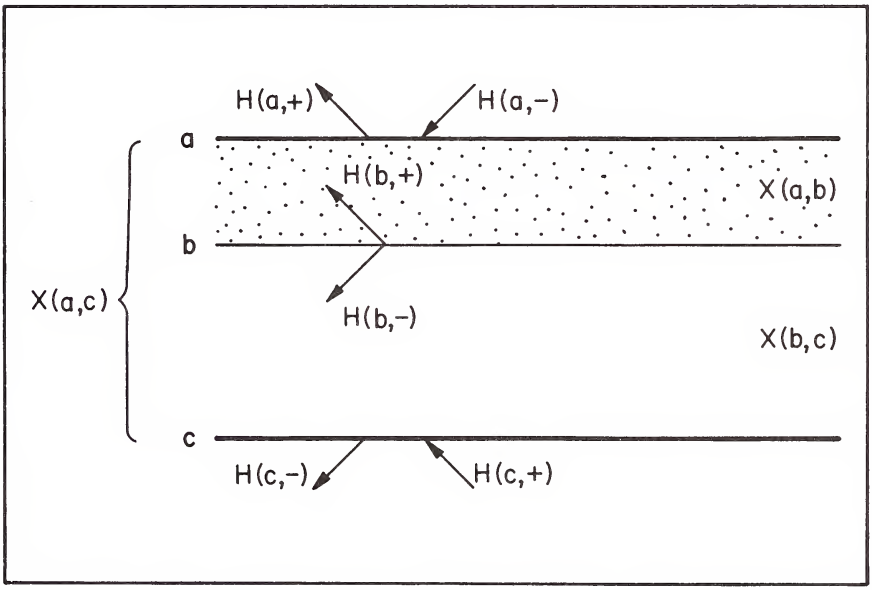

FIG. 1.47 General arrangement for calculating internal irradiances at level b from given irradiances at levels a and c, using the invariant imbedding relation.

Solving these four equations for $H(b,\pm)$, we have, analogously to (35), (36):

$$H(b,-) = H(a,-)\mathcal{T}(a,b,c) + H(c,+)\mathcal{R}(c,b,a) \tag{43}$$

$$H(b,+) = H(a,-)\mathcal{R}(a,b,c) + H(c,+)\mathcal{T}(c,b,a) \tag{44}$$

where:

$$\mathcal{R}(a,b,c) = \frac{T(b-a)R(c-b)}{1-R(b-a)R(c-b)} \tag{45}$$

$$\mathcal{T}(a,b,c) = \frac{T(b-a)}{1-R(b-a)R(c-b)} \tag{46}$$

$$\mathcal{R}(c,b,a) = \frac{T(c-b)R(b-a)}{1-R(b-a)R(c-b)} \tag{47}$$

$$\mathcal{T}(c,b,a) = \frac{T(c-b)}{1-R(b-a)R(c-b)} \tag{48}$$

which are the general versions of (37), (38). These may be evaluated using the R and T values tabulated above.

Equations (43), (44) together constitute the *invariant imbedding relation* for the medium X(a,c) which is partitioned at level b, $a \leq b \leq c$ and in which irradiance is the radiometric concept of interest. It may be put into compact matrix form as follows:

$$(H(b,+),H(b,-)) = (H(c,+),H(a,-)) \begin{bmatrix} \mathcal{T}(c,b,a) & \mathcal{R}(c,b,a) \\ \mathcal{R}(a,b,c) & \mathcal{T}(a,b,c) \end{bmatrix} \tag{49}$$

If the one-D model proves inadequate to predict or describe a given radiometric condition in a natural hydrosol, it may be that a more general and flexible model is required. The hierarchy of successively more refined irradiance models that may be tried after the present one is as follows: the *decomposed one-D model*, the *undecomposed two-D model*, the *decomposed two-D model*; these are studied in Chapter 8.

For a reversal of the preceding procedures in which the light field in real media may be measured so as to predict $R(\tau)$ and $T(\tau)$, see Examples 1, 2, in Sec. 13.10.

A Theoretical Basis for the Law: $N_*(z,\theta) = N_*(0,\theta)e^{-kz}$

In our derivation of the simple model for radiance leading to (14) of Sec. 1.3 we assumed that the path function N_* decreased exponentially with depth, as indicated in (13) of Sec. 1.3. We shall now do away with the assumption and deduce this form of N_* with the help of the two-flow model. This will place (13) of Sec. 1.3 on a sounder basis and also show how the simple models occasionally may be used to help each other attain their full descriptive powers.

Now the path function value $N_*(z,\theta)$, as defined, gives the amount of radiance generated by scattering at depth z, per unit length along the direction ξ of a path in a hydrosol, as shown in Fig. 1.39. What is scattered is the radiance at depth z impinging on the path in all directions ξ'. Just how much of the stream in the direction ξ' is scattered into the direction ξ, at depth z is given by means of the volume scattering function values $\sigma(z;\xi';\xi)$. Thus

$$N_*(z,\xi) = \int_{\Xi} N(z,\xi')\sigma(z;\xi';\xi)\, d\Omega(\xi') \tag{50}$$

where the notation "Ξ" and "$d\Omega(\xi')$" is explained in Sec. 1.1. We shall carefully define σ and derive (50) from first principles in Chapter 3. For the present we can understand it on simple intuitive grounds, as just explained.

The two-flow model assumes that the radiance distribution $N(z,\cdot)$ has an arbitrary fixed shape in the upper and lower hemispheres Ξ_+, Ξ_- of the unit sphere of directions Ξ. If we assume in particular that for every depth z

$N(z,\cdot)$ on Ξ_+ has the constant value $\overline{N}(z)$

and that

$N(z,\cdot)$ on Ξ_- has the constant value $\underline{N}(z)$

then (50) yields up the following necessary form of N_*:

$$\begin{aligned} N_*(z,\xi) &= \int_{\Xi_+} N(z,\xi')\sigma(z;\xi';\xi)\, d\Omega(\xi') \\ &\quad + \int_{\Xi_-} N(z,\xi')\sigma(z;\xi';\xi)\, d\Omega(\xi') \\ &= \overline{N}(z)\int_{\Xi_+}\sigma(z;\xi';\xi)\, d\Omega(\xi') + \underline{N}(z)\int_{\Xi_-}\sigma(z;\xi';\xi)\, d\Omega(\xi') \end{aligned} \tag{51}$$

In the two-flow model adopted in this chapter, the medium is assumed isotropic and homogeneous.* Further, the light field is such that the path direction ξ can be characterized by a single angle θ as shown in Fig. 1.39. We can therefore write, *ad hoc*:

$$\text{"s}(\theta)\text{"} \quad \text{for} \quad \int_{\Xi_-} \sigma(z;\xi';\xi)\, d\Omega(\xi') \tag{52}$$

We shall also write:

$$\text{"s"} \quad \text{for} \quad \int_{\Xi} \sigma(z;\xi';\xi)\, d\Omega(\xi') \tag{53}$$

so that,

$$\int_{\Xi_+} \sigma(z;\xi';\xi)\, d\Omega(\xi') = s - s(\theta). \tag{54}$$

The quantity s is simply the volume total scattering function introduced during the derivation of the simple model for radiance. The portion of the scattering lobe used in finding $s(\theta)$ is shown unshaded in Fig. 1.39. In view of these conventions, we can write:

$$N_*(z,\theta) = \underline{N}(z)s(\theta) + \overline{N}(z)(s - s(\theta)) \tag{55}$$

From (11) of Sec. 1.1 is is clear that:

$$H(z,-) = \pi \underline{N}(z) \tag{56}$$

$$H(z,+) = \pi \overline{N}(z) \tag{57}$$

and from (57), (56) and (5) we have:

$$\overline{N} = \underline{N}\, R_\infty \tag{58}$$

Therefore:

$$N_*(z,\theta) = \underline{N}(z)[s(\theta) + R_\infty(s - s(\theta))] \tag{59}$$

We are essentially finished, because by (8), (11) of Sec. 1.1 we have (setting ξ equal to **k**)

$$\begin{aligned} h(z) &= h(z,+) + h(z,-) \\ &= 2H(z,+) + 2H(z,-) \\ &= 2\pi(R_\infty + 1)\underline{N}(z) \end{aligned} \tag{60}$$

Using this in (59) and recalling (7), we find:

---

*_Homogeneity_ means σ is independent of z; _isotropy_ means σ depends only on $\xi \cdot \xi'$.

$$N_*(z,\theta) = \frac{h(z)[s(\theta) + R_\infty(s-s(\theta))]}{2\pi(1+R_\infty)}$$

$$= N_*(0,\theta)e^{-kz} \qquad (61)$$

where:

$$N_*(0,\theta) = \frac{h(0)[s(\theta) + R_\infty(s-s(\theta))]}{2\pi(1+R_\infty)} \quad , \qquad (62)$$

which is the desired result. In practice we can therefore use the theoretical k and the empirical K interchangeably. This derivation also shows how, using (50), one can generalize the construction of $N_*(0,\theta)$ to quite realistic angular dependences using existing light fields at or somewhat below the air-water surface. The unshaded region of the σ-lobe in Fig. 1.39 shows the portion of the three dimensional surface of $\sigma(z;\xi';\xi)$ over which the integration takes place to obtain $s(\theta)$, $0 \leq \theta \leq \pi$. Observe that if $s(\theta)$ is a surface of revolution (as it is in practice) then:

$$s(\theta) + s(\pi-\theta) = s \qquad (63)$$

whence:

$$s(\pi/2) = s/2$$

and in particular:

$$s(0) + s(\pi) = s$$

As an example of the use of (62) we observe that in some Pacific coastal waters (cf. [300]) as measured in the wavelength band of a Wratten 57 filter, we have

$$s(0) = .001/m$$

$$s(\pi) = .013/m$$

Observe that $s(0)$ acts like a backward scattering function for *collimated* flux, whereas $s(\pi)$ acts like a forward scattering function for *collimated* flux, so that by (63)

$$s(0) + s(\pi) = s = .014/m$$

This water was also found to have a corresponding volume absorption coefficient of $a = .104/m$, and hence the medium has an $\alpha = .118/m$. Such water is highly forward scattering and also relatively highly absorptive, and will therefore force the simple models to work hard in their descriptive tasks. Since the present medium is highly absorptive, the downward scattered daylight light near the surface will be relatively highly collimated. Accordingly we assume a relatively small distribution factor D, say $D = 1.1$. Since the medium is highly forward scattering, we shall estimate the backward scattering coefficient b for the *scattered* flux field to be .002/m. It follows from the one-D two-flow model ((9) of

1.3 and (9) of 1.4) that aD = .114, and that k = .114/m along with γ =.99; so that R_∞= .01. Let h(0) = 500 watts/m^2 just below the surface.

These assumed conditions allow us to illustrate the path function formula (62). We have, for the downward path function just below the surface:

$$N_*(0,\pi) = \frac{h(0)[s(\pi) + R_\infty s(0)]}{2\pi(1+R_\infty)}$$

$$= \frac{500[.013 + .01 \times .001]}{6.28 \times (1 + .01)}$$

$$= 1.03 \text{ watts/m}^3\text{sr}$$

$$= 1.03 \text{ herschels/m}$$

Further, for the horizontal path function:

$$N_*(0,\pi/2) = \frac{h(0)[1+R_\infty]s}{4\pi[1+R_\infty]} = \frac{sh(0)}{4\pi}$$

$$= \frac{500 \times .014}{4 \times 3.14} = .557 \text{ herschels/m}$$

Finally, for the upward path function:

$$N_*(0,0) = \frac{h(0)[s(0)+ R_\infty s(\pi)]}{2\pi[1+R_\infty]}$$

$$= \frac{500[.001+.01 \times .013]}{6.28(1+.01)}$$

$$= .080 \text{ herschels/m.}$$

Computing Radiances from the Simple Model

Some illustrations of the computation of radiances using (14) of Sec. 1.3 will help fix in mind the typical orders of magnitudes of radiance values in natural waters. Let us begin with the case of a horizontal path of sight some given depth z_o below the surface. Then in (14) of Sec. 1.3, we set $\theta = \pi/2$, and that equation becomes:

$$N_r(z_o,\pi/2) = N_o(z_o,\pi/2)e^{-\alpha r} + \frac{N_*(z_o,\pi/2)}{\alpha}\left[1-e^{-\alpha r}\right] \quad (64)$$

which we can write quite simply as:

$$N_r = N_o e^{-\alpha r} + \frac{N_*}{\alpha}\left[1-e^{-\alpha r}\right]$$

provided the depth and direction of the path are understood. (The right is reserved to disinter the depth and direction variables at any time.) For infinitely long horizontal paths, i.e., for the case $r = \infty$, this formula yields:

$$\boxed{N_q = \frac{N_*}{\alpha}} \tag{65}$$

for the observable horizontal radiance N_q at a given depth in any laterally extensive stratified optical medium. Observe that in such media the N_q defined above does not change with location along the path. For this reason we denote the observable radiance as "N_q" and call it the *equilibrium radiance*.

An estimate of N_q for shallow depths in Pacific coastal water around the blue-green part of the spectrum can be made on the basis of the preceding example, wherein we found that $N_*(0,\pi/2) = .557$ herschels/m. In such waters, for example, $\alpha = a+s = .104 + .014 = .118$/m. Hence:

$$N_q(0,\pi/2) = .557/.118 = 4.72 \text{ herschels}$$

is the equilibrium radiance just below the surface. At a depth of 5 meters, it follows from (61) that

$$\begin{aligned} N_q(5,\pi/2) &= \frac{N_*(5,\pi/2)}{\alpha} = \frac{N_*(0,\pi/2)}{\alpha}\, e^{-5k} \\ &= N_q(0,\pi/2)e^{-5k} \\ &= 4.72 \times e^{(-5 \times .115)} \\ &= 4.72 \times .560 = 2.64 \text{ herschels} \end{aligned}$$

where we have used the k for the water of the preceding example.

As another example of the use of the radiance model, we set $\theta = \pi$, and $\theta = 0$ in (14) of Sec. 1.3, to find that, at depth z at the lower end of a vertical path of length r:

$$\boxed{N_r(z,\pi) = N_o(z_o,\pi)e^{-\alpha r} + \frac{N_*(z,\pi)}{\alpha-K}\left[1-e^{-(\alpha-K)r}\right]} \tag{66}$$

and similarly at depth z, at the upper end of a vertical path of length r:

$$\boxed{N_r(z,0) = N_o(z_o,0)e^{-\alpha r} + \frac{N_*(z,0)}{\alpha+K}\left[1-e^{-(\alpha+K)r}\right]} \tag{67}$$

The reader is reminded of the standing convention that $N_T(z,\pi)$ is the apparent radiance at depth z flowing in the downward direction and to see it, one must direct his eye or radiance meter upward (cf. Fig. 1.39). We persist in using this form of radiance (i.e., surface radiance) because it simplifies the dynamics of photons in scattering-absorbing media.

Suppose the medium is infinitely deep, so that we can set $r = \infty$ in (67) and still keep the path within the medium. Then (67) becomes:

$$N(z,0) = \frac{N_*(z,0)}{\alpha + K}$$

which is the radiance one would see at depth z looking straight down into the infinite deeps. Suppose z = 0, then our preceding example lets us estimate that:

$$N(0,0) = \frac{N_*(0,0)}{\alpha + K}$$

$$= \frac{.080}{.118 + .115}$$

$$= .344 \text{ herschels.}$$

Let the zenith radiance as seen just above an air-water surface be 80 herschels in a given band width of the blue-green part of the spectrum, say at 480 ± 64 mμ, and suppose that $h(0) = 500$ watts/m^2 just below the surface. If the surface is calm, then just below it, by virtue of the n^2-law for radiance, (Sec. 1.1), we would have

$$N_o(0,\pi) = 80 \times \left(\frac{4}{3}\right)^2 = 142 \text{ herschels}$$

where 4/3 is the index of refraction of water. This radiance value is to be modified slightly if surface transmittance and reflectance effects are to be included. These corrections are of secondary importance and so we shall not include these effects at the moment. Now, to the present task: we can estimate $N(z,\pi)$ for z = 5 meters, by means of (66) in which we set z_o= 0m, z = 5m, and use $\alpha = .118/m$, $k = .115/m$. Thus, with the help of our estimate of $N_*(0,\pi)$ above:

$$N_5(5,\pi) = N_o(0,\pi)e^{-.118\times5} + \frac{N_*(0,\pi)e^{-.115\times5}}{.118-.115}\left[1-e^{-(.118-.115)5}\right]$$

$$= 142 \times .554 + (1.03 \times .560) \times 5$$

$$= 78.6 + 2.88$$

$$= 81.5 \text{ herschels}$$

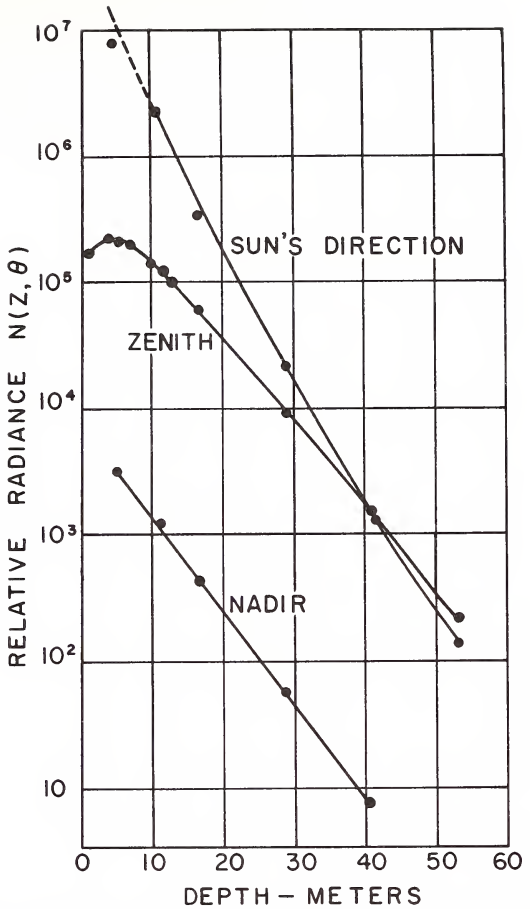

FIG. 1.48 Experimental verification of the simple model for radiance, as measured by Tyler in Lake Pend Oreille, Idaho, April 1957. (From [298], by permission)

The next to last equality shows that at a depth of 5 meters, 78.6 herschels are transmitted from the original 142 just below the surface, and that 2.88 herschels are added by the process of scattering over the 5 meter path.

Figure 1.48, which is based on the work in [298], shows the observed radiance distribution in Lake Pend Oreille and its associated predicted values using (14) of Sec. 1.3 for three important directions. The solid curve is computed from the model, the dots denote measured radiances.

A word or two may be in order here on the rather unintuitive-seeming jump by the radiance function as the flux crosses the air-water surface. We saw in the example above how it jumped from 80 to 142 herschels. To simplify matters suppose for the moment that there are no losses by reflection as the flux crosses the surface. Fig. 1.49 depicts the flux

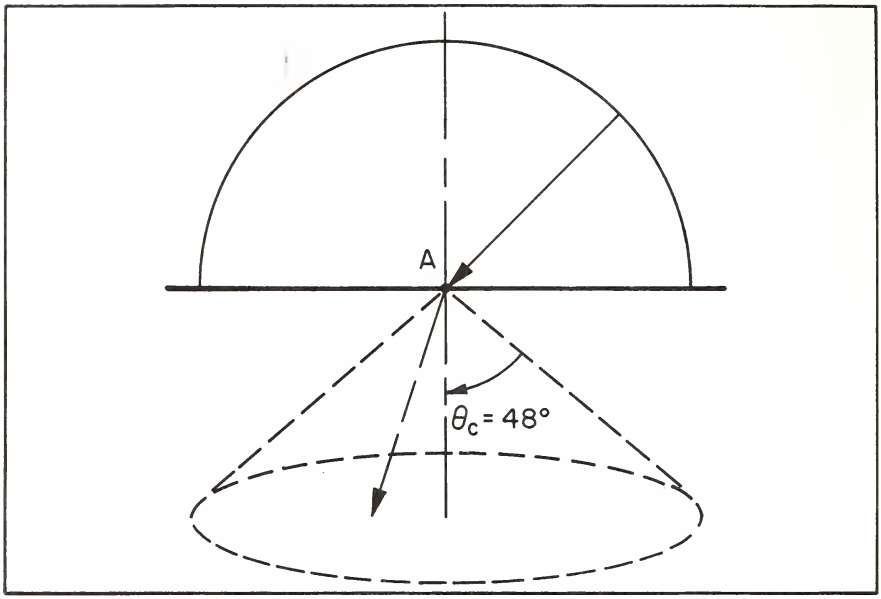

FIG. 1.49 To show that the irradiance conservation law holds despite the n^2 effect on radiance at the air-water level.

incident at a point A on the surface, flowing in from all directions in a hemisphere. The refracted rays below the surface do not fan out in a full hemisphere, but are limited to a right circular cone of half angle $\theta_c = 48°$, or more precisely,

$$\theta_c = \text{arc sin } \left(\frac{3}{4}\right) \quad .$$

Let the incident radiance distribution be of constant magnitude N. Then the irradiance on the air-water surface, by (11) of Sec. 1.1, is simply πN. Let us compute the irradiance just below the surface produced by the refracted incident flux of radiance $(4/3)^2 N$. By (1) of Sec. 1.1 we now find:

$$H = \int_{\theta'=0}^{\theta_c} \int_{\phi'=0}^{2\pi} \left[\left(\frac{4}{3}\right)^2 N\right] \cos\theta' \sin\theta' \, d\theta' \, d\phi'$$

$$= \left(\frac{4}{3}\right)^2 2\pi N \int_{\theta'=0}^{\theta_c} \cos\theta' \sin\theta' \, d\theta'$$

$$= \pi N$$

This shows that, despite the rather odd buildup of refracted radiance across the air-water surface, this buildup is of such a magnitude, and takes place over such a restricted set of directions, that, as expected, energy conservation is observed. The argument just given can readily be extended to ideal transmitting surfaces bounding media of arbitrary index of refraction. When, in addition, reflection processes are to be taken into account, the more extensive calculations discussed in Sec. 12.2 are to be used.

Derivation of the Contrast Transmittance Law and the Radiance Difference Law

The contrast transmittance law:

$$C_r = C_o e^{-(\alpha+K\cos\theta)r}$$

for an inclined path of sight of length r in a homogeneous optical medium was first encountered experimentally (in the special instances of vertical and horizontal directions) as explained in the discussion leading up to (12) of Sec. 1.2. It is now our purpose to show how this law may be deduced from the simple model for radiance (14) of Sec. 1.3, and under what conditions it is expected to hold.

Let the hydrosol X be infinitely deep and consider a path in X as shown in (a) of Fig. 1.50, where the observer is at depth z and the apparent radiance ${}_tN_r(z,\theta)$ of an object of inherent radiance ${}_tN_o(z_t,\theta)$ is observed. The angle θ is such

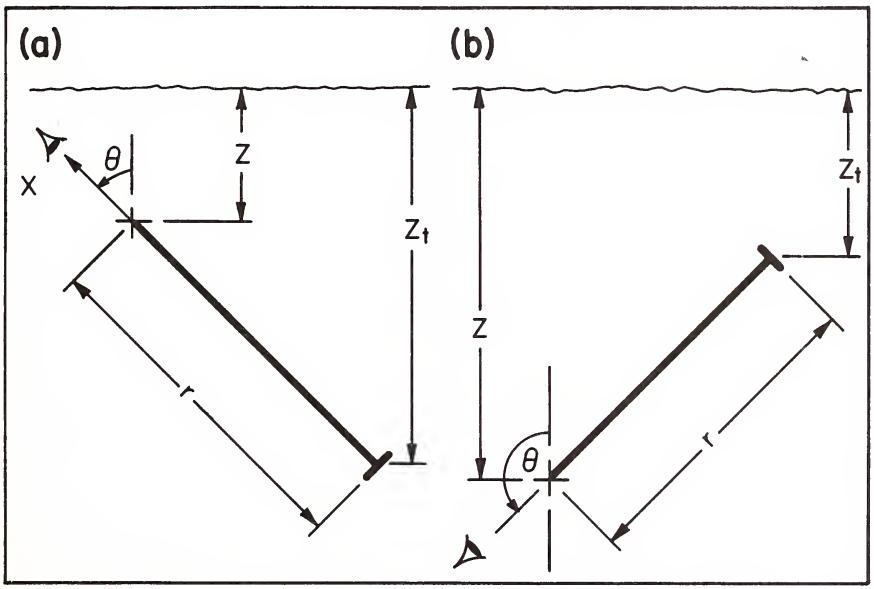

FIG. 1.50 Setting for a theoretical proof of the exponential law for apparent contrast. (cf. Figs. 1.29, 1.30)

that $0 \leq \theta \leq \pi/2$. Recall that θ is the angle from the vertical at which the photons are flowing, as shown by the arrow in the figure.

Now the background apparent radiance ${}_bN_r$ for the present path of length r is obtained from (14) of Sec. 1.3 by setting $r = \infty$ in that general equation:

$$ {}_bN_r(z,\theta) = \frac{N_*(z,\theta)}{\alpha+K\cos\theta} \quad . \tag{68} $$

This is the apparent radiance of the background of the target as seen at a range r from the target. The apparent contrast $C_r(z,\theta)$ of the object against its background (recall (11) of Sec. 1.2) is:

$$ C_r(z,\theta) = \frac{{}_tN_r(z,\theta) - {}_bN_r(z,\theta)}{{}_bN_r(z,\theta)} \quad , \tag{69} $$

wherein we have:

$$ {}_tN_r(z,\theta) = {}_tN_o(z_t,\theta)e^{-\alpha r} + \frac{N_*(z,\theta)}{\alpha+K\cos\theta}\left[1-e^{-(\alpha+K\cos\theta)r}\right] . \tag{70} $$

Observing that:

$$ C_o(z_t,\theta) = \frac{{}_tN_o(z_t,\theta) - {}_bN_o(z_t,\theta)}{{}_bN_o(z_t,\theta)} \quad , \tag{71} $$

it follows from the preceding four relations, by straightforward substitution of (68) and (70) into (69), and a reduction using (71), that:

$$ \boxed{C_r(z,\theta) = C_o(z_t,\theta)e^{-(\alpha+K\cos\theta)r}} \tag{72} $$

which was to be shown. The quotient C_r/C_o is called the *contrast transmittance*. Equation (72) is the requisite contrast transmittance law. The quantity $(\alpha+K\cos\theta)^{-1}$ is called the *attenuation length* L_θ of the medium along the given path. For $\theta = \pi/2$, $L_{\pi/2} = 1/\alpha$, a basic property of the medium, while $L_o = 1/(\alpha+K)$ is associated with secchi disk readings (cf. (84) below). The quantity $4L_\theta$ is mainly of historic interest and is the *hydrologic range* for the given path of sight. Its plot is an ellipse vs θ (cf. Sec. 1.9).

This simple derivation cannot be repeated in its entirety when the photons are streaming in from a nearby boundary, such as depicted in (b) of Fig. 1.40. In this case (68) must be replaced by the full form of (14) of Sec. 1.3. However, by using (69) and (71), which are general definitions of apparent and inherent contrasts, along with (14) of Sec. 1.3

once again, it follows readily by a similar calculation, that quite generally:

$$C_r(z,\theta) = \left[\frac{{}_bN_o(z_t,\theta)}{{}_bN_r(z,\theta)}\, e^{-\alpha r}\right] C_o(z_t,\theta) \qquad (73)$$

The reader may show that this formula holds for both situations depicted in Fig. 1.50, i.e., for $0 \leq \theta \leq \pi$. It reduces to (72) when $0 \leq \theta \leq \pi/2$, i.e., when (14) of Sec. 1.3 reduces to (68). A fuller discussion of contrast and contrast transmittance is given in Chapter 9.

Figures 1.51 and 1.52 illustrate two experimental checks of the contrast transmittance law for the cases of $\theta = 90°$, and $\theta = 58.8°$. The radiometric quantity used was apparent luminance B_r, and the medium (Lake Winnipesaukee, N.H.) had an α of .490/m for Fig. 1.51 and for Fig. 1.52 the medium had $\alpha = .585/m$ and $K = .350/m$. These optical properties therefore pertain to averages of α, K over the visible spectrum. The observation point in each case was about a meter below a calm air-water surface and when the skies were overcast or early

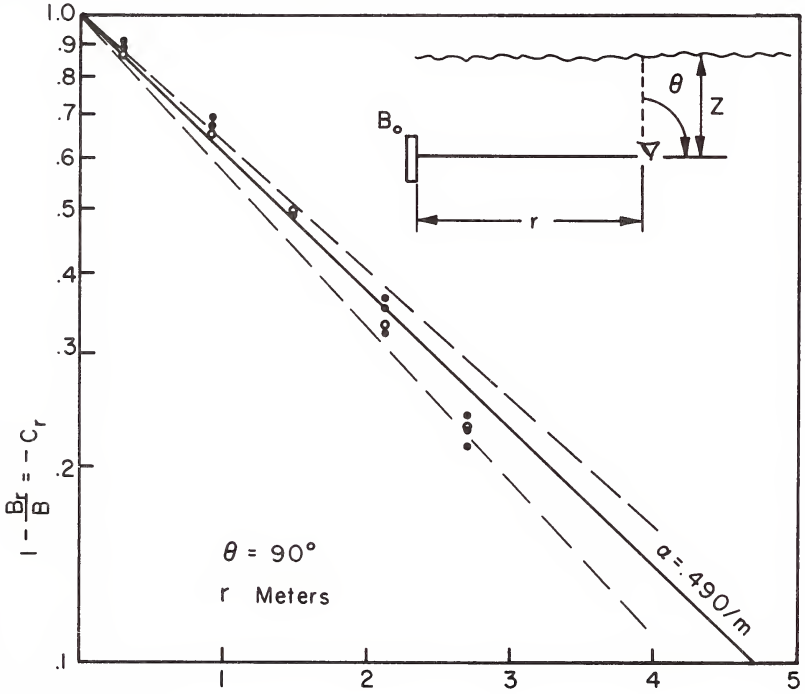

FIG. 1.51 Experimental checks of the exponential law for apparent contrast (cf. Fig. 1.50) by Duntley, Tyler, and Taylor, Lake Winnipesaukee, N.H., Summer 1958.

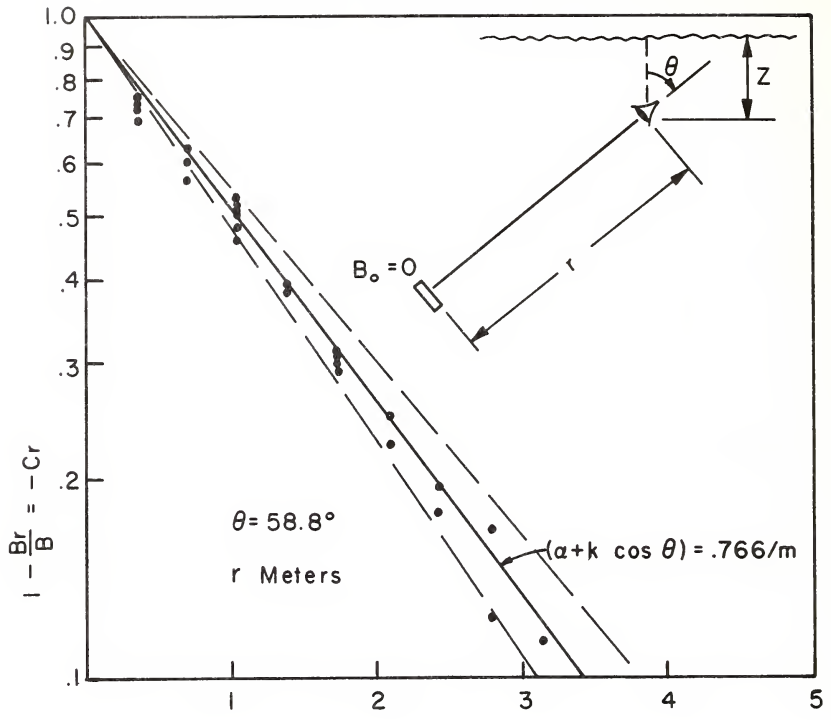

FIG. 1.52 Experimental checks of the exponential law for apparent contrast (cf. Fig. 1.51).

morning skies in each case. Further details may be found in [83].

We conclude with the observation of a useful corollary of (73), namely that *radiance differences propagate exactly according to the exponential law.* Thus

$$\left[{}_bN_r(z,\theta) - {}_tN_r(z,\theta)\right] = \left[{}_bN_o(z_t,\theta) - {}_tN_o(z_t,\theta)\right]e^{-\alpha r} \qquad (74)$$

Contrast Transmittances for General Backgrounds

It should be observed explicitly that formula (73) is of such generality that the apparent contrast C_r of an object need not be with respect to a water background. Rather, if ${}_bN_o$ in (73) is the inherent radiance of a background (as in Fig. 1.53) for a target of inherent radiance ${}_tN_o$ (shaded in the figure), then by computing ${}_bN_r$ according to (14) of

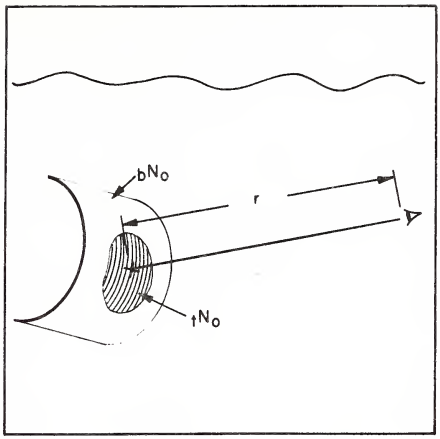

FIG. 1.53 Contrast transmittance for paths with arbitrary backgrounds.

Sec. 1.3 and using this in (73), the requisite apparent contrast transmittance C_r/C_o is determinable.

As a special case of (74) under these circumstances, let the line of sight be horizontal, then it is easy to see that:

$$C_r/C_o = \frac{1}{1+\frac{N_q}{{}_bN_o}\left(e^{\alpha r}-1\right)}, \tag{75}$$

where N_q is the equilibrium radiance for the given horizontal path. Observe that the contrast transmittance of the given path uses only the radiances $_bN_o$ and N_q, i.e., the radiances making up the immediate background of the target. Of course in real media N_q is somewhat affected by both $_tN_o$ and $_bN_o$ (and conversely) so that the classically simple formula (75) does not rigorously hold. But within the framework of the present simple models and for paths of sight under ordinary lighting conditions, (75) is a quite useful and adequate formula.

The Multiplicative Property of Contrast Transmittance

If we take a still closer look at the contrast transmittance law (73), we find a most interesting property held by contrast transmittance in general, whether it be for paths of sight within the sea, or within the atmosphere, or even for paths partly in the sea *and* partly in the atmosphere!

To facilitate our discussions let us write:

$$\text{"}\mathcal{T}_r\text{"} \quad \text{for} \quad C_r/C_o$$

and when necessary we include location and direction variables with "$\mathcal{T}_r$". Now observe that $e^{-\alpha r}$ in (73) can be written as

$$e^{-\alpha r} = \frac{{}_bN_r^o(z,\theta)}{{}_bN_o(z_t,\theta)}$$

where ${}_bN_r^o$ is the *residual radiance* coming directly from the target background over the path of length r. (It is what is left of ${}_bN_o$ after scattering and absorption have taken their toll; cf. (24) of Sec. 1.3). Then we see that (73) can be cast into the form:

$$\mathcal{T}_r = \frac{{}_bN_r^o}{{}_bN_r} \quad .$$

On this basis, we can work solely with the background radiance of a target when discussing beam transmittance of a path along which it is viewed. Hence we need no longer carry the reminder "b" before the radiance symbol. In other words we find that for a *general path of length* r *in a general hydrosol, the contrast transmittance* C_r/C_o *of the path is given by*

$$\mathcal{T}_r = \frac{N_r^o}{N_r} \tag{76}$$

This situation is summarized schematically in (a) of Fig. 1.54.

Next, suppose we have two paths of length r, s, end to end, as shown in (b) of Fig. 1.54. Let the inherent radiance at the far end be N_o. Then at the end of the first path segment of length s, we have, according to the preceding rule:

$$\mathcal{T}_s = \frac{N_s^o}{N_s} = \frac{N_o e^{-\alpha s}}{N_s} \tag{77}$$

where N_s is the apparent radiance associated with N_o, and N_s^o the residual radiance associated with N_o over the path of length s, both reckoned via (12) of Sec. 1.3, for example. The apparent radiance N_s now acts as did the initial radiance N_o, and N_s is transferred over the second segment of length r to give rise to an observed residual radiance $N_s e^{-\alpha r}$ and the apparent radiance N_{r+s} associated with N_s. Hence:

$$\mathcal{T}_r = \frac{N_s e^{-\alpha r}}{N_{r+s}} \tag{78}$$

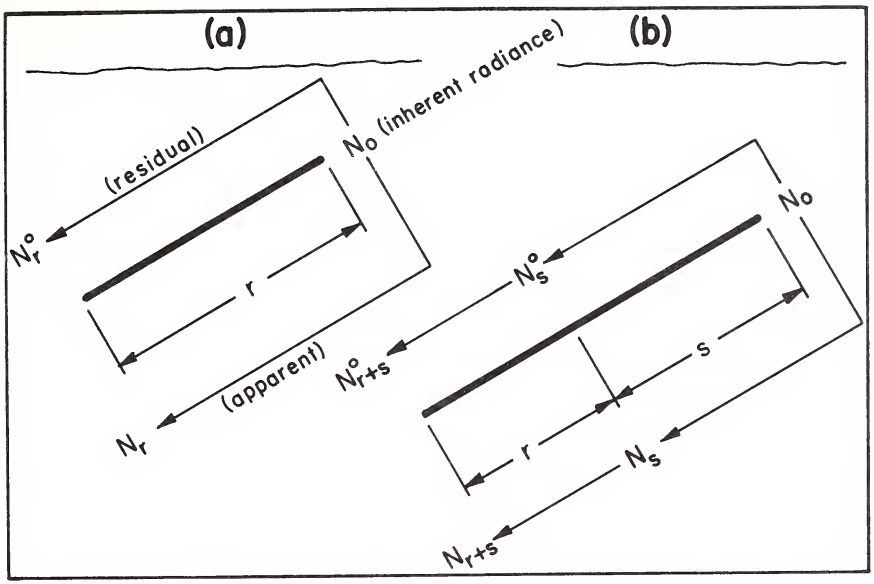

FIG. 1.54 Part (a): Deriving the contrast transmittance as the ratio of a residual radiance and an apparent radiance. Part (b): Deriving the multiplicative (or semigroup) property of contrast transmittance.

But looking at the path as a whole, we can also write:

$$\mathcal{T}_{r+s} = \frac{N_{r+s}^o}{N_{r+s}} \tag{79}$$

Comparing (77)-(79) we find:

$$\boxed{\mathcal{T}_{r+s} = \mathcal{T}_r \mathcal{T}_s} \tag{80}$$

This is the *multiplicative* (or *semigroup*) *property* of the contrast transmittance. The argument just used to derive (80) is readily extended without change of the form of (80) to arbitrary paths in air or water and across places where the index of refraction varies, provided in such cases we work with N/n^2 rather than N, where n is the index of refraction. For by the n^2-law for radiance, N/n^2 is invariant in transparent media with varying index of refraction (see Sec. 9.5).

As an obvious extension of (80), if a path consists of three contiguous, successive segments of arbitrary lengths r, s, t, then the contrast transmittance $\mathcal{T}_{r+s+t}$ of the composite path is simply a product of the three contrast transmittances of the segments:

$$\mathcal{T}_{r+s+t} = \mathcal{T}_r \mathcal{T}_s \mathcal{T}_t \tag{81}$$

As an example of (81), consider a calm air-water surface. A line of sight of length t begins at a submerged object, is refracted at the air-water surface, and runs a length r in the air. Each of the three paths have an associated contrast transmittance. While the path across the surface is of zero length, i.e., s = 0, there is a definite contrast reduction that takes place because of reflected sky light and reflected and transmitted underwater light occurring at the surface. The form of this *singular* contrast transmittance $\mathcal{T}_o$ is given in detail in (20), (23) of Sec. 12.2.

If, in addition, the air-water surface is in motion, then the above analysis must include an additional factor $\overline{\mathcal{T}}_o$ (= $\bar{C}/C$)associated with the time-averaged contrast reduction by refraction (cf. in (5) of Sec. 1.2). Hence now:

$$\overline{\mathcal{T}}_{r+t} = \mathcal{T}_r \mathcal{T}_o \overline{\mathcal{T}}_o \mathcal{T}_t \tag{82}$$

gives the *time averaged* contrast transmittance $\overline{\mathcal{T}}_{r+t}$ for a path of length r in air, and going across a moving air-water surface and plunging a length t in a natural hydrosol (Fig. 1.55). The factors are as follows for a vertical line of sight in air and a small submerged target of half-angle subtense ψ as seen just below the surface:

$$\mathcal{T}_r = e^{-\alpha_1 r} \qquad \text{(in air)}$$

$$\mathcal{T}_t = e^{-(\alpha_2+K)t} \qquad \text{(in water)}$$

$$\overline{\mathcal{T}}_o = \left(1-e^{-\frac{\tan^2\psi}{2\sigma^2}}\right) \qquad \text{(at the interface)}$$

Finally $\mathcal{T}_o$ is as given in (21) of Sec. 12.2 (wherein $N^o(x,\xi')$ is now the *time averaged* vertical upward radiance). The complete analysis of the time averaged radiance transmitted across the air-water surface is made in the latter half of Chapter 12, wherein the more or less intuitive type of factor analysis in (82) is bypassed in a direct, more general, but somewhat more difficult solution of the problem.

Theory of the Secchi and Duntley Disks

It is a part of almost everyone's experience to have thrown or dropped an object into deep water and to have watched it disappear into the depths. If the object is

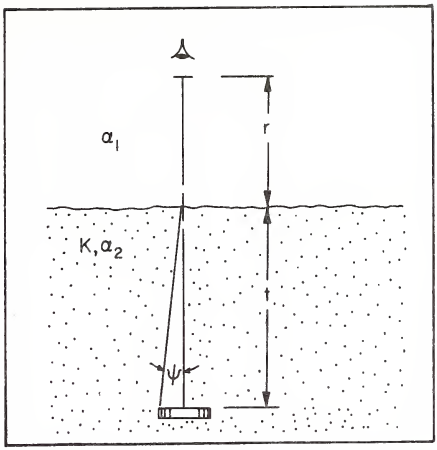

FIG. 1.55 Contrast reduction along a composite path through air, air-water surface, and water.

something bright or white, the eye can easily follow it down into the depths until it seemingly abruptly winks out, to be lost from sight from some depth onward. If the observer were of an inquisitive turn of mind, he may surmise that the general clarity of the water had something to do with the depth at which the object disappeared, and he may wonder if there were indeed a quantitative connection between the depth rate of decay of the light field in the water and also the depth rate of decay of the *whiteness* or *contrast* of the sinking object against the watery background, and maybe even the depth at which it seems to wink into obscurity.

Here is a hypothetical discussion about the radiometric problem of the sinking object, defined above, and which may occur on shipboard between a young eager theorist just learning the ropes and a seasoned experimenter in hydrologic optics just after one of them had accidently dropped a white glass coffee mug over the side of the oceanographic research vessel (which was moored in deep calm water at the time).

Theorist: There you go, being careless with your design of experiments again. You didn't even note the sun altitude or what filter you were using.

Experimenter: I had an irresistable urge to see what would happen if I dropped it in.

Th. Good heavens man! Why the experiment? Have you forgotten Archimedes Law? On theoretical grounds, I predict that the mug will sink!

Ex. (Recovering from the accident) Look--it's turning bilious as it sinks deeper. What an interesting transformation of shades and hues. It looks like it's down 10 meters by now and I can still see it quite clearly!

Th. (Peering down over the railing) It must have reached terminal velocity by now and is surely sinking according to Stokes' law. (Looking at his watch, then a pause) At the sound of the tone it will be exactly 20 meters.

Ex. (Ignoring the other's babbling) There it goes. I lost track of it. There's no doubt about it, this is pretty clear water!

Th. What's the alpha and the kay for this water? Did you measure it again this morning?

Ex. It's the same as yesterday. The alpha's about a tenth per meter and the kay is about fifty thousandths per meter, both in the green. What are you doing?

Th. (Jotting something on a piece of paper so that the other can see it) I'll bet I can connect the mug's depth of disappearance with the alpha and kay of this water.

Ex. (Smiling wearily to himself, and then with a sigh): Here we go again. Take it easy, Einstein, my calculus is buried under a ton of barnacles.

Th. We really don't need it. Didn't you explain to me how it's known that the light level generally goes down exponentially with depth in deep water like this? I can use this fact to figure out how much light gets to the mug at each depth z. It would be (writing on the paper) $H_o e^{-Kz}$, correct?

Ex. Yes, and let's say that H_o is the irradiance on a horizontal surface just below the surface and K is the kay for this water, namely, .050/m. So you can figure out the irradiance on a horizontal surface at depth z. (Then feigning puzzlement) Where does that get you?

Th. Why, this lets you compute the inherent radiance of the mug at depth z, if you know its reflectance.

Ex. Do you know it?

Th. No, but let's just call it "R". Then (writing again) $R(H_o e^{-Kz})$ would give an estimate of the radiance reflected upward by the mug.

Ex. Hmm---Yes, but that's its *inherent* radiance down at depth z. Here we are on deck.

Th. I see what you mean. So we need the *apparent* radiance of the mug. But that'll mean knowing the path radiance generated by scattered light between us and the mug and also the effect of the air-water surface. Gosh, all that's pretty hard to come by isn't it?

Ex. Quite. But if you remember what I told you the other day about radiance *differences* . . .

Th. Radiance *differences*? Oh, of course! They are transmitted exactly according to the exponential law $e^{-\alpha r}$ for beamed light. Let's see, the radiance difference in this case will be between the inherent radiance of the mug at depth z and the inherent radiance of the background water at the same depth. Such a difference is easy to figure.

Ex. Is it? Again you don't know the reflectance of the water at the depth of the mug. At least I haven't measured it yet for this place.

Th. That's O.K. Let's call the reflectance of the water "R_∞". It could not be much different from .02 for all depths. I was looking over some of your old reports, and review articles yesterday. Everywhere you measured R_∞ you got something around .02 for green light, even some deep clear lakes and ponds, *n'est ce pas*?

Ex. (Gritting his teeth) I am afraid so. Very few

surprises left there. Well, where are you leading me next with your paper and pencil?

Th. The average radiance of the water background at depth z is simply R_∞ times the downward irradiance at that depth. That is, we would have $R_\infty(H_o e^{-Kz})$. Right?

Ex. Yes, except for a factor of π--but they'll all cancel out anyway in the end. So don't worry about it now.

Th. (Looking up surprised) Say--how do you know that? Have you worked all this out before?

Ex. (With a straight face, looking out at the horizon) Not exactly. On with it--what is your next step?

Th. Well here is the radiance difference between the mug and the sea at depth z:

$$H_o R e^{-Kz} - H_o R_\infty e^{-Kz}$$

Ex. And then?

Th. And then at long last I can use the radiance difference law. That is I multiply this difference by $e^{-\alpha z}$ to transmit it up to just below the surface--where it'll be what we will actually see if we went there. Thus:

$$\left[H_o R e^{-Kz} - H_o R_\infty e^{-Kz}\right] e^{-\alpha z}$$

Ex. Can you simplify this mess?

Th. Sure, like this:

$$H_o(R-R_\infty)e^{-(\alpha+K)z}$$

Ex. Also I don't like to bother with absolute light levels. Can you take care of that, too?

Th. Yes, I suppose. Why not divide the whole thing by the amount of reflected radiance from the sea just below the surface? Like this:

$$\frac{H_o(R-R_\infty)e^{-(\alpha+K)z}}{H_o R_\infty}$$

Ex. That'll work fine. Now, what have you got for all your trouble?

Th. (A pause, and then) Why this looks like it could be a kind of contrast reduction formula...yes, it is...just let $H_o(R-R_\infty)/H_o R_\infty$ or simply $(R-R_\infty)/R_\infty$ be the inherent contrast of the mug against its background. It looks like this contrast is independent of the depth of the mug. That's fantastic! Is that right?

Ex. (Blanching) Yes, go on...

Th. So if the apparent contrast of the mug at depth z as seen from just below the surface is C_z, then it looks like we have

$$C_z = C_o e^{-(\alpha+K)z}$$

Ex. (A little startled at the equation's quick appearance from an unexpected line of argument) Would you know how to use something like that?

Th. (After a while) Well, if we can agree that the mug

disappears when C_z/C_o is some small number, maybe like 1/50, and measure the z for such a ratio, then we can compute the corresponding $\alpha+K$. It's true we couldn't find α and K separately this way, but the sum is probably still a good index of water clarity.

Ex. (In mock anger) Incredible! Do you know what you've just done, boy?

Th. (Somewhat aghast) No, sir. But I do know that we haven't allowed for the surface effects yet. Is something wrong?

Ex. No, it's just that throughout this discussion I've seen several old friends in a new light. You did well. Now, you run along below and get me a fresh mug of coffee. And on the way back drop into the ship's library. I want to show you something in Sec. 1.4 of "Hydrologic Optics".

It wasn't long until the young theorist saw how to derive the contrast law in the orthodox way (see, e.g., (72)) and how to put in the contrast transmittance factors for the surface, as we have seen for ourselves in (82). It was also made clear to him how Secchi [283] had many years before, in 1865, devised an empirical procedure of just this type for finding a water clarity index which used the depth of disappearance of a standardized disk, and finally of how the meticulous care with which Secchi had stated his measuring procedures had generally been ignored or diluted by subsequent generations of users of his method.

In 1949 Duntley [82] examined the Secchi disk procedure and devised a simple alternative scheme whereby it would be less subject to the vagaries of individual experimenters and lighting conditions during the moment of disappearance of the disk. Duntley observed that one important seat of the difficulty of using Secchi disk readings lay in coping with the contrast transmittance factors $\mathcal{T}_o$ and $\bar{\mathcal{T}}_o$ in (82) (the factor $\mathcal{T}_r$ is essentially unity for work right above the surface).

Suppose then, Duntley reasoned, that *two disks were used,* one being white, the other gray. Suppose further that the two disks are lowered together, side by side into the water a meter or two or so below the water surface, say to depth z. An observer above the surface will see them side by side: a white and a gray disk--each a bit dimmer now, but their luminances still quite distinct. Then the white one is slowly lowered farther into the water, the other being held fixed. As it is lowered, the white disk becomes darker (the e^{-Kz} effect setting in) and soon, at some depth d below the gray disk, there appears to be a luminance match between the two disks (see Fig. 1.56). At this stage of the experiment, we see that by (72) and (82):

$$C_z = \left[C_o e^{-(\alpha+K)z}\right] \mathcal{T}_o \bar{\mathcal{T}}_o$$

for the gray disk, and that:

$$C'_{z+d} = \left[C'_o\, e^{-(\alpha+K)(z+d)}\right] \mathcal{T}_o \bar{\mathcal{T}}_o$$

for the white disk, and indeed, that:

$$C_z = C'_{z+d} \quad .$$

(As they stand, either of these formulas for C_z or C'_{z+d} by itself comprises the theory of the Secchi disk.) By taking the ratio of these contrasts, we eliminate the troublesome contrast transmittances $\mathcal{T}_o$, $\overline{\mathcal{T}}_o$, to find:

$$1 = \frac{C_z}{C'_{z+d}} = \frac{C_o}{C'_o} e^{(\alpha+K)d} = \frac{R-R_\infty}{R'-R_\infty} e^{(\alpha+K)d} \tag{83}$$

Hence

$$\boxed{\alpha+K = \frac{1}{d} \ln \left(\frac{R'-R_\infty}{R-R_\infty} \right)} \tag{84}$$

Using the experimental fact that in green light R_∞ is on the order of .02 (but of course with some variation possible) for most natural hydrosols, and that the R of the gray disk and the R' of the white disk may be easily chosen much greater than the R_∞ of the water to be measured, (84) can be written very nearly as:

$$\alpha+K = \frac{1}{d} \ln \left(\frac{R'}{R} \right) \tag{85}$$

Since the number ln (R'/R) is known and fixed for a pair of disks, a table can be made from which one can read off $\alpha+K$ directly from the match-depth-difference d.

Suppose further that someday an optical oceanographer equipped with a scuba and a light-weight pair of Duntley

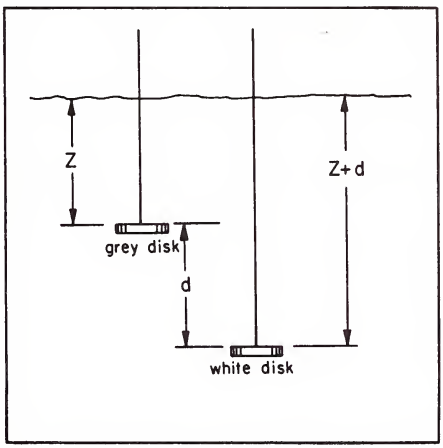

FIG. 1.56 The Duntley-disk procedure for measuring $\alpha+K$.

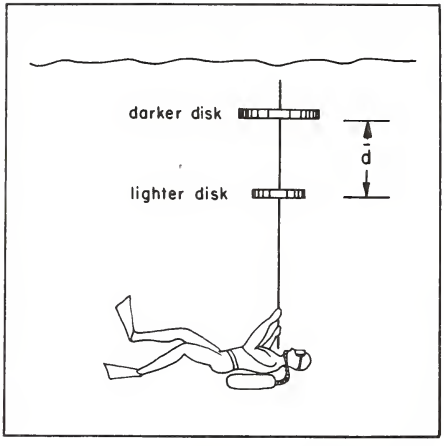

FIG. 1.57 The Duntley-disk procedure for measuring α-K.

disks on a rod (as in Fig. 1.57) will be able to measure the match-depth-difference d for a vertically upward line of sight. Then from an analysis based either on the kind of reasoning by the young theorist in the dialogue above or by simply appealing to (72) with θ = 180°, we could deduce that, analogously to (85):

$$\alpha - K = \frac{1}{d} \ln \left(\frac{R'}{R} \right) \tag{86}$$

From this and (85), we find:

$$\alpha = \frac{1}{2} \left(\frac{1}{d} + \frac{1}{\bar{d}} \right) \ln \left(\frac{R'}{R} \right) \tag{87}$$

and

$$K = \frac{1}{2} \left(\frac{1}{d} - \frac{1}{\bar{d}} \right) \ln \left(\frac{R'}{R} \right) \tag{88}$$

If such a device is used, it should have sectors (or perhaps annuli) on each disk of different whites and grays (when the diver looks upward the darker disk must be farther from him at match time). It is also suggested that the divers wear goggles which transmit in some given small band width of the spectrum around which the K and α values are to be determined. A readily used band width would be centered on the blue-green or yellow-green peaks of transmittance of most natural waters. Some care must also be given to the adaptation of the diver's eyes to the general level of illumination in which the visual match is best made. The importance of levels of illumination in underwater visibility tasks will be illustrated as a matter of course in Sec. 1.9.

Theory of Absorption Measurements in Natural Hydrosols

It is probably a continual source of fascination for highway patrolmen to examine the daily tallies of vehicles that pass over certain continuous road segments on superhighways or relatively desolate roads located between consecutive toll houses, and occasionally to be rewarded with a positive net influx of cars across a given segment. That is, when they subtract from the recorded number of vehicles entering the segment for each day the number of vehicles leaving the segment that same day they occasionally find a *positive difference*! From a purely phenomenological point of view, this means that some vehicles have been absorbed in their passage through the given stretch of highway! Of course, if the tally is correct, this could mean for example that there exist stalled vehicles somewhere along the segment, and a patrol is usually dispatched to investigate.

The principle of detection of the absorption of photons in a given layer of a natural hydrosol is exactly analogous to the toll house tally procedure for wayward vehicles described above. In Fig. 1.58 a laterally extensive layer of water between two levels y and z in a stratified optical medium is monitored by irradiance meters measuring $H(y,\pm)$ and $H(z,\pm)$. The total influx of irradiance to the layer is $H(y,-)+H(z,+)$, and the total efflux is $H(y,+)+H(z,-)$. Therefore the net influx of irradiance is

$$[H(y,-)+H(z,+)] - [H(y,+)+H(z,-)] = \bar{H}(y,-)-\bar{H}(z,-)$$

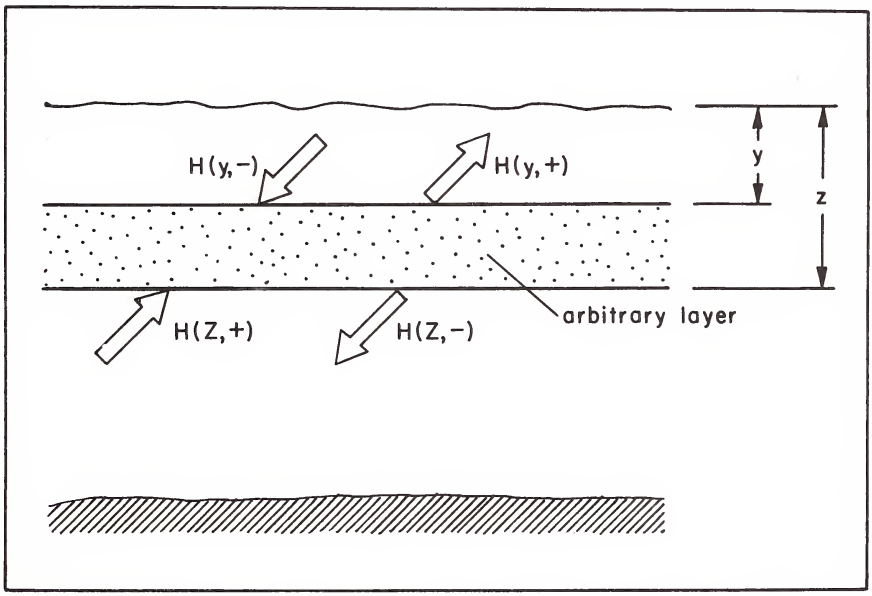

FIG. 1.58 The principle for determining light absorption in a layer of natural hydrosol.

By the same general reasoning leading to (2) we find that (as in the case of the one-D model) in all real natural hydrosols wherein there are no internal sources of radiant flux, this difference is positive, indicating that some fraction of the entering photons is continually being absorbed within the layer. The nature of the absorption is two-fold: if a tally is being kept only of photons of a given color (frequency) then the absorption in this case includes scattering with change in *color*. Secondly, absorption could mean the transformation of radiant energy into non-radiant energy. In practice both of these mechanisms are operative. The difference $\overline{H}(y,-)-\overline{H}(z,-)$ is a direct measure of the amount of radiant flux absorbed by a column of unit horizontal cross section bounded by the upper and lower planes of the layer of water. If a is the volume absorption coefficient of the (homogeneous) layer, then this quantity is directly measurable by means of the relation:

$$a = \frac{\overline{H}(y,-) - \overline{H}(z,-)}{\int_y^z h(z')\, dz'} \tag{89}$$

provided a probe is sent down to find the values h(z') of the scalar irradiance between depths y and z. The reader may check that (89) follows directly from (16) of Sec. 1.3. Hence (89) is an exact formula for homogeneous media with a stratified light field. A discussion of (89) and a systematic derivation of the related formulas below is given in Sec. 13.8.

A local version of (89) comes from (16) of Sec. 1.3 directly:

$$a(z) = \frac{1}{h(z)} \frac{d\overline{H}(z,+)}{dz} \tag{90}$$

To use (90), one need only measure h(z) at depth z, and also $\overline{H}(z,+)$ in a small neighborhood of depths about depth z, so as to be able to compute the derivative of $\overline{H}(z,+)$ at that depth. This method is exact for all inhomogeneous stratified media. An instrument to measure a, and which is based on the principle represented by (90), has been devised by Tyler [299] at the Visibility Laboratory.

It is important to notice two essential features of (90). First, observe that scalar (rather than ordinary irradiance) is used to normalize the derivative; second, the *net* irradiance is used in the derivative. Now it turns out that of these two features, it is the first that is of critical importance and which gives the formula its distinctive power in natural hydrosols. To see this, recall from the preceding discussions that the reflectance R_∞ for green light is quite small in clear deep media, the kind found in most oceanic work, for example, Hence in:

$$\bar{H}(z,+) = H(z,+) - H(z,-)$$

and in:

$$h(z) = h(z,+) + h(z,-)$$

we can ignore with a fair measure of impunity the terms $H(z,+)$ and $h(z,+)$. In that case, (90) becomes:

$$a(z) \cong \frac{-1}{h(z,-)} \frac{dH(z,-)}{dz} \quad .$$

Furthermore, by virtue of the distribution factors $D_{\pm}$ defined in the two-flow model, we can write:

$$h(z,-) = D_{-}H(z,-) \quad . \tag{91}$$

In addition, if we estimate $H(z,-)$ by means of the exponential law:

$$H(z,-) = H(0,-)e^{-Kz}$$

(where K is obtained either via the one-D model, as in (9) of Sec. 1.3, or empirically), then (91) yields:

$$a \cong \frac{-1}{D_{-}H(z,-)} \cdot [-KH(z,-)]$$

$$= \frac{K}{D_{-}} \tag{92}$$

This points up the critical importance of the *scalar* irradiance $h(z)$ in (90); for if we used $H(z,+)+H(z,-)$ in its place, then we would have (90) yield up the estimate

$$a \cong K \qquad \text{(wrong)}$$

which is clearly false. Indeed, the factor D_{-} is often on the order of 1.0-2.0 in natural optical media with values clustering about 1.3 for blue-green light, so the use of H rather than h to normalize the derivative in (90) could lead to errors anywhere from 0 to 100 percent in the estimate of $a(z)$, but mostly on the order of 30 percent.

From (90) we can also obtain a crude but occasionally useful estimate of the *rate of absorption of radiant energy per unit volume of a layer of water.* First:

$$\frac{d\bar{H}(z,+)}{dz} = a(z)\, h(z) \tag{93}$$

is the exact formula for the required depth rate of absorption, i.e., of net influx of irradiance to a unit layer at depth z. It is simply the product of $a(z)$ at depth z with $h(z)$ at depth z. Now if we again drop off $H(z,+)$ and $h(z,+)$ as being small compared to $H(z,-)$ and $h(z,-)$, we have:

$$\frac{dH(z,-)}{dz} \cong -a(z)\, h(z,-)$$

$$= -a(z) D_{-} H(z,-)$$

$$\cong -KH(z,-) = -KH(0,-)e^{-Kz}$$

as the depth rate of absorption of radiant flux per unit volume at depth z. The last approximation comes from (92) and by means of the exponential law for irradiance. It should be noted that (93) is exact only for stratified media. If one wishes to compute exactly the rate of absorption of a small volume of water in a general light field in a generally inhomogeneous optical medium he may use (1) of Sec. 13.8 and the general instructions given there.

As an illustration of (90) as a means of estimation of the volume absorption coefficient, consider the sample light field given in Table 1.

TABLE 1

Irradiance and Scalar Irradiance in
Lake Pend Oreille, Idaho. (Relative values)

z(meters)	H(z,-)	H(z,+)	h(z,-)	h(z,+)
4.24	721,000	15,500	899,000	41,900
10.42	329,000	6,040	413,000	16,500
16.58	109,000	2,230	141,000	6,190
28.96	13,100	298	17,200	830
41.30	1,660	39	2,190	108
53.71	221	5	289	14

These data were obtained by Tyler, Richardson, and Holmes from radiance distribution measurements in Lake Pend Oreille, Idaho [306]. Radiance filters were centered on 480 ± 64 mμ. Observe first that D_{-} at 4.24 meters is 1.25, and that its value at 53.71 meters is 1.31. This shows, incidentally, the general magnitude of D_{-} found in most natural waters for blue-green light. Similar values may be found at the other depths. By computing the slope of the $\bar{H}(z,+)$-plot derived from the tabulations above, and using the computed h(z) values, it was found via (90) that the lake was essentially homogeneous with an a on the order of .117/m. The K for this medium was found to be .169/m, and α = .442/m.

We can invert the formulas (89) and (90) to find the rate of absorption of radiant energy in a given medium, given the volume absorption function and some radiometric samplings of the medium. For example in infinitely deep media in which

scalar irradiance decreases according to the exponential law, we can estimate the total rate of absorption as follows. In (89) set y = 0 and z = ∞, so that $\bar{H}(\infty,-) = 0$. This leaves:

$$\bar{H}(0,-) = a\int_0^\infty h(z')\, dz'$$

Using the exponential law for h(z):

$$\bar{H}(0,-) = ah(0)\int_0^\infty e^{-Kz'}\, dz'$$

That is:

$$\bar{H}(0,-) = \frac{a}{K}\, h(0) \qquad (94)$$

This formula holds actually for any depth z below the surface. (Simply multiply each side by e^{-Kz}.) If z is used in place of 0, then $\bar{H}(z,-)$ in (94) is a measure of the radiant flux absorbed by the entire medium *below* the level z.

As an illustration of (94), suppose that h(0) = 250 watts/m² on some sunny day just below the surface, for the wavelength band 480 ± 64 mμ. The total rate of absorption throughout the lake per square meter of lake surface is therefore:

$$\bar{H}(0,-) = \frac{.117}{.169} \times 250$$

$$= 173 \text{ watts/m}^2 \quad .$$

The remaining power, namely 250-173 = 77 watts/m² goes on to initiate and sustain the scattered light field within the body of the lake.

As another illustration of (94), suppose that measurements of $\bar{H}(y,-)$ and h(y) are made at some depth y in a deep homogeneous medium, and also that K is known for the same wavelength interval. We can then estimate a as follows. From (94):

$$a = K\, \frac{\bar{H}(z,-)}{h(z)} \qquad (95)$$

For example, from Table 1, at depth 28.96 meters, we have

$$\bar{H}(28.96,-) = 13{,}100 - 298$$

$$= 12{,}802 \text{ watts/m}^2$$

Also,

$$h(28.96) = h(28.96,+) + h(28.96,-)$$

$$= 830 + 17{,}200$$

$$= 18{,}030 \text{ watts/m}^2$$

Hence:

$$a = .169 \quad \frac{12,802}{18,030}$$

$$= .120/m \quad .$$

which agrees to within .003/m with the estimate .117/m for a obtained by light field measurements using (90).

We conclude with some observations on the radiant energy content of natural hydrosols, a concept which is closely related to the absorption concept presently under discussion. Recall the general relation between scalar irradiance h(z) and radiant density u(z) as given in (5) of Sec. 1.1:

$$u(z) = \frac{1}{v} h(z) \tag{96}$$

Here v is to the speed of light in homogeneous water:

$$v = 2.25 \times 10^8 \text{ m/sec} \quad .$$

By integrating h(z) from the surface (z = 0) down to depth z in an infinitely deep medium we find:

$$U(z) = \int_0^z u(z)\, dz = \frac{1}{v}\int_0^z h(z)\, dz = \frac{h(0)}{vK}\left[1-e^{-Kz}\right] \tag{97}$$

provided h follows the exponential law. This gives the amount of radiant energy U(z) in a vertical column of unit horizontal cross section with upper end at the surface and lower end at depth z. Observe that by (89) this also can be written

$$U(z) = \frac{\bar{H}(0,-) - \bar{H}(z,-)}{va} = \frac{h(0)}{vK}\left[1-e^{-Kz}\right] \tag{98}$$

For very shallow media, (98) yields

$$U(z) \cong \frac{h(0)z}{v} \tag{99}$$

For very deep media (98) yields

$$U(\infty) = \frac{h(0)}{vK} \tag{100}$$

In the present medium, (Lake Pend Oreille) which is very deep, with K = .169/m and h(0) = 250 watts/m^2 (say), we find

$$U(\infty) = \frac{250}{2.25 \times 10^8 \times .169}$$

$$= 6.6 \times 10^{-6} \text{ joules/m}^2$$

Hence over a region of one square kilometer (10^6 m^2) the present medium contains below the surface about 7 joules of radiant energy in the blue-green wavelength interval in scattered or directly transmitted form. Observe by (98) that nearly 95% of this radiant energy is stored within the first three diffuse attenuation lengths below the surface, i.e., within $3/K = 3/.169 = 17.7$ meters of the surface. Equation (98) shows how $U(z)$ can be estimated if the net influx of radiant energy over the depth interval $[0,z]$ is known, along with the volume absorption coefficient a. Further discussion of light storage phenomena in natural waters is given in Sec. 5.13.

1.5 Some Properties of Artificial Light Fields in Natural Waters

Artificial light fields in seas and lakes are produced by men seeking to illuminate natural underwater environs to carry out search or detection procedures, to study biological processes, or to establish techniques of underwater communication by means of residual and scattered radiant flux. To facilitate these activities some knowledge is desirable of the general quantitative relations between the optical properties of a medium and the light fields produced in that medium by various artificial sources. Such sources commonly range from those that produce highly collimated beams to those that produce conical beams of varying spread, up to uniform point sources. In this section we shall discuss several interesting empirical relations developed for artificial light fields.

Useful models of artificial light fields, which can completely elucidate the empirical findings presented below, may be based on the diffusion models discussed in Chapter 6, in particular in Secs. 6.5-6.7. However, we shall concentrate in this brief survey of artificial light fields only on the diffusion model (27) of Sec. 1.3, as it affords a simple yet adequate base on which to rest the empirical formulas.

The Pure Absorption Case

To see what the difficulties are in describing artificial light fields in the sea, suppose for the moment that sea water or any other natural hydrosol only absorbed radiant flux, and therefore did not scatter it. Suppose that a spherical source S of radius r_o, as in Fig. 1.59, has a uniform inherent surface radiance N_o. Then the apparent radiance N_r of this source's surface is:

$$N_r = N_o e^{-ar} \tag{1}$$

where a is the volume absorption coefficient of the medium. The radiant flux output P_o of the source is:

$$P_o = (4\pi r_o^2)\pi N_o \tag{2}$$

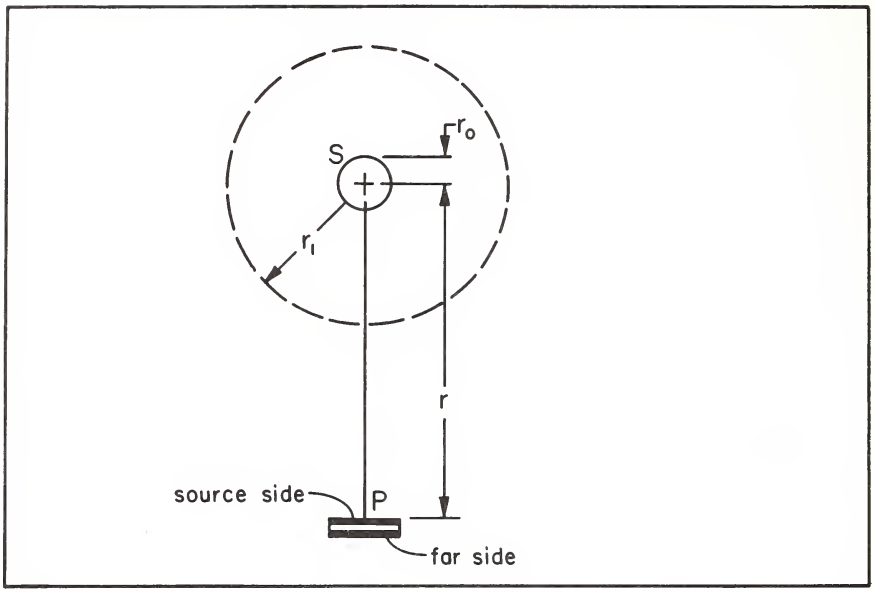

FIG. 1.59 For the derivation of the diffuse light field at P as generated by a small source S via secondary sources limited to the sphere of radius r_1. (Diffusion Model)

Its radiant intensity is:

$$J_o = \frac{P_o}{4\pi} = (\pi r_o^2)N_o \quad , \tag{3}$$

and the apparent irradiance H_r produced by the source is very nearly:

$$H_r = \frac{J_o e^{-a(r-r_o)}}{r^2} \tag{4}$$

for all $r \geq r_o$. The apparent radiance N_r and apparent irradiance H_r in the case of pure absorption are thus quite simply described because of the absence of scattered flux. Even in the present case all is not simple if the radius r_o is large compared to the absorption length 1/a of the medium, for then a relatively complicated integration over direction space must replace (4). However, for $r_o < 1/2a$, (4) is an adequate approximation in normal practice.

Derivation of the Semi-empirical Diffusion Model for Point Sources

When scattering may take place in the medium and to an extent in which the simple formulas (1), (4) no longer adequately describe the apparent radiance and irradiance fields,

we may go on to adopt the next simplest available model for these fields. The required candidate takes the form of (36) of Sec. 1.3 in which the integration in (37) of Sec. 1.3 is no longer over the entire space X but is restricted to a relatively small spherical region of radius r_1 about the luminous source. It is in this spherical region where the primary scattered radiant flux from the source initiates the principal part of the diffuse light field measured at relatively great distances r. The smaller r_o and r_1 are, compared to r, the more nearly will the scalar irradiance h(r) at a distance r from the source S be given by an equation of the form:

$$h(r) = h^{o}(r) + h^{*}(r)$$

$$= \frac{AJ_o e^{-\alpha r}}{r^2} + \frac{BJ_o e^{-\kappa r}}{Dr} \tag{5}$$

where A and B are generally functions of r, or at the very least, constants used to adjust the formula to fit empirical data. It is necessary to introduce A and B because we have sidestepped integrations which could contribute measurable deviations from the simple form (5) for small and large r. We have simply used (4) above and (33) of Sec. 1.3 in a linear combination to obtain (5). A further simplification in the model can be effected if we replace κ, the decay constant indigenous to diffusion theory (cf. (32) of Sec. 1.3), by the more readily empirically determined diffuse attenuation coefficient K obtained from irradiance measurements in the sea. (K is the empirical counterpart to the k of the two-flow model discussed above.) Thus, from (32) of Sec. 1.3 we have:

$$\kappa^2 = \frac{a}{D}$$

From (92) of Sec. 1.4 we can approximate a by the form:

$$a \cong \frac{K}{D_-}$$

where D_- is now the distribution factor for the irradiance measured at point P of Fig. 1.59 produced by flux on the source side of the collector at P. If we identify κ and K, then the two preceding relations yield an estimate of the classical diffusion constant D:

$$D = \frac{1}{D_- K} \tag{6}$$

Using this in (5), dividing each side of (5) by D_-, and keeping A, B arbitrary, we have:

$$\boxed{H(r) = J_o\left(A \frac{e^{-\alpha r}}{r^2} + B \frac{Ke^{-Kr}}{r} \right)} \tag{7}$$

which is the desired semi-empirical form for the irradiance H(r) produced at distance r from a point source of radiant intensity J_0. α is the volume attenuation coefficient for the medium and K is the diffuse attenuation coefficient for the medium. Observe also that in passing to (7) we have dropped as negligible the irradiance on the far side of the surface at P in Fig. 1.59. Despite this conglomeration of assumptions, (7) nevertheless provides a suitable model for H(r) under judicious choice of the A and B as dictated by actual sample measurements of H(r) in real media. We shall now consider two such particular empirical forms of (7).

Two Examples of the Empirical Diffusion Model

Duntley reports in [76] and [77] the results of his empirical study during the summer of 1959 of irradiance fields produced by point sources in Lake Winnipesaukee, N.H.. He determined A and B in (7) in such a way that the resultant empirical formula should be applicable to a large set of natural hydrosols in which are imbedded point sources with a wide range of angular beam spreads.

In the case of a point source with a directionally uniform radiance over all directions, Duntley found that in (7), the constants A, B may be given by:

$$A = 1 \tag{8}$$

$$B = 2.5[1 + 7e^{-Kr}]/4\pi \tag{9}$$

This shows that for relatively small r, B is on the order of 8 times that for large r. A comparison of a real irradiance field (black dots) with that predicted by (7) using (8), (9) (solid curve) is given in Fig. 1.60. The radiant flux wavelengths measured in this experiment were via a Wratten No.61 green filter. The corresponding attenuation length of the water was $1/\alpha = 1.52$ meters, (= 5.00 feet) associated with an $\alpha = .655/m$ (= .200/ft). The K for the same water and wavelength range was found to be .187/m (= .057/ft.).

In a more detailed analysis of the empirical results, Duntley generalized (9) to include the effects of the beam spread of the source, particularly for wide beam spreads. It was found that:

$$A = 1 \tag{10}$$

$$B = \left[2.5\text{-}1.5 \log_{10}\left(\frac{2\pi}{\beta}\right)\right]\left[1+7\left(\frac{2\pi}{\beta}\right)^{1/2} e^{-Kr}\right] \Big/ 4\pi \tag{11}$$

Here the point source is emitting a beam in the form of a circular cone with total angular opening of β. Observe how (11) reduces to (9) for the case of $\beta = 2\pi$. Formula (11) is expected to be a good approximation in the range $\pi/9 \leq \beta \leq 2\pi$, i.e., for all beam spreads not less than about 20°.

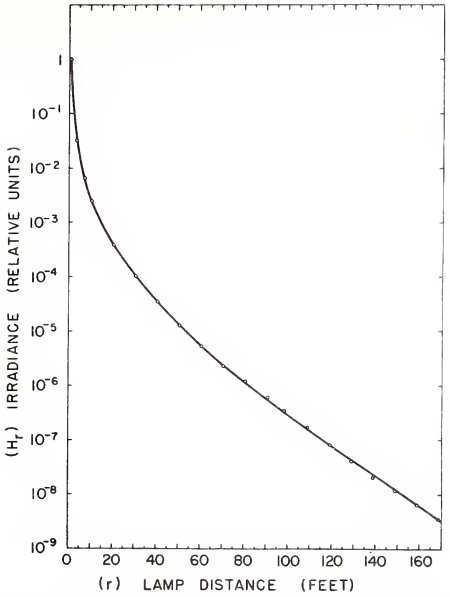

FIG. 1.60 Comparison of calculated irradiance and measured irradiance induced by a point source (small spherical lamp) by Duntley, Lake Winnipesaukee, N.H., 26 August 1959. (Fig. 16 from [78], by permission)

Radiance Distribution Produced by a Submerged Uniform Point Source

In the same set of experiments leading to the empirical determination of the diffusion model (7), (8), (9), Duntley examined the radiance distribution produced at various distances by a submerged point source of nearly uniform radiant intensity. This radiance distribution can be observed and photographed as a function of the direction from the source for various choices of the on-axis distance from the source. For nearby locations, the source (in the form of a spherical lamp) stands out sharply from its luminous halo. As viewing distance increases, the bright disk of the lamp rapidly becomes angularly smaller and also dimmer. Eventually the disk itself vanishes at about 18 to 20 attenuation lengths (i.e., at about $18/\alpha$ to $20/\alpha$ meters), but the luminous glow persists for relatively great distances. Fig. 1.61 depicts the radiance distributions produced by a point source, for a selected set of distances from the source. The lamp was a 1000 watt incandescent "diving lamp", whose 3 inch (7.62 cm) diameter spherical lamp envelope was sprayed with a lacquer to insure that its radiant intensity was uniform.

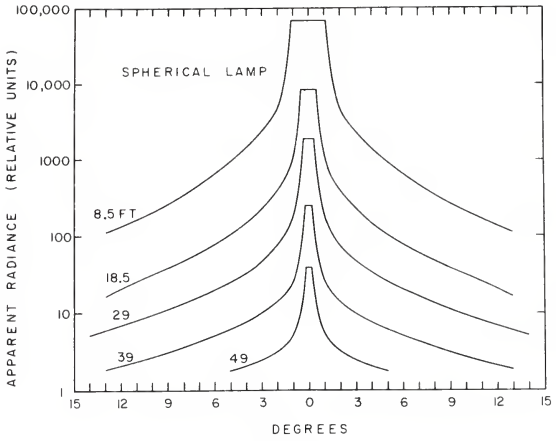

FIG. 1.61 Radiance distributions produced by a point source (small spherical lamp). Measured by Duntley, Lake Winnipesaukee, N.H., 3 August 1961. (Fig. 15 from [78], by permission)

An Empirical Study of Light Fields Produced by Collimated Sources

In the future it is likely that the laser will be used to some extent in underwater communications. It is therefore of interest to study the properties of propagation of highly collimated beams of radiant flux in natural hydrosols. In some preliminary studies in this direction, Duntley [78] had designed and constructed a source of highly collimated radiant flux, shown schematically in Fig. 1.62. Using a lens system designed by J. J. Rennilson, it was possible to produce a long, narrow, very nearly cylindrical beam of light with total beam spread 2ψ as small as 0.01° or 0.00017 of a radian. Smaller beams would begin to be noticeably spread by diffraction effects. By selecting various external beam stops it was possible to produce fine cylindrical beams of variable diameters D which were nearly divergenceless (i.e., cylindrical) over a distance $c = D/\psi$. (The figure gives the ray-geometrical significance of this relation.) Over this range the beam's residual irradiance is essentially free from inverse square effects and is of magnitude $H_r^o = H_o e^{-\alpha r}$, where $r \leq c$, $H_o = J_o/c^2$, and where J_o is the radiant intensity of the lamp used in the collimator. For distances r greater than c, the light beam would depart from its cylindrical shape and thus the residual irradiance of the beam would begin to fall off as the inverse square of r and also be further damped exponentially, so that for $r \geq c$, assuming negligible diffraction effects, we have:

$$H_r^o = \frac{H_o e^{-\alpha r}}{(r/c)^2} \quad . \qquad (12)$$

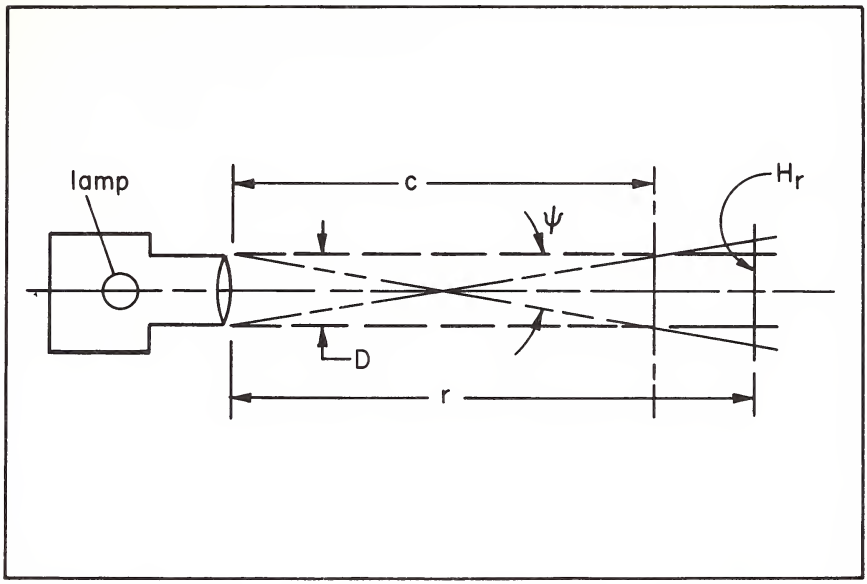

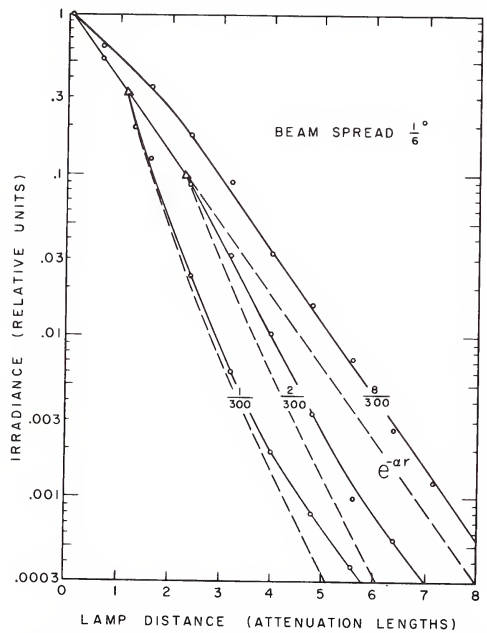

FIG. 1.62 Source for highly collimated beam of radiant flux experiment recorded in Fig. 1.63.

FIG. 1.63 Three determinations of irradiance produced by a highly collimated beam of radiant flux, as made by Duntley in Lake Winnipesaukee, N.H., 14 August 1961. (Fig. 18 from [78], by permission)

Figure 1.63 records three experimental determinations by Duntley of the apparent irradiance H_r of a highly collimated beam of spread 1/6°. The irradiance is that produced at a point on the axis of the beam a distance r from the source, and on a plane normal to the axis. The experimental results were reduced so that the beam diameters D in each of the three cases are in terms of the attenuation lengths of the medium namely 1/300, 2/300 and 8/300 attenuation lengths. In this way it is possible to free the results somewhat from the nature of the particular medium in which they were found. The medium in this case was Lake Winnipesaukee, N.H. whose α was .520/m (= .158/ft.) and whose corresponding attenuation length therefore was $1/\alpha$ = 1.92 meters (= 6.3 ft.), for the wavelength band provided by Wratten No. 61 green filters. The solid lines in Fig. 1.63 are the empirically found H_r values. The dashed lines are the residual irradiances H_r^o computed from (12). The dashed lines depart from the solid lines at the points shown by triangles. These points are located at the distances $c = D/\psi$, which are 1.15 and 2.30 attenuation lengths for the 1/300 and the 2/300 curves, respectively. The point for the 8/300 beam is located 9.20 attenuation lengths away and is not shown. Hence the vertical separation of a

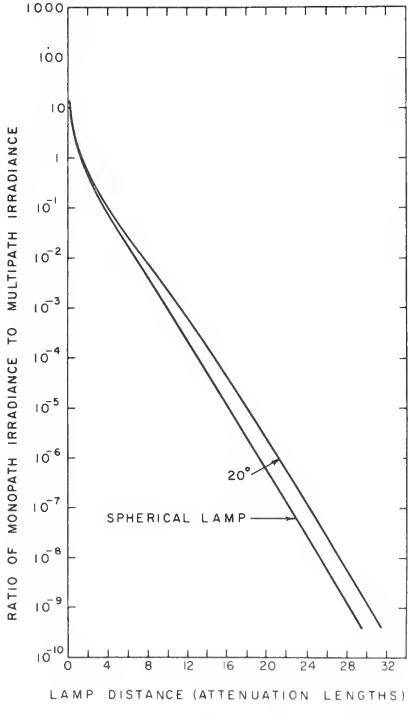

FIG. 1.64 Ratio of monopath (i.e., residual) radiance to multipath (i.e., scattered) radiance for two types of source as measured by Duntley in Lake Winnipesaukee, N.H., 26 August 1961. (Fig. 19 from [78], by permission)

solid curve and its dashed mate gives a measure of the scattered (or diffuse) irradiance H_r^* for each distance r. It should be observed that the data in Fig. 1.63 pertain only to the axis of an aplanatic underwater projection system having a beam spread of 1/6°. In other words the 1/6° beam spread cannot be scaled up and down by factors of 10. Separate and new measurements for different spreads ψ must be made to see how H_r^* depends on ψ.

Some further information on the relative magnitudes of unscattered and scattered irradiances H_r^o (monopath) and H_r^* (multipath) is given in Fig. 1.64, and is also due to Duntley [78]. The ratio H_r^o/H_r^* is plotted versus r for two cases: a spherical point source, and a point source having a total spread of 20°. In the latter case the irradiance is located on-axis and falls on a plane normal to the axis, as usual. As expected, for each fixed distance r, there is relatively more diffuse irradiance H_r^* in the case of the spherical source as for the narrow beam source. These curves are for the medium described in Fig. 1.60. The residual irradiance H_r^o was calculated using the first term of (7) with A = 1. H_r^* was obtained via $H_r - H_r^o = H_r^*$ using the irradiance H_r of Fig. 1.60 for the spherical case, and using recorded H_r data for the 20° case.

Figure 1.65 shows still another experimental finding by Duntley [78] concerning the irradiance produced by collimated beams. In this case the beam had a 2ψ of .046°, and a 2 inch (or 5.08 cm) diameter D. The medium had an α of .685/m (= .209/ft) and hence an attenuation length $1/\alpha$ of 1.46 meters

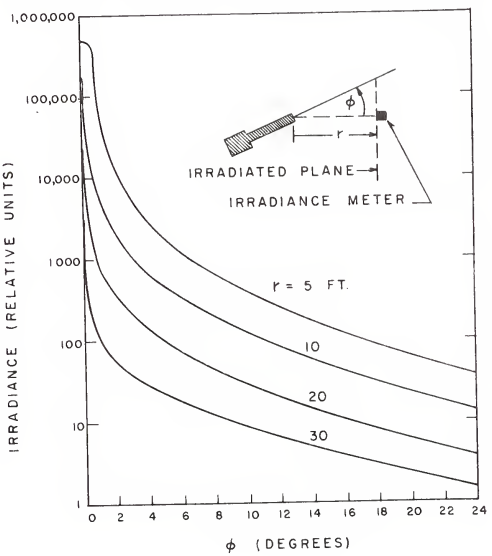

FIG. 1.65 Irradiance on a collecting plane produced by a sweeping collimated beam, as observed by Duntley, Lake Winnipesaukee, N.H., Summer 1961. (Fig. 20 from [78], by permission)

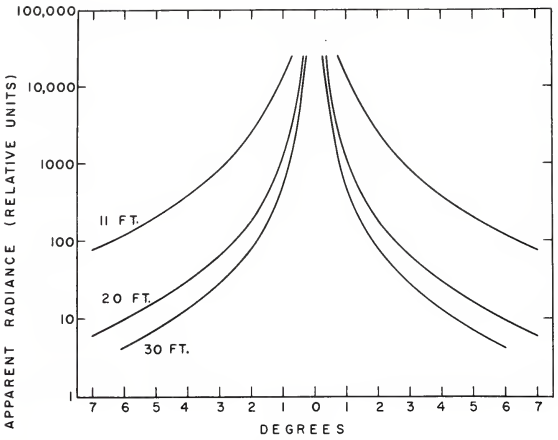

FIG. 1.66 Apparent radiance produced by beam of highly collimated flux (cf. Fig. 1.62), as found by Duntley, Lake Winnipesaukee, N.H., 11 August 1961. (Fig. 17 from [78], by permission)

(= 4.80 ft.) as measured via a Wratten No. 61 green filter, in Lake Winnipesaukee, N.H., summer, 1961. The locations of the measurements within the induced light field are indicated by the inset of the figure. The irradiated plane was swept by the moving beam.

Finally, Fig. 1.66 depicts the apparent radiance as observed under somewhat the same general test condition of Fig. 1.65. Now the beam had a 2ψ of 0.01° and was directed toward the telephotometer so that it completely filled the entrance pupil of the latter at all times. The water was slightly clearer in the present case, having an attenuation length of 2.04 meters (= 6.70 ft.), i.e., an α of .490/m (= .149/ft.) for the same wavelength band. It is of interest to compare Figs. 1.61 and 1.66, which reveal subtle differences between the radiance distributions found by looking at distant point sources and down the barrel of a collimated beam.

Some further discussion of these empirical findings, especially their applicability to underwater communications by scattered light, may be found in [79].

1.6 Inherent and Apparent Optical Properties of Hydrosols

The three simple models describing light fields in the seas and lakes of the earth, as developed in Sec. 1.3, may now be considered as reasonably established descriptions of radiative transfer in natural hydrosols. For as we have seen in our brief survey of their applications in Sec. 1.4 and 1.5, they can be used both to organize our accumulated empirical knowledge of natural light fields by means of faithful symbolic representations of our observations, and also to encourage, via simple mathematical manipulations, the exploration of

new and deeper physical phenomena connected with light fields in the sea. Implicit in the structure of these models are the optical properties we introduced during their construction, such as α, σ, s, a, and κ.

Now, if the theoretical equations of hydrologic optics may be viewed as the *bones* of the subject, then certainly the optical properties α, σ, κ and the various related properties are the *meat* of the subject. Indeed, the equations provide the essential form of our discipline; but the numerical values of their parameters provide it with useful substance. It is our purpose in this section to sort out the principal optical properties used in hydrologic optics and to indicate their representative magnitudes. It is not our purpose at this time, however, to optically catalog the seas and lakes of the world; such a task still awaits a definitive effort, and lies outside the province of a work devoted to the theoretical principles of the subject.

Operational Definitions of the Inherent Optical Properties

The fundamental inherent optical properties of hydrologic optics are the *volume attenuation function* α, and the *volume scattering function* σ. They are *inherent* in the sense that their magnitudes for each wavelength depend only on the substances comprising the hydrosol and not on the geometric structure of the various light fields that may pervade it. The properties α, and σ are *fundamental* in the sense that the entire theory of hydrologic optics (and indeed radiative transfer theory) can be constructed from them, given the concept of the radiance function and the equation of transfer. The greatest contributions an experimental scientist can make to hydrologic optics at this stage of its development (or to any other branch of radiative transfer) lie in the detailed study --on physical, chemical, and optical levels--of these two fundamental properties, along with the simultaneous documentation of the light fields in optical media.* Chapter 13 is devoted to a detailed exposition of the operational definitions of these and other properties. Our immediate aim is to introduce these concepts with a minimum of preamble, though a full and deep understanding of them can come only after the contents of at least Chapters 2, 3, 8, 9 and 13 are mastered.

The Volume Attenuation Function

The volume attenuation function α provides a measure of the loss of radiant flux from a beam of photons of a given wavelength induced by: (a) scattering of flux out of the direction of the beam without change in wavelength or: (b) by scattering of flux of the beam with a change of wavelength, or: (c) by outright absorption of some of the radiant energy

---

*Important problems concerning the physical makeup of α and σ also await interested theoreticians. See problem III of Chapter XVI, Ref. [251].

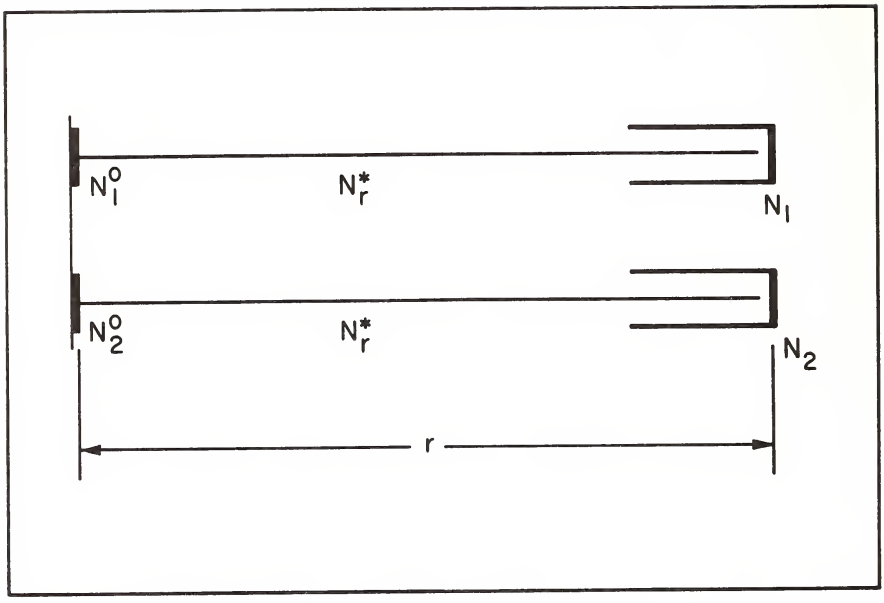

FIG. 1.67 Arrangement for an operational definition of volume attenuation function.

into a form of non-radiant energy. A particularly effective method of defining α is by means of the beam transmittance function using the fact that radiance differences of simultaneous beams propagate precisely in an exponential manner along close parallel paths.

Figure 1.67 depicts two parallel closely spaced paths of length r in an optical medium. The initial radiances at the beginning of the paths are N_1^o and N_2^o, and matters are arranged so that the medium is homogeneous in the vicinity of the paths and that the path radiances of the two paths are essentially the same, and of common value N^*. If T_r is the common fraction of photons comprising N_1^o and N_2^o transmitted along each path without having been scattered or absorbed, then by (24) of Sec. 1.3 the apparent radiances:

$$N_1 = N_1^o T_r + N^*$$

and

$$N_2 = N_2^o T_r + N^*$$

measured at the end of the path may be used to find the *beam transmittance* T_r by means of the relation:

$$T_r = \frac{N_2 - N_1}{N_2^o - N_1^o} \qquad (1)$$

It is very easy to see, using (1), that if two paths of

arbitrary lengths r and s are placed end to end to form a new straight path of length r+s, then:

$$0 \leq T_r \leq 1 \tag{2}$$

and:

$$T_{r+s} = T_r T_s \tag{3}$$

and also:

$$T_o = 1 \tag{4}$$

The second property is the *multiplicative* (or semigroup) property of beam transmittance. It is the basis of the exponential representation of T_r. Indeed, let us write:

$$\text{"}\alpha_r\text{"} \quad \text{for} \quad \frac{1-T_r}{r} \tag{5}$$

The quantity α_r is the (*empirical*) *volume attenuation function* because it gives the average amount of loss of radiance of a beam per unit length of travel of a beam of unit radiance. To see this let N^o be an initial radiance starting out along a path of length r. Then $N^o T_r = N_r^o$ is the *residual radiance*, i.e., the radiance left over in the beam after scattering and absorption losses over the path. Hence $N^o - N_r^o$ is the actual radiance lost, and $(N^o - N_r^o)/r$ the average loss per unit length of the path. Dividing by N^o, we arrive at (5).

Now consider a path of length r+s. Then by (3) and (5):

$$\frac{T_{s+r} - T_r}{s} = \frac{T_s - 1}{s} T_r = -\alpha_s T_r$$

Using the definition of derivative applied to T_r, and letting $s \to 0$, we have:

$$\frac{dT_r}{dr} = -\alpha T_r \tag{6}$$

where we have written:

$$\text{"}\alpha\text{"} \quad \text{for} \quad \lim_{r \to 0} \alpha_r \tag{7}$$

From (4) and (6):

$$T_r = e^{-\alpha r} \tag{8}$$

for homogeneous media. This is the basic connection between beam transmittance and the *volume attenuation function* α defined in (7). The function α has dimensions of L^{-1}, and therefore units of $(\text{meter})^{-1}$. Observe that by (2), α_r and hence α is a non-negative quantity. From (8) we have:

$$\alpha = -\frac{1}{r} \ln T_r \tag{9}$$

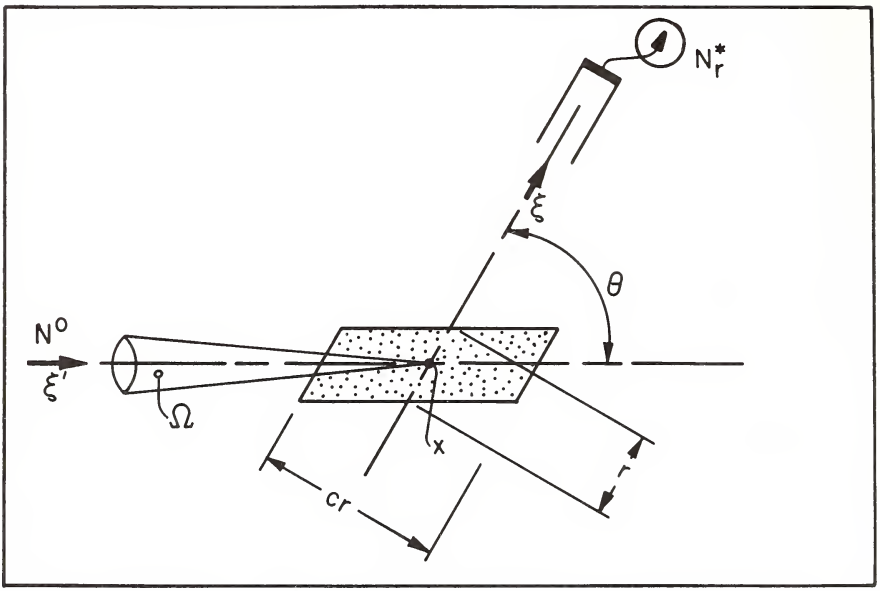

FIG. 1.68 Arrangement for an operational definition of volume scattering function.

which together with (1) provides a useful operational definition of α. For a further discussion of these ideas see Secs. 13.2, 13.4 and 13.5.

The Volume Scattering Function

A small volume of an optical medium is irradiated through a small set of directions of solid angle Ω about a direction ξ' by a radiance N^o of a given wavelength, and the scattered radiant flux in the direction ξ, at an angle θ with ξ', is observed to be N_r^*, where r is the length of the line of sight through the volume. The volume is in the form of a parellelepiped whose dimensions are r × r × cr, where c is a constant. Then we write

$$\text{"}\sigma_{r,\Omega}(\theta)\text{"} \quad \text{for} \quad \frac{N_r^*}{N^o r\Omega} \tag{10}$$

Further, we write:

$$\text{"}\sigma(\theta)\text{"} \quad \text{for} \quad \lim_{\substack{r\to 0 \\ \Omega\to 0}} \sigma_{r,\Omega}(\theta) \tag{11}$$

and call σ the *volume scattering function*. A more detailed discussion of σ is given in Sec. 13.6, and in Sec. 18 of Ref. [251]. The dimensions of σ are $L^{-1}(sr)^{-1}$ and hence its units

are $(\text{meter})^{-1}(\text{steradian})^{-1}$.

The reason for choosing (11) as the basic definition of $\sigma(\theta)$ is that it yields at once the relation:

$$N_* = \frac{N_r^*}{r} = N^o\sigma(\theta)\Omega$$

which with care can be made to blossom into:

$$N_*(x,\xi) = \int_{\Xi} N(x,\xi')\sigma(x;\xi';\xi)\, d\Omega(\xi')$$

and which in turn is the standard representation of the path function in general radiative transfer theory. The correct logical order of appearance of N_* and σ in the theoretical construction of radiative transfer theory is given in the systematic discussions of Chapter 3.

An alternate form of $\sigma_{r,\Omega}(\theta)$ is given by writing

$$\text{"}\sigma_V(\theta)\text{"} \quad \text{for} \quad \frac{J_r^*}{H^oV} \tag{12}$$

where $H^o = N^o\Omega$, V is the volume (e.g., in this case cr^3) of the scattering region in Fig. 1.68, and J_r^* is the radiant intensity of the scattered flux. Clearly

$$\sigma_V(\theta) = \sigma_{r,\Omega}(\theta) \tag{13}$$

and so the two definitions are equivalent. (A careful proof of this is given in Sec. 18 of Ref. [251].) It is found that σ depends, in virtually any given practical setting, only on the angle θ between the incident direction ξ' and the scattered direction ξ. Hence it is possible in practice to write "$\sigma(x;\xi';\xi)$" in the more compact way "$\sigma(\theta)$", adopted above.

Volume Total Scattering Function and Volume Absorption Function

If $\sigma(\theta)$ is integrated over all θ, we obtain the *volume total scattering function* s; where we write:

$$\text{"s"} \quad \text{for} \quad \int_{\phi=0}^{2\pi}\int_{\theta=0}^{\pi} \sigma(\theta)\, \sin\theta\, d\theta\, d\phi \tag{14}$$

The angle ϕ is measured around the direction ξ' (in Fig. 1.68) as a hinge. Clearly we have:

$$s = 2\pi \int_{\theta=0}^{\pi} \sigma(\theta)\, \sin\theta\, d\theta \tag{15}$$

By splitting up the domain of integration $[0,\pi]$ into $[0,\pi/2]$ and $[\pi/2,\pi]$ and writing*:

$$\text{"f"} \quad \text{for} \quad 2\pi\int_{\theta=0}^{\pi/2} \sigma(\theta)\,\sin\theta\,d\theta \tag{16}$$

and

$$\text{"b"} \quad \text{for} \quad 2\pi\int_{\pi/2}^{\pi} \sigma(\theta)\,\sin\theta\,d\theta \tag{17}$$

We then have:

$$s = f + b \tag{18}$$

where f and b are the (volume) *forward* and *backward scattering functions* for collimated radiant flux.

The *volume absorption function* a comes in the back door of the theory by writing

$$\text{"a"} \quad \text{for} \quad \alpha\text{-}s\ , \tag{19}$$

but it redeems itself by possessing the following remarkably powerful operational form:

$$a = \frac{1}{h(z)}\,\frac{d\bar{H}(z,+)}{dz}\ , \tag{20}$$

discussed in the closing paragraph of Sec. 1.4 (see in particular (90) of Sec. 1.4, and also Sec. 13.8).

Considered together, the three operational formulations of α, σ, *and* a *in (9), (10) and (20), respectively, form a complete, mutually consistent, independent set of experimental means of determining these inherent optical properties of natural or artificial hydrosols.* An ideal scientific study of a given hydrosol would determine α,σ and a using these independent means, and then check consistency by requiring the three sets of data to satisfy the relation:

$$\boxed{2\pi\int_{0}^{\pi} \sigma(\theta)\,\sin\theta\,d\theta = \alpha\text{-}a} \tag{21}$$

In other words, the measured σ values are first integrated to yield the left side of (21). Then the measured a is subtracted from the independently measured α, and, hopefully, this difference is equal within a reasonable error allowance, to the computed σ-integral, for each wavelength from the infrared to the ultraviolet parts of the electromagnetic spectrum, and for each point in a hydrosol at which the

*The general definitions are given in (1), (2) of Sec. 9.6.

three determinations were made. This check is expected to hold, in principle, for all unpolarized light fields (Sec. 13.11).

Selected Physical Measurements of the Inherent Optical Properties

The following three tables provide representative samples of the inherent optical properties α, σ, s, f, b and a, measured for distilled water, ocean water, and lake water. The measurements were made by Tyler [300] and may serve as an example of the careful and consistent types of measurements that may be used to optically document the natural waters of the world. Such types of measurements, when performed for a sufficiently finely spaced set of wavelengths, will begin to move hydrologic optics into its final stage of development as a mature scientific discipline.

In Table 1 the distilled water was of the commercially available kind, and is not "distilled" in the strictest sense of the word. The two samples do, however, provide a reasonably good basis for comparison with the σ's of natural hydrosols. The wavelength band for the measurements was centered at 522 ± 80 mμ. The results compare favorably with those of Hulburt [115]. The Table 2 measurements were made in January 1961 in the four numbered locations shown in Fig. 1.69, and over the same wavelength band used for Table 1. Table 3

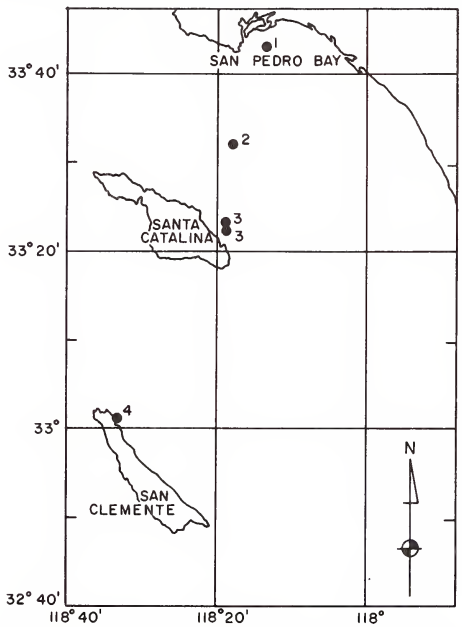

FIG. 1.69 Locations of Tyler's measurements off Southern California coast, winter 1960-1961, and as recorded in Table 2. (Fig. 1 from [300], by permission)

TABLE 1

Scattering properties of commercial "distilled" water samples. Bandwidth limited by a Wratten No. 57 filter.

Sample		A	B
Volume attenuation coefficient α/m		.062	.047
Volume total scattering coefficient s/m		.00845	.00457
Volume absorption coefficient a/m		.0536	.0424
Forward scattering coefficient f/m		.00763	.00396
Backward scattering coefficient f/m		.00082	.000620
Ratio f/s		.900	.870
Volume scattering function $\sigma(\theta)$			
	θ = 0°		
	10		
	20	.00648	.00316
	30	.00223	.00107
	40	.000941	.000520
	50	.000473	.000294
	60	.000271	.000191
	70	.000181	.000128
	80	.000140	.000096
	90	.000117	.000083
	100	.000110	.000079
	110	.000118	.000082
	120	.000126	.000092
	130	.000134	.000102
	140	.000139	.000112
	150	.000146	.000119
	160	.000171	.000141
	170	.000193	.000161
	180	.000201	.000169

(From [300], by permission)

TABLE 2

Scattering properties of Pacific Coastal and offshore water at the Stations shown in Figure 1.69. Bandwidth limited by a Wratten No. 57 filter.

Station number	1	2	3	4
Volume attenuation coefficient α/m	.736	.129	.118	.111
Volume total scattering coefficient s/m	.125	.01094	.01420	.0120
Volume absorption coefficient a/m	.611	.1181	.1038	.099
Forward scattering coefficient f/m	.119	.01010	.01321	.0110
Backward scattering coefficient b/m	.00630	.000847	.000982	.000984
Ratio f/s	.950	.925	.930	.915
Volume scattering function $\sigma(\theta)$				
θ = 0°				
10				
20	.1014	.00881	.01192	.00959
30	.0360	.00268	.00358	.00313
40	.0152	.00117	.00145	.00129
50	.00739	.000616	.000698	.000661
60	.00419	.000356	.000396	.000388
70	.00266	.000232	.000253	.000249
80	.00181	.000164	.000179	.000175
90	.00134	.000132	.000145	.000142
100	.00109	.000120	.000134	.000130
110	.000940	.000120	.000135	.000135
120	.000903	.000124	.000146	.000146
130	.000912	.000134	.000158	.000159
140	.000944	.000145	.000175	.000176
150	.001003	.000156	.000192	.000193
160	.001028	.000175	.000202	.000208
170	.001036	.000191	.000206	.000219
180	.001037	.000197	.000207	.000223

(From [300], by permission)

TABLE 3

Volume scattering function for Lake Pend Oreille, Idaho, Spring 1960 before and after a high wind. Bandwidth limited by a Wratten No. 45 filter.

Sample date		April 26	April 27
Volume attenuation coefficient α/m		.589	.909
Volume total scattering coefficient s/m		.258	.585
Volume absorption coefficient a/m		.331	.324
Forward scattering function f/m		.248	.559
Backward scattering coefficient b/m		.00976	.0256
Ratio f/s		.960	.955
Volume scattering function $\sigma(\theta)$			
	θ = 0°		
	10		
	20	.222	.470
	30	.0715	.166
	40	.0291	.0758
	50	.0137	.0380
	60	.00712	.0206
	70	.00416	.0121
	80	.00271	.00780
	90	.00198	.00559
	100	.00162	.00448
	110	.00147	.00394
	120	.00143	.00379
	130	.00145	.00372
	140	.00149	.00371
	150	.00156	.00383
	160	.00163	.00396
	170	.00168	.00406
	180	.00170	.00410

(From [300], by permission)

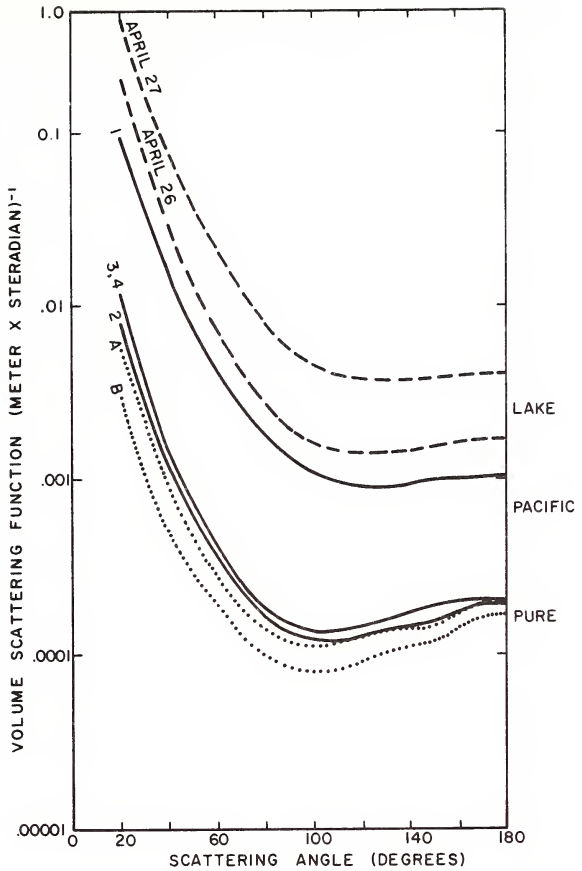

FIG. 1.70 Plot of Tables 1, 2, 3.

summarizes Tyler's Lake Pend Oreille measurements of the Spring of 1960. The wavelength band in this case was centered at 480 ± 64 mμ. These tabulations are compared graphically in Fig. 1.70 wherein the relative clarity of the waters may be seen at a glance. Curves 3, 4 of Table 2 essentially coincide in the figure.

Figure 1.71 provides three more comparisons of distilled, lake and ocean waters. In this case, the distilled water measurements were by Dawson and Hulburt [63], the lake water measurements by Duntley [78], and the Atlantic (between Madeira and Gibralter) measurements by Jerlov [123]. The latter graph is keyed in with the measurements listed in Table 4 below. The lake measurements by Duntley are of particular interest because of the relatively small angles for which σ was obtained using special equipment [78]. A detail of σ for the range 0.5° to 1.7° is given in Fig. 1.72. The ordinates of the lake curve in Fig. 1.71 are continued in Fig. 1.72.

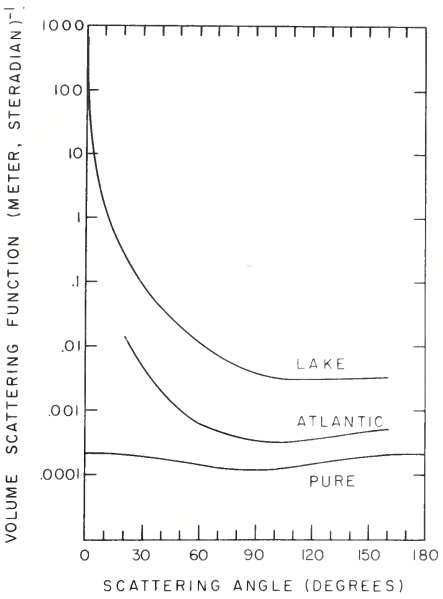

FIG. 1.71 Plots of data taken at various times and locales by Dawson and Hulburt (pure), by Duntley (lake), and by Jerlov (Atlantic). See text for details. (Fig. 9 from [78], by permission)

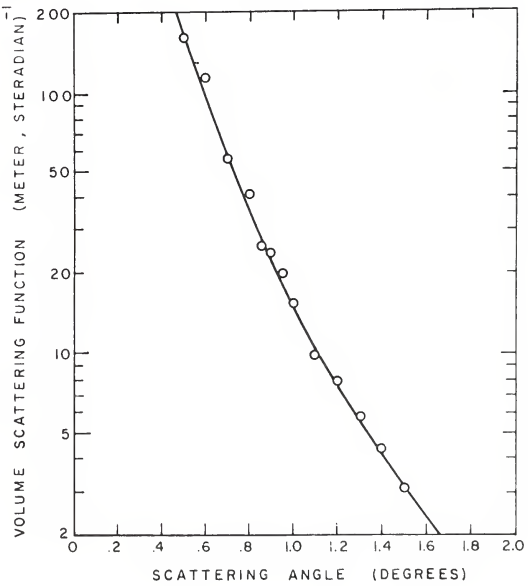

FIG. 1.72 Extreme detail of forward scattering values of volume scattering function in Duntley's lake water curve of Fig. 1.71.

TABLE 4

Comparison between relative values of the scattering function. (All data normalized at 90°)

	In vitro measurements			In situ measurements		
Angle θ	Poole and Atkins (1954) English Channel	Hulburt (1945) Chesapeake Bay	Kozlyaninov (1957) East China Sea	Sasaki (1960) Japan Trench	Jerlov (1961) East North Atlantic	Tyler (1961) Californian coast
	blue light	white light	blue light	576 mμ	465 mμ	522 mμ
1°			7200			
5°			1100		(690)	
10°	232	247	312		292	
20°	62	61	62	39	74	67
30°	18	22	22	22	23.5	20
45°	6.0	8.5	6.9	5.5	7.5	6.7
60°	2.5	3.0	3.1	2.9	2.96	2.70
75°	1.5	1.4	1.8	1.2	1.72	1.51
90°	1.0	1.0	1.0	1.0	1.00	1.00
105°	0.82	1.0	0.49	0.8	0.95	0.91
120°	0.67	1.2	0.44	0.7	1.05	0.94
135°	0.90	1.5	0.50	1.0	1.30	1.05
150°		2.2		1.2	1.55	1.18
165°		3.1			1.90	1.38
180°					(2.12)	1.49

(From [127], by permission)

This shows how, in the space of 1°, near-forward scattering values soar two more orders of magnitude. The associated wavelengths are those transmitted by a No. 61 Wratten filter.

Further comparisons of σ values are made in Table 4 (patterned after [127]). Observe that Tyler's measurements are those listed for location 2 in Table 2. The main purpose of Table 4 is to show the remarkable similarity in shape of the σ curves, after normalization at 90°. This fact is reproduced graphically in Fig. 1.73. The curve labeled "Duntley (Green)" in Fig. 1.73 is the normalized lake curve of Fig. 1.71. The remaining references for the σ values of Table 4 and Fig. 1.73 are as follows: Atkins and Poole [6], Hulburt [115], Kozlyaninov [144], Sasaki et. al. [271], and Jerlov [123]. A relatively recent and somewhat extensive experimental study of σ in the Atlantic was made by Spilhaus [290]. This work makes new progress toward workable classifications of optical media via the volume scattering function.

The highly forward scattering character of natural waters observed in all of the preceding results is one of the

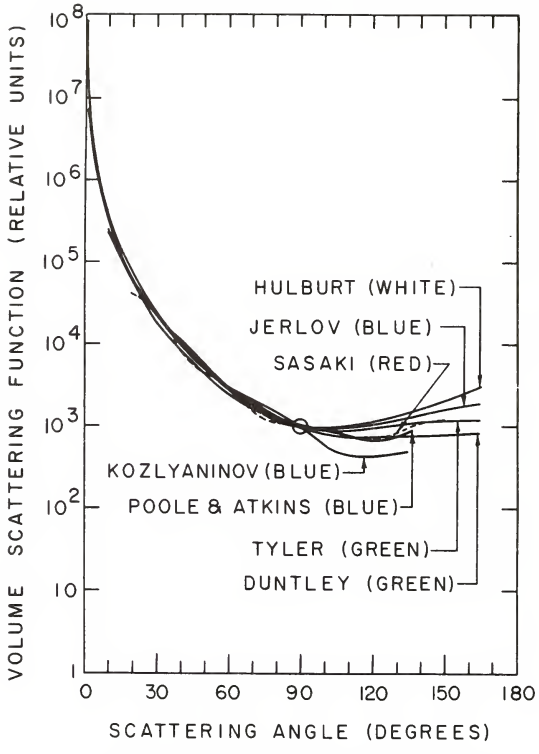

FIG. 1.73 Illustrating the stability of shape of the volume scattering function as measured in various locations and times. See text for details. (Fig. 12 from [78], by permission)

outstanding, and not yet fully understood features of the function. In particular, does the σ-curve have a vertical or horizontal tangent at 0°? Despite the absence of detailed knowledge, we know that the high forward scattering is due principally to the great variety of dissolved and suspended organic and mineral matter in the sea. The ebb and flow of the life processes and geologic processes within natural hydrosols constantly alters the concentration of these substances, and the basic Rayleigh-type scattering that absolutely pure water would exhibit is heavily masked by the scattered light produced by these 'foreign' substances. If water in its pristine state is examined optically, then (cf. [63]) the scattered radiance N_r^* in (10) would have the general form:

$$N_r^*(\theta,\lambda) = \frac{Ar}{\lambda^4}(1 + B\cos^2\theta) \qquad (22)$$

where A and B are suitable constants (see [63]). Observe that $N_r^*(\theta,\lambda)$ increases sharply for the smaller wavelengths,

thereby tending to suffuse extensive masses of very pure water with scattered blue light, much in the way that the clear sunlit atmosphere above one's head appears blue to the sight. It was shown by Kalle [132] that the relatively heavy concentration of decaying organic matter in the form of phenol-humic acids and carbohydrate-humic acids (or melanoidines), respectively contribute the brownish and yellowish components to the otherwise clear blue water, the net result being the blue-green appearance of most natural hydrosols. Hence the greater the concentrations of these organic materials, the yellower or browner the water will become. Unlike the sharp λ^{-4} wavelength-behavior of scattered light in pure water, we have, by contrast, in oceanic or lake water which contain particles and organisms whose dimensions are large compared with wavelengths of light, the scattered light nearly independent of wavelength. Hence when one measures α (= a+s) or k ($\cong \sqrt{aD(aD+2b)}$) as a function of wavelength and observes great variations, these variations are due principally to the absorption mechanism operative in the solutes and suspensoids within the water. For example, while the scattered light in pure water increases nearly 10 fold as λ goes from 700 to 400 mμ, the absorption coefficient for plankton-infested water or for suspensoids of the yellow substance increases on the order of 100 fold over the same range (cf., e.g., [115]). By virtue of these reasons, the striking similarity of shape of the σ curves in Fig. 1.73 becomes more understandable. If this sensitivity of σ to wavelength λ is sufficiently weak, a great simplification of the documentation of optical properties of natural waters is possible; for then the burden of describing the spectral variation of the inherent optical properties falls on α or, equivalently, a. Table 5, adapted from Hulburt [115], gives the spectral dependence of α, s, and a for two types of water. These tabulations bear out the rationalizations enunciated above. Table 6 shows the spread of α values over oceanic regions, as found by Jerlov [122].

TABLE 5

Spectral dependence of volume attenuation (α), total scattering (s) and absorption functions (a) for distilled and Chesapeake Bay waters (per meter)

Wavelength (mμ)	Distilled			Bay		
	α	s	a	α	s	a
400	.080	.038	.042	-	-	-
420	.061	.030	.031	.800	.175	.625
440	.046	.025	.021	.628	.180	.448
480	.037	.017	.020	.447	.180	.267
520	.040	.013	.028	.351	.180	.171
560	.053	.009	.044	.323	.180	.143
600	.197	.007	.190	.429	.180	.249
640	.292	.005	.287	.500	.180	.320
680	.406	.004	.402	.589	.180	.409
700	.576	.004	.572	.740	.180	.560

(From [115], by permission)

TABLE 6

Representative values of the volume attenuation function for various oceanic locations for 480 mμ wavelength.

Location	α/meter	Attenuation length 1/α meters
Caribbean	.125	8
Pacific N. Equatorial Current	.083	12
Pacific counter current	.083	12
Pacific Equatorial Divergence	.100	10
Pacific S. Equatorial Current	.111	9
Gulf of Panama	.167	6
Galapagos Islands	.250	4

(From [122], by permission)

Before concluding this brief survey of the inherent optical properties of natural hydrosols we wish to point up an apparent dissimilarity between the spectral dependence of α in air and in water. The dissimilarity is with respect to the fine structure of the λ-dependence of α. In the meteorologic optics context, α experiences rather spectacular increases and decreases in values at frequent intervals along the λ-axis (see, e.g., Refs. [128], [296], and [177]). Where α decreases rapidly to some minimum at λ_j, the atmosphere is said to have a *window* at λ_j, for the beam tramsmittance $T_r = e^{-\alpha(\lambda)r}$ will have a *maximum* at λ_j, and so one can 'look through' the atmosphere with relative ease using light having wavelengths in the immediate neighborhood of λ_j. The infrared region of the spectrum, e.g., has windows through the atmosphere, and this fact has important consequences for communication applications of radiative transfer theory. These observations lead one to consider the possibility of a fine structure for α in natural waters. This possibility does not seem too bright, at least on the basis of Table 5. However, perhaps the measurements of α yielding the values in Table 5 were too crude, and accordingly smeared out possible sharp dips in α. That is, the minimum of α in the vicinity of 480 mμ for distilled water may harbor a still sharper minimum if the spectral resolution of α-meters were increased. Recently, a careful spectroscopic study of α for "battery-grade" distilled water was made in the region from 375 mμ to 685 mμ by Drummeter and Knestrick [68]. The spectral resolution achieved by the grating spectrograph used was .02 mμ. A path of water of 9.75 meters was used for the transmission experiment. Variations of α per meter as small as two parts in a hundred were capable of detection by the apparatus, i.e., the apparatus could detect changes Δα of 2×10^{-2}/m. No spectral fine structure of α of any significance was detectable.

Operational Definitions of the Apparent Optical Properties

The *apparent optical properties* of a natural hydrosol are those radiometrically determined scattering- and absorbing-induced quantities which generally depend on the geometrical structure of the light field (i.e., whether the light field is more or less collimated or diffuse) but which have enough regular features and enough stability to be entitled to the appellation, "optical property". The main apparent optical properties are all measurable by means of the four irradiances: $h(z,\pm)$ and $H(z,\pm)$. (See (9), (10) of Sec. 1.1.) Thus we write:

$$\text{"D}(z,\pm)\text{"} \quad \text{for} \quad \frac{h(z,\pm)}{H(z,\pm)} \qquad \text{(Distribution functions)} \tag{23}$$

$$\text{"K}(z,\pm)\text{"} \quad \text{for} \quad -\frac{1}{H(z,\pm)}\frac{dH(z,\pm)}{dz} \qquad \text{(K-functions for irradiance)} \tag{24}$$

$$\text{"k}(z)\text{"} \quad \text{for} \quad -\frac{1}{h(z)}\frac{dh(z)}{dz} \qquad \text{(K-function for scalar irradiance)} \tag{25}$$

$$\text{"R}(z,\pm)\text{"} \quad \text{for} \quad \frac{H(z,\mp)}{H(z,\pm)} \qquad \text{(Reflectance function for irradiance)} \tag{26}$$

The distribution functions are simple indicators of the collimatedness or diffuseness of the light field in the downward (-) or upward (+) flows. The three K-functions are the depth rates of decay of the various irradiances. They are in principle generally distinct, though numerically they are quite close in value. The R functions give the reflectance of the entire medium to upward (+) or downward (-) flux at level z. Each of these is implicitly a function of wavelength. The theory of their interconnections is quite simple and will be discussed briefly in the following section. Their full theory is established in Chapters 9, 10 and 13. Table 7, adapted from [306], is a representative sample of the magnitudes of these properties.

These measurements were made in the spring of 1957 before the onset of the plankton bloom and appearance of the thermocline. The lake was essentially homogeneous so that the values of α, s, and a are representative of the entire medium. As the biologic activity within the lake increases throughout the remainder of the year, the values of α, s and a will rise accordingly, thereby providing an optical biometer of such activity. Furthermore, since 95% of the radiant energy content of the lake is essentially confined to within 3 diffusion lengths 1/K of the surface (cf., (98) of Sec. 1.4) and is therefore within the arena of most biologic activity, we would expect the homogeneity of the lake to disappear with the onset of spring and summer. Furthermore, rain run-offs will introduce still further mixtures of organic and inorganic materials into the entire body of the lake and change the optical properties. In short, it appears quite possible for

TABLE 7

The apparent and inherent optical properties of Lake Pend Oreille at depth 29 meters and for a wavelength band centered on 480 ± 64 mμ

Property	28 April 1957 Computed from Radiance Dist. (sunny)	16 March 1957 Measured Directly (overcast)	Calculated Indirectly
D(29,+)	2.78		
D(29,-)	1.31		
K(29,+)	.164/m		
K(29,-)	.169/m	.184/m	
R(29,+)	43.5		
R(29,-)	.023		
α(29)		.442/m	
s(29)			.325/m
a(29)	.117/m		

(From [306], by permission)

one to form an optical portrait of the biology and geology of a lake or oceanic region by monitoring its α, σ, a and K, at given times over a yearly cycle. The more of these properties one records, the more complete will the optical portrait be, and the more likely will be the usefulness of the findings to scientists in neighboring disciplines to hydrologic optics.

In order to increase our intuitive and objective knowledge about the relations between the clarity of water and its α and K properties, we append Table 8, adapted from [74]. This table, while ostensibly a rather limited sample, exhibits some interesting relations between α and K. For example the list of values shows a remarkable stability of the ratio K/α considering the range of waters in which the measurements were made. Thus while α varies over an eightfold range and K over a sevenfold range, K/α varies only over about a twofold range. The stability of K/α within a given region of water is even greater, indicating a possible basis for simple rules of variation of α and K which may be used to estimate one of those properties in the absence of the other. This stability of K/α will be seen to be an important factor in the description of the shape of the light field at moderate and great depths in the seas and lakes (Sec. 10.7, in particular (29) of Sec. 10.7).

TABLE 8

A sampling of α, K values for the 480 ± 64 mμ range.

	α	K	K/α
Coronados Islands, Mexico (depth: 3 to 10 meters)	0.499 meter^{-1}	0.180 meter^{-1}	.361
San Diego Bay and Approaches (Average of data within 1/2 meter of the bottom)			
Open Sea Southwest of Point Loma	0.439 meter^{-1}	0.177 meter^{-1}	.404
Coast at Mexico-California border	0.654	0.226	.346
San Diego Harbor Opening	0.727	0.162	.223
Zuniga Point, Harbor Opening	1.065	0.396	.372
Entrance Channel, South	1.156	0.280	.242
Entrance Channel, North	1.770	0.565	.320
North Bend of Harbor	1.462	0.584	.400
Midpoint of Harbor Pocket	3.20	1.07	.334
Proceeding East through Straits of Juan de Fuca to Admiralty Inlet (Averages of data from 5 to 30 meters depth)			
Ocean Entrance	0.543 meter^{-1}	0.262 meter^{-1}	.483
	0.630	0.278	.442
Central Region	0.600	0.315	.525
	0.724	0.321	.445
Opposite Victoria, Vancouver Island	0.651	0.340	.522
Fresh Water Lakes*			
El Capitan Reservoir (Aug. 1955), San Diego County (turbid water)	1.853 meter^{-1}	1.062 meter^{-1}	.575
Diamond Island Field Station (Summer 1956) Lake Winnipesaukee, N.H. (moderately clear)	0.756	0.374	.495
Lake Pend Oreille, Idaho (Apr 1957) (Clear water)	0.413	0.195	.472

*The coefficients α and K were found to be the same at all depths at these locations and times.

Preliminary Observations on the Classification of Natural Hydrosols

From the preceding samplings, we see that one of the difficulties in forming a well-rounded optical picture of a natural hydrosol from most of the currently existing literature in hydrologic optics is that each investigator has looked at only one or two fragments of the entire radiometric picture according to his momentary interests. As a result, such findings have only transient interest because they cannot be incorporated by subsequent investigators into any systematic study of the radiative transfer processes occurring in the hydrosol. It is true that the preceding examples are very helpful in forming an intuition of the principal optical properties of natural hydrosols. However, the completeness of experimental studies to the degree shown in Tables 1, 2, 3 are all too rare and we can be hopeful that they will be emulated by other investigators in future scientific studies of light fields in oceans and lakes. The recent works of Tyler cited above and those of Jerlov [125], [126], [127], have begun to show a trend in the direction of exhaustive systematic optical analyses of natural hydrosols. Thus in Jerlov's work [127], potentially fruitful classifications of different types of ocean waters are made, and are elaborated in the book version of [125]. For example, Fig. 1.74 shows a classification of ocean water types by means of the irradiance

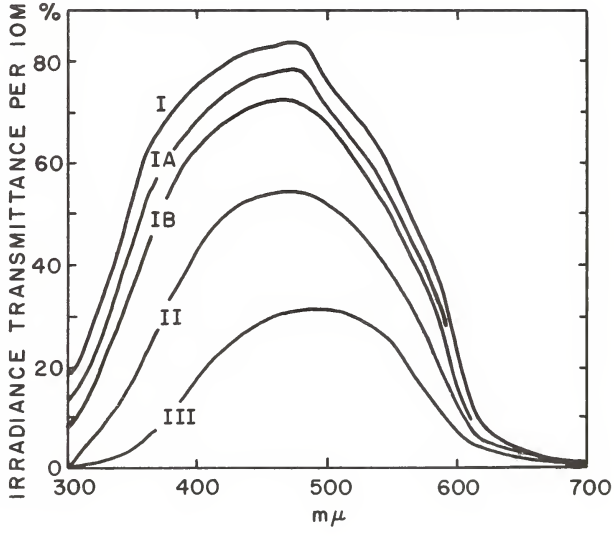

FIG. 1.74 Irradiance transmittance for a 10 meter layer of water, as sampled by Jerlov, and illustrating a possible classification scheme for natural hydrosols. (From [127], by permission)

transmittance e^{-Kz} of a given layer of water ($z = 10$ meters in this case) as a function of wavelength. While it would be generally more desirable and more directly useful to simply plot the K-function for $H(z,-)$ as a function of λ, even as they stand, the graphs give an informative picture of the five general types of oceanic water encountered by Jerlov in his long series of careful studies of Atlantic and peripheral waters. These graphs could be of even greater service if someday they or their kind are supplemented by similar plots of α as a function of λ, along with σ, as a function of both θ and λ, if the patience and funds for such a pioneering effort could ever be assembled. The rationale behind these observations will be outlined in the following section.

1.7 Some General Modes of Classification of Natural Optical Media

Our studies in the preceding sections, especially those in the section just concluded, lead us to seek out those of the manifold optical properties used in the mathematical models of light fields in natural hydrosols that are fundamental and most useful. This problem has no simple solution, and indeed has different answers depending on one's view of the role of hydrologic optics in the study of natural waters. If one were a mathematician interested primarily in the intricate geometrical relations among the radiance distributions and their connections with the physics of the medium then, unquestionably, the inherent optical properties α and σ as functions of position and wavelength (or equivalently α and a) constitute the only scientific answer to the query. If one were interested mainly in engineering calculations leading to estimates of the visibility of submerged objects in natural or artificial light fields then, equally clearly, the full spatial and spectral measurement of the properties α and K would suffice for most such purposes. On the other hand, a biologist interested in the problem of photosynthesis may find it possible to conduct a large portion of his work using only the volume absorption function a or only the diffuse attenuation function K. If one were a physicist or chemist concerned mainly with the analysis of water for the detection of certain dissolved and suspended substances, then quite likely σ and α (or equivalently σ and a) would suffice, but for vastly different reasons than those given by the mathematician mentioned above. For the mathematician would use α and σ to compute $N(z,\xi)$ at each depth z and for each direction ξ, while the physicist or chemist would use α and σ to yield concentrations of solutes and suspensoids in the irradiated sample of the hydrosol.

Modes of Classification

In view of the preceding observations, several alternate modes of classification of natural optical media are possible. We now list the main modes of classification and indicate how much information about the hydrosol is inherent in each.

Mode IA *Specifying* α,σ *as functions of position, direction (for* σ*) and wavelength through the medium* X.

The measurements of α,σ are envisioned here as done by means of specially designed α-meters and σ-meters (cf. [78]). The deductions that are possible using this mode are indicated schematically as follows under the column labeled "Mode IA":

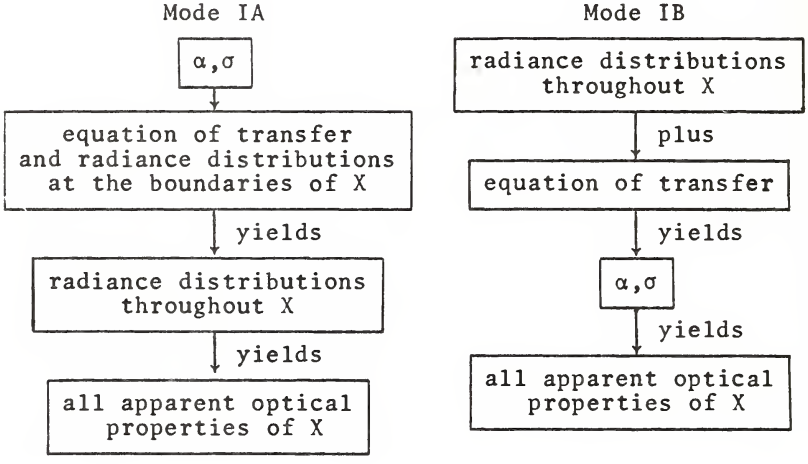

The procedure by which the radiance distributions throughout the medium are obtained from α, σ, the equation of transfer, and the boundary lighting conditions on the hydrosol is now a well established procedure which may take several alternate forms. The main techniques for such calculations are summarized in Chapters 4, 5, 6, 7 and 8 below, and in Part Three of Ref. [251]. The determination of the apparent optical properties from radiance distributions proceeds as outlined in (23)-(26) of Sec. 1.6.

Mode IB *Specifying radiance distributions throughout* X *as functions of wavelength.*

This mode of classification is extremely fruitful, for as the deduction diagram for Mode IB shows, this information will yield all the inherent and apparent optical properties of the medium. Table 7 of Sec. 1.6, except for α, s and a, was constructed using this mode of classification. The manners in which the inherent optical properties α, s and a of a medium are forthcoming from radiance distribution measurements are explained in Chapter 13. Modes IA and IB are in principle mathematically equivalent modes of classification and rank highest in the hierarchy of possible modes of classification as regards completeness of information about the hydrosol studied.

Mode II *Specifying* $H(z,\pm)$ *and* $h(z,\pm)$ *as functions of position and wavelength throughout* X.

From the four irradiances of Mode II comes the set of all apparent optical properties discussed in Sec. 1.6. An extraordinary amount of information is forthcoming from such a mode of classification when it is realized that we are replacing the radiance distribution $N(z,\cdot)$ at each depth z by just four numbers $H(z,\pm)$, $h(z,\pm)$ at that depth. A number of deductions of the relations among the inherent optical properties s and a and a wealth of subsidiary properties are possible from a carefully conducted Mode II classification. The bases for these deductions are explored in Chapters 9, 10 and 13.

It may seem odd to suggest modes of classification which are comprised only of radiometric documentations of light fields. However, when one reflects on the matter, it becomes clear that this is precisely how all the usual apparent optical properties are found in the first place! Therefore if an investigator accompanies the listing of the deduced optical properties, of current interest, with a listing of the complete $H(z,\pm)$ and $h(z,\pm)$ measurements (or preferably the $N(z,\xi)$ measurements) from which he made his deductions, he thereby makes available to subsequent investigators potential information he is presently uninterested in or which his technology may not yet be able to extract. Imagine, for example, if scientists in Galileo's time documented the light fields by means of radiance distributions, however crudely, we would now be able to extract information about those hydrosols that the original investigators hardly could conceive of. Flights of fancy to one side, the reader should perceive the underlying intent of this observation and its pertinence to Mode II.

Mode III *Specifying* α *and* K *as functions of position and wavelength throughout* X.

The collection of α and K measurements is here envisioned as made by a single instrument assembly so designed as to simultaneously measure α and K as it is lowered into and moved about in the optical medium. For example, such a device, designed by R.W. Austin of the Visibility Laboratory, University of California [7], has been used in coastal surveys by the U.S. Oceanographic Office.

By a judicious choice of near-surface radiance distributions and by virtue of the near-universality of shape of the σ curves (cf. Fig. 1.73) one may be able to estimate $N_*(z,\theta)$, using (50) or (61) of Sec. 1.4 with the K values supplied by Mode III of the classification scheme. Then with (14) of Sec. 1.3 and the α as found by Mode III, excellent estimates may be obtained of the radiance distributions within a medium probed in a Mode III fashion. Once these radiance distributions are obtained, then we are in effect in possession of a Mode IB wealth of knowledge, provided the simple model for radiance fields is applicable.

Further members are possible in the preceding hierarchy of modes of classification of natural hydrosols. However, a proliferation of such modes at this time is not desirable, as it would detract attention from the only mode really worth considering in the establishment of a science of hydrologic optics, namely Mode I in either of its equivalent guises A or B. However, this ideal may not soon be reached, and accordingly the two lesser but yet extremely useful modes of classification are included in our present survey. Finally, *whenever possible and in the interests of consistency and completeness, measurements in the preceding modes should be done in the polarized light context and also as a function of time, if such is indicated by the physical (or biological) state of the medium* (cf., Sec. 13.6, 13.11).

A complete theoretical analysis and classification of the optical properties in arbitrary optical media is made in Sec. 9.6.

1.8 Colorimetric Radiative Transfer

An interesting application of radiative transfer theory can be made to the studies of the apparent colors of objects located within media that scatter and absorb radiant energy in a selective fashion. The application of the principles of radiative transfer to such studies is straightforward and requires no new concepts to be introduced into the theory beyond those we have been considering. For this purpose we need only adopt the well-known standard C.I.E. (*Commission Internationale de l'Eclairage*) color coordinate system, within which any spectral sample of radiant flux may be located and assigned a unique color, in a manner to be briefly explained below. By coupling the concepts of radiative transfer theory to the C.I.E. color coordinate system, an accurate, quantitative basis for the description of color phenomena within the atmosphere and the sea is achieved, which for the purposes of the present discussion we shall call *colorimetric radiative transfer theory*. Our goal in this section is to outline the union of the two theories and indicate the nature of its applications.

The color phenomena within the domain of colorimetric radiative transfer theory are manifold: a precise description and prediction is possible of the blue of the sky and of the reds and golds of sunsets; of the onset and growth of the blue and purple hazes between distant mountains and a receding observer; the odd yellowing of mercury vapor street lamps with distance in strange blue fogs [177]; the conventional but ever pleasant sight of a reddish-orange rising moon; the yellowing and reddening of extremely shiny surfaces such as corrugated aluminum roofs and sidings seen through long paths of sight in the atmosphere; the sickening brown smear of smog smothering a city. In the underwater domain, the colorimetric radiative transfer phenomena are overpowered and dominated by the highly selective absorption of reds and violets (and their neighboring colors), resulting in a powerful filtering of all sky light into a blue-green residue of greater or lesser luminance that pervades almost all submarine scenes.

Brightly-colored submerged tropical scenes of plants and animals with their reds, yellows and deep blues quickly transform with distance into shades of brighter or dimmer greens and blues with reds and purples washed to pink and then attenuated away. Such scenes are now easily witnessed firsthand with modern scuba devices. However, only one or two generations ago, such sights were a rare delight.

In his 1927 Haiti expedition, Beebe [12] noted that:

> "Toward the end of the dive I sat on white sand [in his diving helmet rig] and watched the surface above me. The sea breeze had sprung up and it was fairly rough. The view from beneath was of green, wrinkled, translucent ceiling cloth, never still for a moment, crinkling and uncrinkling, waving and flapping as in a breeze, or rather cross breezes. It was decidely green in comparison with the ever more blue distance--turquoise green in the sunlight, changing toward greenish glaucous in shadow. As to the distance, I can never get away from the idea of the most diluted, ethereal ultramarine, and yet my mind knows that a dozen other colors are somehow in it."

All of these phenomena can be quantitatively and quite accurately described by means of such simple models for radiance and irradiance as developed in Sec. 1.3, which need only use information on optical properties obtainable by Mode III classification procedures of optical media (cf., Sec. 1.7).

The Quantitative Description of Color

It is a relatively easy matter to understand the C.I.E. color coordinate system if we recall some similar conventions we have adopted in our everyday tasks of locating objects in space. Part (a) of Fig. 1.75 exhibits an object in space (designated by "A") which can be located by means of its three coordinates in an xyz cartesian frame of reference. There is nothing unique about this frame as far as being adequate to locate A in space. The alternate frame depicted in (b) of Fig. 1.75 will do just as well. In each diagram, object A is located at the same spot. That spot, fixed relative to the first frame, is designated by a vector **u** which is specified by giving its coordinates (x,y,z). These coordinates are found by dropping perpendiculars from **u** to each of the three axes, in short, by finding the dot products:

$$\mathbf{u} \cdot \mathbf{i} \tag{1}$$

$$\mathbf{u} \cdot \mathbf{j} \tag{2}$$

$$\mathbf{u} \cdot \mathbf{k} \tag{3}$$

of the vector **u** with the mutually orthogonal unit vectors **i**, **j**, **k** along the x, y, z axes respectively. This is called *analyzing* **u** relative to the x, y, z frame. The next step is to *synthesize* **u** (i.e., get it back) by means of the equation:

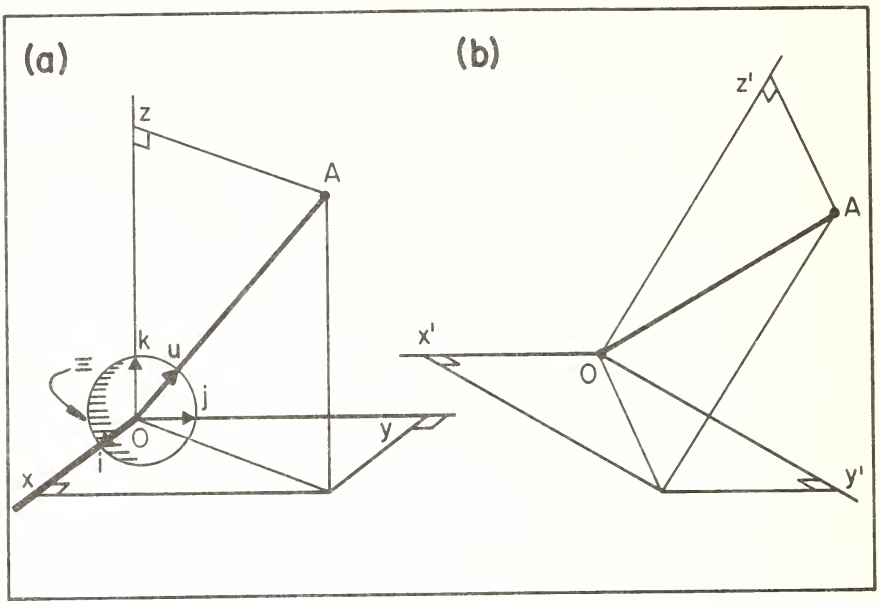

FIG. 1.75 For illustrating the analogy between coordinate systems in the real three dimensional world and the C.I.E. tristimulus color coordinate system.

$$\mathbf{u} = (\mathbf{u}\cdot\mathbf{i})\mathbf{i} + (\mathbf{u}\cdot\mathbf{j})\mathbf{j} + (\mathbf{u}\cdot\mathbf{k})\mathbf{k} \qquad (4)$$

Now, we can perform such an analysis and synthesis not only on a simple location vector such as **u**, but also on any radiant flux function P defined on the electromagnetic spectrum Λ (the set of all wavelengths from $\lambda = 0$ to $\lambda = \infty$). Instead of the **i**, **j**, **k** unit vectors, we now use the (dimensionless) *tristimulus functions* $\bar{x}$, $\bar{y}$, $\bar{z}$ on Λ adopted by the C.I.E.. A plot of each of these is given, to scale, in Fig. 1.76. If we form samples of radiant flux with just the power spectra given by the forms of these three functions, then the visual sensation of the $\bar{x}$ sample would be red, that of $\bar{y}$ would be green, and that of $\bar{z}$, blue.

To analyze a given radiant flux sample P (watts/mμ) into its red, green and blue components, we write:

$$\text{"P}\cdot\bar{x}\text{"} \quad \text{for} \quad 680\int_0^\infty P(\lambda)\ \bar{x}(\lambda)\ d\lambda \quad \text{(lumens)} \qquad (5)$$

$$\text{"P}\cdot\bar{y}\text{"} \quad \text{for} \quad 680\int_0^\infty P(\lambda)\ \bar{y}(\lambda)\ d\lambda \quad \text{(lumens)} \qquad (6)$$

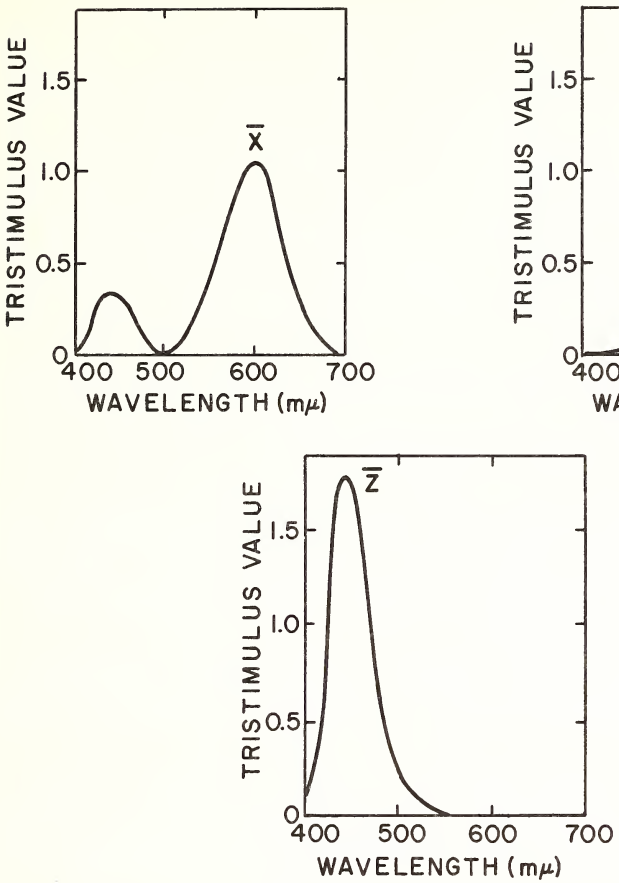

FIG. 1.76 The tristimulus functions. The $\bar{y}$ curve is the photopic luminosity function of Fig. 1.10.

$$\text{"P}\cdot\bar{z}\text{"} \quad \text{for} \quad 680\int_0^\infty P(\lambda)\ \bar{z}(\lambda)\ d\lambda \quad \text{(lumens)} \qquad (7)$$

which are closely analogous to the simple vector operations (1), (2), (3). The number 680 has dimensions of lumens/watt, and serves as a connection with photometry--(cf., Sec. 2.12). To point up this similarity to the vector operations we have written "P$\cdot\bar{x}$", "P$\cdot\bar{y}$", and "P$\cdot\bar{z}$" for (5), (6), (7), respectively. Then analogously to (4) we can synthesize these components. We do this and write:

$$\text{"}\subset[P]\text{"} \quad \text{for} \quad (P\cdot\bar{x})\bar{x} + (P\cdot\bar{y})\bar{y} + (P\cdot\bar{z})\bar{z} \qquad (8)$$

We call $C[P]$ the *color* or *chromaticity* of P. $C[P]$ is a function defined on Λ and it is designed to give a very close visual color match to the original function P. The point to observe here is that whereas P could be of quite an arbitrary structure over Λ, its color $C[P]$ is the linear superposition of three suitably weighted amounts of standard red, green, and blue radiant flux samples. The weighting numbers $P\cdot\bar{x}$, $P\cdot\bar{y}$, $P\cdot\bar{z}$ are the *color components* of P, and the ordered triple of numbers $(P\cdot\bar{x}, P\cdot\bar{y}, P\cdot\bar{z})$ is the *color vector* associated with P. In this way we have set up a one-to-one transformation of given radiant flux samples P into their associated colors $C[P]$, each with three well defined color components* $P\cdot\bar{x}$, $P\cdot\bar{y}$, $P\cdot\bar{z}$. For brevity let us write (in accordance with C.I.E. notation):

$$\text{"X"} \quad \text{for} \quad P\cdot\bar{x} \tag{9}$$

$$\text{"Y"} \quad \text{for} \quad P\cdot\bar{y} \tag{10}$$

$$\text{"Z"} \quad \text{for} \quad P\cdot\bar{z} \tag{11}$$

We observe in passing that the component $P\cdot\bar{y}$ of a sample P of radiant flux is simply its photometric counterpart. Thus, for radiance N, $N\cdot\bar{y}$ is the associated luminance B; for irradiance H, $H\cdot\bar{y}$ is the associated illuminance E; and so on (cf., Sec. 1.1). Tables of $\bar{x}$, $\bar{y}$, $\bar{z}$ along with further descriptions of colorimetry may be found in [50].

We may summarize the analogy between simple location vectors and chromaticity vectors by means of the parallel listings below in Table 1.

TABLE 1

A vector analogy for chromaticity concepts

Location Vectors	Chromaticity Vectors
(1) Original vector $\mathbf{u}$	(1) Original radiant flux function P
(2) $\mathbf{i},\mathbf{j},\mathbf{k}$ unit vectors	(2) $\bar{x},\bar{y},\bar{z}$ tristimulus functions
(3) Components of $\mathbf{u}$ with respect to $\mathbf{i},\mathbf{j},\mathbf{k}$:	(3) Color components of P with respect to $\bar{x},\bar{y},\bar{z}$:
$\mathbf{u}\cdot\mathbf{i} = \alpha$	$P\cdot\bar{x} = X$
$\mathbf{u}\cdot\mathbf{j} = \beta$	$P\cdot\bar{y} = Y$
$\mathbf{u}\cdot\mathbf{k} = \gamma$	$P\cdot\bar{z} = Z$
(4) The representation of $\mathbf{u}$:	(4) The representation of P:
$\mathbf{u} = \alpha\mathbf{i} + \beta\mathbf{j} + \gamma\mathbf{k}$	$C[P] = X\bar{x} + Y\bar{y} + Z\bar{z}$

*The mathematical reader will see that this vector terminology is completely appropriate, for what we can postulate initially is the vector space $\mathcal{P}$ of all Riemann integrable functions P on Λ. The mapping C is therefore a non-identity linear transformation of $\mathcal{P}$ into itself. It turns out that C is one-to-one and not onto, but its range is sufficiently large to encompass most colors seen by the human eye.

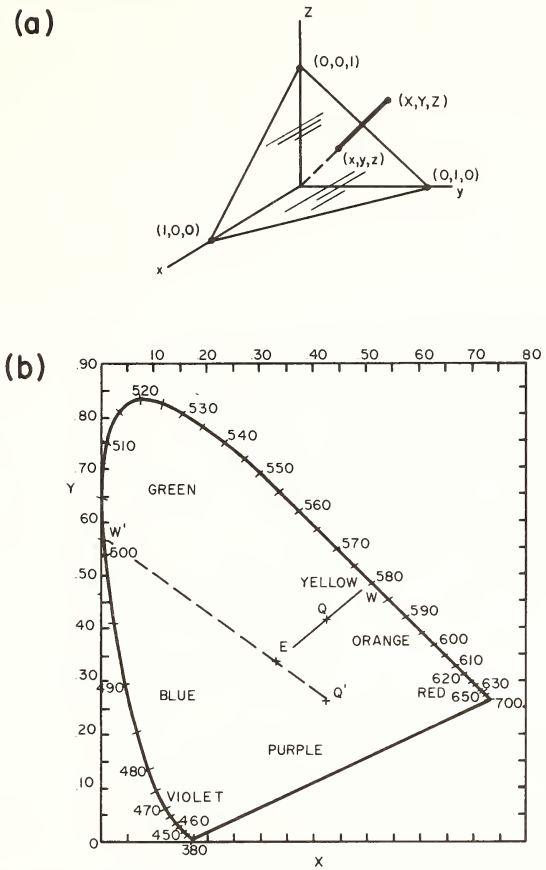

FIG. 1.77 Chromaticity plane (part (a)) and chromaticity diagram (part (b)). Point E is the white-light point.

In the usual location vector theory, a special place is reserved for vectors of unit length, namely the unit sphere Ξ shown in (a) of Fig. 1.75. Analogous to the unit sphere is the *chromaticity plane* shown in (a) of Fig. 1.77. This plane has the property that for all points p (= (x,y,z)) on it we have $x+y+z = 1$. If (X,Y,Z) is a chromaticity vector, then the vector

$$\frac{1}{(X+Y+Z)} \cdot (X,Y,Z) = \left(\frac{X}{X+Y+Z}, \frac{Y}{X+Y+Z}, \frac{Z}{X+Y+Z} \right)$$

lies on the chromaticity plane. Observe that only the part of the chromaticity plane that lies in the first octant (shown in (a) of Fig. 1.77) is needed in colorimetry. For, since P and the functions $\bar{x}$, $\bar{y}$, $\bar{z}$ are never negative, all chromaticity vectors accordingly lie in the first octant. Observe further

that one need only use two numbers to locate a point on the chromaticity plane. These numbers are conventionally chosen to be the x and y components, where we write

$$\text{"x"} \quad \text{for} \quad \frac{X}{X+Y+Z} \tag{12}$$

$$\text{"y"} \quad \text{for} \quad \frac{Y}{X+Y+Z} \tag{13}$$

$$\text{"z"} \quad \text{for} \quad \frac{Z}{X+Y+Z} \tag{14}$$

The x,y,z are the *chromaticity components* (or *coordinates*) of P. By projecting all chromaticity vectors (X,Y,Z) down onto the chromaticity plane, as shown in Fig. 1.76, we are in effect normalizing the associated luminances of the radiant flux function P. Once the chromaticity plane is defined we can excise it from its spatial context, or simply work with a plane diagram copy of the chromaticity plane, as in (b) of Fig. 1.77. The x and y chromaticity coordinates are displayed in a way once again reminiscent of the usual location vector conventions.

Once the setting in (b) of Fig. 1.77 is achieved, we can locate within it all manners of points which represent the conventional colors of familiar everyday objects and scenes. For example, suppose that we begin with a sample P of radiant flux which has a constant value P_o for all λ. From (5)-(7) this gives:

$$X = 680\ P_o \int_0^\infty \bar{x}(\lambda)\ d\lambda \tag{15}$$

$$Y = 680\ P_o \int_0^\infty \bar{y}(\lambda)\ d\lambda \tag{16}$$

$$Z = 680\ P_o \int_0^\infty \bar{z}(\lambda)\ d\lambda \tag{17}$$

Now the $\bar{x}$, $\bar{y}$, and $\bar{z}$ functions are so designed that their integrals over $\Lambda = [0,\infty]$ have essentially a single common value, namely 21.37. Hence the associated chromaticity components for this P are

$$x = 1/3$$

$$y = 1/3$$

$$z = 1/3$$

Such a flux sample has the appearance of a pure white color and is analogous to pure noise in acoustics. In fact, in the

theory of stochastic processes, if the spectrum of a given function is of constant value, it is said that the function represents *white noise* (all the analogies we are touching here and there in the present exposition are quite deep and far more than superficial in appearance).

The point (x,y) = (1/3,1/3) in the chromaticity plane corresponding to *white light* is denoted by "E", in (b) of Fig. 1.77 and is the central base of operations in the practical task of specifying colors. If we go on to obtain the chromaticity coordinates of all the pure monochromatic colors of the spectrum Λ (their sample functions P are Dirac delta functions), we sweep out a horseshoe shaped locus in the plane of (b) of Fig. 1.77, starting approximately at the point x = .74, y = .26 (red), and sweeping around to the point x = .07, y = .84 (green), and ending up at x = .17, y = .01 (violet). This curve is called the *spectrum locus*. We can close the locus by drawing the straight line from the violet to the red point. The closed plane region so formed is the *chromaticity diagram*. The colors associated with the points of the spectrum locus are the purest colors attainable in the present system. Suppose that a given sample of radiant flux has chromaticity coordinates (x,y) which land it at point Q on the chromaticity diagram. Draw a straight line from E through Q to intersect the spectrum locus at W. The wavelength λ associated with W is called the *dominant wavelength* or *color* of Q, and the fraction p = EQ/EW (where "EQ", "EW" denote the lengths of the respective straight line segments) is called the *purity* of the color of Q. If a point such as Q' is considered, we extend Q'E back to W', and the associated purity is by definition EQ'/EW'. *In this way, we finally achieve the first part of our goal for the present exposition, namely, the explanation of how a given sample* P *of radiant flux defined on the spectrum* Λ *can be assigned two numbers: its dominant wavelength* λ *and the purity* p *of the dominant wavelength of* P.

These two numbers act very much like the polar coordinates of points in the chromaticity diagram, with the point E as the pole. The purity is often given as a percentage rather than a fraction. Hence the pair (x,y) of chromaticity coordinates have their polar equivalents (λ,p). We shall use the term "chromaticity coordinates" interchangeably for these equivalent representations.

An Example of Experimentally Determined Chromaticity Coordinates

We shall now cite some examples of the preceding concepts. These examples are drawn from various colorimetric studies of natural hydrosols. Fig. 1.78 depicts the spectral dependence of the apparent radiance of submerged sandy shoals and reefs as studied in 1944 by Duntley through a glass-bottomed boat surveying parts of the east coast of Florida (near Dania). The same submarine area surveyed from an altitude of 4300 feet (1300 meters) is depicted in Fig. 1.79. If $N(\lambda)$ is the apparent radiance of a particular point of the underwater

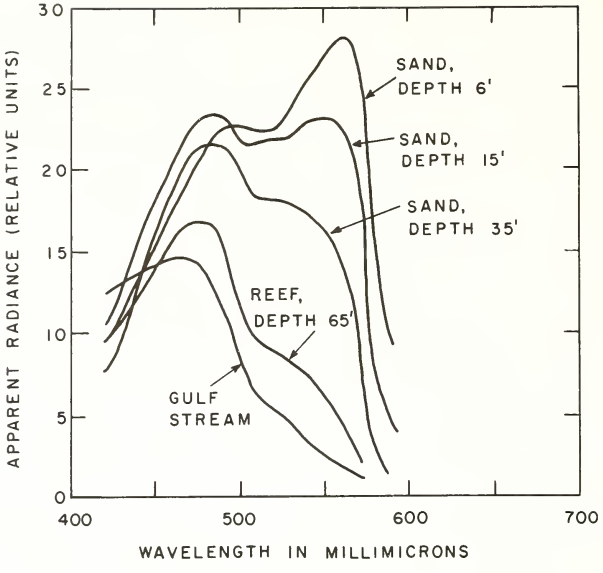

FIG. 1.78 Spectroradiometric curves of sandy bottom of shoals near Dania, Florida, by Duntley, March 1944. (Fig. 1 from [78], by permission)

scene for a given λ, as plotted on Fig. 1.78, then the color components x, y, z of $N(\lambda)$, $0 \leq \lambda \leq \infty$, are obtained by using these plotted radiance values in (5)-(7) and (12)-(14) with $N(\lambda)$ replacing $P(\lambda)$. Seventy-six chromaticity coordinates x, y, were computed according to (12), (13) for each of the five curves in Fig. 1.78, and their locations are shown along the upper curve on the chromaticity diagram of Fig. 1.80. The corresponding

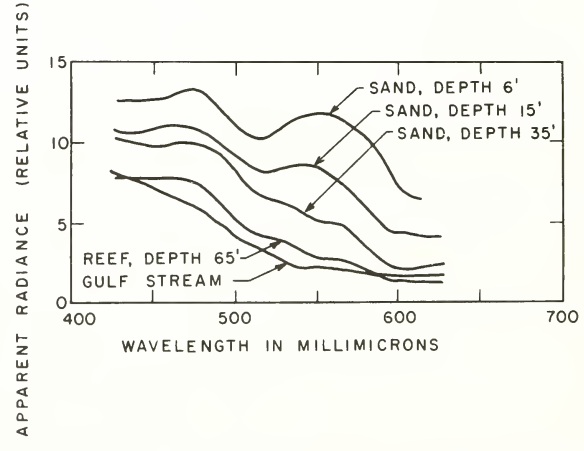

FIG. 1.79 Same scene as Fig. 1.78, viewed from an altitude of 4300 feet. (Fig. 2 from [78], by permission)

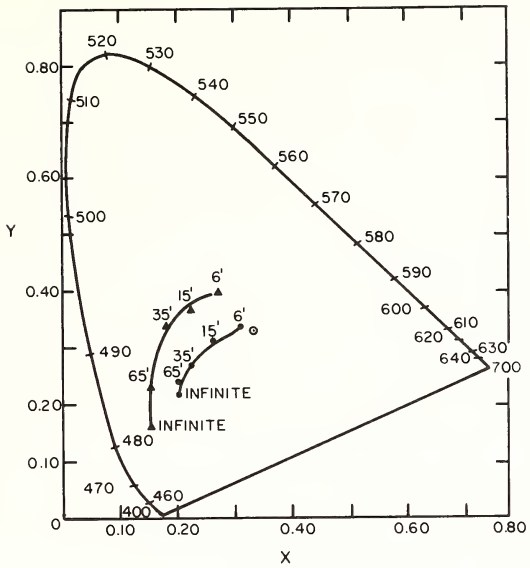

FIG. 1.80 Chromaticity diagram associated with the curves of Figs. 1.78, 1.79. The five curves of Fig. 1.78 yield the five points of the upper curve in the chromaticity diagram. The five curves of Fig. 1.79 yield the five points of the lower curve in the diagram. (Fig. 3 from [78], by permission)

locus of the chromaticity coordinates for the aerial view of the shoals is given by the lower curve in Fig. 1.80. This example is taken from the review article [78] by Duntley. Further examples may be found in [126], and [302].

We now turn to the second part of our goal in this section, the theory of colorimetric radiative transfer.

On the Use of Simple Models for Theoretical Predictions of Chromaticity Coordinates

A relatively unexplored area of application of the simple models for radiance and irradiance developed in Sec. 1.3 is colorimetric radiative transfer theory. We shall consider the essential steps that may be taken in this direction of application. Starting quite generally with the apparent radiance form of the equation of transfer (12) of Sec. 1.3, let us take the wavelength λ out of wraps and write the equation with λ explicitly shown, as follows:

$$N_r(z,\theta,\lambda) = N_o(z_o,\theta,\lambda)e^{-\alpha(\lambda)r} + \int_0^r N_*(z',\theta,\lambda)e^{-\alpha(\lambda)(r-r')}dr' \quad (18)$$

By specifying $N_o(z_o,\theta,\lambda)$, $\alpha(\lambda)$, and $N_*(z',\theta,\lambda)$ we are able in principle to compute $N_r(z,\theta,\lambda)$ for every z, θ, r, and λ over given paths and for a preselected set of λ values in Λ. Then by (5)-(7), we can compute:

$$X_r(z,\theta) = 680\int_0^\infty N_r(z,\theta,\lambda)\ \bar{x}(\lambda)\ d\lambda \tag{19}$$

$$Y_r(z,\theta) = 680\int_0^\infty N_r(z,\theta,\lambda)\ \bar{y}(\lambda)\ d\lambda \quad (=B_r(z,\theta)) \tag{20}$$

$$Z_r(z,\theta) = 680\int_0^\infty N_r(z,\theta,\lambda)\ \bar{z}(\lambda)\ d\lambda \tag{21}$$

From these color components of $N_r(z,\theta,\lambda)$, using (12), (13), we can find the two chromaticity coordinates:

$$x_r(z,\theta) = \frac{X_r(z,\theta)}{X_r(z,\theta) + Y_r(z,\theta) + Z_r(z,\theta)} \tag{22}$$

$$y_r(z,\theta) = \frac{Y_r(z,\theta)}{X_r(z,\theta) + Y_r(z,\theta) + Z_r(z,\theta)} \tag{23}$$

and from these, as explained above, we derive the dominant wavelength λ and the purity p of this wavelength. Such a pair (λ,p) is a function of z, θ, and r, and we thus may write the pair as: $(\lambda_r(z,\theta),\ p_r(z,\theta))$.

The simple model for apparent radiance (14) of Sec. 1.3 should be a rich source of colorimetric predictions for the light fields in natural hydrosols. Thus we can now write the equation as:

$$N_r(z,\theta,\lambda) = N_o(z_o,\theta,\lambda)e^{-\alpha(\lambda)r} + \\ + \frac{N_*(z,\theta,\lambda)}{(\alpha(\lambda)+K(\lambda)\cos\theta)}\left[1-e^{-(\alpha(\lambda)+K(\lambda)\cos\theta)r}\right] \tag{24}$$

where

$$N_*(z,\theta,\lambda) = N_*(0,\theta,\lambda)e^{-K(\lambda)z}$$

By setting $\theta = 0$, $\pi/2$ and π in (24), for example, we can predict the spectral apparent radiance of the hydrosol in these directions at depth z and via (22), (23), assign dominant wavelengths to these directions and depths, and purities to these wavelengths. To use (24) one need only specify $\alpha(\lambda)$, $K(\lambda)$ and $N_*(0,\theta,\lambda)$ along with $N_o(z_o,\theta,\lambda)$. The equation will then automatically take care of and predict the effects of the radiative transfer processes on the apparent radiances $N_r(z,\theta,\lambda)$.

The quantitative study of the colors of distant objects was apparently first systematically done by Middleton [177] in the meteorologic optics setting. He used a special case of (24) in which $\theta = \pi/2$, and computed the change in color of various objects as a function of r. His computation may serve as a model for the more extensive computations that can be made using (24) with a general value of θ.

In a completely similar way we may use the two-flow model for spectral irradiance $H(z,\pm,\lambda)$ described in (6), (7) of Sec. 1.3, and particularly in (8)-(10) of Sec. 1.4, to predict the chromaticity coordinates of the upward and downward irradiances as a function of optical depth in a given medium. The λ-dependence of $H(z,\pm,\lambda)$ enters this theory via the γ parameter and also the initial irradiances $H(0,\pm,\lambda)$ (or any equivalent pair of irradiances, as suggested by (43), (44) of Sec. 1.4).

It should be observed that in the employment of the simple model for radiance and the two-flow model for irradiance, we require only information on the Mode III level of classification of natural hydrosols (cf., Sec. 1.7).

Our purpose in this brief excursion into the world of submarine color has been to lay the foundations for a scientific description of the myriads of colors and their many hues as seen beneath the surface of seas and lakes illuminated by natural light. The simple theory evolved above and culminating in (22) and (23) goes a long way toward a quantification of the otherwise inexpressible color sensations experienced by all who explore and study underwater environs. Even such skilled expositors of natural phenomena as Minnaert [182] or William Beebe were hard pressed in their explorations of the atmosphere and the sea to describe adequately what they saw. In his studies of the coral reefs of Haiti in 1927, Beebe, in particular, observed that [12]:

> "Someday, when I can carry a color book in my helmet, I will be able to enumerate an exact color code of distance. Even in our colder, thinner atmosphere the green of mountain slopes softens to purple a long way off, but on the bottom of the sea, still greater changes take place within a few feet or yards. I have walked backward and seen a feathery-crowned sea-worm of dragon's blood alter, in my vision, within a few seconds and steps, to the palest of coral pink; while a sea-weed, deep olive-green when within reach, comes gently to the eye, when five yards away, as faintest glaucus."

The relatively precise expression of these transformations of colors with distance in scattering-absorbing media is now within our grasp. But the placing of a coordinate grid over our visual impressions can go only so far--something of our impressions of the real world will always slip through such a coarse net. This was sensed by Beebe; and for us, now in possession of the relatively powerful tools forged above, we are inclined to agree when he goes on to reflect that [12]:

> "An artist of great skill and patience can approximate the oxydized royal purple of a gorgonia, even

the pink and ivory sunset of a conch shell--but the vanishing point of distance beneath the water, where the coral reef ends and the mysteries of the unknown deeps begin--the illusion, too subtle for color, of submarine visual infinity--this is not to be whelmed by man-made brushes nor imprisoned on any terrestrial dimension."

1.9 Applications of Hydrologic Optics to Underwater Visibility Problems

In this section we shall apply the simple model for radiance (14) of Sec. 1.3 to the problem of predicting the visibility of underwater objects illuminated by natural light fields and as seen by underwater swimmers. In order to achieve this goal we must take into account not only the geometrical structure of the light field at each depth z, and its general exponential decrease with depth, but also the inherent properties of the eyes of the underwater swimmer and their mode of adaptation to the light levels in the underwater environs. These rather delicate features of the problem must be blended with great care in order to achieve a synthesis which is at once readily applicable under rugged field conditions, and yet accurate enough to make useful and dependable predictions.

Such a synthesis has recently been achieved by Duntley and it is on his results reported in [75] that the present section is based. Except for minor changes of the text of [75], in order to insure continuity within the framework of the present work, the exposition of the use of the nomographs is essentially that given in [75]. Successful experimental field tests of the theory underlying the simple model are recorded in [83]. (See Figs. 1.51, 1.52.)

We observe that the optical properties required for the application of the nomographs in this section are the volume attenuation coefficient α and the diffuse attenuation coefficient K, so that we require only a Mode III classification of optical media, as defined in Sec. 1.7, in order to implement the theoretical results summarized below. These optical properties may be measured simultaneously by means of a water clarity meter designed and developed at the Visibility Laboratory of the Scripps Institution of Oceanography [7] and which has been in use now for several years by the U.S. Oceanographic Office.

Introduction to the Nomographs

The limiting range at which a swimmer can sight any specified underwater object can be calculated from α and K if sufficient information is available concerning the nature of the object, its lighting, its background, and the visual characteristics of the observer. Consider, for example, the two underwater photographs shown in Fig. 1.81. In part (a) of the figure the camera is looking steeply downward through twenty

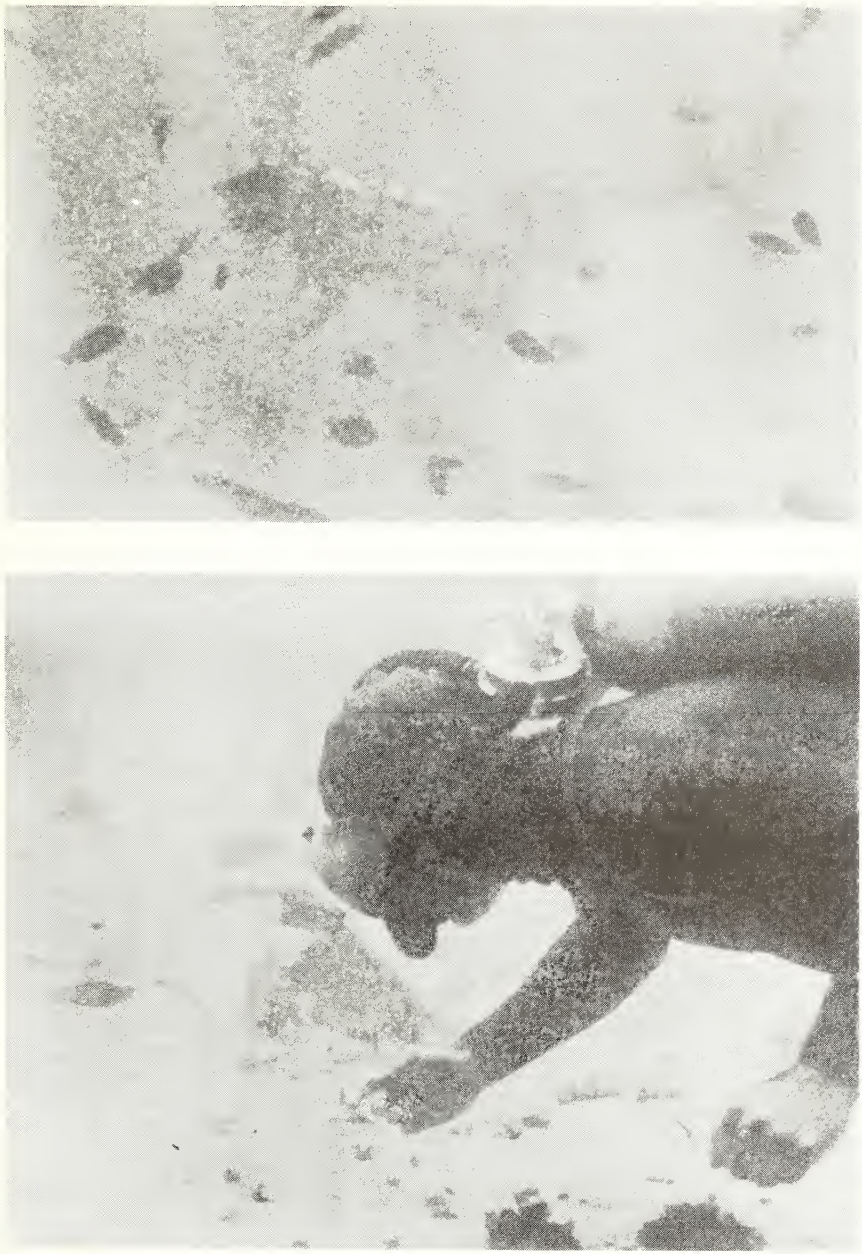

FIG. 1.81 Parts (a) and (b) illustrate the effect of distance on the apparent contrast of a swimmer against his background. The nomographs below give a quantitative means for predicting and describing the visibility of the swimmer for various parts of his underwater environs. *Courtesy of S.Q. Duntley*

feet or more of water at a black-suited swimmer close to the bottom. At short range, as in part (b) of the figure, the swimmer's suit appears very black compared with the near-white bottom, but at twenty feet (part (a)) its apparent contrast is low; only the nearest fish and kelp leaves appear "black". At a slightly greater camera distance the swimmer would not be seen in the photograph because of insufficient apparent contrast. The greatest distance at which the swimmer can be seen by his companion, the photographer, may be calculated by means of the nomographic charts presented in this section.

The nomographic charts in this section can be applied to nearly every underwater viewing task if adequate input data concerning the object, its lighting, and its background are available. The applications discussed and illustrated in this section are visual tasks for which adequate input data are readily available.

The main body of this section is concerned with the prediction of sighting ranges along paths of sight which are inclined downward, and the nomographs are designed especially for this case. The visibility of flat, horizontal, non-glossy surfaces lying on the bottom or suspended far above the bottom can be calculated with great accuracy; but three-dimensional objects, particularly those with rounded surfaces, will be treated with slightly less certainty until additional development work, in progress at the time of the present writing, has been completed. Accordingly, sightings of complex surfaces and sightings along upward-looking paths of sight are not treated per se in the present set of nomographs.

A. Selection of the Proper Chart

A.1 *Introduction*

The detection capabilities of any swimmer depend upon the level of light to which his eyes are adapted. This, in turn, depends upon the quantity of natural illumination on the surface of the sea, the depth of the swimmer, and the clarity of the water.

We shall present nomographic charts for nine adaptation conditions covering the entire range of light levels at which the human eye can operate, a range which extends from brightest day to darkest night. The first step in any visibility calculation is to ascertain the adaptation luminance to which the swimmer will be exposed and to select the appropriate chart.

A.2 *Natural Illumination*

The Bureau of Ships, U.S. Navy, has made a comprehensive study of natural illumination on the surface of the sea and has published an unclassified handbook-type report entitled "Natural Illumination Charts", (Ref. [35]) from which the illuminance in lumens per square foot (i.e., "footcandles") can be found for any location on earth at any time of day on

any day in any year. A summary page from that report is reproduced as Figure 1.12. By means of this figure the illumination on the surface of the sea can be found if the altitude of the sun and type of sky is known.

A.3 *Effect of Depth and Water Clarity*

If the illuminance on any fully exposed upward-facing horizontal surface is measured at various depths in any uniform stratum of sea water, we have seen (in (7) of Sec. 1.2, and (7) of Sec. 1.4) that, to a useful approximation, the illumination level decreases exponentially with depth. Graphs of the exponential law, constructed especially for the purposes of the present section, are given in Figures 1.82, 1.83. The slopes of the straight lines are measured by the various values of the diffuse attenuation coefficient K, which is defined by the equation

$$E_z = E_o e^{-Kz} \quad , \tag{1}$$

where E_o is the downward illuminance at the top of the uniform stratum, z is depth within the stratum, and E_z is the downward illuminance at depth z. Strictly, this equation relates to monochromatic light only, as shown in (7) of Sec. 1.4, but it is a sufficient approximation to illuminance data for the practical purposes of this section.

If the measured value of K is the same from the sea surface to the target, z may be taken as the depth of the swimmer and the illuminance at his depth determined by multiplying the illuminance at the sea-surface (from Figure 1.12) by the appropriate factor read from Figure 1.82.

Stratified Water

If the water above the target is composed of two or more layers having different values of K, it will be necessary to use the appropriate straight line in Figure 1.82 or 1.83 to obtain the factor for calculating the illuminance at the bottom of the first layer and use this value as the illumination incident on the top of the second layer, and so on until the level of the swimmer is reached. In other words, Figure 1.82 is used to determine factors for each successive layer, and the product of these factors is multiplied by the illuminance at the surface of the sea in order to obtain the illuminance at the depth of the swimmer.

The assumption of an average or weighted-average K for the entire distance from sea-surface to swimmer is often a sufficient approximation for the calculation of adaptation luminance and the subsequent selection of the proper nomographic chart. Even in extreme cases the use of a single K is often sufficient for this purpose.

Effect of Sea-state

Sea-state, i.e., wave conditions, have no significant effect on underwater visibility tasks except near the surface, where small waves and ripples may cause the water to be filled

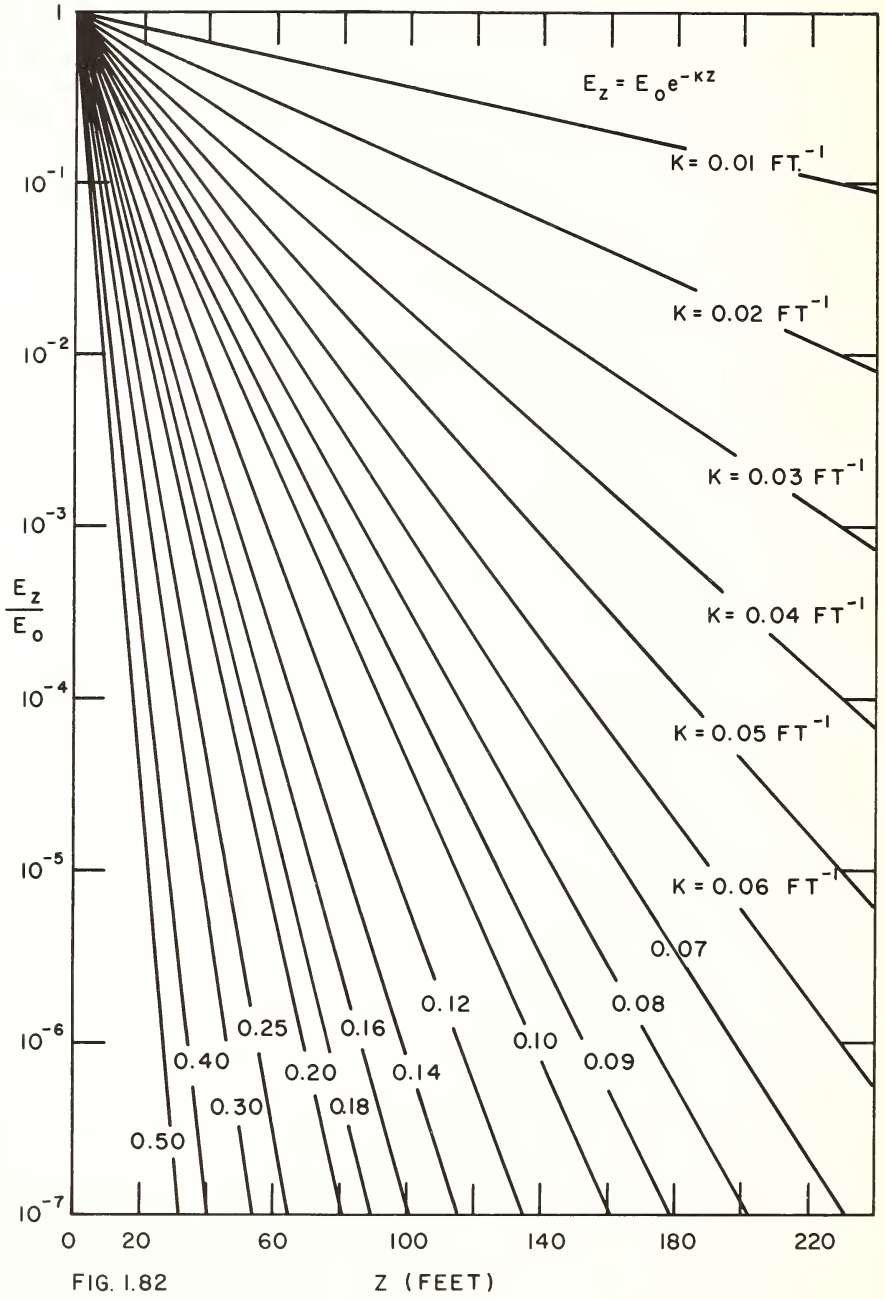
$E_z = E_o e^{-Kz}$
K = 0.01 FT^{-1}
K = 0.02 FT^{-1}
K = 0.03 FT^{-1}
K = 0.04 FT^{-1}
K = 0.05 FT^{-1}
K = 0.06 FT^{-1}
0.07
0.08
0.09
0.10
0.12
0.14
0.16
0.18
0.20
0.25
0.30
0.40
0.50
$\frac{E_z}{E_o}$
1
10^{-1}
10^{-2}
10^{-3}
10^{-4}
10^{-5}
10^{-6}
10^{-7}
0
20
60
100
140
180
220
Z (FEET)

FIG. I.82

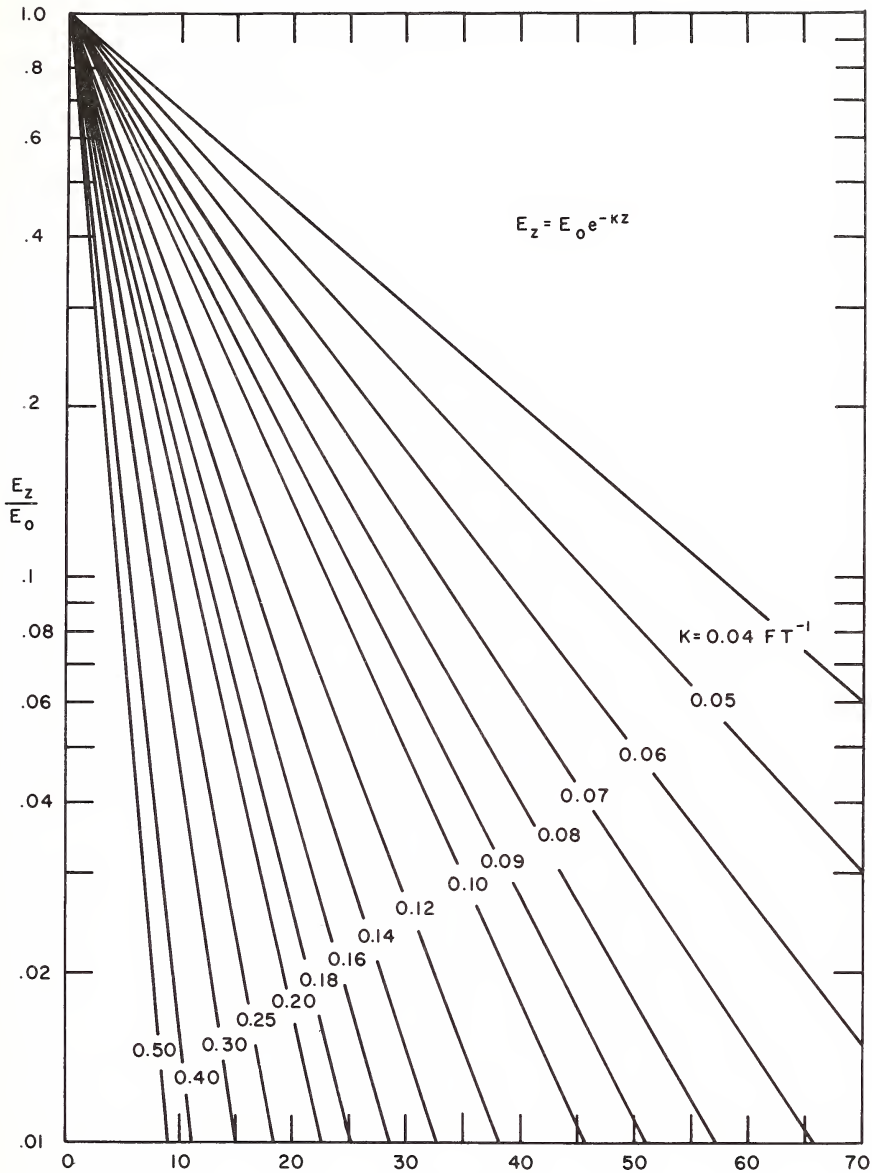
1.0
.8
.6
.4
.2
.1
.08
.06
.04
.02
.01
$\frac{E_z}{E_o}$
$E_z = E_o e^{-kz}$
K= 0.04 FT^{-1}
0.05
0.06
0.07
0.08
0.09
0.10
0.12
0.14
0.16
0.18
0.20
0.25
0.30
0.40
0.50
0
10
20
30
40
50
60
70
Z (FEET)

FIG. 1.83

with a rapidly moving ensemble of dancing beams of sunlight and where large waves may cause noticeable lighting fluctuations due to the effectively variable depth of the swimmer (cf., discussions on subsurface refractive phenomena in Sec. 1.2). When the sun is within 5 degrees of the horizon, slightly more sunlight penetrates the water surface when it is rough than when it is calm, as described in the discussions of Table 3, Sec. 1.2, but the effect is ordinarily negligible in terms of visibility by swimmers.

Examples

On a certain cloudless sunny morning the illuminance at a point 40 feet beneath the surface in the entrance channel of a harbor was found by measurement to be 176 lumens/ft^2 and K at this depth was measured as 0.0943 per foot. A deck-cell showed the illuminance on the surface of the water to be 7600 lumens/ft^2. Reference to Figure 1.82 or insertion of these numbers in Equation (1) yields a predicted illuminance of 175 lumens/ft^2, in excellent agreement with the measured value. A diver reported that no major stratification was observable above 40 feet.

Half an hour earlier, however, the diver had reported a dense cloud of organic material between depths 10 and 15 feet. The surface illuminance at that time was 5200 lumens/ft^2 and K at 40 feet was 0.0943 per foot. The illuminance at 40 feet predicted from these numbers is 120 lumens/ft^2, but measurement disclosed only 90 lumens/ft^2. Obviously the cloudy stratum between 10 and 15 feet had lowered the illuminance at 40 feet by 30 lumens/ft^2, and it would have been necessary to know K for this stratum in order to correct for its presence.

A.4 *Adaptation Level*

If the swimmer were just above a perfectly reflecting white bottom he would be adapted to a luminance level (expressed in foot-lamberts) numerically equal to the illuminance at his depth. If, however, he is in water so deep that the bottom produces no influence on the light-field he will see, when looking straight down, a luminance numerically equal to approximately 1/50 of the illuminance from above (see paragraph B.7 below). Thus, if the illuminance on the top of the swimmer is 100 lumens/ft^2 he will observe an adaptation luminance of 2 foot-lamberts when looking straight down.

Inclination Factor

If the swimmer looks along an inclined path rather than straight down he will see an adaptation luminance which is greater by an amount known as the *inclination factor*. This factor depends upon depth and the downward direction in which he looks, as shown by the small graphs in the lower left corner of Figure 1.84. For example, if the swimmer is at a depth 9/K (i.e., 90 feet if K = 0.1 per foot) and looks downward in a direction having a zenith angle of 120 degrees in the azimuth of the sun he will observe approximately twice as much luminance as if his path of sight were straight down. In

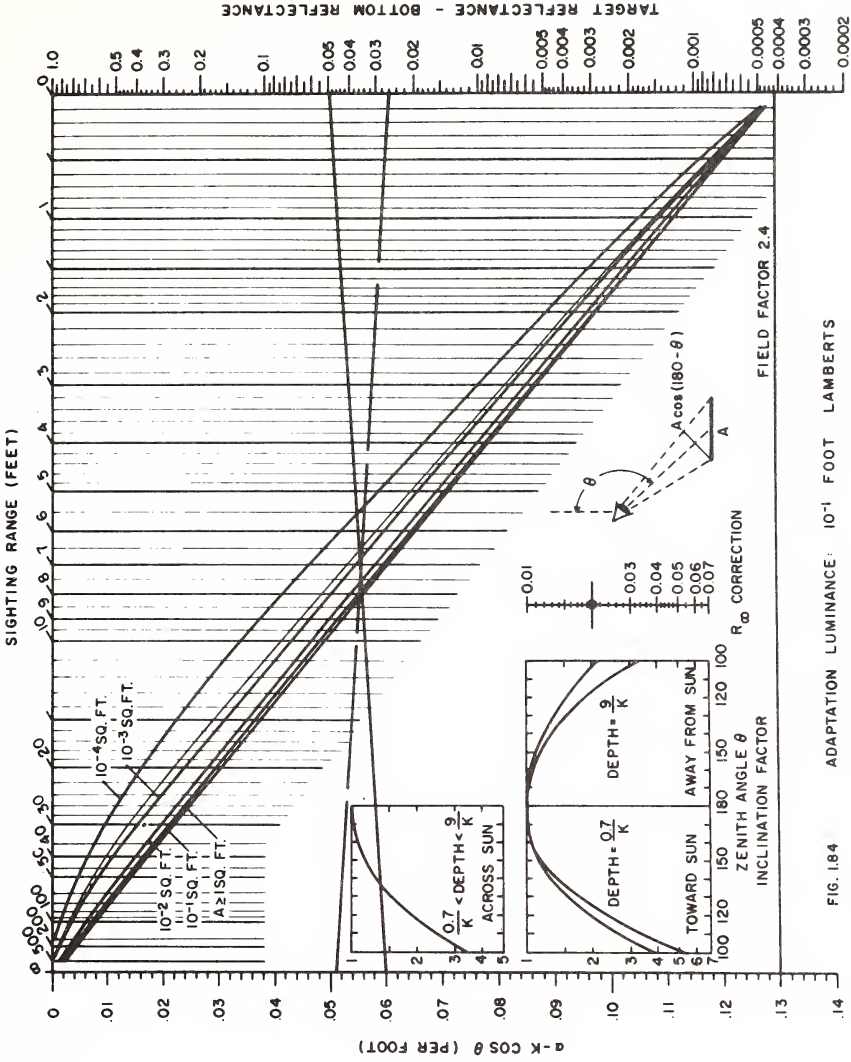
TARGET REFLECTANCE - BOTTOM REFLECTANCE
SIGHTING RANGE (FEET)
a-K COS θ (PER FOOT)
FIELD FACTOR 2.4
ADAPTATION LUMINANCE: 10⁻¹ FOOT LAMBERTS
10⁻⁴SQ. FT.
10⁻³SQ.FT.
10⁻²SQ. FT.
10⁻¹SQ. FT.
A≥1SQ. FT.
0.7/K < DEPTH < 9/K
ACROSS SUN
DEPTH = 0.7/K
DEPTH = 9/K
TOWARD SUN
AWAY FROM SUN
ZENITH ANGLE θ
INCLINATION FACTOR
R∞ CORRECTION
A cos (180-θ)

FIG. 1.84

terms of the numerical example in the preceding paragraph, his adaptation luminance is 2×2 = 4 foot-lamberts. The theoretical basis for the inclination factor is (68) of Sec. 1.4.

Bottom Influence

If the swimmer is near the bottom, his adaptation may be affected, depending (i) on how greatly the bottom differs in reflectance from 1/50, (ii) on the clarity of the water, and (iii) upon its distance from the swimmer. Generally speaking, dark mud bottoms have little or no effect on adaptation and light-colored bottoms have negligible influence when the sighting range is the order of 3/K or greater. Even at a sighting range of only one diffuse attenuation length 1/K, few bottoms are white enough to affect the swimmer's adaptation significantly. Generally speaking, therefore, the influence of the bottom upon adaptation can be neglected in calculating visibility by swimmers. It should be noted, however, that the reflectance of the bottom may have a major effect on the inherent contrast of the object and, therefore, upon its visibility, as discussed in Section B.2 below.

A.5 *Calculation of Adaptation Luminance*

The foregoing discussion can be summarized and illustrated by concrete examples: let it be required to find the adaptation luminance for a swimmer 60 feet beneath the surface of deep water characterized by a diffuse attenuation coefficient K of 0.10 per foot, or 0.328 per meter which, as we have seen in Tables 7 and 8 of Sec. 1.6, is on the order of K-values found in clear lake water. It is also a value typical of coastal water. Let it be assumed that the sun is 16.8 degrees above the horizontal plane on a clear sunny day.

Reference to Figure 1.12 shows that the illuminance on the sea-surface is 2000 lumens/ft^2. Inspection of the line marked K = 0.10 per foot in Figure 1.82 shows that the horizontal plane containing the swimmer receives 2.5×10^{-3} as much downward light as does the sea-surface, or $2000 \times 2.5 \times 10^{-3} = 5$ lumens/ft^2.

If the swimmer looks straight downward his adaptation luminance will be 5 × 1/50 = 0.1 foot-lamberts if there is no bottom influence.

If the swimmer looks along a downward slant path having a zenith angle of 110 degrees in a plane at right angles to the azimuth of the sun, the inclination factor graph in Fig. 1.84 shows that his adaptation luminance is 2.5 times greater than if he looks straight down. Along this inclined path of sight the swimmer's adaptation luminance is, therefore, 0.10 × 2.5 = 0.25 foot-lamberts. The user of Figure 1.84 should verify that the "across sun" curve is applicable by noting that the depth (60 feet) of the swimmer is 6/K, since K = 0.10 per foot, and that this depth lies between limits specified in the figure.

Had the solar elevation been 65 degrees, Figure 1.12

shows that the illumination at the sea-surface would have been 10,000 lumens/ft^2 and the adaptation luminances of the swimmer at 60 feet would, therefore, have been five times higher; i.e., 0.50 foot-lamberts when looking straight down and 1.25 foot-lamberts when looking at right angles to the azimuth of the sun along a downward path of sight having a zenith angle of 110 degrees.

A.6 *Chart Selection*

Paragraph B below (in Figs. 1.89-1.106) contains nine pairs of nomographic charts, each pair representing a decimal value of adaptation luminance, as follows: 1000, 100, 10, 1, 10^{-1}, 10^{-2}, 10^{-3}, 10^{-4}, 10^{-5} foot-lamberts. One member of a pair is for low clarity, the other for high clarity water. After the adaptation luminance of the swimmer has been calculated the chart closest to this level is selected. If the adaptation luminance is not close to any decimal value, sighting range for the visual target should be calculated by means of charts for higher and lower light levels respectively in order to bracket the desired answer and provide for interpolation between these sighting ranges.

B. Using the Nomographs

B.1 *Introduction*

Once the adaptation luminance for the swimmer has been determined and the proper nomographic chart selected, sighting ranges can be predicted. The calculation procedures are slightly different for each type of visual task and, therefore, they will be discussed separately. The basic nomographs are given in Figs. 1.89-1.106. However, for illustrative purposes, two charts have been excised from that group and appear in Figs. 1.84 and 1.85. This is the low-clarity, high-clarity pair for 10^{-1} foot-lambert adaptation.

B.2 *Objects on the Bottom*

The nomographic visibility charts can be used to calculate the sighting range of flat, horizontal objects of uniform reflectance lying on the bottom.

Object Size and Shape

The size of the object is measured by its area, expressed in square feet; the shape of the object is unimportant unless it is an extremely elongated form (10:1 or greater) and unless adaptation luminance is 10 foot-lamberts or greater. Even in such unusual cases the effect of object shape on sighting range is usually small.

Vertical Path of Sight

Sighting range calculations are simplest when the path of sight is vertically downward. Each nomograph requires

five items of input data: target area, target reflectance, bottom reflectance, the volume attenuation coefficient α, and the diffuse attenuation coefficient K. The coefficients α and K must be for the water between the swimmer and the target.

The vertical scales on the nomographs are labeled "α-K cos θ". (The use of a minus sign here, relative to the use of a plus sign in Sec. 1.3 wherein the theory of the simple radiance model was developed, is to facilitate the direction specifications *by the swimmer*. In other words we adopt here field luminances and the *swimmer-centered direction convention*.) A downward vertical path of sight has a zenith angle θ = 180 degrees, and cos 180 = -1. A point representing the sum of α and K, expressed in reciprocal feet, is marked on the left vertical scales.

The right vertical scales of the nomographs are labeled "target reflectance minus bottom reflectance". The algebraic sign of this difference is of no importance; if the bottom is more reflective than the target the difference will, of course, be a negative number; disregard the negative sign and plot the magnitude of the difference on the right vertical scale. Reflectance must be expressed as a decimal; i.e., as 0.06, not as six percent. Bottom reflectance should be measured at the sea-bottom with great care to avoid disturbing any fine silt which may be present. Bottom samples cannot be brought to the surface for measurement without disturbing the material sufficiently to alter its reflectance. Target reflectance may be measured at the sea-bottom or on ship-board by means of a technique described in paragraph B.5 of this section.

The curved lines which cover the upper right corner of the nomographic visibility charts represent visual threshold data for the target area with which each curve is identified. (The refractive effect of the swimmer's flat face-plate has been allowed for in constructing these nomographs.) Curves representing decimal values of target area are marked accordingly. Intermediate unmarked curves refer respectively to 2, 4, 6, and 8 times the decimal value except in those cases when only a single line appears between decimal curves; in this case the unmarked curve related to 5 times the decimal value.

Special Charts for Water of Low-clarity. Two series of nine nomographic charts are presented below. In the first series, the scales have been optimized for use in clear oceanic and coastal waters where sighting ranges of 20 feet to 100 feet or more often occur. The second series of charts are designed for waters of poor to medium clarity where sighting ranges of 1 foot to 20 feet or more prevail. Either series of charts may be used for any problem having input data within the range of its scales, but experience will eventually indicate which chart is best suited for any given problem.

Sighting Range Calculations, Clear Water. To calculate sighting range, connect the appropriate points on the left

and right vertical scales by a straight line and note its intersection with the curve corresponding to the area of the target. From this intersection proceed vertically to the sighting range scale. The following numerical example will illustrate this procedure with the aid of Figure 1.84.

Let the following input data be assumed:

Adaptation luminance = 10^{-1} foot-lamberts
Target: flat; horizontal; on the bottom
Target area = 10 square feet
Target reflectance = 0.080; non-glossy
Bottom reflectance = 0.030
Volume attenuation coefficient = α = 0.073 per foot
Diffuse attenuation coefficient = K = 0.027 per foot

From these data, (recalling that paths of sight at present are vertical) $\alpha + K = 0.100$, and target reflectance minus bottom reflectance is 0.050. The solid line drawn on Figure 1.84 intersects the curve marked "10 square feet" at the vertical line denoting a sighting range of 47.6 feet. The same line drawn on Figure 1.84 indicates that a swimmer looking straight down under the assumed conditions can sight a 0.1 square foot object at 43 feet, an object of 1 square foot at 46 feet, and all objects of area 100 square feet or more when he is 48.5 feet or less from the bottom.

Sighting Range Calculations, Low-clarity Water. The same example may be solved by means of the low-clarity chart (Figure 1.85) and corresponding sighting ranges obtained, but with far less precision.

In an hypothetical water of lesser clarity, characterized by α = 0.43 per foot and K = 0.17 per foot, the sum $\alpha+K$ is 0.60 per foot. If all other input data remain unchanged the high-clarity nomograph (Figure 1.84) cannot readily be used because its left vertical scale goes only to 0.14. Actually, this chart can be adapted by extending the left vertical scale linearly downward to 0.60 and constructing a diagonal line from that point to 0.05 on the right vertical scale, but such a procedure is unnecessary because the low-clarity nomograph (Figure 1.85) is available. The straight line drawn on that figure indicates by its intersection with the lower-most curve that flat horizontal objects of all sizes greater than 1 square foot can be seen by a swimmer looking straight down under the assumed conditions when he is 8 feet or less from the bottom. The same line shows by other intersections, that he must descend to within 7.5 feet of the bottom to see an object 10^{-2} square feet in area and to 5.5 feet from the bottom before a tiny object of area 10^{-4} square feet can be seen.

Inclined Paths of Sight

The nomographic visibility charts can be used for the calculation of sighting range along inclined paths of sight. Three additional items of input data are necessary: (1) the approximate azimuth of the path of sight relative to the sun,

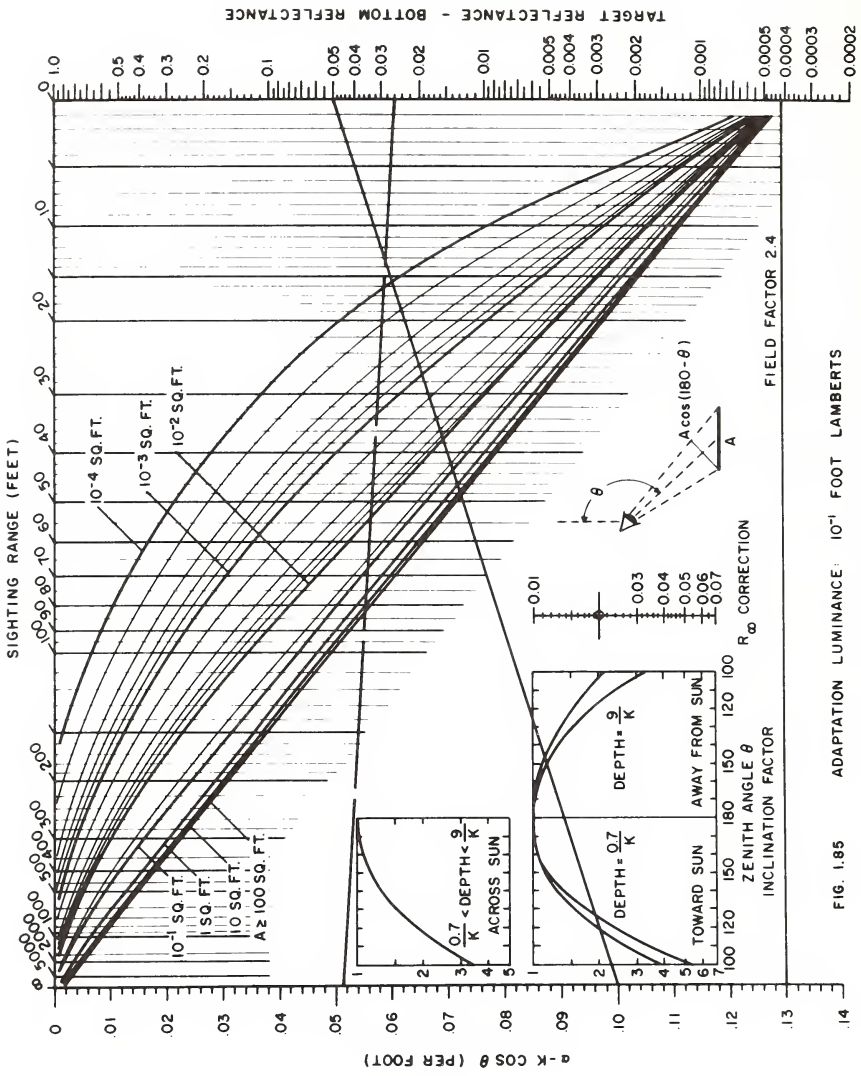
TARGET REFLECTANCE - BOTTOM REFLECTANCE
SIGHTING RANGE (FEET)
α - K COS θ (PER FOOT)
10^{-4} SQ. FT.
10^{-3} SQ. FT.
10^{-2} SQ. FT.
10^{-1} SQ. FT.
1 SQ. FT.
10 SQ. FT.
A ≥ 100 SQ. FT.
$\frac{0.7}{K}$ < DEPTH < $\frac{9}{K}$
ACROSS SUN
DEPTH = $\frac{0.7}{K}$
TOWARD SUN
DEPTH = $\frac{9}{K}$
AWAY FROM SUN
ZENITH ANGLE θ
INCLINATION FACTOR
R_∞ CORRECTION
A cos (180 - θ)
FIELD FACTOR 2.4
ADAPTATION LUMINANCE 10^{-1} FOOT LAMBERTS

FIG. 1.85

(2) the depth of the swimmer expressed in units of 1/K, and
(3) the zenith angle of the path of sight.

The first two items of data are used to estimate the increase in adaptation luminance associated with the inclined path. This is accomplished by means of the *inclination factor* curves in the lower left corner of Figure 1.84. (Identical curves appear on all of the nomographic visibility charts.) A continuation of the numerical example begun in the preceding section will illustrate this step:

Let the following input information be assumed:

(1) *Azimuth of the path of sight:* at right angles to the azimuth of the sun; i.e., the path of sight is "across sun".

(2) *Depth of swimmer* = 2.7/K. This would be the case if his depth is 100 feet and K = 0.027. The depth, 2.7/K, falls within the range for which the "across sun" curve applies.

(3) *Zenith angle of the path of sight* = 120 *degrees.*

Effect of Zenith Angle on Adaptation. Reference to the "across sun" inclination factor graph discloses that the inclination factor for this zenith angle is 1.9. This means that the adaptation luminance is 1.9 times as great as that experienced by the swimmer when looking vertically downward; i.e., $1.9 \times 10^{-1} = 0.19$ foot-lamberts. Since this adaptation luminance falls between the nomograms for 1 and 10^{-1} foot-lamberts, both charts should be used in order to bracket the sighting range. The effect of adaptation on sighting range will be discussed further in a later part of this section and illustrated by Figure 1.86.

Effect of Zenith Angle on Left Vertical Scale. The zenith angle of the path of sight (120 degrees) affects the value plotted on the left vertical scale of the nomograph:

$$\alpha\text{-}K \cos \theta = 0.43 - (0.17)(-0.50) = 0.51 .$$

(A table of cosines is available in Table 7 of Sec. 12.1) Use the relation $\cos \theta = -\cos (180\text{-}\theta)$ for θ in the range $90 \leq \theta \leq 180$.

Effect of Zenith Angle on Effective Area. The *effective area* of the object depends on the observer's line of sight; thus $A \cos (180\text{-}\theta) = 10 \times 0.50 = 5$ square feet. Inspection of the curves in Figure 1.85 shows that, in this case, no sighting range will be lost by the foreshortening because all targets having an effective area greater than 1 square foot are visually detectable at the same distance under the conditions assumed in this numerical example.

Effect of Inclination Factor on Right Vertical Scale. The inclination factor affects the value plotted on the right vertical scale as follows: the difference between target reflectance and bottom reflectance must be divided by the inclination factor before the number is plotted. Thus,

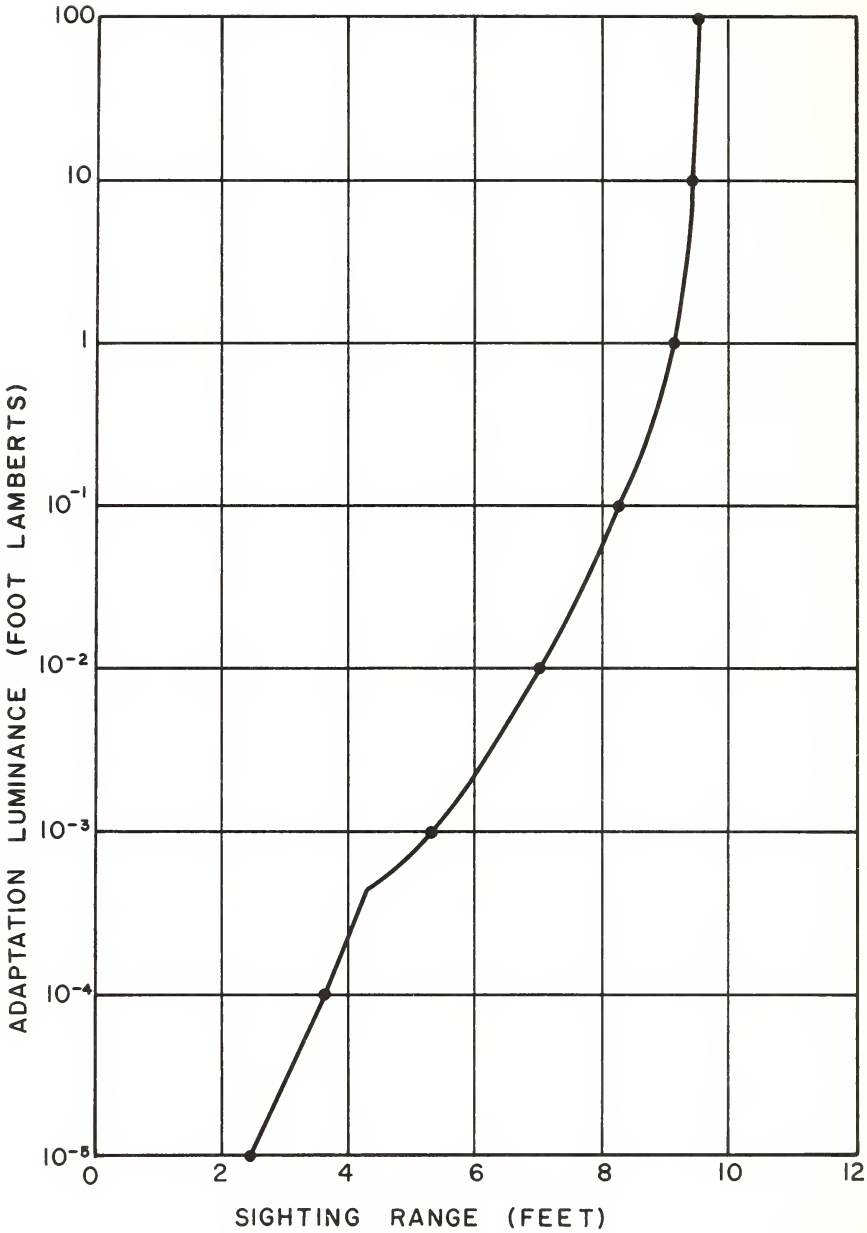

FIG. 1.86 The effect of adaptation on sighting range (see text).

(0.050/1.9) = 0.026. The inclination factor curves which appear on each chart have been plotted on an inverted logarithmic scale having the same modulus as the right vertical scale of the nomograph in order that the division can be accomplished graphically. Draftsman's dividers can conveniently be used for this purpose: measure downward from the top border of the figure to the inclination factor curve and transfer this setting to the right vertical scale of the nomograph, using it to *reduce* the plotted value of target reflectance minus bottom reflectance.

Calculation of the Sighting Range. The broken line on Figure 1.85 shows that the sighting range would be 8.1 feet for the inclined path if the adaptation luminance was 10^{-1} foot-lamberts. Since, as shown above, the adaptation luminance is 1.9×10^{-1} foot-lamberts a minor correction to the sighting range should be made in the following manner:

Effect of Adaptation on Sighting Range. Since the luminance to which the swimmer's eyes are adapted is 0.19 foot-lamberts, an interpolation should be made between the sighting range 9.1 feet indicated by the nomograph for 1 foot-lambert and the sighting range 8.2 feet indicated by the nomograph for 10^{-1} foot-lambert. By linear arithmetic interpolation, $8.2 + (9.1-8.2)(1.9 \times 10^{-1}) = 8.4$ feet. This value compares with the sighting range of 8.5 feet found by the graphical interpolation provided by Figure 1.86, which illustrates the effect of adaptation on sighting range in this illustrative example. Figure 1.86 has been prepared by assuming successively all decimal values of adaptation luminance and plotting the resulting sighting ranges given by the entire series of nomographic charts.* Linear arithmetic interpolation of sighting range between adjacent decimal levels of adaptation luminance suffices for the needs of most problems.

Implication of the Sighting Range. Although the sighting range for the inclined path (8.5 feet) happens to be only slightly longer than the sighting range for the vertical case, it should be recognized that the swimmer must be within 4.25 feet of the bottom in order to see the target at this inclination angle.

B.3 *The Secchi Disk*

The underwater sighting range of a flat horizontal surface of uniform reflectance, suspended in (optically) deep water, e.g., a Secchi Disk, can be calculated by means of the nomographic visibility charts. Ordinarily, Secchi Disk readings are obtained by an observer above the surface of the sea

*The discontinuity in curve slope at about 4.4×10^{-4} foot-lamberts results from a change from central fixation to averted vision on the part of the swimmer, in order to achieve maximum sighting range in the dim light; this change of fixation is built into the nomographs.

who must look downward through the surface (see the analysis of the Secchi Disk theory in Sec. 1.4). Sky reflection and complex refractive effects resulting from water waves greatly complicate the interpretation of the greatest depth at which the disk can be seen. If, however, a swimmer lowers a Secchi Disk beneath him and observes its disappearance, the sighting range can be predicted by means of the nomographic visibility charts if α and K are known. Conversely, the observed sighting range can be inserted in the nomograph in order to find the sum of the attenuation coefficients, α+K.

Let it be assumed that the water is so deep beneath the disk that the bottom has no significant effect upon the light field. The nomographs are so constructed that they will correctly predict the sighting range of the disk if the right vertical scale of the nomograph is imagined to be labeled "Secchi Disk reflectance minus 0.02". All other details of the calculation are identical with those described in the preceding paragraphs of this section which deal with objects on the sea-bottom. Attention is called, however, to subject matter of Section B.7, entitled "The R_∞ Correction".

B.4 *Target Markings*

The preceding paragraphs of this section have dealt with the sighting ranges of the whole target. It is sometimes required to calculate the sighting ranges of certain details or markings on a target. This is readily accomplished by means of the nomographic visibility charts. The only modifications of the procedure described in the preceding paragraphs are (i) to imagine the right vertical scale to be labeled "reflectance of marking-reflectance of target", and (ii) to use the curve which applies to the area of the marking.

B.5 *The Measurement of Target Reflectance*

The reflectance of painted surfaces differ, often markedly, when dry and when wet. The values of target reflectance required for use in the nomographic visibility charts are those which would be measured by a water-filled reflectometer submerged with the target. This *submerged reflectance* differs from reflectances measured by conventional laboratory reflectometers *even if the painted surface is wet.*

Target reflectance may be measured at the sea-bottom, or, with greater convenience, it may be measured on shipboard by means of a technique developed by the Visibility Laboratory of the University of California (San Diego) and described in [82]. Excerpts from that report have been assembled and are reproduced in Fig. 1.87.

B.6 *Horizontal Paths of Sight*

The visibility nomographs can be used for calculating sighting ranges along horizontal paths of sight provided the inherent contrast of the object against its horizontal water background is known. Such contrasts are determinable in any of several ways. For example, one may use irradiance

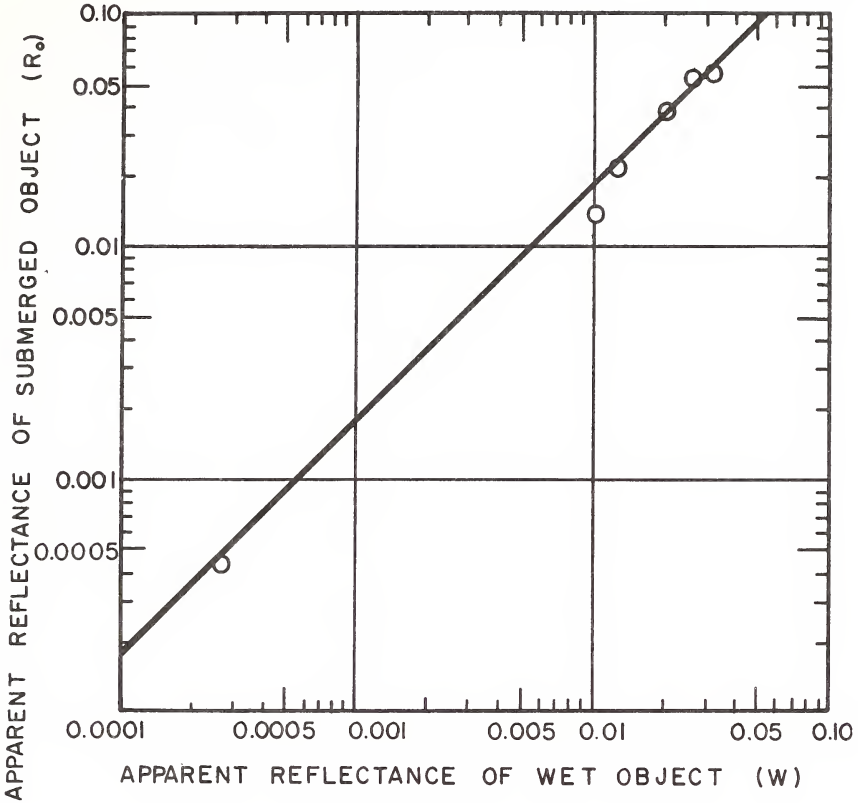

FIG. 1.87 Graphical means of determining the reflectance R_o of a submerged surface given its wet reflectance. The technique involves wetting the sample with a thin film of water, irradiating it with a beam at 45°, and viewing it normally, say with a conventional refractometer. This determines the abscissa of the graph. The associated ordinate yields R_o. This scheme was designed by Duntley, and the plotted points are the results of his experimental check of the graph.

distributions of the kind shown in Figs. 1.25, 1.26, for the general class of medium (specified by Mode III of Sec. 1.7) under study. Such irradiance distributions are also readily made from radiance distributions obtained via a Mode IB classification of media. Finally, one may use the simple radiance model of Sec. 1.3 to provide such estimates.

For the calculation of horizontal sighting ranges, the right vertical scale should be imagined to be labeled "inherent contrast ÷ 50". Thus an inherent contrast of ±1 plots at the point marked 0.02 on the right vertical scale.

For horizontal paths of sight the zenith angle $\theta = 90$

degrees and, since cos 90 = 0, the left vertical scale involves only the volume attenuation coefficient α. The areas associated with the curved lines on the nomograph refer to the projected area of the target as seen from the position of the swimmer.

Sighting ranges are calculated by connecting the right and left vertical scales with a straight line, and reading the sighting range from the scale division directly above the intersection of this line with the curve which applies to the target area. When the nomographic charts are used in this manner for horizontal sighting range calculations no approximations are involved so that neither of the corrections described in the next two sections of this report are required.

B.7 *The R_∞ Correction*

In nearly all optically deep natural waters and at all depths approximately 50 times more illuminance reaches any horizontal plane from above than from below. The ratio of the illuminance from below to the illuminance from above is denoted by the symbol "R_∞". This notation implies that the (optically) infinite deep water beneath any horizontal plane in the sea could be replaced, for optical purposes, by a surface of reflectance R_∞. This quantity is often measured by means of two photoelectric cells mounted back-to-back and facing upward and downward respectively.

Because $R_\infty = 0.02$ for most natural waters of moderate to high clarity, the nomographic visibility charts have this value built into their scales. If R_∞ is known to be different than 0.02 in any specific instance, this information can be entered in the calculation by dividing the value of "target reflectance - bottom reflectance" by 50 R_∞ before plotting the point on the right vertical scale of the nomograph. Alternatively, the "R_∞ CORRECTION" scale printed on the nomograph can be used to apply a correction after the point has been plotted but before the line is drawn across the chart. Draftsman's dividers are a convenient tool for this purpose: set one leg of the dividers at the circled point on the "R_∞ CORRECTION" scale and adjust the other leg to the known value of R_∞. Transfer this setting to the right vertical scale, maintaining the direction of the correction indicated by the "R_∞ CORRECTION" scale; i.e., the plotted point on the right vertical scale is moved downward when R_∞ exceeds 0.02, and upward when R_∞ is less than 0.02.

B.8 *Correction of the Sighting Range*

The nomographic visibility charts involve certain algebraic approximations which may lead to invalid sighting ranges when the indicated value of sighting range is short and when the reflectance of the bottom departs markedly from 0.02. Figure 1.88 is provided as a means for testing any indicated sighting range for error and indicating the needed correction. The following numerical example will illustrate the use of Figure 1.88.

A sighting range of 4 feet is indicated by the

nomographic visibility chart when:

Adaptation luminance is 10^{-1} foot-lamberts
Target area = 10^{-3} square feet
α-K cos θ = 0.50
Bottom reflectance = 0.10
Inclination factor = 2
Target reflectance - bottom reflectance = 0.010

Since the sighting range is short and the reflectance of the bottom departs markedly from 0.02, the predicted sighting range should be tested and corrected by means of Figure 1.88 as follows:

On the vertical scale of Figure 1.88, labeled "sighting range × (α-K cos θ)" enter the data 4 × 0.5 = 2. On the horizontal scale labeled "bottom reflectance/inclination factor" enter the data 0.10/2 = 0.05. These entries locate a point on Figure 1.88 which falls close to the curve marked "0.83". The factor 0.83 is to be applied to the value of "target reflectance - bottom reflectance". Thus, 0.010 × 0.83= 0.0083. If this corrected value is plotted on the right vertical scale on the nomographic visibility chart the corrected sighting range is 3.72 feet.

Except in extreme cases the corrected sighting range will differ but little from the uncorrected value. In most cases the point on Figure 1.88 will plot above the highest curve, indicating thereby that no correction is required.

Like the nomographic visibility charts, Figure 1.88 has been constructed with the assumption that R_∞ = 0.02. If R_∞ is known to differ from this value this information can easily be inserted in the correction process by dividing the value of "bottom reflectance/inclination factor" by 50 R_∞ before plotting the point on Figure 1.85. Thus, in the foregoing example if R_∞ = 0.0154, the horizontal coordinate of the point on Figure 1.85 is 0.050/(50 × 0.0154) = 0.065, and the correction factor is 0.77 rather than the value 0.83 obtained before the insertion of the R_∞ information, and the new corrected sighting range is 3.60 feet.

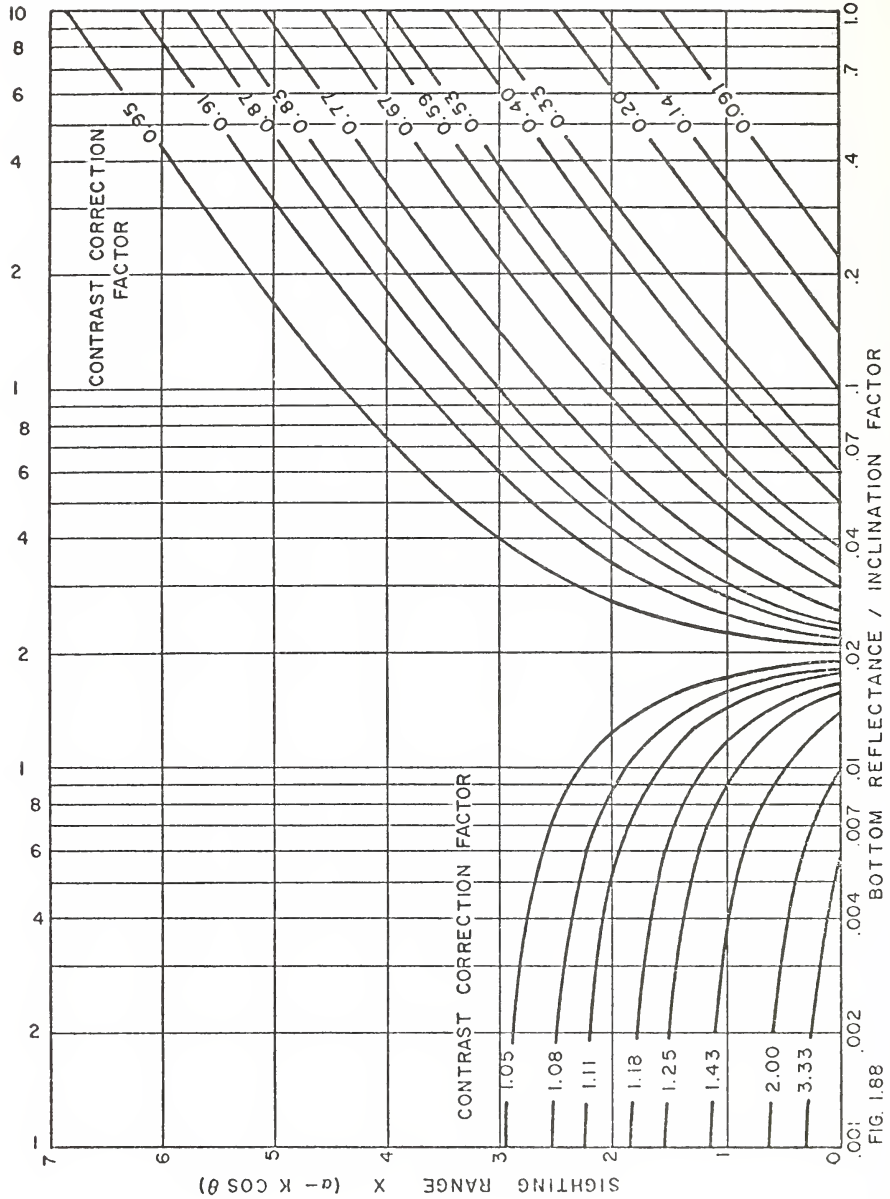
CONTRAST CORRECTION FACTOR
0.95
0.91
0.87
0.83
0.77
0.67
0.59
0.53
0.40
0.33
0.20
0.14
0.0
CONTRAST CORRECTION FACTOR
1.05
1.08
1.11
1.18
1.25
1.43
2.00
3.33
SIGHTING RANGE X (a − K COS θ)
BOTTOM REFLECTANCE / INCLINATION FACTOR

FIG. 1.88

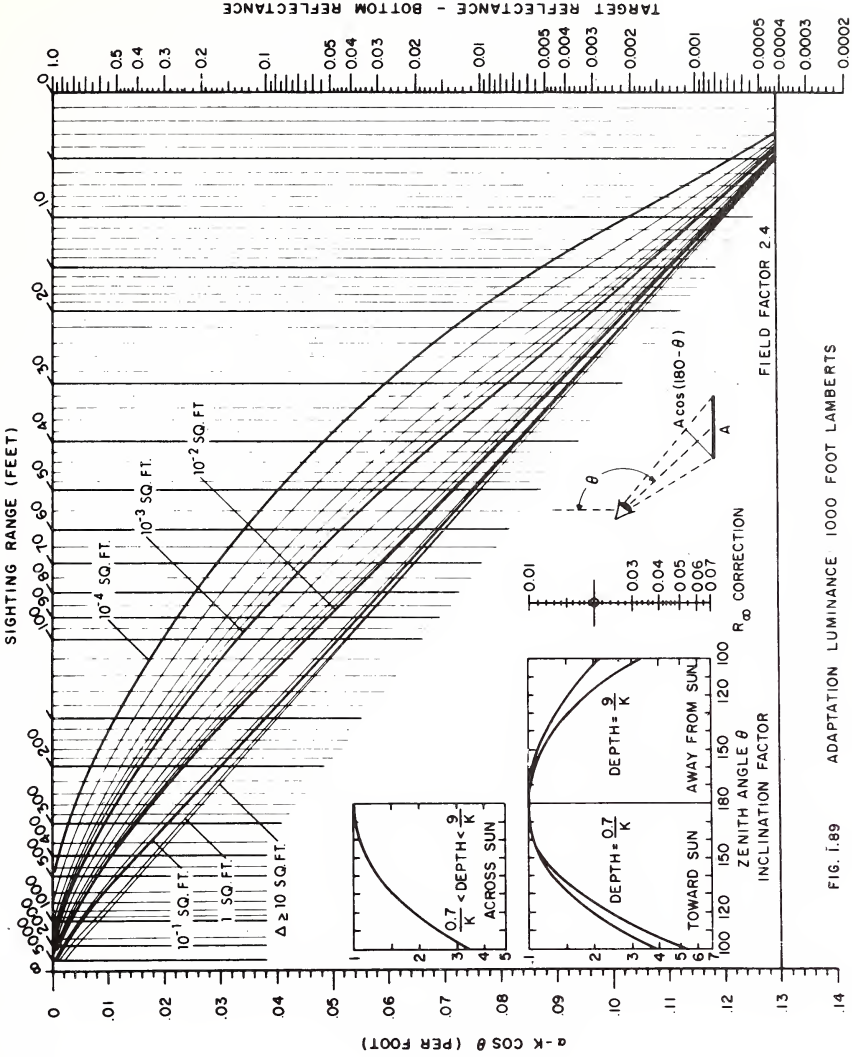
TARGET REFLECTANCE - BOTTOM REFLECTANCE
SIGHTING RANGE (FEET)
$a - K \cos\theta$ (PER FOOT)
10^{-4} SQ. FT.
10^{-3} SQ. FT.
10^{-2} SQ. FT.
10^{-1} SQ. FT.
1 SQ. FT.
$\Delta \geq 10$ SQ. FT.
FIELD FACTOR 2.4
R_∞ CORRECTION
$A\cos(180-\theta)$
θ
$\frac{0.7}{K} < \text{DEPTH} < \frac{9}{K}$
ACROSS SUN
DEPTH = $\frac{0.7}{K}$
DEPTH = $\frac{9}{K}$
TOWARD SUN
AWAY FROM SUN
ZENITH ANGLE θ
INCLINATION FACTOR
ADAPTATION LUMINANCE 1000 FOOT LAMBERTS

FIG. 1.89

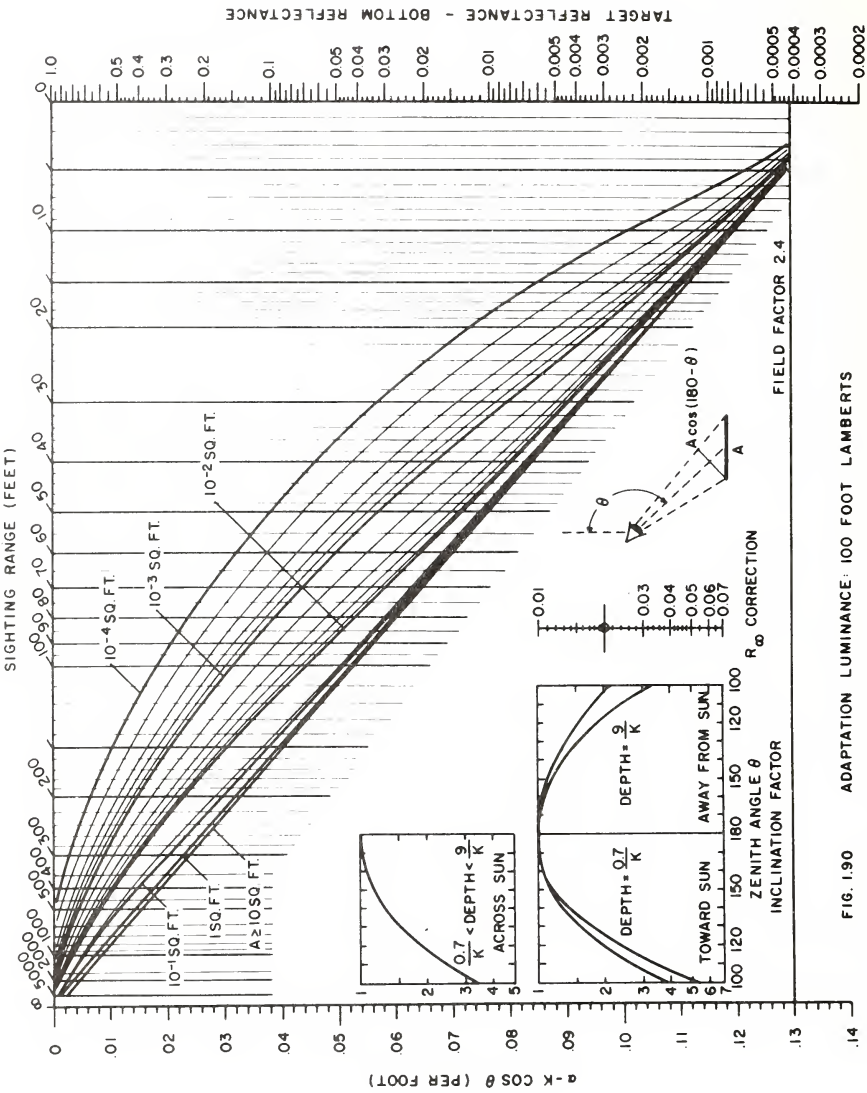
TARGET REFLECTANCE - BOTTOM REFLECTANCE
SIGHTING RANGE (FEET)
α-K COS θ (PER FOOT)
10^{-4} SQ. FT.
10^{-3} SQ. FT.
10^{-2} SQ. FT.
10^{-1} SQ. FT.
1 SQ. FT.
A ≥ 10 SQ. FT.
$\frac{0.7}{K}$ < DEPTH < $\frac{9}{K}$
ACROSS SUN
DEPTH = $\frac{0.7}{K}$
TOWARD SUN
DEPTH = $\frac{9}{K}$
AWAY FROM SUN
ZENITH ANGLE θ
INCLINATION FACTOR
R_∞ CORRECTION
A cos (180-θ)
A
θ
FIELD FACTOR 2.4
ADAPTATION LUMINANCE: 100 FOOT LAMBERTS

FIG. 1.90

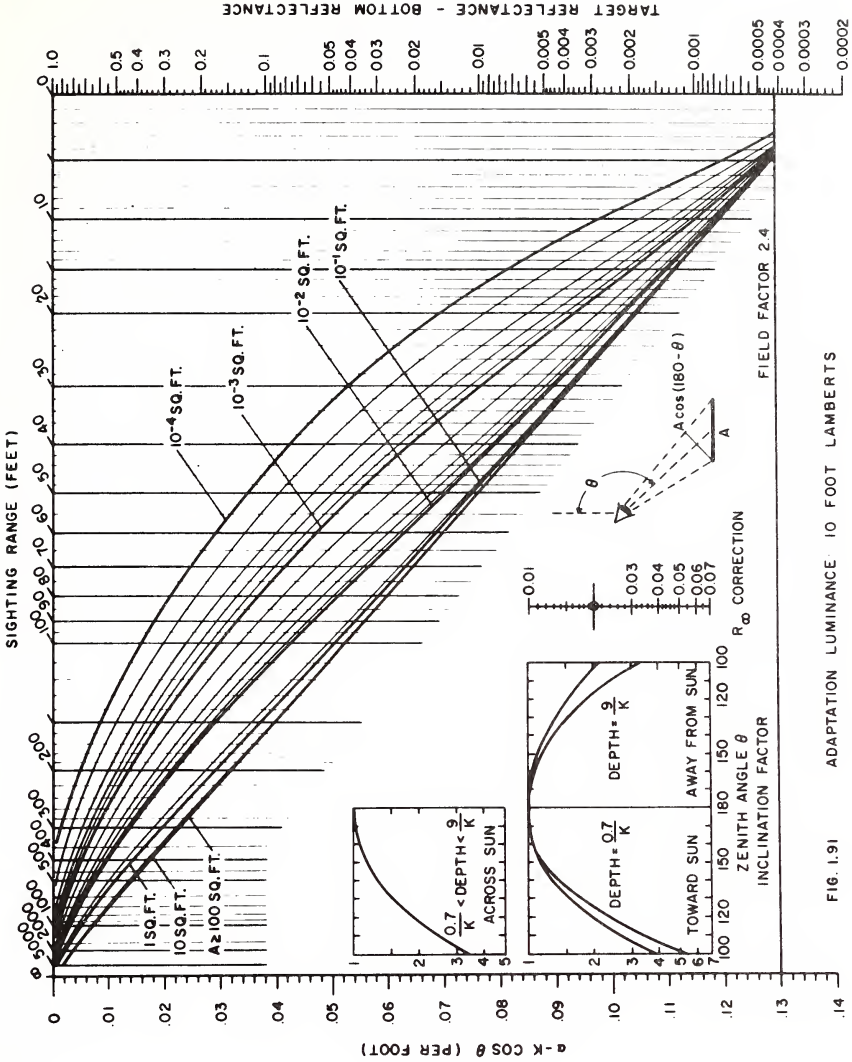

FIG. 1.91 ADAPTATION LUMINANCE 10 FOOT LAMBERTS

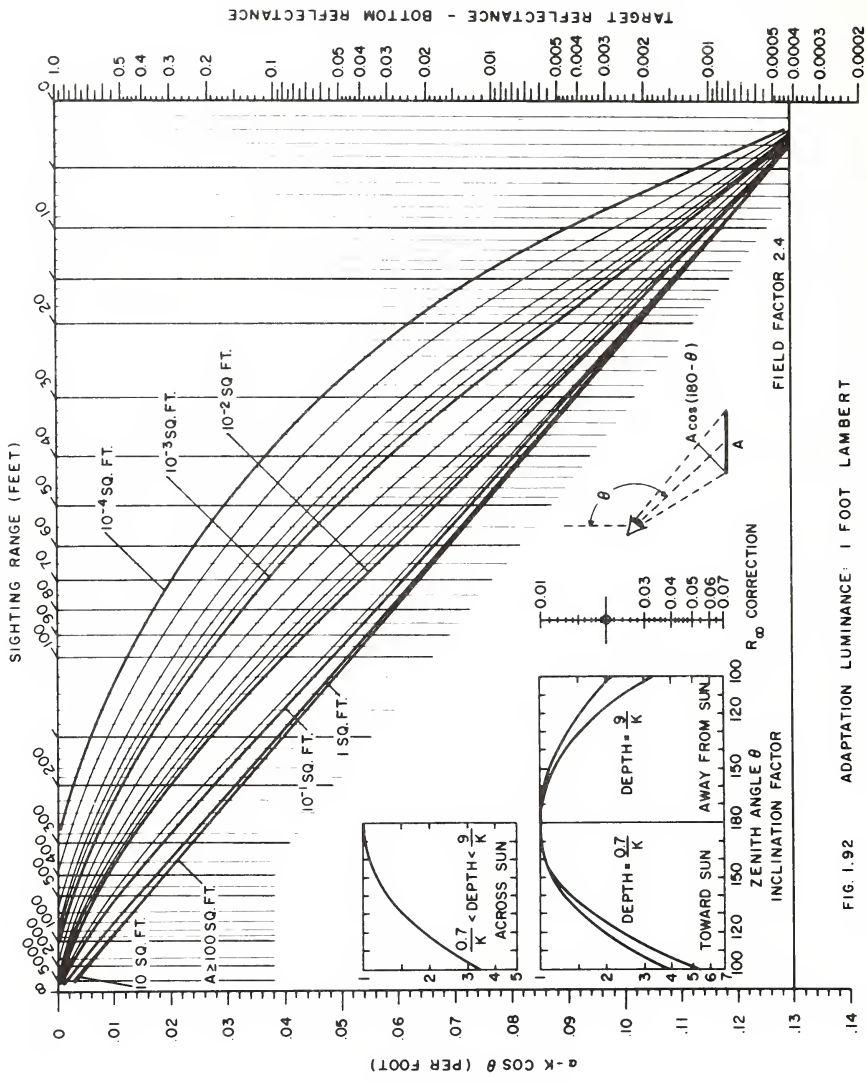

FIG. 1.92 ADAPTATION LUMINANCE: 1 FOOT LAMBERT

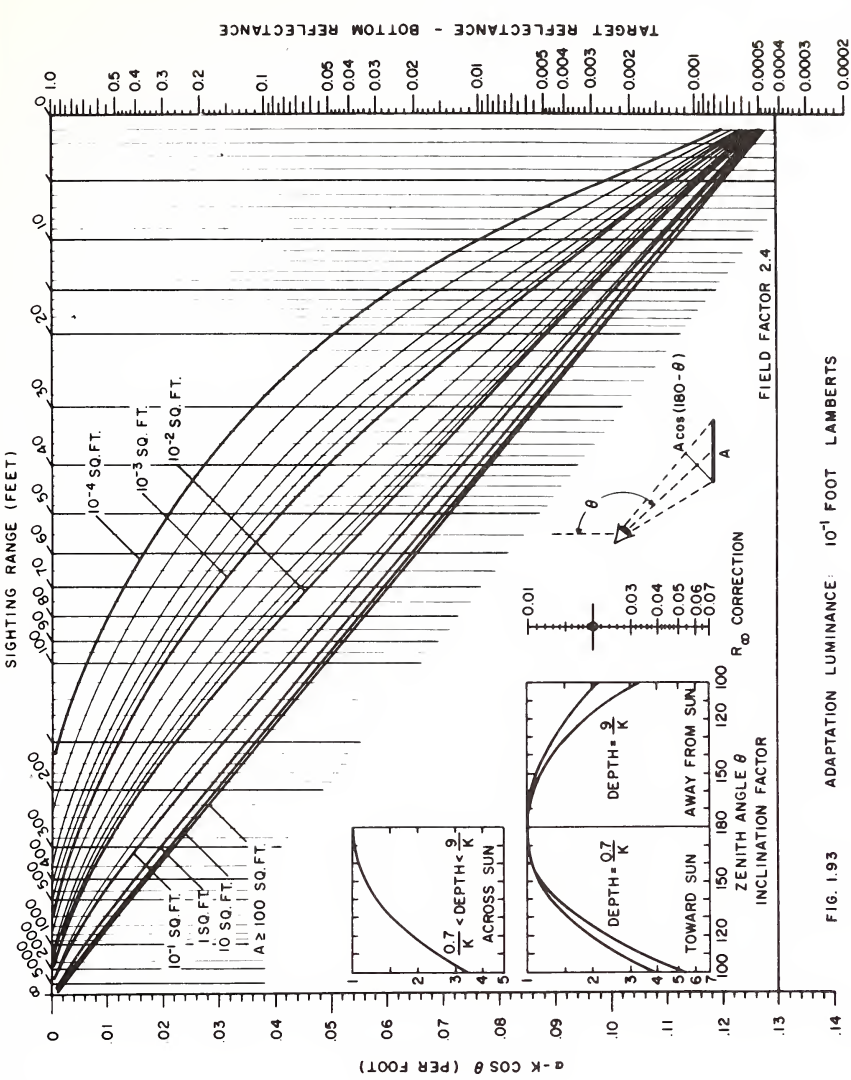

FIG. 1.93 ADAPTATION LUMINANCE: 10^{-1} FOOT LAMBERTS

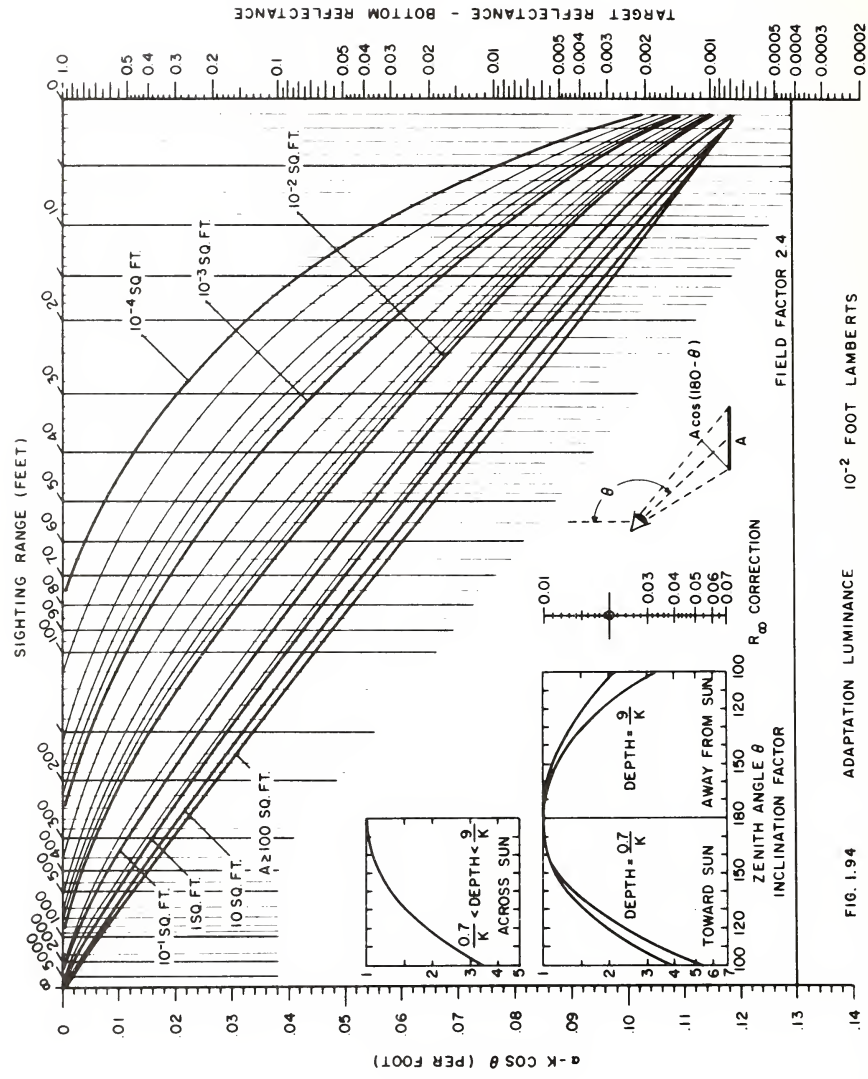
TARGET REFLECTANCE - BOTTOM REFLECTANCE
SIGHTING RANGE (FEET)
α-K COS θ (PER FOOT)
10^{-4} SQ FT
10^{-3} SQ FT
10^{-2} SQ FT
10^{-1} SQ. FT.
1 SQ. FT.
10 SQ. FT.
A≥100 SQ. FT.
$\frac{0.7}{K}$ < DEPTH < $\frac{9}{K}$
ACROSS SUN
DEPTH = $\frac{0.7}{K}$
DEPTH = $\frac{9}{K}$
TOWARD SUN
AWAY FROM SUN
ZENITH ANGLE θ
INCLINATION FACTOR
R_∞ CORRECTION
A cos (180-θ)
FIELD FACTOR 2.4
ADAPTATION LUMINANCE 10^{-2} FOOT LAMBERTS

FIG. 1.94

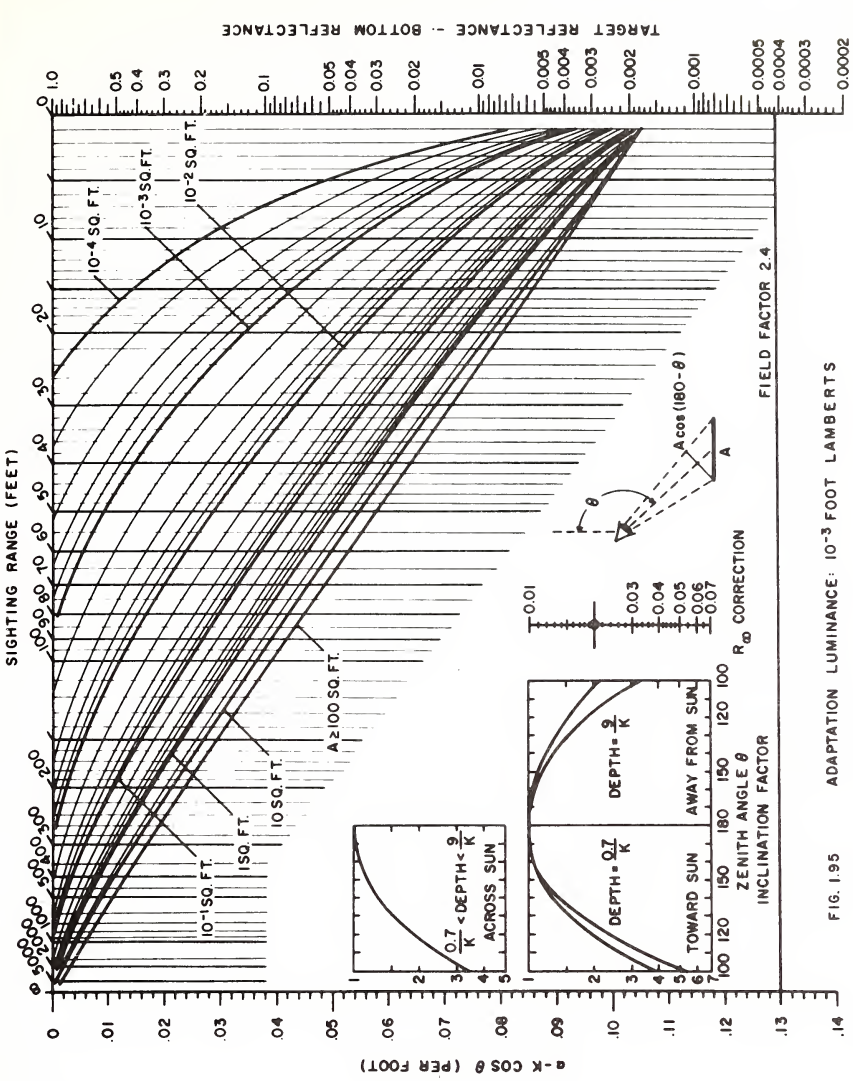

FIG. 1.95 ADAPTATION LUMINANCE: 10^{-3} FOOT LAMBERTS

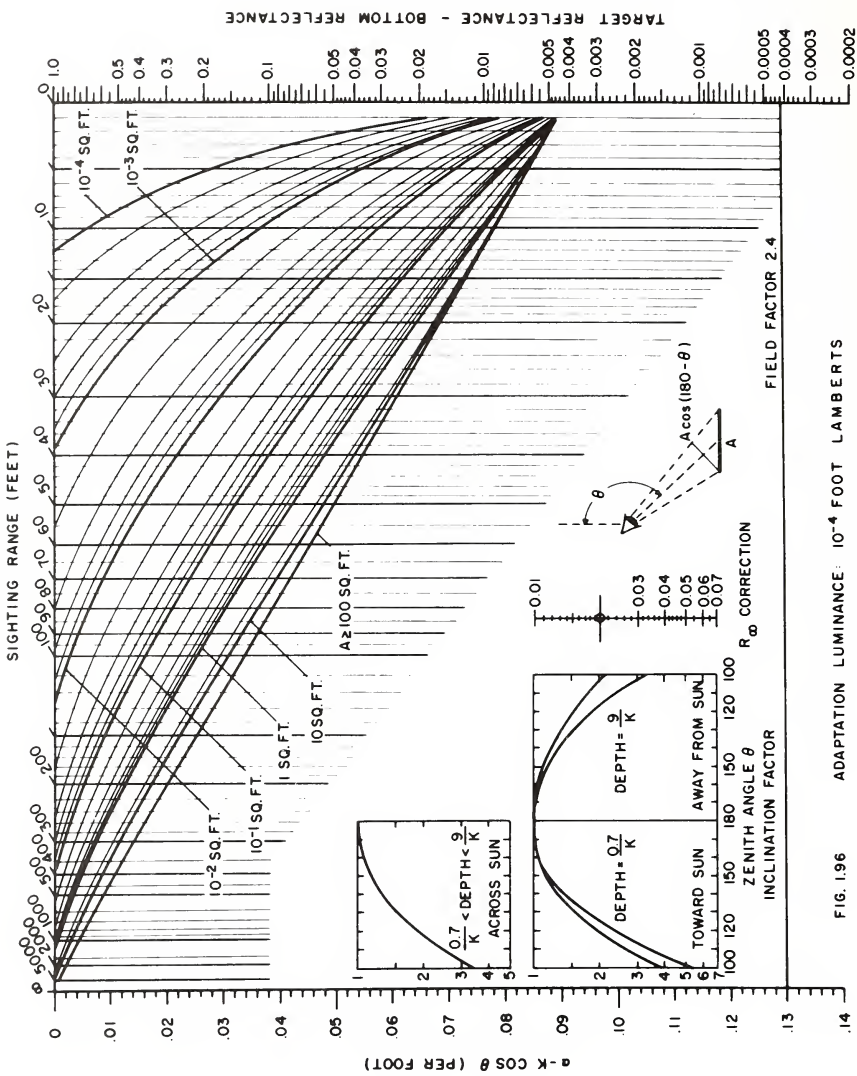
TARGET REFLECTANCE - BOTTOM REFLECTANCE
SIGHTING RANGE (FEET)
α-K COS θ (PER FOOT)
10^{-4} SQ.FT.
10^{-3} SQ.FT.
10^{-2} SQ.FT.
10^{-1} SQ.FT.
1 SQ.FT.
10 SQ.FT.
A≥100 SQ.FT.
FIELD FACTOR 2.4
R_∞ CORRECTION
0.01
0.03
0.04
0.05
0.06
0.07
A cos(180-θ)
θ
A
$\frac{0.7}{K}$ < DEPTH < $\frac{9}{K}$
ACROSS SUN
DEPTH = $\frac{0.7}{K}$
DEPTH = $\frac{9}{K}$
TOWARD SUN
AWAY FROM SUN
ZENITH ANGLE θ
INCLINATION FACTOR
ADAPTATION LUMINANCE: 10^{-4} FOOT LAMBERTS

FIG. 1.96

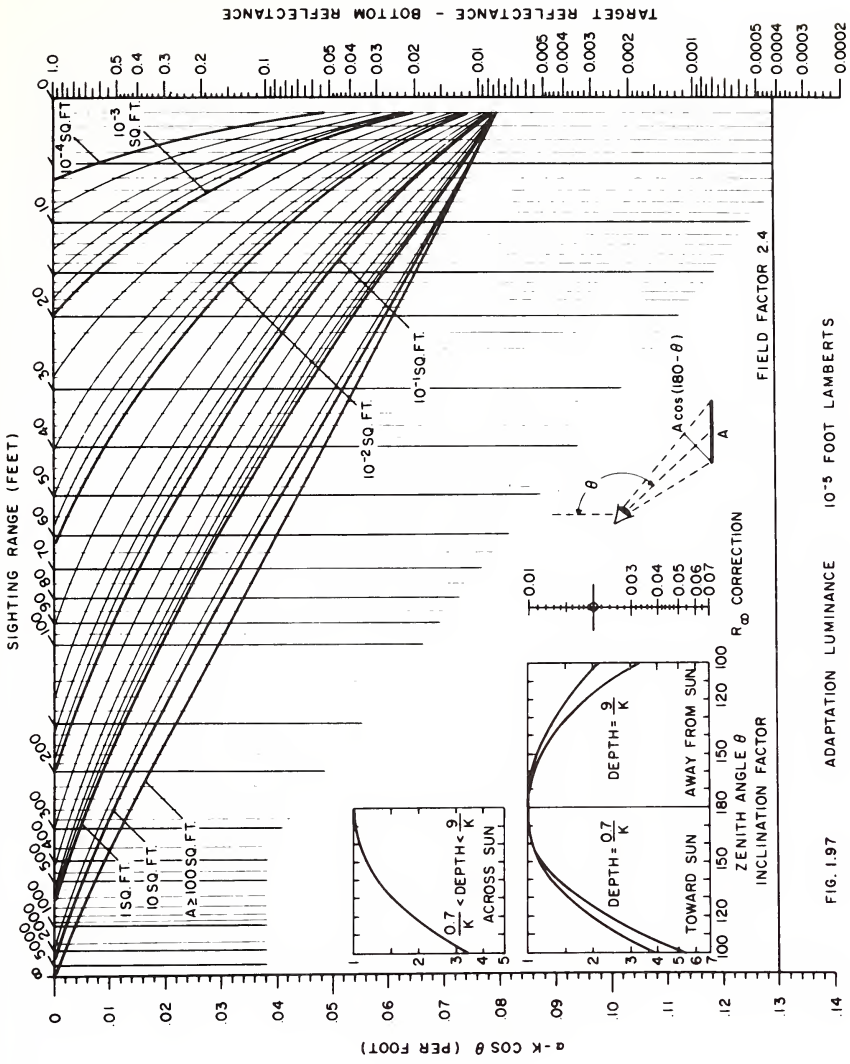
TARGET REFLECTANCE - BOTTOM REFLECTANCE
SIGHTING RANGE (FEET)
a-K COS θ (PER FOOT)
10⁻⁴ SQ FT
10⁻³ SQ FT
10⁻² SQ FT
10⁻¹ SQ FT
1 SQ FT
10 SQ FT
A≥100 SQ FT
FIELD FACTOR 2.4
ADAPTATION LUMINANCE 10⁻⁵ FOOT LAMBERTS
R∞ CORRECTION
A cos (180-θ)
θ
A
0.7/K < DEPTH < 9/K ACROSS SUN
DEPTH = 0.7/K TOWARD SUN
DEPTH = 9/K AWAY FROM SUN
ZENITH ANGLE θ
INCLINATION FACTOR

FIG. 1.97

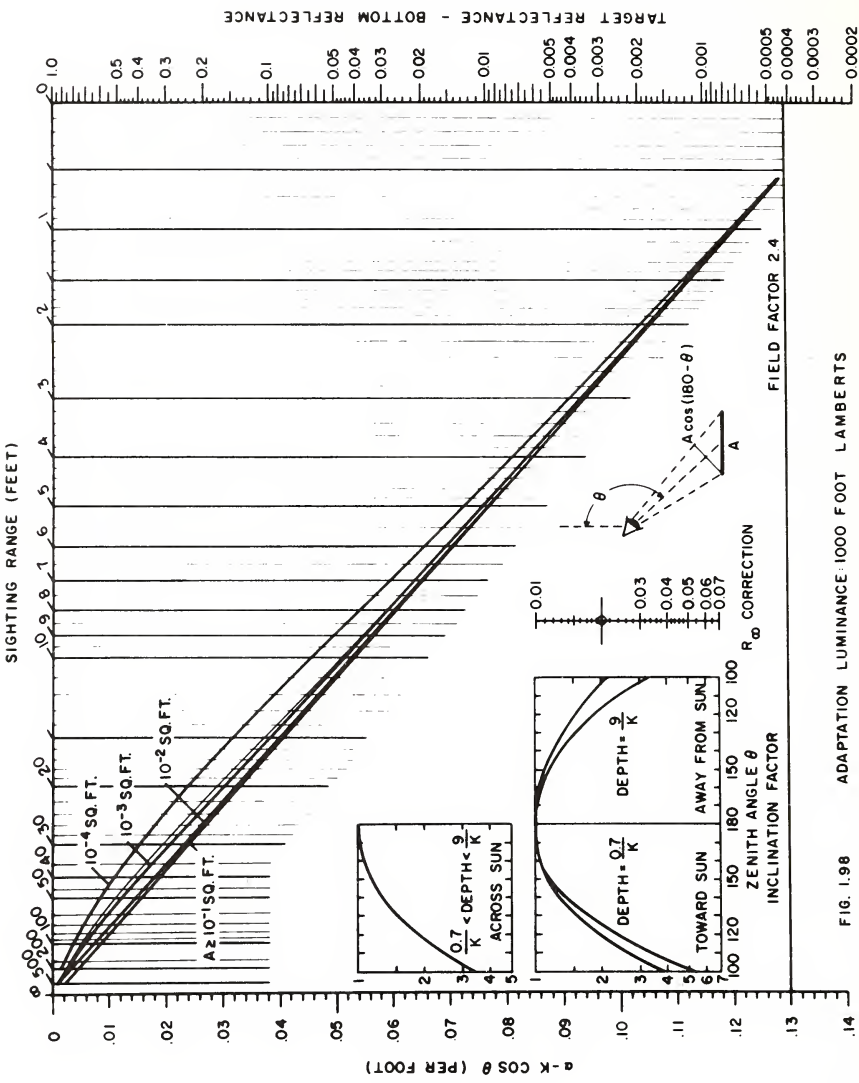
TARGET REFLECTANCE - BOTTOM REFLECTANCE
SIGHTING RANGE (FEET)
a-K cos θ (PER FOOT)
A ≥ 10⁻¹ SQ. FT.
10⁻² SQ. FT.
10⁻³ SQ. FT.
10⁻⁴ SQ. FT.
FIELD FACTOR 2.4
A cos (180-θ)
R∞ CORRECTION
0.01
0.03
0.04
0.05
0.06
0.07
0.7/K < DEPTH < 9/K
ACROSS SUN
DEPTH = 0.7/K
DEPTH = 9/K
TOWARD SUN
AWAY FROM SUN
ZENITH ANGLE θ
INCLINATION FACTOR
ADAPTATION LUMINANCE: 1000 FOOT LAMBERTS

FIG. 1.98

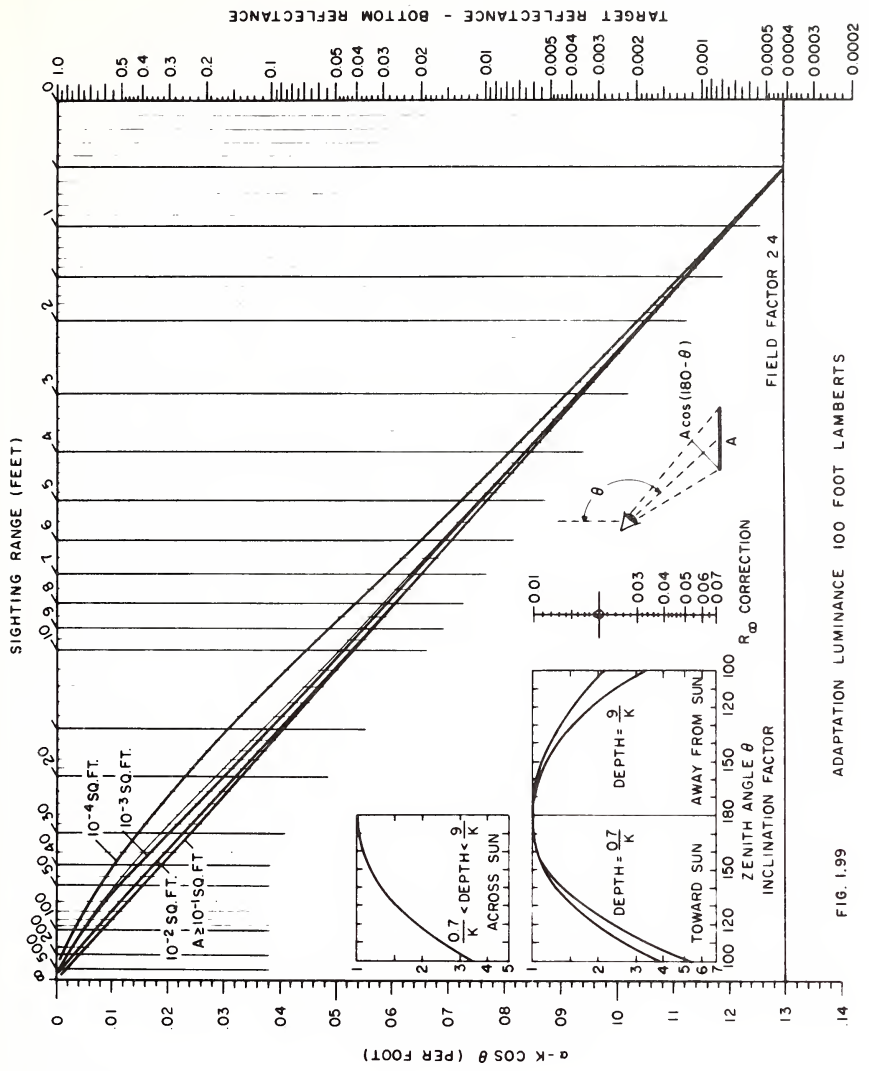
TARGET REFLECTANCE - BOTTOM REFLECTANCE
1.0
0.5
0.4
0.3
0.2
0.1
0.05
0.04
0.03
0.02
0.01
0.005
0.004
0.003
0.002
0.001
0.0005
0.0004
0.0003
0.0002
SIGHTING RANGE (FEET)
a-K COS θ (PER FOOT)
10^{-4} SQ.FT.
10^{-3} SQ.FT.
10^{-2} SQ.FT.
$A \geq 10^{-1}$ SQ.FT
$\frac{0.7}{K}$ < DEPTH < $\frac{9}{K}$
ACROSS SUN
DEPTH = $\frac{0.7}{K}$
DEPTH = $\frac{9}{K}$
TOWARD SUN
AWAY FROM SUN
ZENITH ANGLE θ
INCLINATION FACTOR
$A\cos(180-\theta)$
θ
A
R_∞ CORRECTION
.001
.003
.004
.005
.006
.007
FIELD FACTOR 2.4
ADAPTATION LUMINANCE 100 FOOT LAMBERTS

FIG. 1.99

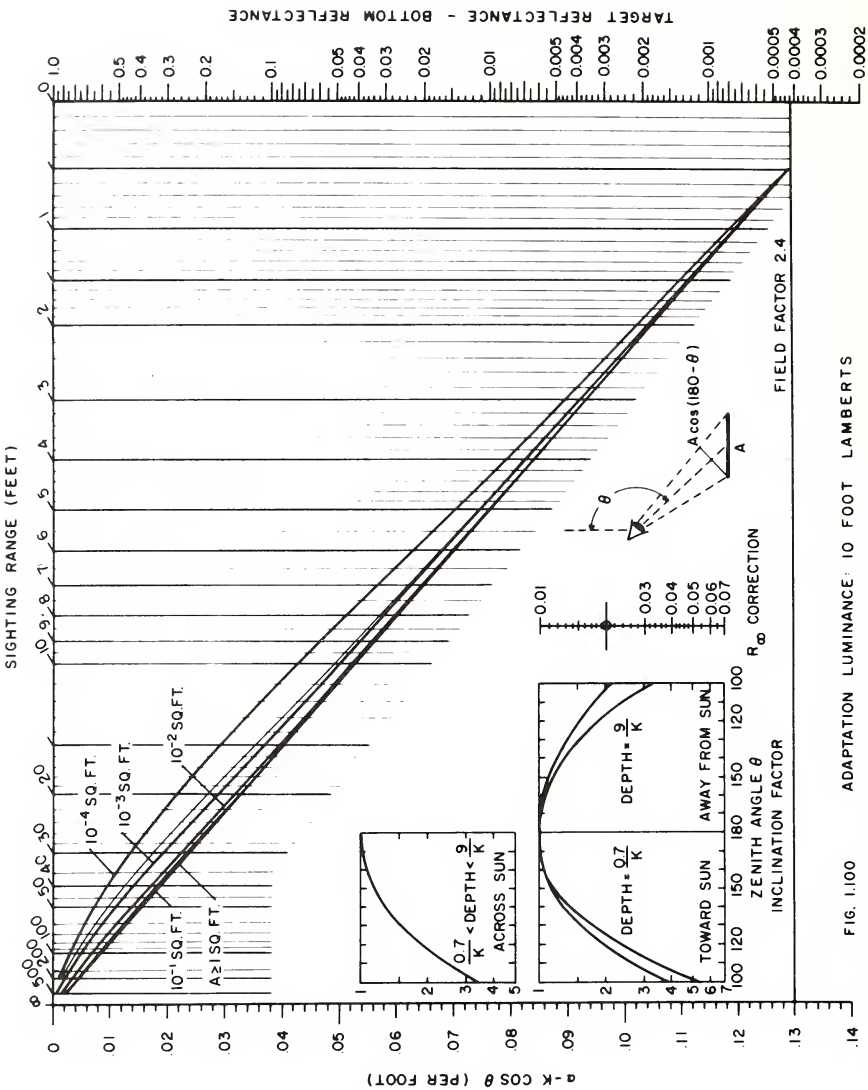
TARGET REFLECTANCE - BOTTOM REFLECTANCE
SIGHTING RANGE (FEET)
α - K COS θ (PER FOOT)
10^{-4} SQ. FT.
10^{-3} SQ. FT.
10^{-2} SQ. FT.
10^{-1} SQ. FT.
A ≥ 1 SQ. FT.
$\frac{0.7}{K}$ < DEPTH < $\frac{9}{K}$
ACROSS SUN
DEPTH = $\frac{0.7}{K}$
TOWARD SUN
DEPTH = $\frac{9}{K}$
AWAY FROM SUN
ZENITH ANGLE θ
INCLINATION FACTOR
R_∞ CORRECTION
A cos (180 - θ)
A
θ
FIELD FACTOR 2.4
ADAPTATION LUMINANCE: 10 FOOT LAMBERTS

FIG. 1.100

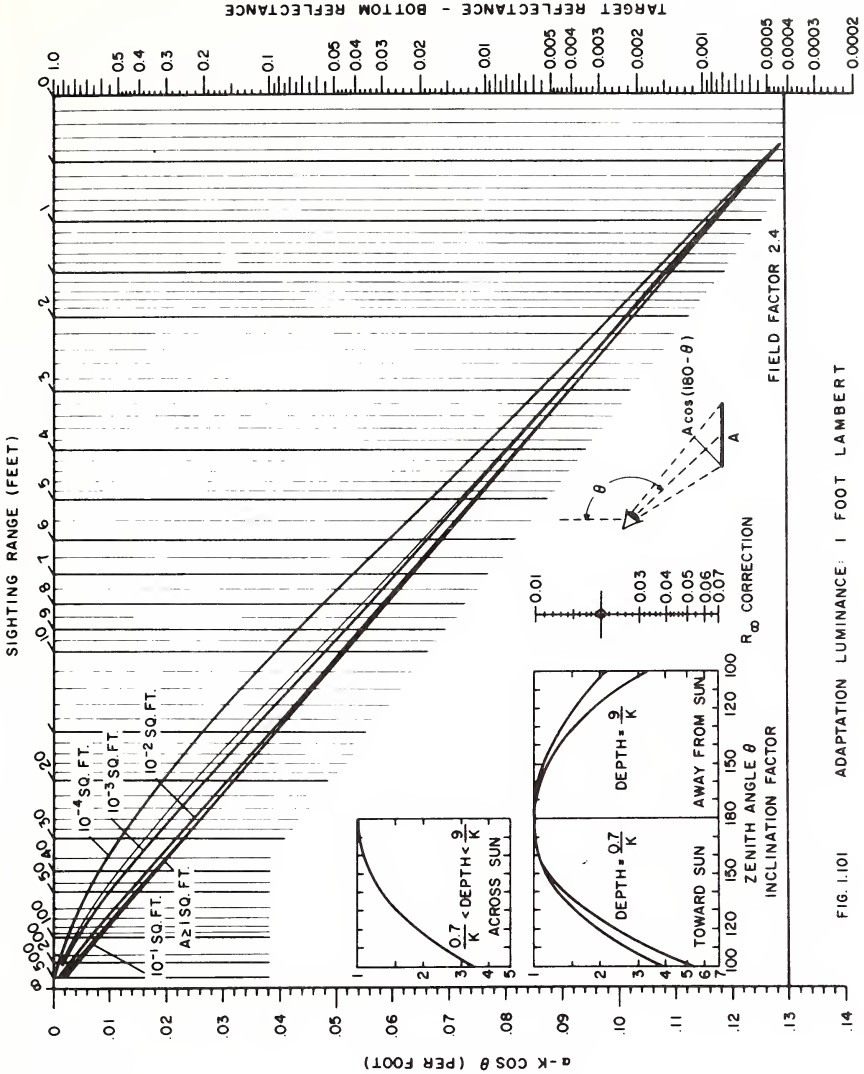

FIG. 1.101 ADAPTATION LUMINANCE: 1 FOOT LAMBERT

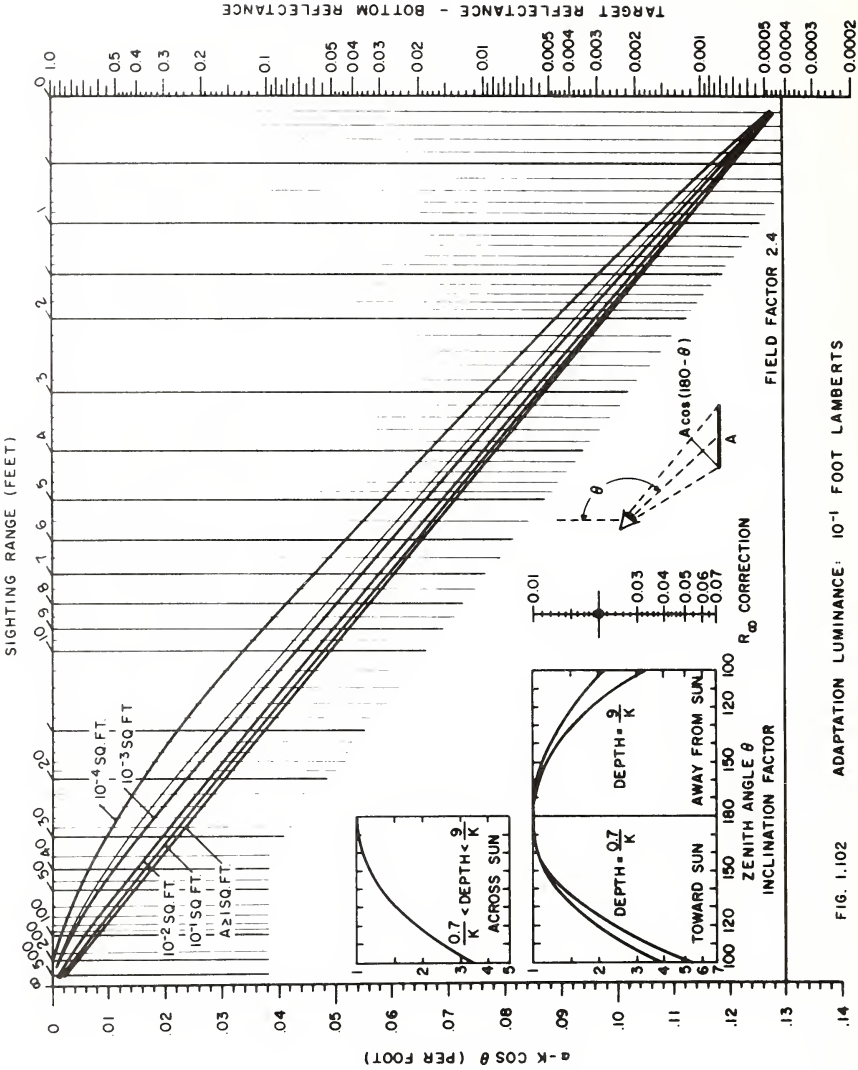
TARGET REFLECTANCE - BOTTOM REFLECTANCE
SIGHTING RANGE (FEET)
α-K COS θ (PER FOOT)
10^{-4} SQ FT
10^{-3} SQ FT
10^{-2} SQ FT
10^{-1} SQ FT
A≥1 SQ FT
$\frac{0.7}{K}$ < DEPTH < $\frac{9}{K}$
ACROSS SUN
DEPTH = $\frac{0.7}{K}$
DEPTH = $\frac{9}{K}$
TOWARD SUN
AWAY FROM SUN
ZENITH ANGLE θ
INCLINATION FACTOR
A cos (180-θ)
R_∞ CORRECTION
FIELD FACTOR 2.4
ADAPTATION LUMINANCE: 10^{-1} FOOT LAMBERTS

FIG. 1.102

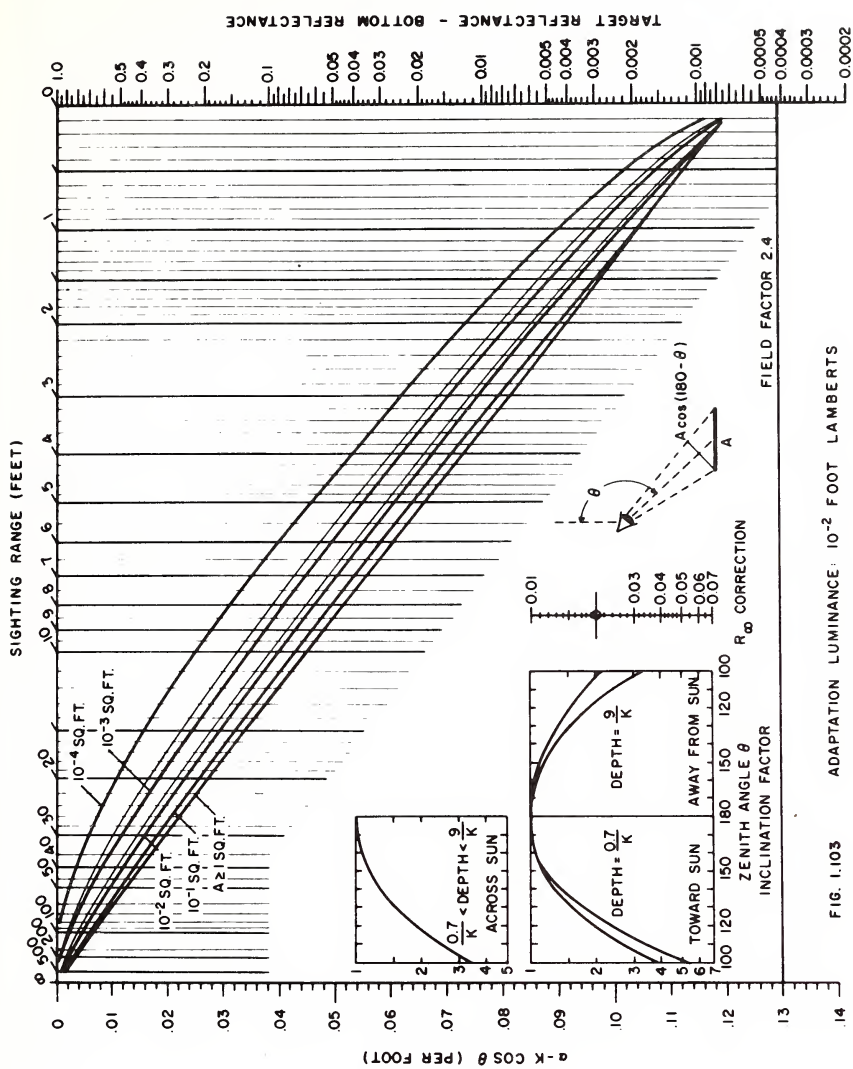

FIG. 1.103 ADAPTATION LUMINANCE: 10^{-2} FOOT LAMBERTS

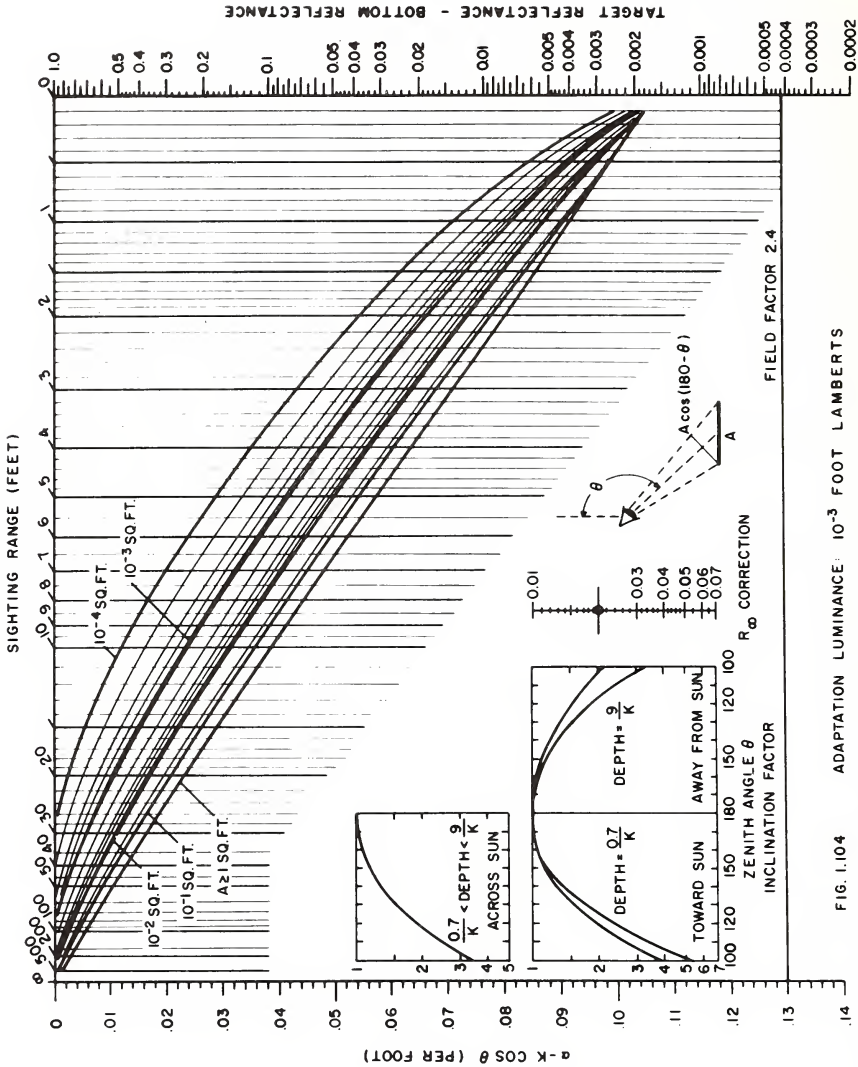

FIG. 1.104 ADAPTATION LUMINANCE: 10^{-3} FOOT LAMBERTS

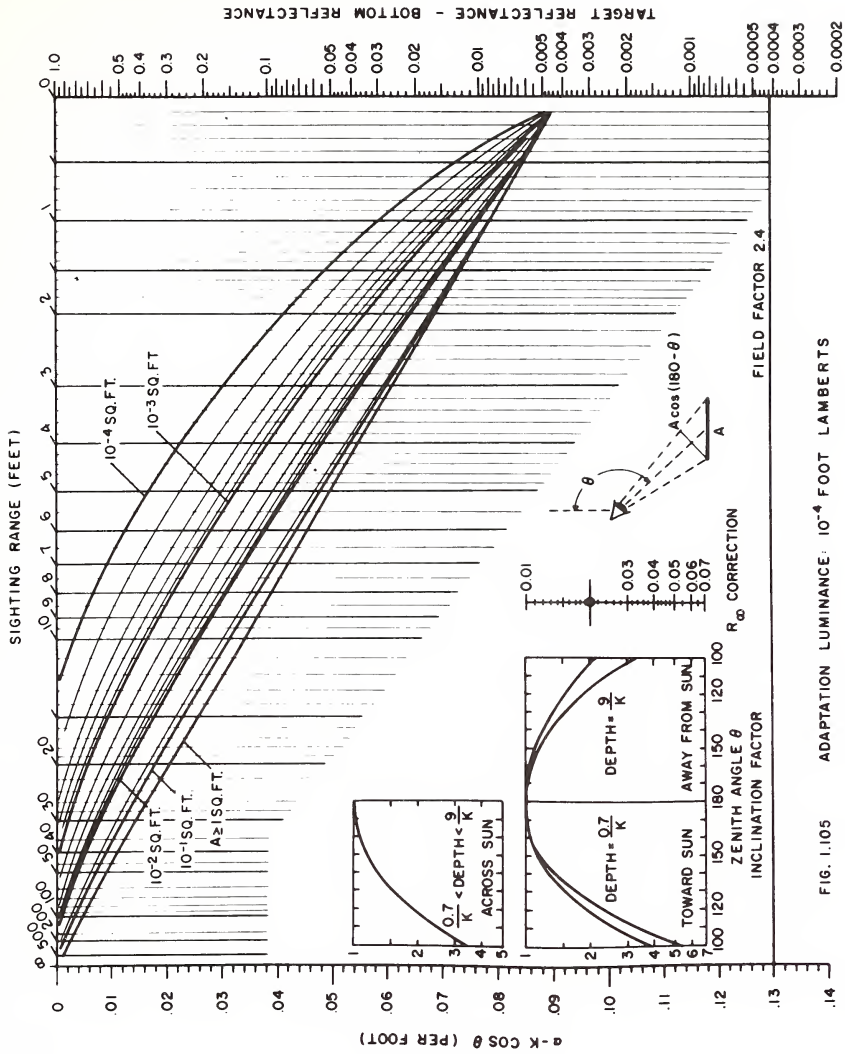

FIG. 1.105 ADAPTATION LUMINANCE: 10^{-4} FOOT LAMBERTS

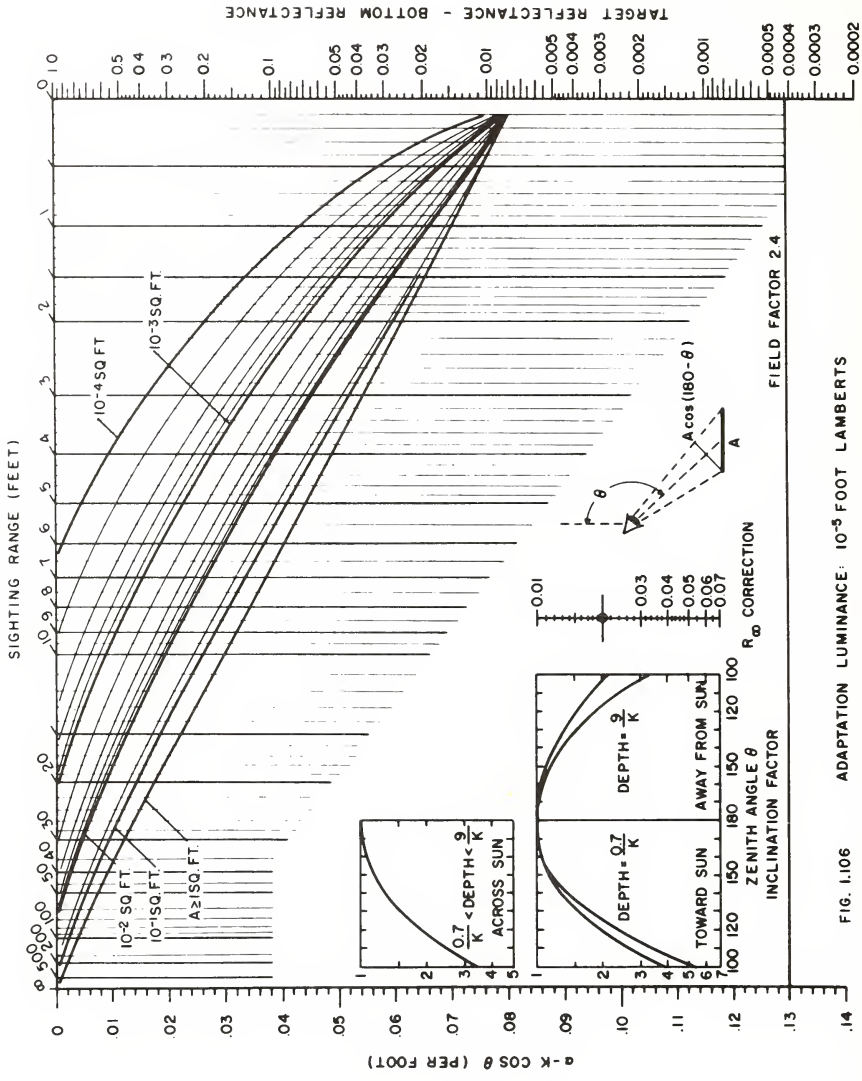

FIG. I.106 ADAPTATION LUMINANCE: 10^{-5} FOOT LAMBERTS

C. Interpretation of Sighting Range

C.1 *Introduction*

The sighting ranges calculated by means of the nomographic visibility charts are the limiting distances at which a swimmer will be aware of seeing the object. It is assumed that he is fully familiar with the underwater environment, well acquainted with the objects for which he looks, and possessed of perfect vision. It is not assumed, however, that his training has included a lengthy special training period devoted to maximizing his ability to produce long sighting ranges.

It is assumed that the swimmer knows the direction in which to look and that he expects to see the visual target. In other words, the swimmer is not required to search his visual field and there is no problem of vigilance.

The above described interpretation of "sighting range" is indicated on the nomographic visibility charts by the inscription "field factor 2.4". This notation, meaningful only to specialists in visibility calculations, implies that nomographic charts can be constructed to depict other levels of observer performance, i.e., other values of "field factor". A general discussion of visual search, field factors, and observer characteristics is out of place in this work, but three common effects will be discussed in simplified form in the following paragraphs.

C.2 *Effect of Lack of Warning*

When an underwater object is encountered by a swimmer without warning, the sighting range will be somewhat shorter than otherwise. This is to say that unexpected objects will be less well detected initially than will those whose existence is known and whose appearance is expected. This effect is independent of training, experience, or visual capability. Its effect upon the sighting range can be allowed for by dividing the value of "target reflectance minus bottom reflectance" by 1.2 before entering the right vertical scale of the nomographic charts.

C.3 *Effect of Observer Training*

Extensive practice in sighting underwater targets at limiting distances will enable good observers to exceed slightly the normal sighting range. A correction for the effect of training can be made by multiplying the value of "target reflectance - bottom reflectance" by a training factor between 1 and 2 before entering the right vertical scale of the nomographic charts. A training factor of 1.0 represents the usual capability of experienced swimmers who are fully familiar with the underwater environment and are well acquainted with the

object for which they look; this value (unity) should ordinarily be used. If an experienced swimmer is considered to be unusually good at underwater sightings a training factor of 1.2 is recommended.* Laboratory experience indicates that only after many thousands of careful attempts to achieve sightings at maximum range can even the most experienced personnel achieve a training factor of 2.

C.4 *Effect of Observer Visual Capability*

All human eyes are not created equal with respect to their capability to detect underwater objects at limiting range; this is not a matter of training but represents subtle physiological differences between men which are beyond detection by ordinary eye-examinations. The nomographic charts have been drawn to represent the performance of average "perfect" young eyes. Some estimate of the effect on sighting range of the spread in visual capability within the population of "perfect" observers can be obtained by successively doubling and halving the value of "target reflectance minus bottom reflectance" before entering the right vertical scale of the nomographic chart.

D. Visualization of Water Clarity

D.1 *Introduction*

The clarity of natural waters can be visualized directly in terms of the attenuation coefficients α and K on the basis of experience gained through the use of the nomographic visibility charts. It will be found that most objects can be sighted at 4 to 5 times the distance $1/(\alpha - K \cos \theta)$ unless the adaptation level is low; exceptions to this rough rule-of-thumb are common but they can easily be categorized. Alternatively, a convenient conceptualization of the appearance of any underwater environment can be obtained from $1/\alpha$ and $1/K$.

D.2 *Estimation of Sighting Range*

The rough rule-of-thumb stated in the preceding paragraph is illustrated by the examples in paragraph B.2 of this section. In the first (clear water) case $1/(\alpha - K \cos \theta) = 1/0.10 = 10$ feet and the vertical sighting range of the large (10 square feet) object is 48 feet, or 4.8 times $1/(\alpha - K \cos \theta)$. In the second (low-clarity water) case $1/(\alpha - K \cos \theta) = 1/0.60 = 1.67$ feet, and the vertical sighting range of the same target is 8.0 feet, or 4.8 times $1/(\alpha - K \cos \theta)$.

---

*It will be recognized that the factor 1/1.2 for lack of warning and the training factor 1.2 cancel; thus the nomographic charts as drawn apply without correction to the case of the experienced, highly trained swimmer who comes upon objects without warning.

The value 4.8 is not universal; it will be altered by changing target size, adaptation luminance, zenith angle, target reflectance, etc. For example, it was noted in paragraph B.2 that in the low-clarity water the vertical sighting range of a small target 10^{-2} square feet in area is 5.5 feet or 3.3 times $1/(\alpha - K \cos \theta)$. If, however, the reflectance of the original 10 square foot visual target had been 0.330 (instead of the value 0.080 assumed in paragraph B.2), thus forming a high inherent contrast with the dark (0.030) bottom, its vertical sighting range is found to be 11.0 feet or 6.6 times $1/(\alpha - K \cos \theta)$. In summary, small values of target size or low values of adaptation luminance (or both) will produce sighting ranges shorter than 4 times $1/(\alpha - K \cos \theta)$ whereas high values of "target reflectance minus bottom reflectance" make large objects visually detectable at ranges in excess of 5 times $1/(\alpha - K \cos \theta)$.

An important and common special case is that of large dark objects viewed horizontally. In this case $1/(\alpha - K \cos \theta) = 1/\alpha$, since $\cos 90° = 0$, and the sighting range will be approximately 4 times $1/\alpha$ unless the adaptation luminance is low.

D.3 *Estimation of Adaptation Luminance*

Inspection of Figure 1.12 will enable convenient order-of-magnitude values of illuminance on the surface of the sea to be noted for, say, noon and sunset, clear and cloudy. Translation of these values to the approximate illuminance at the depth of the swimmer is often facilitated by noting that the illuminance, and, therefore, the adaptation luminance is reduced by a factor of 1/10 for each $(\ln 10)/K$ of depth. Figures 1.82 and 1.83 provide convenient illustrations of this concept.

D.4 *Estimation of* α *and* K

In some, but by no means all, waters the distance $2.3/K$ is about 50% greater than the distance $4/\alpha$; i.e., about $6/\alpha$; thus the natural illuminance (and the adaptation level) may decrease by a factor of 1/10 for each unit of depth equal to 1.5 times the horizontal distance at which a swimmer can see a large dark object at high light levels. If measured values of α and K are not available, these constants can be estimated by means of the relations $\alpha = 4/d$ and $K = 1.5/d$, where d is the horizontal sighting range for large dark objects at high light levels. The estimate of α is more reliable than the estimate of K. Rules of thumb such as these can be given a better basis after more extensive Mode III classifications of natural hydrosols have been made (cf. Sec. 1.7; see also (11)-(13) of Sec. 10.8).

D.5 *Characterization of Natural Waters*

For purposes of easy visualization, it is possible for natural waters to be characterized by the distances $4/\alpha$ and

2.3/K, though the numbers $1/\alpha$, and $1/K$ can do just as well. In the clearest known natural waters* these distances $4/\alpha$ and 2.3/K are believed to be less than 230 feet and 340 feet respectively. In the first numerical example given in paragraph B.2 the distances were found to be $4/\alpha$ = 55 feet and 2.3/K = 85 feet; in the second, $4/\alpha$ = 9.3 feet and 2.3/K = 13.5 feet.

1.10 Applications of Hydrologic Optics to the Food-Chain Problem in the Sea

In this section we shall discuss, from the point of view of radiative transfer theory, the problem of food-chain relations in the ocean. The theory of food-chain relations attempts to describe, in quantitative terms, the distribution in time and space, within a given oceanic region, of the food supply of the main animal populations of that region. The food supply is an essentially self-sustaining collection of biological organisms, inorganic matter, and radiant energy. Aside from radiant energy, the chain consists principally of the following four links: nutrients (e.g., phosphate), phytoplankton, herbivores, and predators. This set of interacting organisms is arranged so that each item in the list constitutes the food of the next item in the list, and in this sense forms a *food-chain* in an oceanic region. This food-chain is initiated and sustained by solar radiant energy penetrating into the sea. The radiant energy sustains the photosynthesis within the phytoplankton and the life processes of the herbivores and predators. Furthermore, the continued decomposition into nutrient material of each of the last three links in the chain also contributes to its maintenance. Thus, any complete theory of food-chain relations in the ocean must take into explicit account, among other things, the role of radiant energy in the food-chain relations. A survey of the present state of the theory (ref. [265]) indicates that the systematic inclusion of radiant energy terms into the food-chain relation has been avoided because of the additional difficulties attendant on such an inclusion in an already complex theory. In the present discussion, it will be shown how the general inclusion of radiant energy terms into the description of the food-chain relations can be carried out in such a way that the attendant increase in the complexity of the theory will not render the result altogether impracticable. Furthermore, it will be shown that the resultant formulations point to some novel, detailed descriptions of the depth distributions of the light field in a region containing the members of the food-chain. By doing so, the main purpose of the discussion will be fulfilled, namely, to round out the classical Volterra prey-predator equations [309] which describe

---

*Probable values: α = 0.017 per foot = 0.056 per meter
K = 0.0067 per foot
= 0.022 per meter at 480 millimicrons

Compare this α with that in Table 1 of Sec. 1.6.

food-chain relations, by including one more equation which specifically--and in a manner uniform with the other equations--incorporates the photons of the light field into the list of interacting members of the the food-chain. The manner in which light particles can generally be considered as "prey" or "predator" will become clear as the discussion proceeds.

The General Exponential Law of Change

The simple differential law:

$$\frac{dA}{dt} = KA \tag{1}$$

has been found to describe a wide variety of natural phenomena, among which are: growth of yeast cultures and bacterial cultures, decay of radioactive substances, growth and decay of animal populations, damped or resonating oscillations of mechanical and electrical systems, and the darkening of light fields with depth in scattering-absorbing media, to name a few. Up until now we have been concerned in this work principally with the latter use of the exponential law. As we shall see in the latter stages of this discussion, we may very well view (1), under suitable interpretations, as the alpha and the omega--that is, the beginning and the end--of the general theory of the food-chain relations. However, for the present, we view (1) as the ostensibly simple equation it appears to be, with constant coefficient K, and thereby obtain the general solution of (1) in the form:

$$A(t) = A(0)e^{Kt} \tag{2}$$

where A(t) is the amount at time t of the entity under consideration. When K is positive, then there is growth of A(t); when K is negative, there is decay of A(t), as time t increases.

The description of natural growth and decay processes summarized in (1) and (2) is known as the *exponential law* and pertains as it stands basically to isolated and relatively simple systems. When the systems are no longer isolated or no longer simple in internal structure, then (1) is replaced by a correspondingly modified equation. For example, by removing the isolation restriction, two new features appear: a source term A_η may be added to the right side of (1); and the possibility arises of a non-constant growth rate term K. From the present point of view, the inclusion of a source term A_η presents no essential modification of the equation (1), and so will not be studied in this discussion. However, the practical and theoretical possibilities inherent in a non-constant growth rate term K are endless, and some of them hold the key to the solution of the general problem of the food-chain relation; some of these possibilities will now be considered.

The Volterra Prey-Predator Equations

A theory of food-chains can be made to rest in the classical equations postulated by Volterra [309] which govern the evolution in time of the number P of prey and number A of predators feeding on the prey. Thus, for example, if P is the number of plants and A the number of animals in a symbiotic relation, then their evolution in time may be governed by general equations of the form:

$$\frac{dP}{dt} = K_P P \tag{3}$$

$$\frac{dA}{dt} = K_A A \tag{4}$$

where we have written

$$"K_P" \quad \text{for} \quad p\text{-}bA \tag{5}$$

and

$$"K_A" \quad \text{for} \quad cP\text{-}a \quad . \tag{6}$$

That is, the growth rate term K_P for the prey is the sum of the intrinsic growth rate p for the prey population and the interaction decay term -bA, where b is a coupling constant between the populations of A and P. Similarly a is the coefficient of decay of the predator population, and c is the coupling constant between A and P in this instance. The coupling constants b and c are usually taken as equal or as connected by some given relation.

Now each equation (3), (4) is of the general type as (1) and, assuming K_P and K_A known as functions of time along with the initial values P(0) and A(0) of P and A, are directly integrable:

$$A(t) = A(0) \exp\left\{\int_0^t K_A(t')\, dt'\right\}$$

$$P(t) = P(0) \exp\left\{\int_0^t K_P(t')\, dt'\right\}$$

However, equations (3) and (4) are generally coupled (i.e., $b \neq 0$ and $c \neq 0$) so that the preceding solutions, while formally correct, are of no immediate practical use, since knowledge of K_P and K_A is tantamount to knowledge of P and A themselves.

The equations (3) and (4), despite their analytically unpleasant nonlinear coupling, form a workable starting point in the quantitative description of the food-chain relation.

It is clear, however, that the equations as they stand describe only the herbivore and predator components of the chain and so cannot adequately describe the complete food-chain relation as defined above. The other members of the chain, namely the phytoplankton and the nutrients (which also constitute a prey-predator pair), along with the radiant energy, are excluded from (3), (4).

The General Food-Chain Equations

We turn now to a formulation of the Volterra-type prey-predator equations which goes beyond that of (3), (4) and which takes into account the interactions of all five members of the food-chain relation. To keep the geometric and physical variables down to a comfortable minimum at the outset, we shall assume that all quantities of the chain depend on depth and time only, over the oceanic region of interest. Thus let:

- $U(z,t)$ be the radiant density (radiant energy per unit volume) at depth z, time t
- $P(z,t)$ be the number of *phytoplankton* per unit volume at depth z, time t
- $B(z,t)$ be the number of *herbivores* per unit volume at depth z, time t
- $C(z,t)$ be the number of *carnivores* per unit volume at depth z, time t
- $N(z,t)$ be the amount of *nutrient* per unit volume at depth z, time t

We postulate a food-chain ordering among the members of the food-chain, and which is schematically summarized below:

	C	B	P	N	U
C	0	+	+	±	+
B	-	0	+	±	+
P	-	-	0	±	+
N	±	±	±	0	±
U	-	-	-	-	0

(7)

This ordering is to be interpreted as follows: consider the carnivore row. Carnivores in the present hierarchy are understood to grow at the expense of most other members of the chain (hence the + signs in the row). Herbivores, on the other hand, grow at the expense of phytoplankton, nutrients and radiant energy (hence + signs) but are preyed upon by carnivores (hence - sign). The zero entries indicate that in the present model, members of the chain do not increase or decrease at the expense of their own numbers. (In mathematical

terms the food-chain ordering relation in (7) is an irreflexive, asymmetric, transitive relation.) The double signs (±) in the nutrient row indicate that at times, N may increase(+) in the direct presence of the other members and at other times may decrease (-) in the direct presence of the other members.

The food-chain ordering associated with each pair of the food-chain is given a quantitative measure by assigning interaction functions to each pair of members of the chain. Thus to the pair (C,B) we assign a function K_{CB} which on the basis of the food-chain ordering relation tabulated above, is positive for all z and t. Similarly to (C,P) we assign the interaction function K_{CP} which is also positive-valued. Continuing in this way we assign to the pair (U,N) the function K_{UN} which is negative-valued for all z,t. The functions K_{CC}, K_{BB}, etc. are all zero-valued, and K_{NC} may be positive, zero or negative-valued for various z, and t.

Once a food-chain ordering has been established and the 20 non zero interaction functions have been assigned, the Volterra interaction equations can be written down:

$$\left.\begin{aligned} \frac{dC}{dt} &= K_C C \\ \frac{dB}{dt} &= K_B B \\ \frac{dP}{dt} &= K_P P \\ \frac{dN}{dt} &= K_N N \\ \frac{dU}{dt} &= K_U U \end{aligned}\right\} \qquad (8)$$

where we have written

$$\left.\begin{aligned} \text{"}K_C\text{"} \quad &\text{for} \quad k_C + K_{CB}B + K_{CP}P + K_{CN}N + K_{CU}U \\ \text{"}K_B\text{"} \quad &\text{for} \quad k_B + K_{BC}C + K_{BP}P + K_{BN}N + K_{BU}U \\ \text{"}K_P\text{"} \quad &\text{for} \quad k_P + K_{PC}C + K_{PB}B + K_{PN}N + K_{PU}U \\ \text{"}K_N\text{"} \quad &\text{for} \quad k_N + K_{NC}C + K_{NB}B + K_{NP}P + K_{NU}U \\ \text{"}K_U\text{"} \quad &\text{for} \quad k_U + K_{UC}C + K_{UB}B + K_{UP}P + K_{UN}N \end{aligned}\right\} \qquad (9)$$

The five functions k_C, ..., k_U are inherent growth-decay rates, which are operative independently of the presence of other members of the chain. Furthermore, the differentiation operator d/dt in (8) is a total derivative operator, i.e., we have written

$$\text{"d/dt"} \quad \text{for} \quad \partial/\partial t + v(\partial/\partial z) \tag{10}$$

where in each case v is an averaged speed of propagation in the z direction. In the case of U it is the speed of light. In the case of C and B, it is variable with time and space according to the vertical movements of the animals. In the case of P and N, v represents rate of rising and sinking, plus eddy diffusion rates. The theoretical basis for the equation governing U in (8) which is one of the novel features of (8), rests in the general theory of K-functions for directly observable radiometric quantities as developed in Chapter 9 below. For practical purposes, one may, however, use (7) of Sec. 1.4 with each side divided by v (recall (5) of Sec. 1.1).

Once the interaction functions are known and the initial states C(z,0), K(z,0),...,U(z,0) are known over all depths z in the region of interest, the system (8) is in principle solvable by iteration techniques. Thus, for example, by writing

$$\text{"A"} \quad \text{for} \quad (C, B, P, N, U) \tag{11}$$

and

$$\text{"K"} \quad \text{for} \quad \begin{bmatrix} K_C & & & 0 \\ & K_B & & \\ & & \ddots & \\ 0 & & & K_U \end{bmatrix} \tag{12}$$

The system (8) becomes transformed into the vector equation:

$$\boxed{\frac{dA}{dt} = A\,K} \tag{13}$$

which may be solved by any of several modern iteration techniques (see, e.g., [23]) using large scale computers. It is therefore no longer necessary to limit the generality of a food-chain theory because of the possible intractability of the analytic solution procedure (e.g., the impossibility of obtaining closed forms for the integrations).

An Illustration of the Food-Chain Theory with A Radiant Energy Term

As a simple illustration of the general theory outlined above, let us consider a three-member food-chain consisting of phytoplankton, herbivores, and radiant energy. Hence we will study the effect of adding to the classical prey-predator equations (3), (4), another equation which specifically includes

radiant energy in the prey-predator interactions. The following discussion is actually independent of the number of members in the food-chain, so that a reader following the general line of argument developed below may extend the arguments and their results to arbitrarily large food-chains.

The General Three-Term Equations

The requisite equations for the present illustration are:

$$\frac{dU}{dt} = (k_U + K_{UB}B + K_{UP}P)U \quad \text{(photons)} \tag{14}$$

$$\frac{dB}{dt} = (k_B + K_{BP}P + K_{BU}U)B \quad \text{(herbivores)} \tag{15}$$

$$\frac{dP}{dt} = (k_P + K_{PB}B + K_{PU}U)P \quad \text{(phytoplankton)} \tag{16}$$

The Quasi-Steady State Equations

We shall be interested for the present in a *quasi-steady state solution of the preceding system* of equations. By 'quasi-steady state' we mean that the time rates of change of the magnitudes of P and B are negligible compared to that of U, so that the light field U adjusts to and settles down to steady state almost instantly in accordance to the prevailing spatial distributions of P and B at time t. Therefore, in (14) we may drop the time derivative and consider only change of U in depth for fixed t and adjust the definitions of the K-functions to absorb the speed constant v; and in (15) and (16) we may drop the spatial derivatives, and consider only the change of B and P in time for a fixed depth z:

$$\frac{dU}{dz} = (k_U + K_{UB}B + K_{UP}P)U \tag{17}$$

$$\frac{\partial B}{\partial t} = (k_B + K_{BP}P + K_{BU}U)B \tag{18}$$

$$\frac{\partial P}{\partial t} = (k_P + K_{PB}B + K_{PU}U)P \tag{19}$$

This set of equations like the general equations, is readily solvable in principle for given arbitrary constants k_U, K_{UB}, etc., and initial conditions. The steady state spatial distributions of U, P, B are of especial interest, and we shall devote the remainder of this section to the study of these distributions.

The Equilibrium Solutions

When $\partial B/\partial t = 0$ for every z at a given time t, the existing spatial distribution of B is called the *equilibrium population* and denoted by "B_q"; similarly for P. The equilibrium populations of P or B are readily characterized in terms of the spatial distribution of the radiant energy. Thus from (18) we have:

$$\frac{\partial B_q}{\partial t} = 0$$

which implies

$$k_B + K_{BP}P_q + K_{BU}U = 0$$

so that

$$\boxed{P_q = -(k_B + K_{BU}U)/K_{BP}} \tag{20}$$

Similarly from (19), for steady state:

$$\frac{\partial P_q}{\partial t} = 0$$

so that

$$k_P + K_{PB}B_q + K_{PU}U = 0$$

whence

$$\boxed{B_q = -(k_P + K_{PU}U)/K_{PB}} \tag{21}$$

Equations (20) and (21) show that if the steady state radiant energy distribution U is known, the equilibrium P and B distributions are determinable over the range of depths of interest.

We now show that the relations (20) and (21) together with (17) uniquely determine the steady state radiant energy distribution through the medium so that P_q and B_q are uniquely determinable, in turn. Substituting P_q and B_q as given by (20) and (21) into (17), and rearranging, we have:

$$\frac{dU}{dz} = \left\{k_U - \frac{K_{UB}}{K_{PB}}\left(k_P + K_{PU}U\right) - \frac{K_{UP}}{K_{BP}}\left(k_B + K_{BU}U\right)\right\}U$$

That is:

$$\boxed{\frac{dU}{dz} = aU + bU^2} \tag{22}$$

where we have written:

$$\text{"a"} \quad \text{for} \quad k_U - \left(k_P \frac{K_{UB}}{K_{PB}} + k_B \frac{K_{UP}}{K_{BP}} \right) \tag{23}$$

and

$$\text{"b"} \quad \text{for} \quad -\left(\frac{K_{UB}K_{PU}}{K_{PB}} + \frac{K_{UP}K_{BU}}{K_{BP}} \right) \tag{24}$$

If "U(0)" denotes the initial value of U at some fiducial depth (here z = 0), then (22) resolves into:

$$U(z) = \frac{aU(0)e^{az}}{-bU(0)e^{az} + [bU(0) + a]} \tag{25}$$

This solution may now be used in (20) and (21) to obtain detailed descriptions of the depth distribution of the steady state populations of P and B. The solution (25) exhibits some interesting mathematical properties for various choices of a and b. For b = 0, we have simple exponential growth (a > 0) or decay (a < 0). For a = 0, by a limiting argument, we have

$$U(z) = \frac{U(0)}{1-bU(0)z} \quad .$$

Some General Properties of Equilibrium Solutions

The equilibrium solutions found above have several interesting practical properties, one of which we isolate for particular attention here. This is the property of predicting a possible band of depths below the ocean surface outside of which the P and B populations cannot exist. To find the limits of this band of depths, we return to equations (20) and (21) and require that $P_q \geq 0$ and $B_q \geq 0$. These conditions merely state that real distributions of phytoplankton and herbivores must not have negative populations. The non negativity condition applied to (20) yields:

$$-(k_B + K_{BU}U)/K_{BP} \geq 0$$

From the interaction table (7) we find that $K_{BP} \geq 0$, so that

$$k_B + K_{BU}U \leq 0$$

whence

$$U \leq -k_B/K_{BU}$$

Similarly, from (21) with the help of the nonnegativity condition we find:

$$U \geq -k_P / K_{PU}$$

Hence a necessary condition for the existence of steady state P and B equilibrium distributions at depth z is that

$$\boxed{-k_P/K_{PU} \leq U(z) \leq -k_B/K_{BU}} \qquad (26)$$

It is to be noted that (26) are *necessary* conditions (i.e., *if* a band exists, *then* it must be such that (26) holds) and not sufficient conditions, except insofar as the steps can be retraced from (26) to (20) and (21). This can be done if K_{PB} and K_{BP} are strictly negative and strictly positive, respectively, and if the left side of (26) is indeed less than the right side.

Now according to (25), U(z) is under certain conditions a decreasing function of z (for negative a). Thus if U(0) is greater than $-k_B/K_{BU}$, then (26) shows that no steady state population should exist for depths $z = 0$ down to where $U(z) = -k_B/K_{BU}$. Then there is expected a band of depths within which $P > 0$ and $B > 0$. Since U(z) decreases monotonically, there will be depths below which the left side of (26) no longer holds, so that $P = 0$ and $B = 0$ in those depths. It appears then that the present model can in principle predict a euphotic zone in natural hydrosols in which the food-chain is in a quasi-steady state condition.

We have reached the main goal of the discussion, namely to supplement the classical Volterra prey-predator equations with a third equation governing the flow of radiant energy in the sea, and to briefly explore the consequences of the interactions of the prey-predator-photon system.

1.11 Future Problems of Hydrologic Optics

The present introductory chapter to hydrologic optics is brought to a close with a small, carefully selected list of important problems which are as yet only partially resolved. The list is deliberately kept small so as not to overwhelm prospective students of the subject with a mass of more or less obvious types of applicational problems they soon would encounter in their own fashion as their studies proceed. Rather, we have selected for presentation and discussion here three archetype problems which, if eventually satisfactorily resolved, would elevate the discipline of hydrologic optics to the level of a mature science which could predict and describe, in the fullest sense of these terms, all aspects of the transfer of radiant energy in the seas, lakes and other natural hydrosols of the world.

Problem One: To Establish Theoretically the Physical Basis of the Inherent Optical Properties of Natural Hydrosols

The two main inherent optical properties α, σ, of the hydrosols, and of optical media in general defined in Sec. 1.6, together with the equation of transfer ((10) or (12) of Sec. 1.3) form the core of modern radiative transfer theory. This theory is by definition (i.e., by actual considered choice) predominantly phenomenological in outlook, and accordingly the optical properties α, σ are left unspecified in the general theory. The theory thus contains no formalism which predicts the values of α and σ in a given medium *in terms of the inherent physical structure of that medium.* It is important to understand the significance of this observation. It does *not* maintain that the theory of radiative transfer is incapable of providing procedures to measure α and σ in natural optical media. The operational procedures in Sec. 1.6 and in Chapter 13 below supply abundant methods for arriving at α and σ in given media. Rather, what is intended is the observation that *the connections between α and σ and the electromagnetic structure, and more basically, the molecular structure of these media is beyond the ken of the principles of the theory.* The purpose of Problem One is to establish *theoretical* connections between α and σ and the physical properties of an hydrosol--i.e., the properties of a given solution or suspension (or both) of substances in H_2O. One such connection is possible on the electromagnetic level wherein α and σ could be related *theoretically* to the permittivity, permeability, and conductivity functions of the hydrosol. Such connections have received initial attention in Chapters XIV and XVI of Ref. [251], and the results there suggest further directions in which to pursue this problem. Observe that the approach in [251] is not the approach of the Mie theory of scattering, since the latter applies only to single scatterers. The suggested approach attempts to obtain a basis for σ as actually measured *in situ.* The motivation for Problem One is quite clear: if this problem is solved, it may someday be possible to predict, by calculation, the α and σ of an hydrosol, given its physical analysis; and conversely, from a spectral radiometric analysis of α and σ, to determine the physical components of the hydrosol. It may then also be possible to resolve once and for all the quantitative and conceptual problems of the nature of forward scattered light for very small and very large angles of scatter (see Sec. 1.6, in particular Fig. 1.72; Sec. 18 of Ref. [251], and [78]) and also to provide a rational basis for such interesting findings as displayed in Table 4 and Fig. 1.73 of Sec. 1.6, of the uniformity of shape of σ. Furthermore, by solving Problem One, we may also resolve such questions as the existence of spectral windows in the sea which even though seemingly settled on an empirical level (cf., Sec. 1.6) will continually nag at the analytically inclined individual who would prefer such an important question to be resolved in a way which rests on necessary inferences drawn from established physical principles;

principles which are, incidentally, on a more fundamental level than those on which radiative transfer theory is made to rest. Still further, the problem of the structure of σ in the polarized context (using the matrix $\mathbf{p}$) may be solved (see Sec. 13.11). Last, but not least, the resolution of the present problem will securely anchor the discipline of hydrologic optics, and radiative transfer in general, to the mathematical and physical bedrock of the mainland of modern physics.

Problem Two: To Establish Complete Empirical Classifications of Natural Hydrosols

The discussion of this problem was essentially presented in Sec. 1.7, and so need not be repeated here. It should perhaps be emphasized that this problem is unquestionably the single most important problem facing experimenters in the field of hydrologic optics. A moment's reflection will show the experimenter (who is for example bent on the problem of the connections between the ideal photosynthesis in a region and the measurement of radiant energy in that region) that this problem is essentially one of classification of an optical medium in either of the three main modes (Modes I, II, III) described in Sec. 1.7. Or again, a scientist concerned with the problem of underwater optical communication or visibility will benefit from complete empirical classifications of the media of interest. Even theoreticians, on descending from their ivory towers after making some inroads into Problem One above, will require corroboration of the kind that only a truly exhaustive solution of the present problem can supply.

Perhaps we can put the nature of the present problem into perspective by enjoining the prospective experimenter on what *not* to do if his work is to contribute to the solution of Problem Two and is to be of lasting worth and importance to the discipline of hydrologic optics:

(i) Do not omit to mention the spectral range and accuracy of your determinations of the optical properties.

(ii) Avoid broad-band measurements whenever narrow-band measurements are possible, even if considerably more effort is entailed for the latter.

(iii) Do not measure α alone or σ alone; measure them together (Mode IA), over at least the visible spectrum.

Alternatively:

(iv) Do not measure α alone or K alone; measure them together (Mode III), over at least the visible spectrum.

Alternatively:

(v) Do not measure $H(z,-)$ alone or $h(z)$ alone; measure all four irradiances: $H(z,\pm)$ and $h(z,\pm)$ together (Mode II), or preferably $N(z,\cdot)$ (Mode IB), over at least the visible spectrum.

Of course with these *don'ts* go important positive observances of the usual kind, especially for alternatives (iv) and (v): recording of lighting conditions above the air-water surface, the state of the air-water surface, the proximity and state of the bottom, the state of polarization, and so on.

Problem Three: To Establish A Unified Automatic Computation Program for Prediction Computations and Data Reduction Computations in Geophysical Optics (the GEOVAC)

The theory of radiative transfer is now well founded with many excellent means of solution of the equations of the theory, as explained at length at appropriate points throughout the remainder of this work, or in Ref. [251], and in other works on the subject. In need at present are workable *computer programs* which will take α and σ and boundary lighting conditions (either unpolarized or polarized) and yield internal radiance distributions throughout the medium of interest, regardless of its shape and size. In other words we envision a hardware realization of the Mode IA classification of natural optical media. Conversely, the computation programs should be able to convert experimental documentations of the (unpolarized or polarized) radiance distributions (or at least irradiance quartets), as a function of wavelength and depth, into the appropriate determination of the inherent and apparent optical properties of the medium. In this way we can also achieve a hardware realization of the Mode IB (or, respectively, the Mode II) classification of natural optical media. The applications of such a program-complex to the problems cited in the opening remarks of Sec. 1.0 are manifold, and many uses of such a program are undoubtedly yet to be conceived. The geophysical optics automatic variable computer--the'GEOVAC'--program envisioned above will serve to tie together efforts on both Problems One and Two above, as well as help solve the everyday problems arising in the engineering applications of meteorologic and hydrologic optics.

1.12 Bibliographic Notes for Chapter 1

In addition to the mention of various references given at the appropriate points in the discussions of this chapter, the following references are noted for especial attention, as they form a relatively immediate point of entry into the domain of hydrologic optics, either directly or via their references. First there is the survey article of light in the sea by Duntley [78] which covers the gist of the hydrologic optics work of the Visibility Laboratory of the University of California over the twenty year period 1944-1964. Contemporary and earlier work in hydrologic optics by other organizations and individuals is surveyed in the annotated bibliography on transmission of light in water by Du Pré and Dawson [84]. This bibliography covers approximately 650 abstracts

by over 400 authors in more than 150 European and American journals, extending over the period from 1818 to 1959. Two symposia on radiant energy in the sea resulted in published papers relevant to hydrologic optics: the Helsinki meeting of I.U.G.G. in August 1960 is summarized in [124]; and papers presented at the Hawaiian meeting of the tenth Pacific Science Congress are in [303]. Reference [109] contains a summary of a small amount of theory and a relatively larger amount of practical experimental results along with descriptions of instrumentation used in hydrologic optics. Reference [109], accordingly, is a useful supplement to the present work. The paper and recent book by Jerlov [125] also surveys recent developments in the field. Of some historical interest in the developmental aspects of the field of hydrologic optics are Chapters I-IV of [82] which are the synthesis of the experimental work by Duntley and the early theoretical work of the author. The roots of this chapter trace back in part to some early studies presented in [210]. The basis of the subsequent chapters of this work are given in the bibliographic notes appended to each chapter.

The numbering of the bibliography items in this volume and succeeding volumes follows that of the master bibliography given in the final volume (VI) of the present work.

BIBLIOGRAPHY FOR VOLUME I

6. Atkins, W.R.G. and Poole, H.H., "The angular scattering of blue, green and red light by sea water," Sci. Proc. Roy. Dublin Soc. *26*, 313 (1954).

7. Austin, R.W., *Water Clarity Meter, Operating and Maintenance Instructions,* (Scripps Inst. of Ocean. Ref. 59-9, University of California, San Diego, 1959).

12. Beebe, W., *Beneath Tropic Seas* (Blue Ribbon Books, New York, 1928).

23. Birkhoff, G., and Rota, G., *Ordinary Differential Equations* (Ginn and Co., New York, 1962).

35. Brown, D.R.E., *Natural Illumination Charts* (Report No. 374-1, Proj. NS 714-100, Bureau of Ships, Dept. of the Navy, September 1952).

36. Burton, H.E., "The optics of Euclid," J. Opt. Soc. Am. *35*, 357 (1945).

50. Committee on Colorimetry (Optical Society of America), *The Science of Color* (Thomas Y. Crowell Co., New York, 1953).

56. Cox, C., and Munk, W., "Measurement of the roughness of the sea surface from photographs of the sun's glitter," J. Opt. Soc. Am. *44*, 838 (1954).

58. Cox, C., and Munk, W., "Some problems in optical oceanography," J. Mar. Res. *14*, 63 (1955).

63. Dawson, L.H., and Hulburt, E.O., "Angular distribution of light scattered in liquids," J. Opt. Soc. Am. *31*, 554 (1941).

68. Drummeter, L.F., and Knestrick, G.L., *A High Resolution Investigation of the Relative Spectral Attenuation Coefficients of Water--Part I: Preliminary* (Report 5642, U.S. Naval Research Laboratory, May 24, 1961).

74. Duntley, S.Q., *Examples of Water Clarity, I, II* (Visibility Laboratory, Univ. of California, San Diego, Report 3-7, Task 3, Contract NObs-72039 Bureau of Ships, May 1959; and Report 5-7, Task 5, same contract, June 1960).

75. Duntley, S.Q., *Improved Nomographs for Calculating Visibility by Swimmers (Natural Light)* (Visibility Laboratory, Univ. of California, San Diego, Report 5-3, Task 5, Contract NObs-72039, Bureau of Ships, Feb-

76. Duntley, S.Q., *Measurements of the Transmission of Light from an Underwater Point Source* (Visibility Laboratory, Univ. of California, San Diego, Report 5-11, Task 5, Contract NObs-72039, Bureau of Ships, October 1960).

77. Duntley, S.Q., *Measurements of the Transmission of Light from an Underwater Source Having Variable Beam-Spread* (Scripps Inst. of Ocean. Ref. 60-57, Univ. of California, San Diego, 1960).

78. Duntley, S.Q., "Light in the Sea", J. Opt. Soc. Am. *53*, 214 (1963).

79. Duntley, S.Q., *Underwater Communication by Scattered Light* (Visibility Laboratory, Univ. of California, San Diego, Report 5-12, Task 5 (Final Report), Contract NObs-72039, Bureau of Ships, September 1963).

81. Duntley, S.Q., Culver, W.H., Richey, F., and Preisendorfer, R.W., "Reduction of contrast by atmospheric boil," J. Opt. Soc. Am. *53*, 351 (1963).

82. Duntley, S.Q., and Preisendorfer, R.W., *The Visibility of Submerged Objects* (Final Report N5ori-07864, Visibility Laboratory, Massachusetts Institute of Technology, 31 August 1952).

83. Duntley, S.Q., Tyler, J.E., and Taylor, J.H., *Field Test of a System for Predicting Visibility by Swimmers from Measurements of the Clarity of Natural Waters* (Scripps Inst. of Ocean. Ref. 59-39, Univ. of California, San Diego, 1959).

84. DuPré, E.F., and Dawson, L.H., *Transmission of Light in Water: An Annotated Bibliography* (U.S. Naval Research Laboratory, Bibliography No. 20, April,1961).

96. Gates, D.M., *Energy Exchange in the Biosphere* (Harper and Row, New York, 1962).

109. Hill, M.N., ed., *The Sea* (Interscience Pub., New York, 1962), vol. I, Physical Oceanography.

113. Hulburt, E.O., "The polarization of light at sea," J. Opt. Soc. Am. *24*, 35 (1934).

115. Hulburt, E.O., "Optics of distilled and natural water," J. Opt. Soc. Am. *35*, 698 (1945).

117. Ivanoff, A., and Waterman, T.H., "Elliptical polarization of submarine illumination," J. Mar. Res. *16*, 255 (1958).

118. Ivanoff, A., and Waterman, T.H., "Factors, mainly depth and wavelength, affecting the degree of underwater polarization," J. Mar. Res. *16*, 283 (1958).

122. Jerlov, N.G., "Optical studies of ocean water, " Reports of the Swedish Deep-Sea Expedition *3*, 1 (1951).

123. Jerlov, N.G., "Optical measurements in the eastern North Atlantic," Discovery II exp. of August and September 1959, Medd. Oceanogr. Inst. Göteborg *30*, 1 (1961).

124. Jerlov, N.G., ed., *Symposium on Radiant Energy in the Sea*, International Union of Geodesy and Geophysics, Helsinki Meeting, August 1960 (L'Institute Géographique National, Monograph No. 10, Paris, 1961).

125. Jerlov, N.G., "Optical oceanography," Oceanogr. Mar. Biol. Ann. Rev. *1*, 89 (1963). See also: *Optical Oceanography* (Elsevier Publishing Co., N.Y., 1968).

126. Jerlov, N.G., "Factors influencing the colour of the oceans," in *Studies on Oceanography* (1964), p. 260.

127. Jerlov, N.G., "Optical classification of ocean water," in *Physical Aspects of Light in the Sea* (Univ. of Hawaii Press, 1964), J.E. Tyler, ed.

128. Johnson, F.S., "The solar constant," J. Met. *11*, 431 (1954).

132. Kalle, K., "What do we know about the 'Gelbstoff'?," *Symposium on Radiant Energy in the Sea*, International Union of Geodesy and Geophysics, Helsinki Meeting, August 1960 (L'Institute Géographique National, Monograph No. 10, Paris, 1961).

133. Kampa, E.M., and Boden, B.P., "Light generation in a sonic-scattering layer," Deep Sea Res. *4*, 73 (1957).

144. Kozlyaninov, M.V., "New instrument for measuring the optical properties of sea water," Trudy Inst. Okeanol. Akad. Nauk S.S.S.R. *25*, 134 (1957), (trans. available Off. Tech. Serv., U.S. Dept. of Comm., Washington, D.C.).

160. Limbaugh, C., and Rechnitzer, A.B., "Visual detection of temperature-density discontinuities in water by diving," Science *121*, 1 (1955).

173. Malkus, J.S., "Large scale interactions," in *The Sea* (Interscience Pub., New York, 1962), M.N. Hill, ed., vol. I, Chapt. 4.

177. Middleton, W.E.K., *Vision Through the Atmosphere* (Univ. of Toronto Press, 1952).

182. Minnaert, M., *The Nature of Light and Color in the Open Air* (Dover Pub., Inc., New York, 1954), trans. by H.M. Kremer-Priest, revised by K.E. Brian Jay.

185. Moon, P., *The Scientific Basis of Illuminating Engineering* (Dover Pub., Inc., New York, 1961), rev. ed.

210. Preisendorfer, R.W., *Lectures on Photometry, Hydrologic Optics, Atmospheric Optics* (Lecture Notes, vol. I, Visibility Laboratory, Scripps Inst. of Ocean., Univ. of California, San Diego, Fall 1953).

225. Preisendorfer, R.W., *On the Existence of Characteristic Diffuse Light in Natural Waters* (Scripps Inst. of Ocean. Ref. 58-59, Univ. of California, San Diego, 1958).

251. Preisendorfer, R.W., *Radiative Transfer on Discrete Spaces* (Pergamon Press, New York, 1965).

260. Redmond, P.M., *Light Refraction by a Free Ocean Surface* (AIAA paper No. 65-238, Am. Inst. of Aeronautics and Astronautics, New York, March 1965).

265. Riley, G.A., "Theory of food-chain relations in the ocean," in *The Sea* (Interscience Pub., New York, 1963), M.N. Hill, ed., vol. II, Chapt. 20.

271. Sasaki, T., Okami, N., Oshiba, G., and Watanabe, S., "Angular distribution of light in deep water," Records of Ocean. Works in Japan *5*, 1 (1960).

272. Schenck, H., "On the focusing of sunlight by ocean waves," J. Opt. Soc. Am. *47*, 653 (1957).

283. Secchi, P.A., *Relazione della Esperienze Fatte a Bordo della Pontificia Pirocorvetta L'Immacolata Concezione per Determinare la Trasparenza del Mare* (circa 1866) [Reports on Experiments Made on Board the Papal Steam Sloop L'Immacolata Concezione to Determine the Transparency of the Sea] (Translation available, Dept. of the Navy, Office of Chief of Naval Operations, O.N.I. Trans. No. A-655, Op-923 M4B, 21 Dec. 1955).

290. Spilhaus, A.F., *Observations of Light Scattering in Sea Water* (PhD Thesis, Dept. of Geology and Geophysics, M.I.T., February 1965, prepared under ONR Contract Nonr 1841 (74). NR 083-157).

296. Thekaekara, M.P., "The solar constant and spectral distribution of solar radiant flux," Solar Energy *9*, 7 (1965).

298. Tyler, J.E., "Radiance distribution as a function of depth in an underwater environment," Bull. Scripps Inst. Ocean. *7*, 363 (1960).

299. Tyler, J.E., *An Instrument for the Measurement of the Volume Absorption Coefficient of Horizontally Stratified Water* (Report No. 5-4, Task 5, Contract NObs-72039, Bureau of Ships Project NS 714-100, Visibility Laboratory, Univ. of California, San Diego, February 1960).

300. Tyler, J.E., "Scattering properties of distilled and natural waters," Limnology and Oceanography *6*, 451 (1961).

301. Tyler, J.E., "Estimation of percent polarization in deep oceanic water," J. Mar. Res. *21*, 102 (1963).

302. Tyler, J.E., "Colour of the ocean," Nature *202*, 1262 (1964).

303. Tyler, J.E., ed., *Physical Aspects of Light in the Sea*, A Symposium at the Tenth Pacific Science Congress, Honolulu, Hawaii, August 1961 (Univ. of Hawaii Press, Honolulu, Hawaii, 1964).

304. Tyler, J.E., and Shaules, A., "Irradiance on a flat object underwater," Applied Optics *3*, 105 (1964).

305. Tyler, J.E., and Preisendorfer, R.W., "Light," in *The Sea* (Interscience Pub., New York, 1962), M.N. Hill, ed., vol. I, Chapt. 8.

309. Volterra, V., *Theory of Functionals and of Integral and Integro-differential Equations* (Dover Pub., Inc., New York, 1959).

315. Whitney, L.V., "The angular distribution of characteristic diffuse light in natural waters," J. Mar. Res. *4*, 122 (1941).

α (alpha), 60
a (ay), 55, 58, 60
Absorbed flux, 55, 58
Absorption (of a finitely deep slab of water, A_γ), 70; measurements, 103; length, 110
Adaptation level (for visibility), 160
Apparent optical properties, 118; defined, listed, 135
Apparent radiance, 60
Astrophysical Optics, defined, 1
Asymptotic radiance hypothesis, 41
Atmospheric radiative transfer, gross features, 27
Attenuation length, 90

Back scattered flux, 55
Beam transmittance, 120
Beebe, L., 143, 153
Biological sources, underwater light field, 53
Blondel, 21
Boundaries, 55
Brightness (monochromatic) of radiant flux, 10; 'Brightness' is an untechnical term for the precise concepts of radiance or luminance (as the case may be).

Candela, 20
Carnivores (in food chain), 199
Chromaticity (color), 146; components, 148; plane, 147; diagram, 149; coordinates, 149
Classification of natural hydrosols, 138
Collimated flux, scattering functions for, 83; produced by sources, 114
Color, 146; components, 146; purity, 149; dominant wavelength, 149
Colorimetric radiative transfer, 142
Complete reflectance (for irradiance), 79
Complete transmittance (for irradiance), 79
Consistency, check for inherent optical properties, 124
Contrast; apparent, inherent, 44; transmittance law, 89,90, 99; multiplicative (semigroup) property, 95
Contrast reduction; subsurface, by scattering and absorption, 44; by refractive effects, 48
Conventions (used in this work) nature of radiant flux, 6; unpolarized flux, 7; frequency density (footnote)
Cosine law, for irradiance, 13; for radiant emittance, 14

Decomposed (light field), 63
Diffusion constant (D), 64; in terms of K, 111
Diffusion equation (for h), 64
Diffusion length, 135
Diffusion model, 61; for point sources, 110; empirical examples, 112
Distribution factor, 55
Divergence law, 44; for vector irradiance, 62
Dominant wavelength, 149
Duntley Disks, 96

Equation of transfer, 60
Equilibrium radiance, 85
Equilibrium solutions (food chain), 203
Exponential law of change (general), 197; differential form, 201

Fick's law (of diffusion), 64
Field interpretations of radiant flux, 12
Finitely deep hydrosols, reflectance and transmittance, 68
Flux density (radiant), 10
Food chain problem (in the sea), 196
Foot candle, 20
Frequency density convention (in this work), 7

Geophysical Optics, defined, 1
GEOVAC (geophysical optics variable automatic computer), 208
Glitter patterns, on air-water surface, 32

Herbivore (in food chain), 199
Herschel (luminance unit), 21
Homogeneity (of σ), 82
Hydrologic Optics, defined, 1; future problems, 205
Hydrologic range, 90

Illuminance, 19; measured at earth's surface, 25
Inherent optical properties, 118; defined, listed, 119
Inherent radiance, 60
Intensity (radiant), 10; field, 12; surface, 12
Interaction principle, 4
Interdependence (Plan) of chapters in this work, 5
Invariant Imbedding Relation (for irradiance), 71, 80
Irradiance, 12; scalar, 15, 106; hemispherical scalar, 16; vector, 15; net, 16, 61; upwelling (upward), 16, 55, 58, 106; downwelling (downward), 16, 55, 58, 106; measured at earth's surface, 24; reflectance of air-water surface, 30; reflectance in deep water, 67; invariant imbedding relations, 71
Irradiance distributions, underwater, 42
Isotropy (of σ), 82

κ (kappa)(k-function or diffuse attenuation function for diffusion model), 65
k (little kay), 58; interchangeable with K (big kay), 83

Lambert, 20
Light. This term is used throughout the present work as an informal correspondent to any one of the defined concepts of geometrical radiometry and photometry. The meaning intended for the term 'light' will be implicit in each context of its use. Thus 'light field' may, e.g., correspond informally to 'radiant energy', 'radiant flux', 'radiance distribution', 'irradiance function', 'luminous energy', 'luminous flux', 'luminance distribution', 'illuminance function', etcetera.
Light field, decay with depth, 37, 66; polarization, underwater, 50; biological sources, 53; artificial, 109; decomposed, 63
Lumen, 19
Luminance, 19
Luminosity function (photopic), 145
Luminous energy, 19

Manhole (optical), 34
Melanoidines (Gelbstoff), 133
Modes of classification of natural hydrosols, 140
Multiplicative (semigroup) property, of contrast transmittance, 93; of beam transmittance, 120

Natural hydrosols, classified, 138; characterization (for visibility), 195
Natural illumination, 156
Nomographs for underwater visibility, 154
Nutrient (in food chain), 199

One-D (two-flow irradiance) model, 56
Operational definitions of the densities, 10
Optical properties, inherent, apparent, 118

Path function, 60
Path radiance, 63
Perfectly diffusing (surface), 21
Phase density, of radiant flux, 10
Photometry, geometrical, 18
Photons, as viewed in this work, 7

Photopic luminosity curve, 18, 145
Phytoplankton (in food chain), 199
Polarization, defined, 51; underwater properties, 52
Plane-parallel medium, 55
Prey-predator equations, 198
Principles of invariance for irradiance, 73, 79
Problems of hydrologic optics, 2, 205

Quantum, 7
Quasi-steady state (food chain), 202

Radiance, 10; field, 12; surface, 12; n^2-law, 18, 87; inherent, 60; apparent, 60; equilibrium, 85; -difference law, 92; residual, 120; path, 63
Radiance distribution, behavior with depth, 39; asymptotic hypothesis, 41; by submerged point source, 113
Radiance model, 58
Radiant density, 16
Radiant emittance, 12
Radiant energy. In this work radiant energy is the undefined, primitive concept, taken as given by nature and axiomatized by radiometrists as their primary physical notion. In other fields, such as electromagnetics, it can be made to rest on one step lower: on the constructs (E,D,B,H) of the electromagnetic field. These steps into physical primitivity descend even lower. But this nether region is of no concern to us in this work.
Radiant flux, defined, 7; monochromatic brightness of, 10; field and surface interpretations, 121
Radiant intensity, 10; field and surface, 12
Radiative transfer theory, defined, 1; basic constructs, 4; atmospheric features, 27; across air-water surface, 28;
Radiative transfer theory (con't.)
colorimetric, 142
Radiometric concepts, operational definitions, 11
Radiometry, geometrical, 7
Rationalized units (polemic on), 21
Reflectance, for irradiance at air-water surface, 30; for infinitely deep homogeneous water, 67; for finitely deep homogeneous water, 68; complete (for irradiance), 79
Refraction, subsurface, 33
Residual radiance, 63, 120
Riccati Equation, in food chain, 203
R-infinity (R_∞), 67; correction in visibility, 172

σ (sigma), 122
s (ess), 58
Scattered flux, 58, for collimated flux, 83; forward, backward, 124
Schuster, A., 57
Secchi Disk, 96; in visibility calculations, 169
Semigroup (multiplicative) property, of contrast transmittance, 95; of beam transmittance, 120
Sighting range (interpretations), 195
Simple model for radiance, 61
Solar (irradiance) constant, 22; (illuminance), 22
Source term (for scalar irradiance), 64
Spectrum locus, 149
Stratified media, 62
Subsurface refractive phenomena, 33
Surface interpretation of radiant flux, 12

Thermocline phenomena, 36
Transmittance, for irradiance at air-water surface, 30; (t=1-r), for finitely deep homogeneous water, 68; complete (for irradiance), 79; beam, 120; contrast, 93
Tristimulus functions, 144
Two-flow (irradiance) model, 55-57

Unpolarized-Flux convention (in this work), 7

Vector analogy with color, 146
Visibility underwater, 154; effect of depth and water clarity, 157; use of nomographs, 163; along inclined paths of sight, 165; horizontal paths of sight, 170
Volterra prey-predator equations, 198
Volume absorption function, 60; measurement, 103; operational definition, 124
Volume attenuation function, 60; operational definition, 119; empirical, 120
Volume backward scattering functions, 124
Volume forward scattering functions, 124
Volume scattering function, 122
Volume total scattering function, 60; operational definition, 123

Water clarity (visualization), 194
Wavelength, dominant, 149
White light, 149
Window (spectral), 134

☆ U.S. GOVERNMENT PRINTING OFFICE: 1976—677-881/ 36 REGION NO. 8